Miscellaneous Paper GL-93-14
August 1993

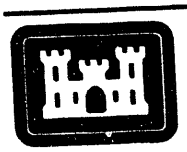

US Army Corps of Engineers
Waterways Experiment Station

Site-Specific Earthquake Response Analysis for Paducah Gaseous Diffusion Plant, Paducah, Kentucky

by *David W. Sykora, Jennifer J. Davis*
Geotechnical Laboratory

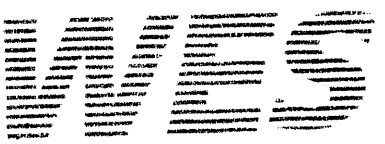

Prepared for U.S. Department of Energy, Oak Ridge Operations

DISCLAIMER

Miscellaneous Paper GL-93-14
August 1993

Site-Specific Earthquake Response Analysis for Paducah Gaseous Diffusion Plant, Paducah, Kentucky

by David W. Sykora, Jennifer J. Davis
Geotechnical Laboratory

U.S. Army Corps of Engineers
Waterways Experiment Station
3909 Halls Ferry Road
Vicksburg, MS 39180-6199

Final report

Approved for public release; distribution is unlimited

Prepared for U.S. Department of Energy
Oak Ridge Operations
Oak Ridge, Tennessee 37831-8650

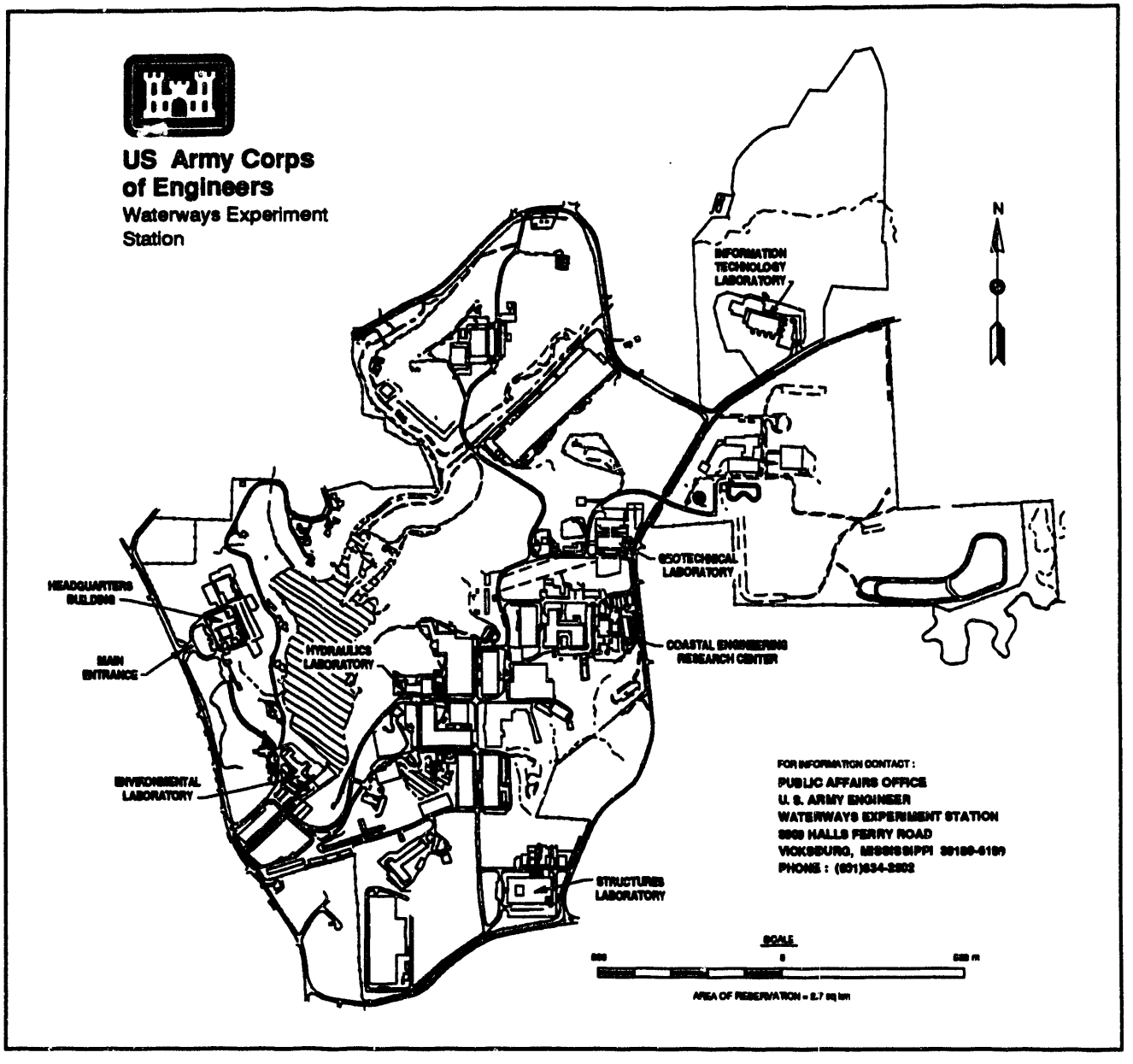

Waterways Experiment Station Cataloging-In-Publication Data

Sykora, David W.
Site-specific earthquake response analysis for Paducah Gaseous Diffusion Plant, Paducah, Kentucky / by David W. Sykora, Jennifer J. Davis; prepared for U.S. Dept. of Energy, Oak Ridge Operations.
266 p.: ill.; 28 cm. -- (Miscellaneous paper; GL-93-14)
Includes bibliographical references.
1. Earthquake hazard analysis -- Kentucky -- Paducah. 2. Gaseous diffusion plants -- Kentucky -- Paducah. 3. Nuclear facilities -- Kentucky -- Paducah. I. Davis, Jennifer J. II. United States. Dept. of Energy. Oak Ridge Operations Office. III. U.S. Army Engineer Waterways Experiment Station. IV. Title. V. Series: Miscellaneous paper (U.S. Army Engineer Waterways Experiment Station) ; GL-93-14.
TA7 W34m no.GL-93-14

EXECUTIVE SUMMARY

A site-specific earthquake response study was conducted for the U.S. Department of Energy (DOE) Paducah Gaseous Diffusion Plant (PGDP), located near Paducah, Kentucky, to provide guidance for the seismic safety analysis and future design of structures and facilities there. The methods used generally follow widely-accepted and validated practices of the geotechnical earthquake engineering profession as documented in professional literature.

Three earthquake events developed using probabilistic methodologies were considered. Two horizontal components of rock outcrop motion in terms of acceleration versus time were used independently (uncoupled). The peak horizontal accelerations at rock outcrop are 0.19, 0.27, and 0.63 g for the 500-year, 1000-year, and 5000-year events, respectively.

Input parameters describing soil column idealization, geotechnical engineering properties, and seismic velocities for four individual soil columns were obtained from reports by others summarizing investigations around the perimeter of the plant area. Soils at PGDP generally consist of Pleistocene-age alluvium overlying Tertiary-age deposits and then hard limestone. Idealized soil column heights range from 322 to 364 ft.

The computer program *SHAKE* was used to calculate the site response corresponding to each of the four sites. The predominant site period is in the range of 0.9 to 1.2 sec. Secondary response peaks occurred at periods around 0.2 and 0.4 sec. The peak horizontal accelerations at (free field) ground surface were calculated to be 0.20, 0.27, and 0.36 g for the 500-year, 1000-year, and 5000-year events, respectively. Peak spectral velocities of 18, 26, and 70 in./sec for the 500-year, 1000-year, and 5000-year events, respectively, occur in this range of periods at 5 percent damping. Peak spectral accelerations of 0.75, 1.1, and 1.0 g for these three events, respectively, occur at a period of 0.2 sec.

A sensitivity study was conducted using an average soil column and the 1000-year earthquake event. The effects of including a measured velocity inversion at Site 3 and reasonable ranges of impedance ratio, depth to bedrock, and modulus relationships were found to be negligible to small. The effect of damping ratio relationships and maximum shear modulus using very large bounds was found to be considerable at lower periods.

PREFACE

This report documents the site response evaluations performed for the U.S. Department of Energy (DOE) Paducah Gaseous Diffusion Plant (PGDP) located southwest of Paducah, Kentucky. The U.S. Army Engineer Waterways Experiment Station (WES) was authorized to conduct this study from FY91 to FY93 by the DOE, Oak Ridge Operations (ORO), Oak Ridge, Tennessee, through Inter-Agency Agreement (IAG) No. DE-AI05-91OR21971. The study was conducted under the Gaseous Diffusion Plant Safety Analysis Report (GDP SAR) Program. Dr. Ronald O. Hultgren and Mr. James A. Reafsnyder, ORO, were the DOE Program Officers.

The IAG was managed for Martin Marietta Energy Systems, Inc., by Ms. Karen E. Shaffer, Uranium Enrichment, Martin Marietta Energy Systems, Inc., Oak Ridge, Tennessee. Mr. William R. Brock, Deputy Engineering GDP SAR Manager, Technical Operations, and Mr. R. Joe Hunt, Center for Natural Phenomena Engineering, Technical Operations, provided technical requirements and oversight for the study. The overall project manager was Mr. Anthony Angelelli, GDP SAR Manager, Uranium Enrichment. A similar study was conducted for the DOE Portsmouth Gaseous Diffusion Plant (PORTS), located near Portsmouth, Ohio, under the same IAG and is reported under separate cover. A reassessment of liquefaction potential and estimation of earthquake-induced settlements at PGDP are also reported under separate cover.

The WES Principal Investigator was Mr. David W. Sykora, Earthquake Engineering and Seismology Branch (EESB), Earthquake Engineering and Geosciences Division (EEGD), Geotechnical Laboratory (GL), WES. Ms. Jennifer J. Davis, a co-op student from Mississippi State University, assisted Mr. Sykora. Mr. Gregory D. Comes, EESB, provided additional engineering assistance, and Messrs. William M. McGeehee and Daniel M. Habeeb, EEGD, helped to prepare report figures. Dr. Mary Ellen Hynes was the Chief, EESB, during this study.

Overall direction at WES was provided by Dr. A. G. Franklin, Chief, EEGD, and Dr. William F. Marcuson III, Director, GL.

At the time of publication of this report, Director of WES was Dr. Robert W. Whalin. Commander was COL Bruce K. Howard, EN.

CONTENTS

LIST OF TABLES

LIST OF FIGURES

LIST OF FIGURES (cont'd)

LIST OF FIGURES (cont'd)

CONVERSION FACTORS, NON-SI to SI (METRIC)
UNITS OF MEASUREMENT

Non-SI units of measurement used in this report can be converted to SI (metric) units as follows:

Multiply	Abbreviation	By	To Obtain
acre	-	0.4047	square kilometers
feet	ft	0.3048	meters
inches	in.	2.54	centimeters
miles (US statute)	mis.	1.609	kilometers
pounds (mass) per cubic foot	pcf	16.01846	kilograms per cubic meter
pounds (mass) per square foot	psf	4.882428	kilograms per square meter
pounds (force) per inch	psi	6.894757	kilopascals

SITE-SPECIFIC EARTHQUAKE RESPONSE ANALYSIS FOR PADUCAH GASEOUS DIFFUSION PLANT, PADUCAH, KENTUCKY

PART I: INTRODUCTION

1. The Paducah Gaseous Diffusion Plant (PGDP), owned by the U.S. Department of Energy (DOE) and operated under contract by Martin Marietta Energy Systems, Inc., is located southwest of Paducah, Kentucky. An aerial photograph and an oblique sketch of the plant are shown in Figures 1 and 2, respectively. The fenced portion of the plant consists of 748 acres.* This plant was constructed in the 1950's and is one of only two gaseous diffusion plants in operation in the United States; the other is located near Portsmouth, Ohio.

2. The facilities at PGDP are currently being evaluated for safety in response to natural seismic hazards. Design and evaluation guidelines to evaluate the effects of earthquakes and other natural hazards on DOE facilities follow probabilistic hazard models that have been outlined by Kennedy et al. (1990). Criteria also established by Kennedy et al. (1990) classify diffusion plants as "moderate hazard" facilities.

3. The U.S. Army Engineer Waterways Experiment Station (WES) was tasked to calculate the site response using site-specific design earthquake records developed by others and the results of previous geotechnical investigations. In all, six earthquake records at three hazard levels and four individual and one average soil columns were used.

Purpose

4. The purpose of this study was to calculate a reasonable range of expected site-specific, free-field earthquake response at PGDP to three hazard-level earthquakes, a 500-year, a 1000-year and a 5000-year event, using geotechnical and geophysical information collected by others specifcally for this site response analysis. The response was calculated independently for two components of horizontal motion at each hazard level. The emphasis of the

---

* A table of factors for converting US customary units of measurement to metric (SI) units is presented on page 8.

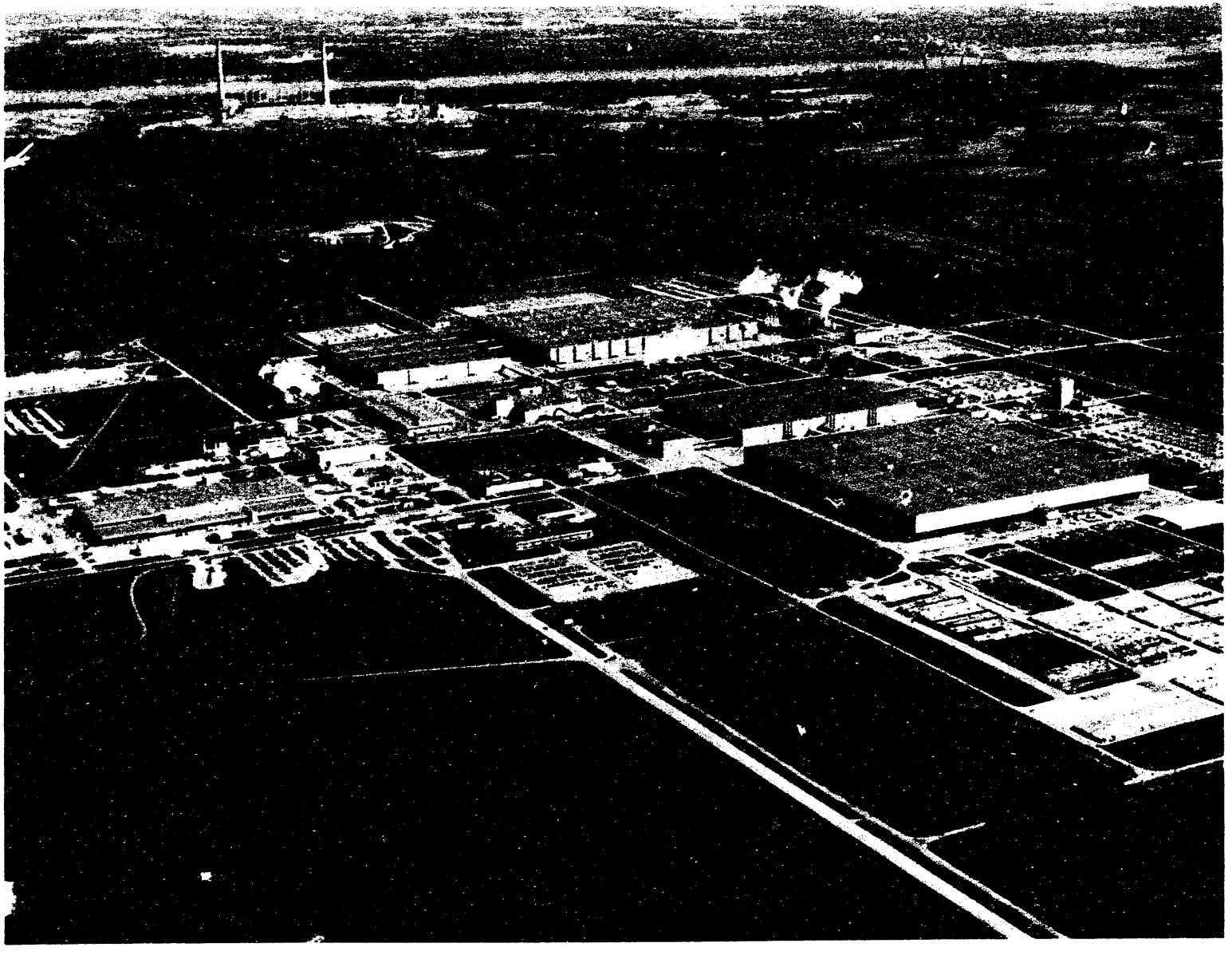

Figure 1. Aerial photograph of Paducah Gaseous Diffusion Plant looking northeast

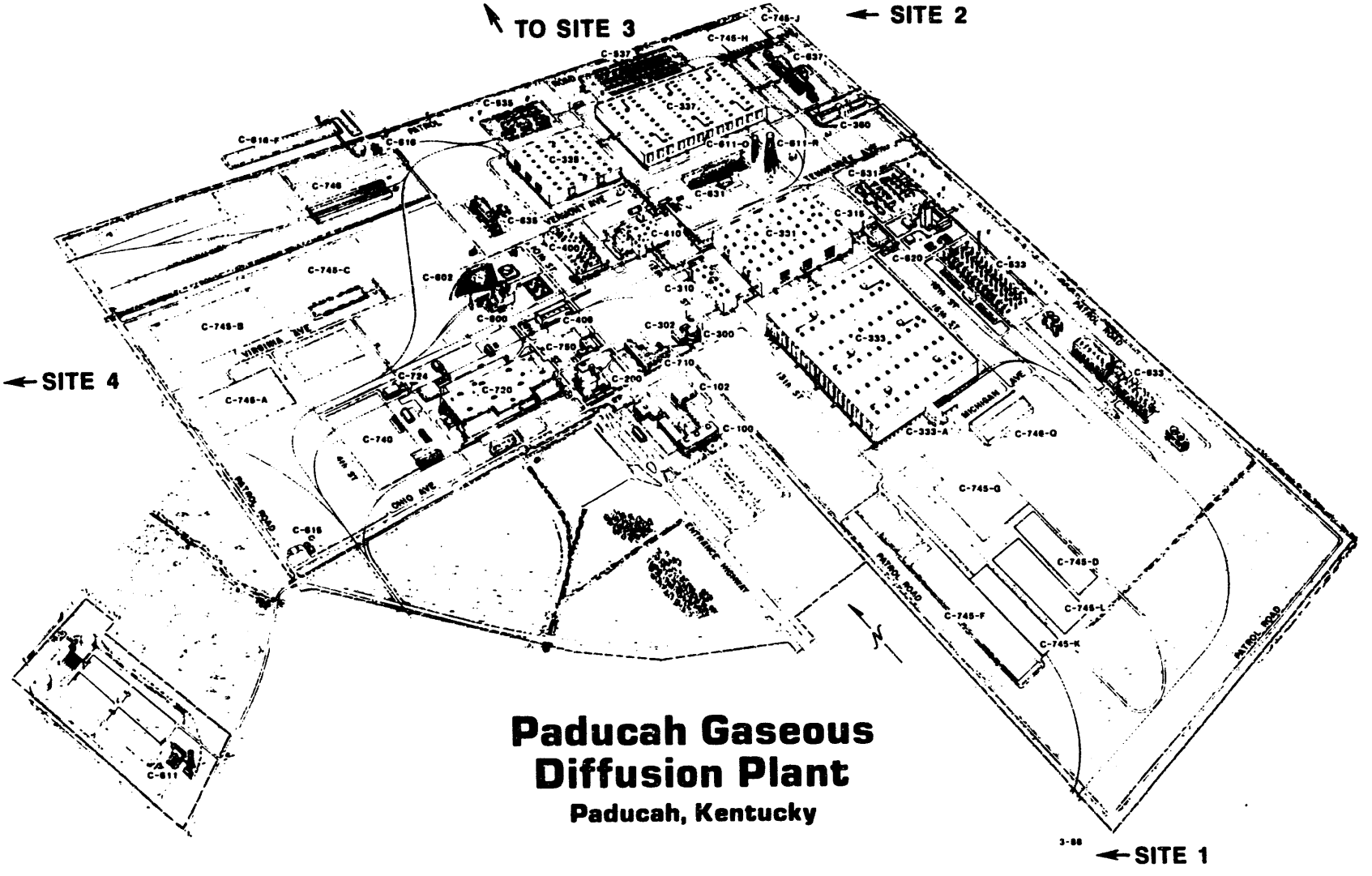

Figure 2. Oblique sketch of PGDP showing general locations of four sites used in the analysis

evaluation was on the 1000-year event which represents the Design Basis Earthquake (DBE) for design and seismic evaluation studies at moderate hazard DOE facilities. Calculated free field response spectra will be used by structural engineers to evaluate the stability of sensitive structures and facilities and to design future systems at PGDP. To our knowledge, no previous detailed site response analysis has been conducted for PGDP. Calculated acceleration records will be used by WES to update the study of liquefaction potential at the site and estimate earthquake-induced settlements.

Procedure of Site Response Analysis

5. A site response analysis, sometimes referred to as a soil amplification analysis, involves the determination of components of ground motion for design or seismic evaluation. Typically, as in this study, that determination is made for a "free-field" response—the response at the ground surface of an ideal soil deposit (horizontal layers extending to infinity) to a spatially-uniform, horizontal motion applied at the base. The conceptual relationship between free-field response with respect to two other primary control points—rock outcrop and base rock—in a site response analysis is shown in Figure 3. The motions at these three points, as well as any other point in the vertical profile, are unique. Design earthquake motions are most often specified as corresponding to rock outcrop. Mathematical expressions (transfer functions) are then used to find the equivalent motion for the baserock, and then the seismic waves are propagated through the soil column to determine the free-field motion at the surface.

6. The determination of site-specific earthquake response of soil deposits generally involves three basic steps:

a. Determination of earthquake hazard and the selection or derivation of design motions.

b. Idealization of stratigraphy and selection of material properties.

c. Calculation and evaluation of site response.

For this study, step (a) and part of step (b), listed above, were conducted by others (Risk Engineering, Inc. 1993, Automated Science Group, Inc. 1991, ERCE 1990b, and Staub, Wang, and Selfridge 1991) and submitted to WES by Martin

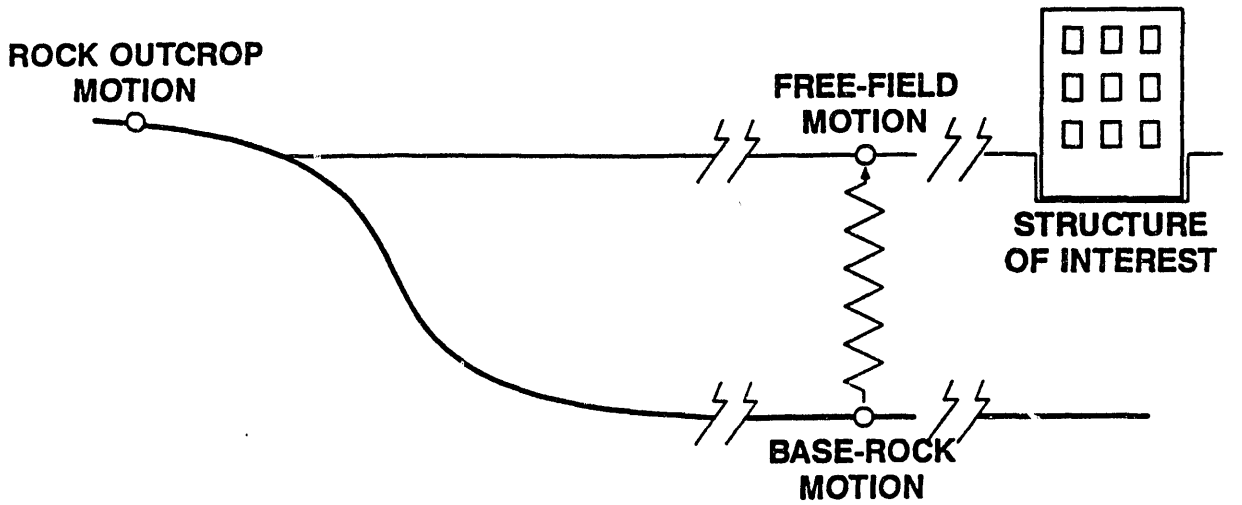

Figure 3. Three primary control points for a site response analysis

Marietta Energy Systems, Inc. WES was wholly responsible for the calculation and evaluation of site-specific earthquake response (step (c) listed above). WES also derived the average column used for sensitivity analysis.

7. At the direction of Martin Marietta Energy Systems, Inc., the computer program *SHAKE* (Schnabel, Lysmer, and Seed 1972) was used to calculate site response for purposes of this study. *SHAKE* is a one-dimensional, total stress code that solves the wave equation in the frequency domain (complex response technique). The soil profile is represented with an idealized soil column of homogeneous, visco-elastic layers of infinite extent.

8. *SHAKE* is widely used by the geotechnical earthquake engineering profession for the calculation of site response for horizontal motions. Several investigators have reported close comparisons between the results using *SHAKE* and the measured horizontal response from strong-motion instruments triggered during earthquakes at periods less than 2 sec (e.g., Seed et al. 1987 and Seed, Dickenson, and Idriss 1991). The experience of these investigators suggest that for periods greater than 4 sec, motions are likely to be significantly affected by two-dimensional effects and surface wave energy and are not well represented with *SHAKE*.**

** Personal communication, Prof. Raymond Seed, University of California at Berkeley, 23 September 1991.

Special Considerations for Study at PGDP

9. The analysis of earthquake response at a site is not only unique to the material properties and site conditions but also to other factors such as the number and spatial distribution of soil columns, assessment of how representative the soil columns are of the range of site conditions, and interpretations or assumptions required to provide the necessary complement of input parameters. At PGDP, some special considerations were required.

10. Soil conditions at Site 1, located on the southern boundary of PGDP (refer to Figure 2), were reported to be considerably different than those at the other three sites (ERCE 1990a). A review of the geology there indicates that this area is underlain almost entirely by Tertiary-age deposits of the Porter's Creek Formation which tends to be stiffer than the Tertiary-age deposits of the Clayton-McNairy Formation. These deposits are expected to exist beneath the southern portion of the C-333 processing building. The calculated response at Site 1 was included to produce a full range of response that could potentially exist in the near vicinity of PGDP. The results of the analysis indicate that the response at Site 1 generally lies near the upper-bound of response but does not differ significantly from the response at other sites.

11. The four sites are spaced a large distance apart (two sites are over 2 miles apart) and exist outside of the fenced boundaries. A number of borings that were made within the fenced area for previous studies suggest that the profiles at Sites 2, 3, and 4 are representative of the conditions for the overall plant. The ranges in measured shear wave velocity with depth at the four sites are relatively small considering the distance between sites. Furthermore, shear wave velocities measured at the nearby Olmsted Lock and Dam Project on the Ohio River in the same geologic formation that exists at PGDP have essentially the same range and variability.

12. A comprehensive sensitivity analysis of inputs was performed to account for reasonable uncertainties in the depth to bedrock, impedance contrast, shear wave velocity, and relationships between shear modulus and damping ratio versus shear strain. Potential variations in shear wave velocity were addressed using guidance by the Nuclear Regulatory Commission (1989).

Report Organization

13. The presentation of information henceforth generally will follow the order of site response analysis listed earlier. First, the synthetic records used in the analysis are presented in Part II. Then, stratigraphic and material property information is presented in Part III. Detailed descriptions of calculations and methods of presentation are given in Part IV. The results of calculations for the 500-year, 1000-year, and 5000-year events are presented in Part V. The sensitivity analysis was conducted using an average column intended to represent all four sites and the 1000-year event. This analysis is summarized in Part VI. A summary and conclusions section completes the report. Figures representing many of the computations conducted for the study are contained in the appendices for reference.

PART II: DESIGN EARTHQUAKE EVENTS

14. The determination of earthquake hazard and the selection or derivation of appropriate design records represent the first step of a site response analysis. Based on current DOE guidelines and the moderate hazard classification assigned to PGDP, probabilistic methods of hazard analysis were used to derive parameters defining the design events and to develop corresponding synthetic records.

15. The probabilistic assessment of seismic hazard was conducted by Risk Engineering, Inc. (1993). They used an extended-source seismic hazard to represent the New Madrid Seismic Zone (NMSZ) for site-specific evaluations at PGDP. Recent seismic activity in the NMSZ is shown in Figure 4. The extended-source model of the NMSZ is a system of parallel faults running in a north-northeasterly direction. Earthquake magnitudes and epicentral distances were smoothed with the dominant magnitudes and epicentral distances being 7.1 at 65 km for the 500-year event, 7.3 at 52 km for the 1000-year event, and 7.3 at 38 km for the 5000-year event. Uniform hazard response spectra were generated at these three levels of hazard.

16. Three sets of synthetic earthquake records representing rock outcrop motions were developed corresponding to three median levels of hazard (500-year, 1000-year, and 5000-year events). Synthetic earthquake records were developed by Risk Engineering, Inc. (1992) to completely envelop the uniform hazard spectra. Two horizontal components of motion were provided for each earthquake event. A time step of 0.01 sec (i.e., 100 samples per second) was used corresponding to a Nyquist frequency of about 50 Hz, a value well above the free-field natural frequency at the site. Records of the variation of acceleration, velocity, and displacement with time and absolute acceleration response spectra are presented below for the three design events using a constant vertical plot scale for consistency. The acceleration and velocity records were integrated exactly by WES to allow inspection of the variations of velocity and displacement, respectively, with time.

500-Year Event

17. The two components of the synthetic 500-year design earthquake event for rock outcrop are shown in Figure 5, and particular characteristics

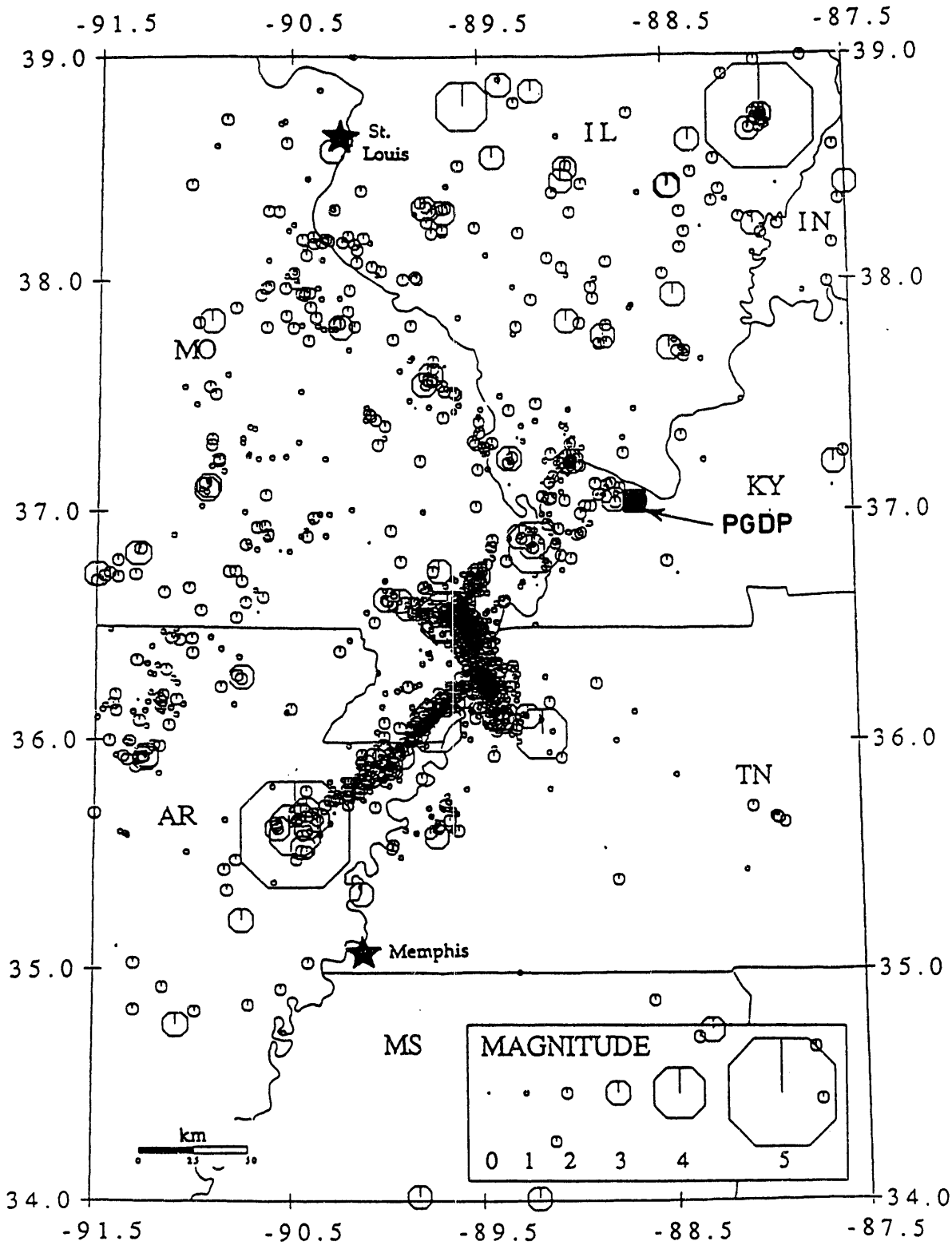

Figure 4. Seismic activity in central U.S. during 189-month period between 1974 and 1990 (courtesy of Saint Louis University)

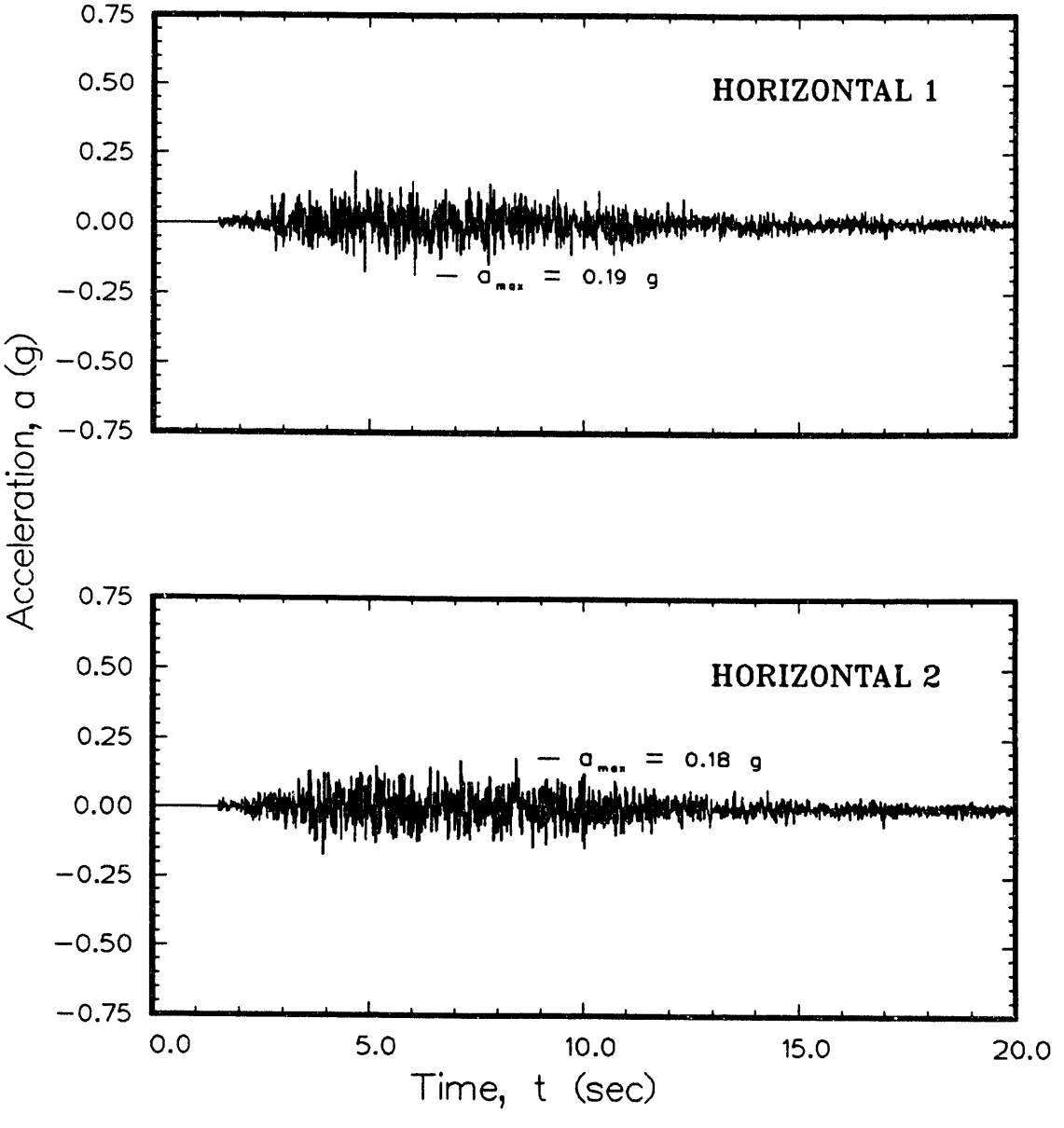

Figure 5. Horizontal components of acceleration versus time for the 500-year design earthquake event (Risk Engineering, Inc. 1992)

are summarized in Table 1. The peak horizontal ground accelerations are 0.19 and 0.18 g for the Horizontal 1 and Horizontal 2 components, respectively, and the durations of strong motion (accelerations $\geq$ 0.05 g) are 11 and 15 sec. The variation of acceleration, velocity, and displacement for the two horizontal components of the 500-year event are shown in Figure 6.

Table 1

Characteristics of 500-Year Event Outcrop Motions

Component	Peak Acceleration (cm/sec^2)	Peak Velocity (cm/sec)	Peak Displacement (cm)	Duration Strong Motion (sec)
Horizontal 1	183	11.0	8.0	11
Horizontal 2	178	6.8	2.9	15

18. The variations of velocity and displacement for the two horizontal components differ noticeably both in the peak amplitude and the number of times that the zero amplitude line is crossed. The peak velocity and displacement for the Horizontal 1 component are on the order of twice those for the Horizontal 2 component.

19. The absolute acceleration response spectra at six levels of system damping for the 500-year event are shown for both components of rock outcrop motion in Figure 7. The spectra corresponding to 5 percent damping are similar with spectral accelerations ranging up to 0.50 g. At 5 percent damping, the Horizontal 1 component has a peak ordinate of 0.5 g at 0.042 sec, and the Horizontal 2 component has dual peak ordinates at 0.021 and 0.035 sec. The Horizontal 2 component consistently has a greater response at periods less than 0.04 sec.

1000-Year Event

20. The two horizontal components of the synthetic 1000-year design earthquake event for rock outcrop are shown in Figure 8, and particular characteristics are summarized in Table 2. The peak horizontal ground

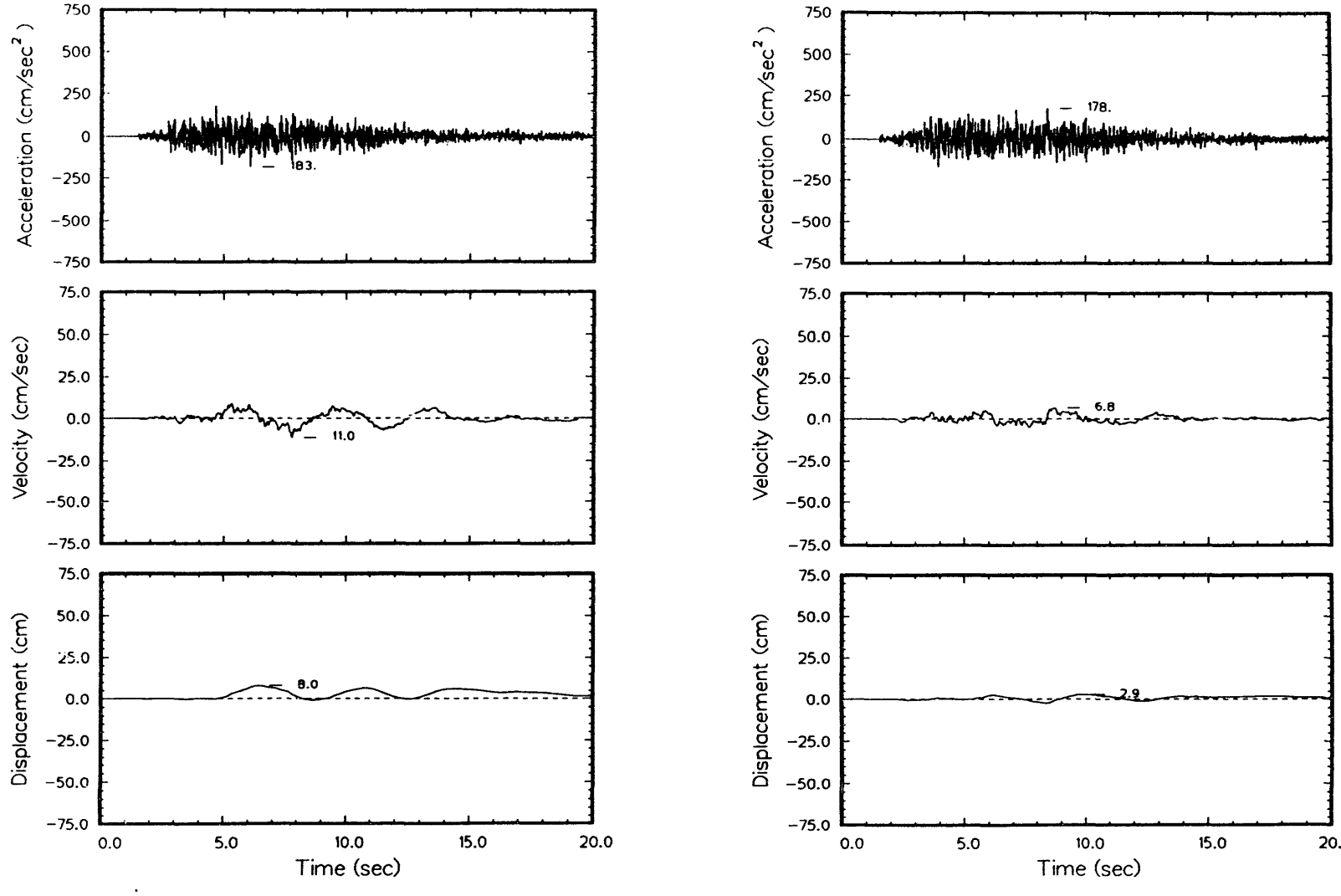

a. Horizontal 1 component

b. Horizontal 2 component

Figure 6. Variations of acceleration, velocity, and displacement for 500-year design earthquake event

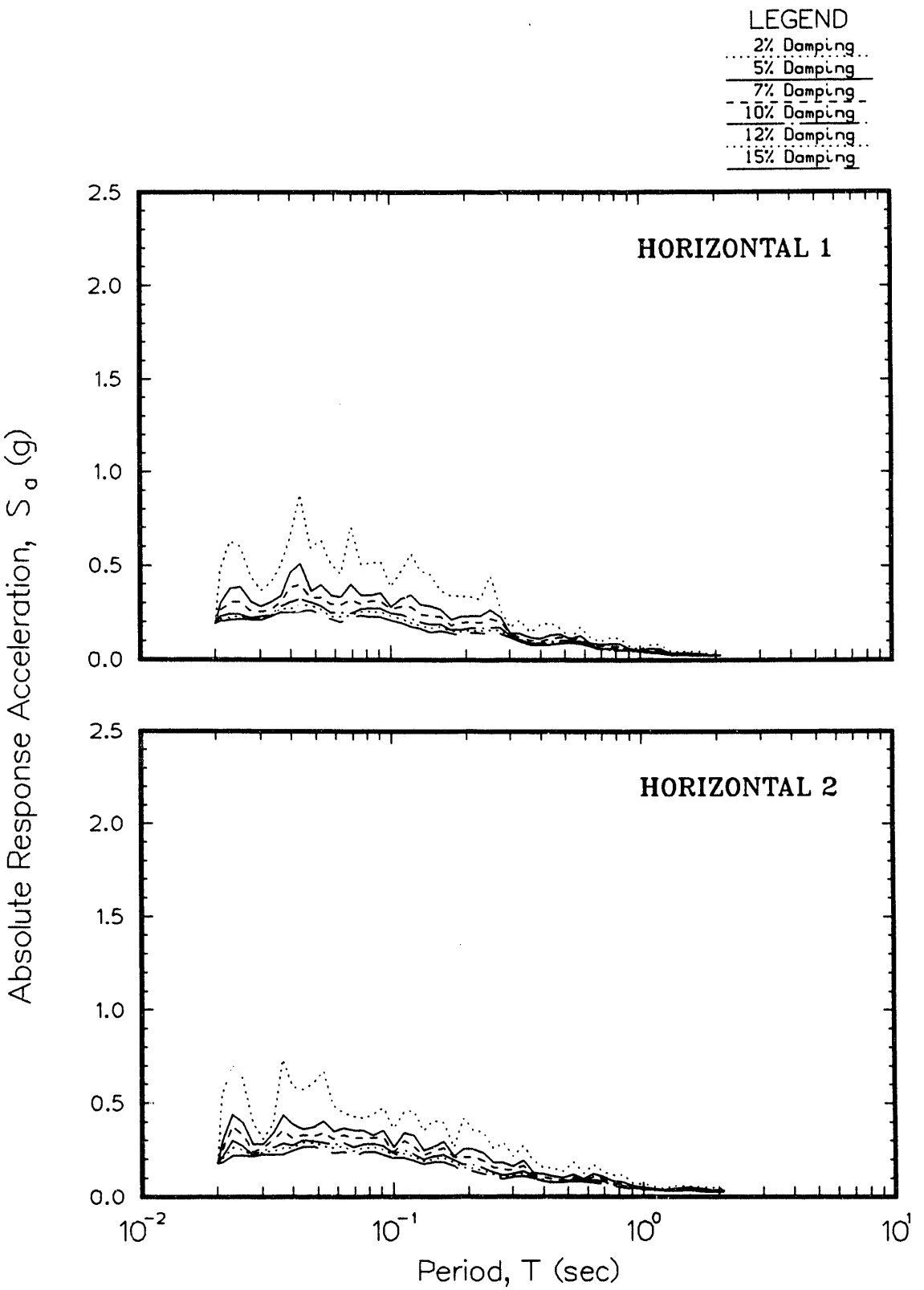

Figure 7. Acceleration (outcrop) response spectra for the 500-year design earthquake event

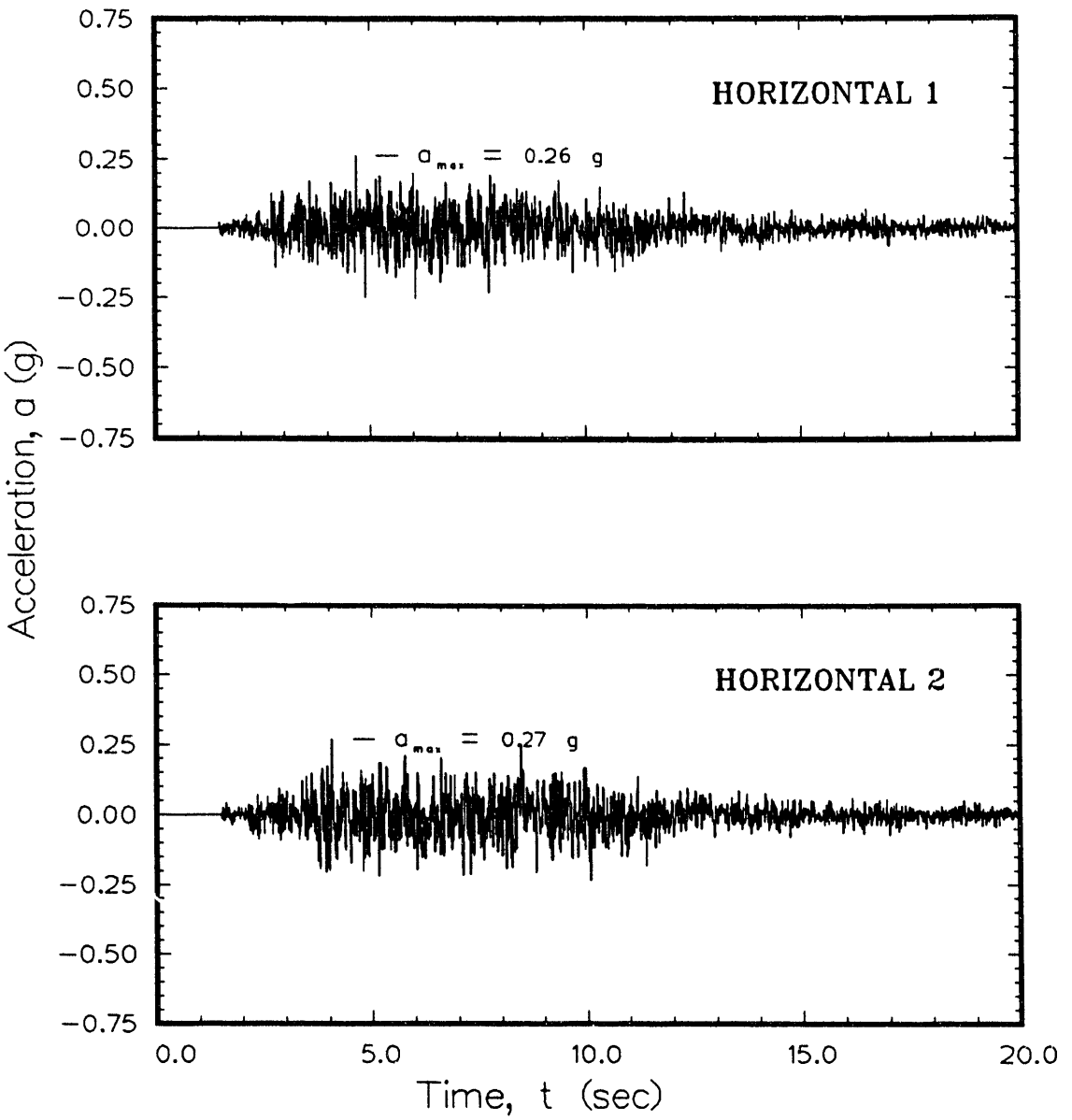

Figure 8. Horizontal components of acceleration versus time for the 1000-year design earthquake event (Risk Engineering, Inc. 1992)

accelerations are 0.26 and 0.27 g for the Horizontal 1 and Horizontal 2 components, respectively, and the durations of strong motion (accelerations $\geq$ 0.05 g) are 15 and 17 sec. The variation of acceleration, velocity, and displacement for the two horizontal components of the 1000-year event are shown in Figure 9.

Table 2

Characteristics of 1000-Year Event Outcrop Motions

Component	Peak Acceleration (cm/sec^2)	Peak Velocity (cm/sec)	Peak Displacement (cm)	Duration Strong Motion (sec)
Horizontal 1	258	18.1	13.7	15
Horizontal 2	265	14.7	11.1	17

21. The variations of velocity and displacement for the two horizontal components are similar. The Horizontal 1 component has slightly larger peak values of velocity and displacement. The variations of displacement for each component are slightly skewed to one direction or the other.

22. The absolute acceleration response spectra at six levels of system damping for the 1000-year event are shown for both components of rock outcrop motion in Figure 10. The spectra corresponding to 5 percent damping are similar with peak spectral accelerations up to 0.77 g. At 5 percent damping, the peak spectral accelerations are 0.68 and 0.77 g, about one-and-a-half times greater than the peaks for the 500-year event. Predominant periods for the two components are again 0.042 and 0.035 sec, and the Horizontal 2 component has a consistently greater response at periods less than 0.04 sec.

5000-Year Event

23. The three components of the synthetic 5000-year design earthquake event for rock outcrop are shown in Figure 11 and particular characteristics are summarized in Table 3. The peak horizontal ground accelerations are 0.54

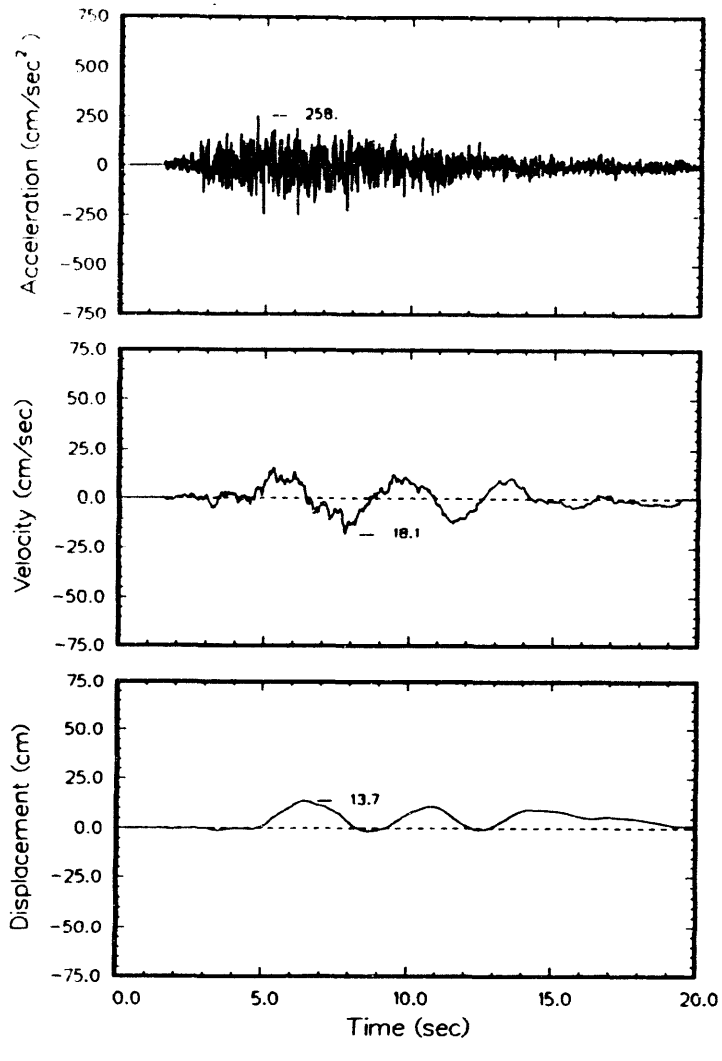

a. Horizontal 1 component

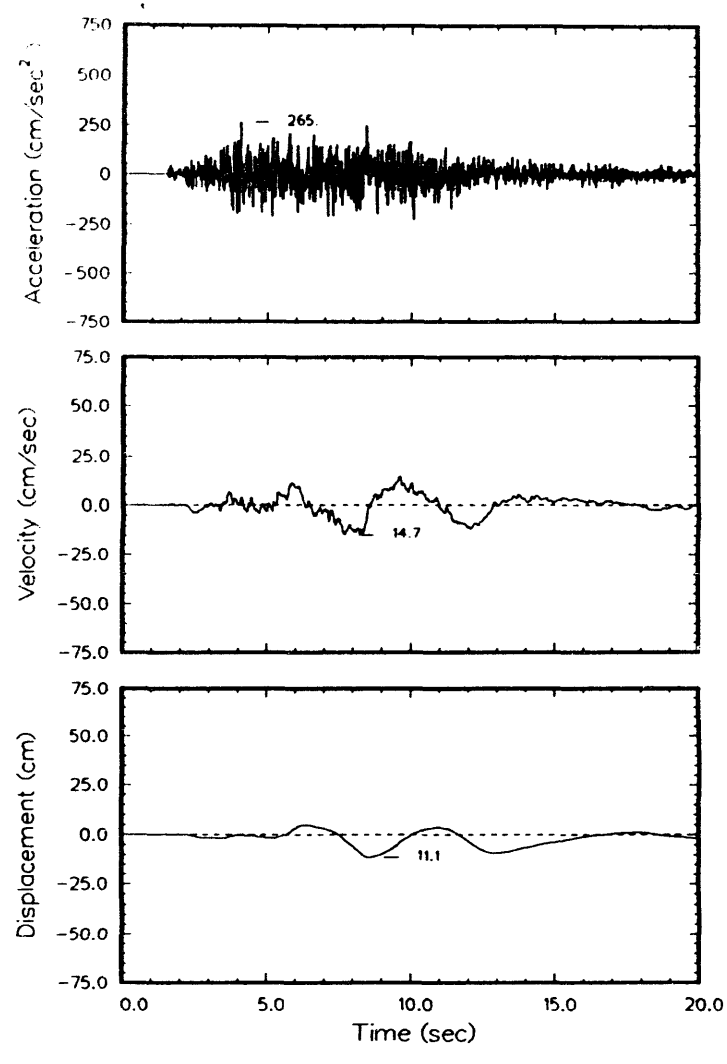

b. Horizontal 2 component

Figure 9. Variations of acceleration, velocity, and displacement for 1000-year design earthquake event

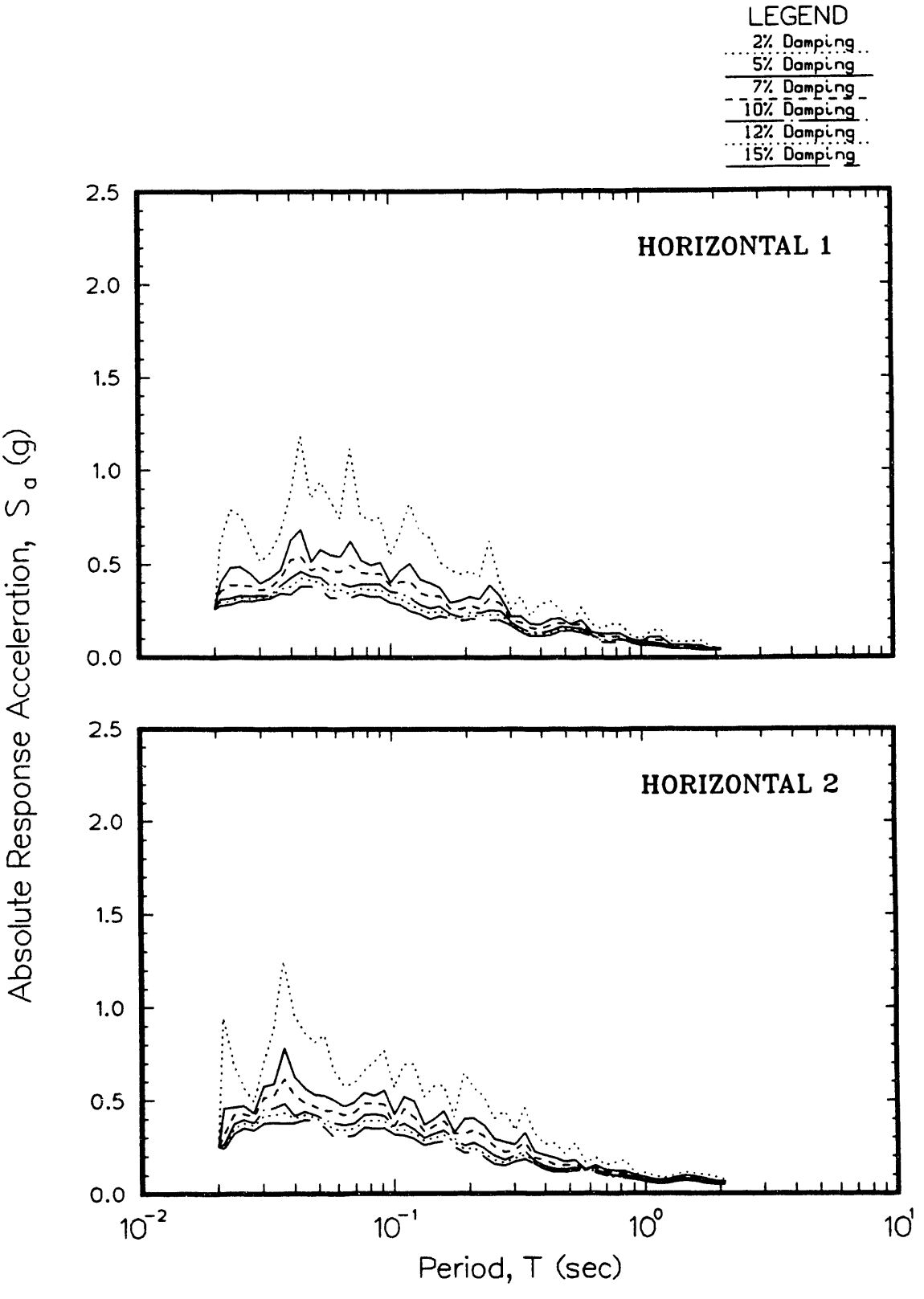

Figure 10. Acceleration (outcrop) response spectra for the 1000-year design earthquake event

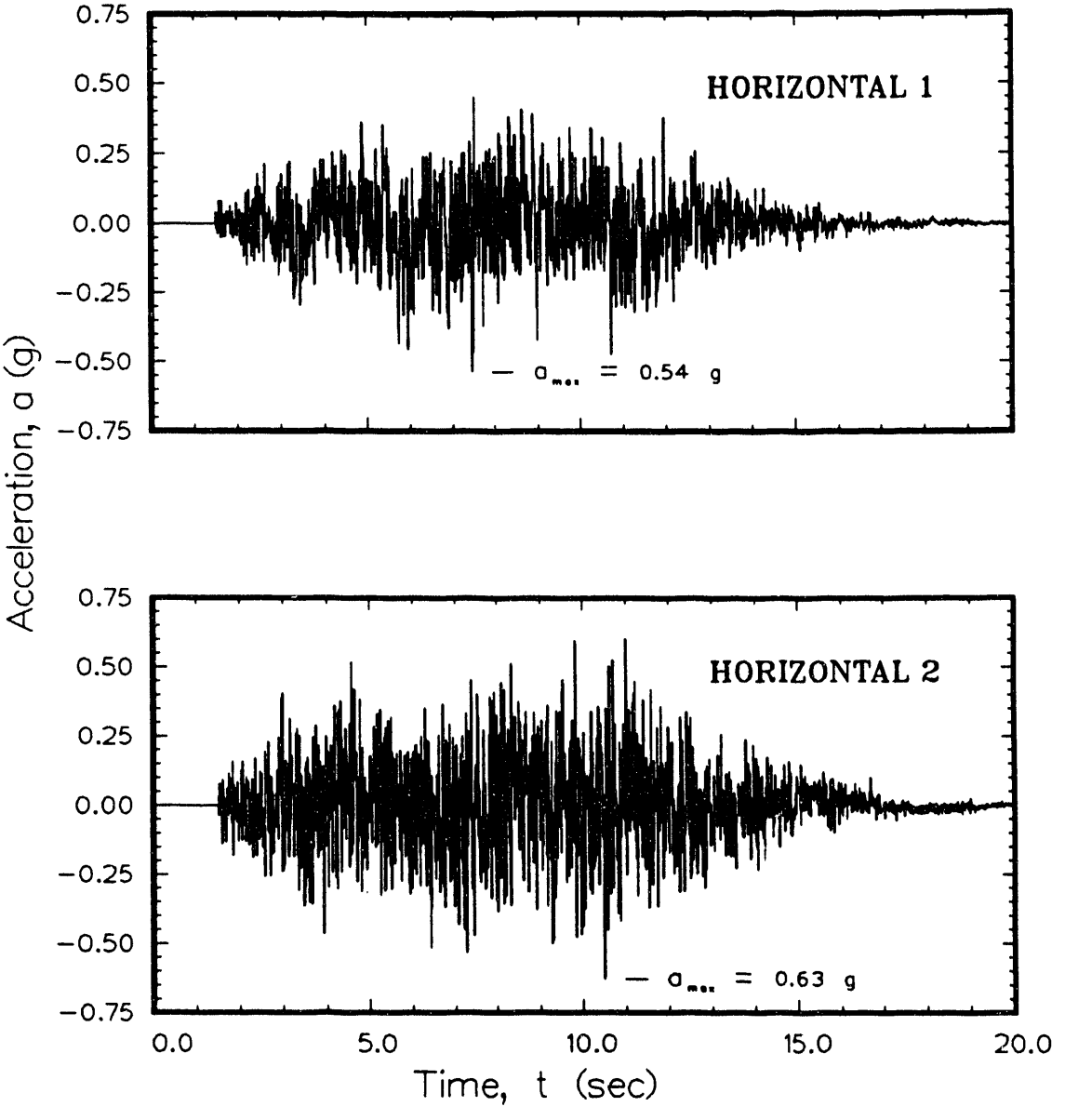

Figure 11. Horizontal components of acceleration versus time for the 5000-year design earthquake event (Risk Engineering, Inc. 1992)

and 0.63 g, respectively, and the durations of strong motion (accelerations ≥ 0.05 g) are 15 and 16 sec. The variation of acceleration, velocity, and displacement for the two horizontal components of the 5000-year event are shown in Figure 12.

Table 3

Characteristics of 5000-Year Event Outcrop Motions

Component	Peak Acceleration (cm/sec^2)	Peak Velocity (cm/sec)	Peak Displacement (cm)	Duration Strong Motion (sec)
Horizontal 1	525	53.5	45.9	13
Horizontal 2	615	59.0	41.8	15

24. The variations of velocity and displacement for the two horizontal components are very similar. The Horizontal 2 component has a slightly larger peak value of velocity, and the Horizontal 1 component has a slightly larger peak value of displacement. The variation of displacement for the Horizontal 1 component is slightly skewed to one direction. The peak values of acceleration, velocity, and displacement for the 5000-year event are about three times the peak values for the 1000-year event.

25. The absolute acceleration response spectra at six levels of system damping for the 5000-year event are shown for both components of rock outcrop motion in Figure 13. The spectra for the two components are significantly different. The Horizontal 2 component produces significantly greater response at periods less than 0.04 sec, much more pronounced than the stronger response at these periods noted for the other two events. For a damping ratio of 5 percent, the peak spectral accelerations are 1.32 at 0.048 sec and 1.55 g at 0.03 sec, about two times the peaks for the 1000-year event and three times the peak values for the 500-year event.

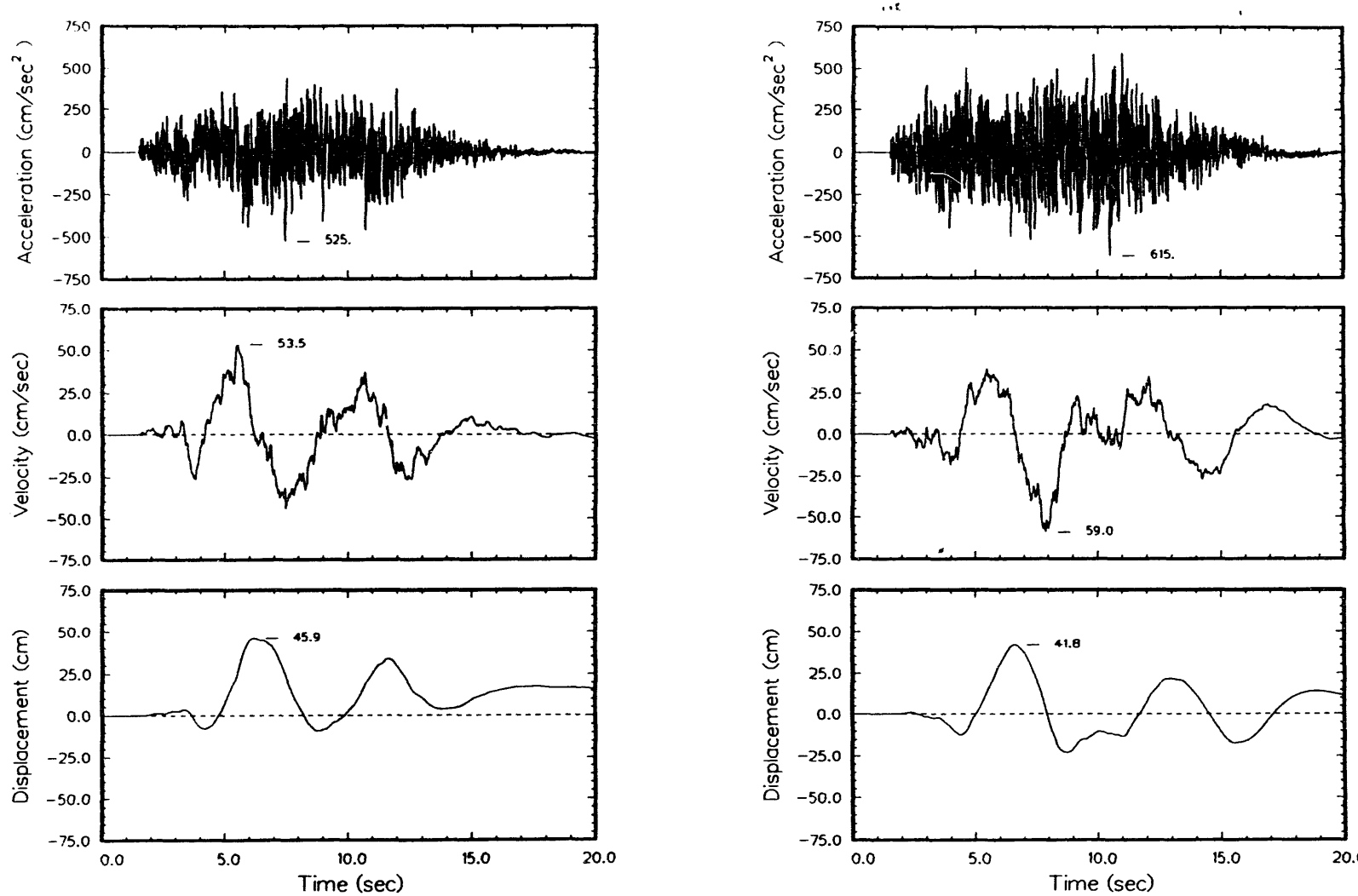

a. Horizontal 1 component

b. Horizontal 2 component

Figure 12. Variations of acceleration, velocity, and displacement for 5000-year design earthquake event

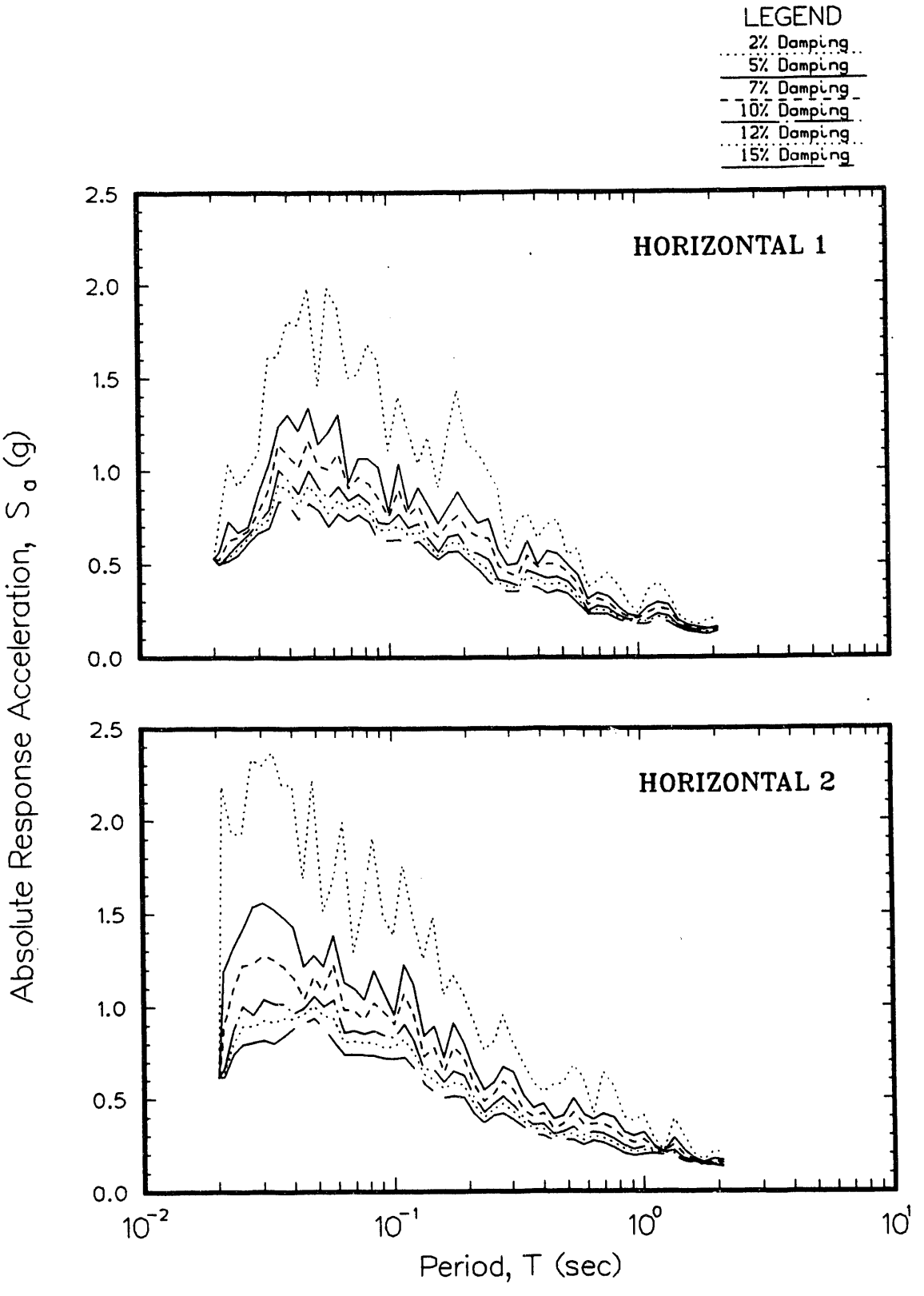

Figure 13. Acceleration (outcrop) response spectra for the 5000-year design earthquake event

PART III: SITE DESCRIPTION AND SOIL COLUMNS

26. PGDP is located about 10 miles west of Paducah, in McCracken County, Kentucky, about 4 miles south of the Ohio River and about 3 miles south of the Ohio River Valley. This area is at the northern boundary of the Coastal Plain Province and the plant is situated on an upland surface that was graded during construction in the early 1950's to between el 370 and 380 MSL.+ (ERCE 1990b) The region around the plant is relatively flat with some upland erosion from nearby streams.

27. An attempt was made at the initiation of this study to obtain information from investigations conducted by USACE in the 1950's at PGDP for original construction of the plant. Despite considerable effort, this information was not found. Therefore, only recently-obtained information was involved.

Site Geology

28. Soil deposits at PGDP are part of the Mississippi Embayment which consists of Cretaceous-age (pre-Tertiary) to Pleistocene-age deposits. The Mississippi Embayment has undergone several cycles of uplifting with consequent erosion and downwarping with consequent deposition. Tertiary-age deposits were placed in marine environments. Pleistocene-age continental deposits were deposited in fresh-water environments on erosional surfaces of Tertiary-age deposits. "These deposits may represent part of a large alluvial fan, and may consist partly of reworked glacial outwash." (ERCE 1990b) The results of consolidation tests were not available to determine the degree of overconsolidation of foundation materials. Based on the history of deposition and erosion, however, soil deposits at PGDP are expected to be normally consolidated or possibly slightly overconsolidated.

29. Soil deposits can be generally described as consisting of a surficial veneer of loess, alluvial continental deposits that consist of gravel, sand, silt and clay overlying Tertiary-age deposits of predominantly clay interbedded with sands and silts, and occasionally a "rubble zone." Fill is expected at the ground surface in isolated locations. Hard limestone

---

+ Mean Sea Level

underlies the entire site. The soil deposits and limestone dip gently downward to the south (ERCE 1990b). An illustrated cross section showing the primary soil deposits along a line projected north-south through the plant area is shown in Figure 14. This figure is not to scale, but it generally shows the distribution of materials along the profile. Brief descriptions of the soil deposits and bedrock are presented below.

Fill

30. Fill was encountered in the upper five feet at Site 2. The fill material is essentially a silty clay with limestone fragments (ERCE 1990b). For this analysis, this material was generally lumped together with loess.

Loess deposits

31. Wind-blown loess deposits cover nearly the entire fenced area of PGDP. These deposits are of Pleistocene age and vary in thickness from 15 to 40 ft (ERCE 1990b). At the four sites used for site response analysis, the thickness only ranged from 10 to 20 ft. The loess generally classifies as a silty clay (CL) with some CL-ML material. The liquid limits and plasticity indices range from 22 to 35 and 4 to 14, respectively; moist unit weights range from 120 to 124 pcf. The range in Standard Penetration Test (SPT) N-values is 5 to 26 with an average of 11 blows per foot indicating a firm to very stiff consistency.

Continental deposits

32. Continental deposits appear to underlie the entire area around PGDP. These alluvial deposits are of Pleistocene age (possibly pre-Pleistocene); they vary in thickness from 20 ft at Site 1 to 93 ft at Sites 3 and 4 and 95 ft at Site 2, and consist of low plasticity clays and silts, silty and clayey sands, and gravels. The liquid limits and plasticity indices range from 14 to 40 and non-plastic to 20, respectively; moist unit weights range from 97 to 136 pcf. The range in SPT N-values is 4 blows per foot to refusal with an average of about 45 blows per foot confirming that there is a wide variation in material densities and consistencies.

Tertiary-age deposits

33. Three primary formations of Tertiary-age exist in the area of the PGDP: the Clayton, McNairy, and Porter's Creek. The Clayton and McNairy Formations are combined for engineering purposes of this study because the materials are very similar. The Porter's Creek and Clayton-McNairy Formations are described separately below.

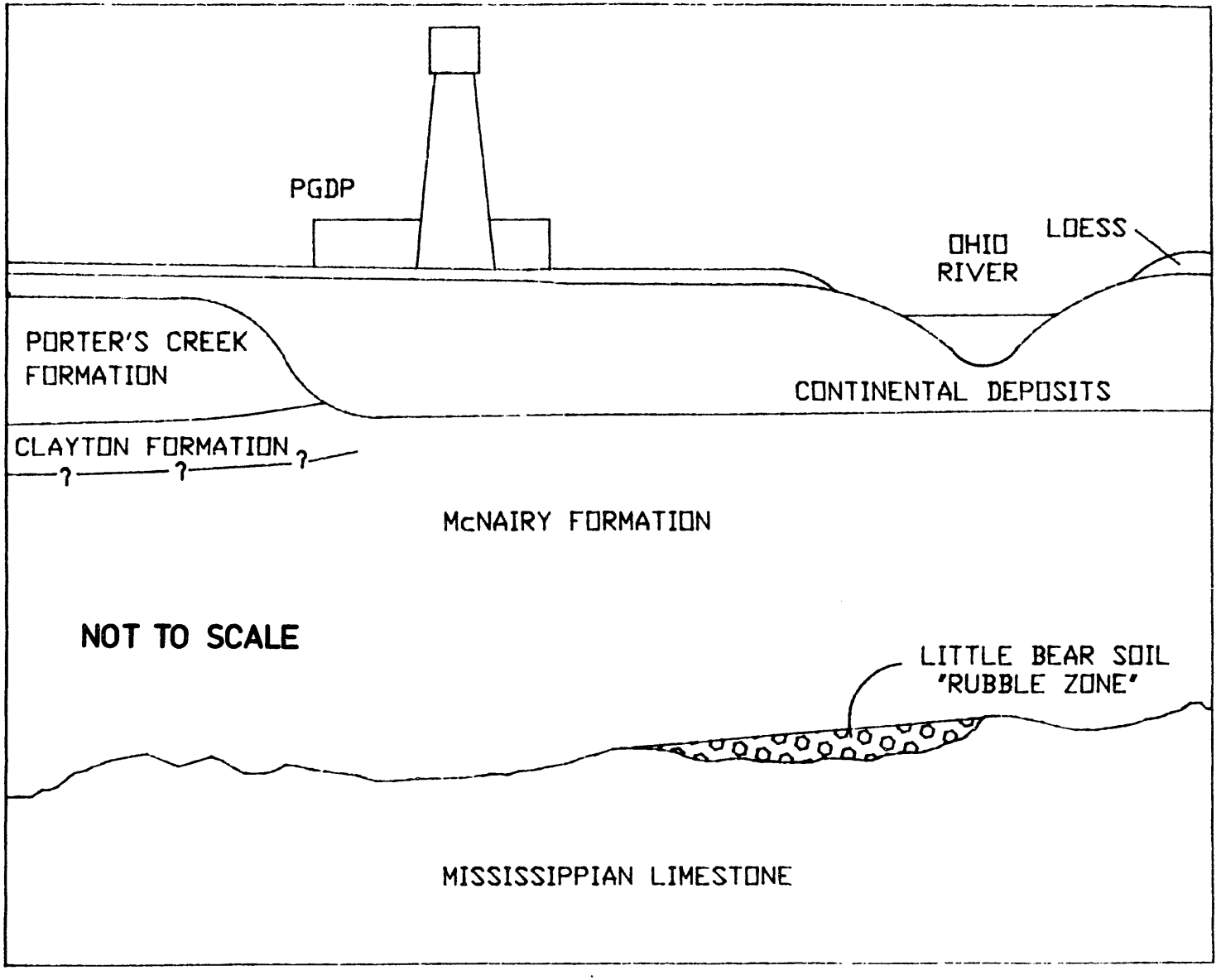

Figure 14. Illustrated cross section through PGDP and Ohio River Valley looking west (adapted from ERCE 1990b)

34. Porter's Creek Formation. The Porter's Creek Formation was encountered at Site 1. The thickness of the deposits within this formation is 84 ft. These materials are micaceous silts and clays with intervals of fine sand, in part glauconitic (ERCE 1990b). The plasticity of these deposits is high and the Atterberg Limits plot well below the "A-line." The liquid limits and plasticity indices range from 88 to 106 and 11 to 25, respectively; moist unit weights were not measured. The range in SPT N-values is 43 to 170 blows per foot with an average of 92 blows indicating a hard to very hard soil consistency.

35. Clayton-McNairy Formation. The Clayton-McNairy Formation was encountered at all four sites beneath Continental Deposits (at Sites 2, 3, and 4) or Porter's Creek Clay (at Site 1). These materials consist of interbedded clay, silt, and fine sand. The thickness of these deposits ranged from 210 to 225 ft at the four sites. The liquid limits and plasticity indices of these materials range from 22 to 43 and non-plastic to 18, respectively; moist unit weights were not measured. The range in SPT N-values is 45 blows per foot to refusal with more than half of the N-values being greater than 100 indicating a hard to very hard soil consistency.

Little Bear Soil

36. Little Bear Soil (rubble zone) was apparently encountered at Site 3 at depths between 334 and 364 ft but not at any of the other three sites. This deposit is believed to generally consist of silty clay with chert fragments and limonite nodules (ERCE 1990b). This material is described from the drilling log as "Probably siliceous limestone and chert fragments (rubble zone)." An SPT sampler could not penetrate material in this zone.

Bedrock

37. Bedrock beneath the plant area at PGDP generally consists of limestone of Mississippian Age, presumably of the Warsaw Formation (Martin Marietta Energy Systems, Inc. 1991b). The limestone tends to be moderately hard to hard with a relatively high shear modulus. Two borings for this study fully penetrated the soils (at Sites 3 and 4) and were extended 5 to 35 ft, respectively, into limestone using a roller bit.

38. Previous investigations by others for major projects in the region on similar types of bedrock provided additional insight into the characteristics of the limestone, particularly on representative shear wave velocities. These previous investigations were for the Bellefonte, Browns

Ferry, and Watts Bar Nuclear Power Plants and the Tennessee Valley Authority (TVA) Yellow Creek Project.

Individual Soil Columns

39. A "soil column" is a one-dimensional idealization of a layered soil deposit. This representation assumes that the soil layers and surface of the deposit are horizontal and that the material properties do not vary over the thickness of any one layer. The primary components of a soil column are: geometry (number of layers and thickness of each layer), geotechnical engineering data, and seismic geophysical data. General descriptions of each of these categories are provided in the following sections.

40. Four individual soil columns were derived from recent drilling and geotechnical engineering investigations (ERCE 1990a) and geophysical measurements (Automated Science Group, Inc. 1991) performed at general locations shown in Figure 2 (ERCE 1990a). Seismic velocities were assimilated by Staub, Wang, and Selfridge (1991). A summary of geotechnical tests and shear wave velocity measurements made at each of the four sites are shown in Figures 15 through 18.

41. All four of the sites are located outside the fenced boundary of PGDP and are separated by great distances. Site 2 is the closest to a large, important building, about 1,500 ft from building C-337. Site 1 is 2,000 ft from building C-333 and Site 3 is 4,000 ft from building C-720. Site 3 is located near the edge of the upland surface where the cooling water pipes emerge and is about 11,700 ft from buildings C-335 and C-337. The distances between each pair of sites are listed in Table 4. Coordinates and surface elevations for all borings drilled at each site are presented in Appendix A.

42. The four idealized soil columns developed by ERCE (1990a) are shown in Figures 19 through 22. Minor modifications to the original soil columns were made by WES by combining some adjacent layers with similar material types and shear wave velocities. Changes in material types are designated with solid horizontal line segments across the column whereas changes in parameters for the same material type are designated with a dashed horizontal line segment. Specifics about each component are described below.

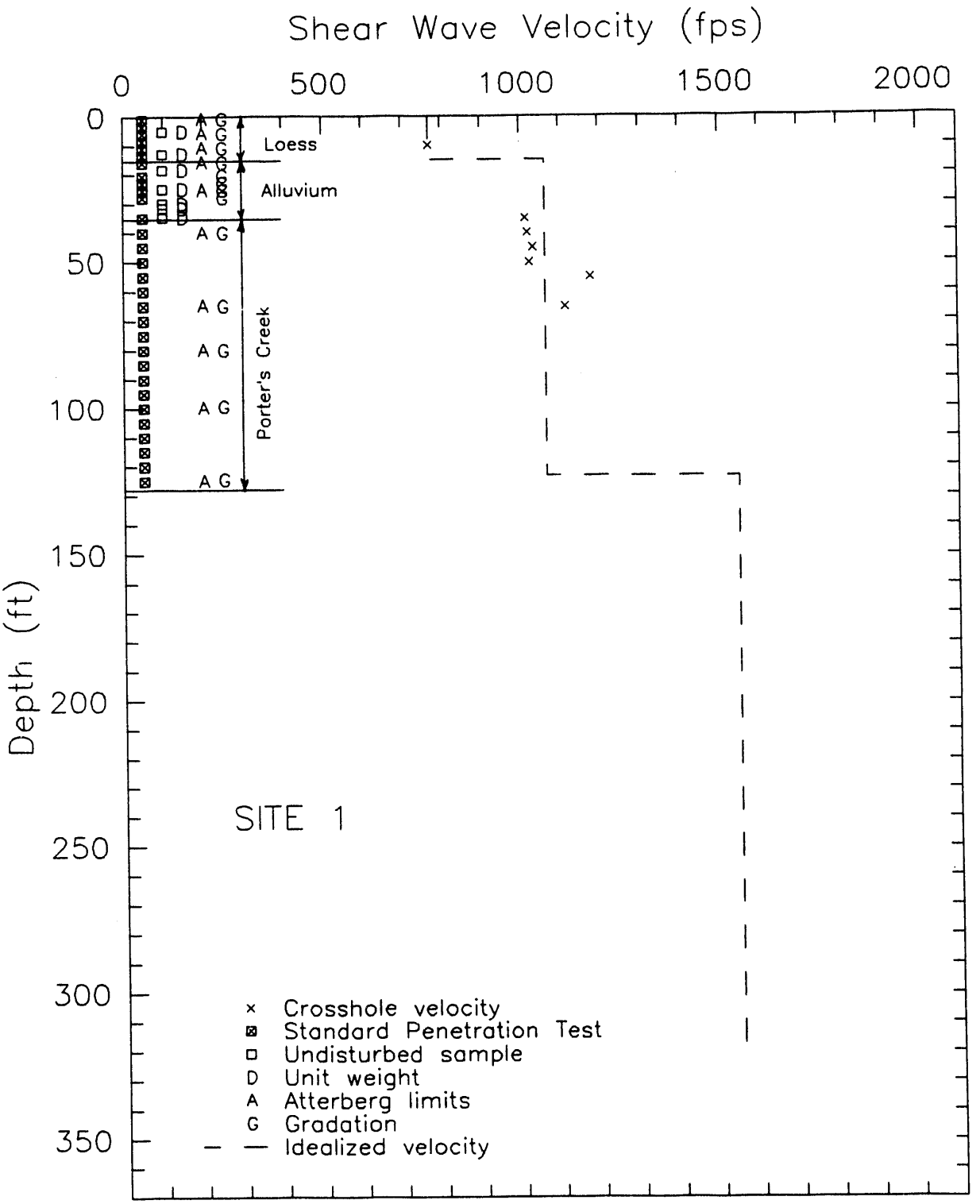

Figure 15. Depths of geotechnical testing and results of shear wave velocity measurements at Site 1

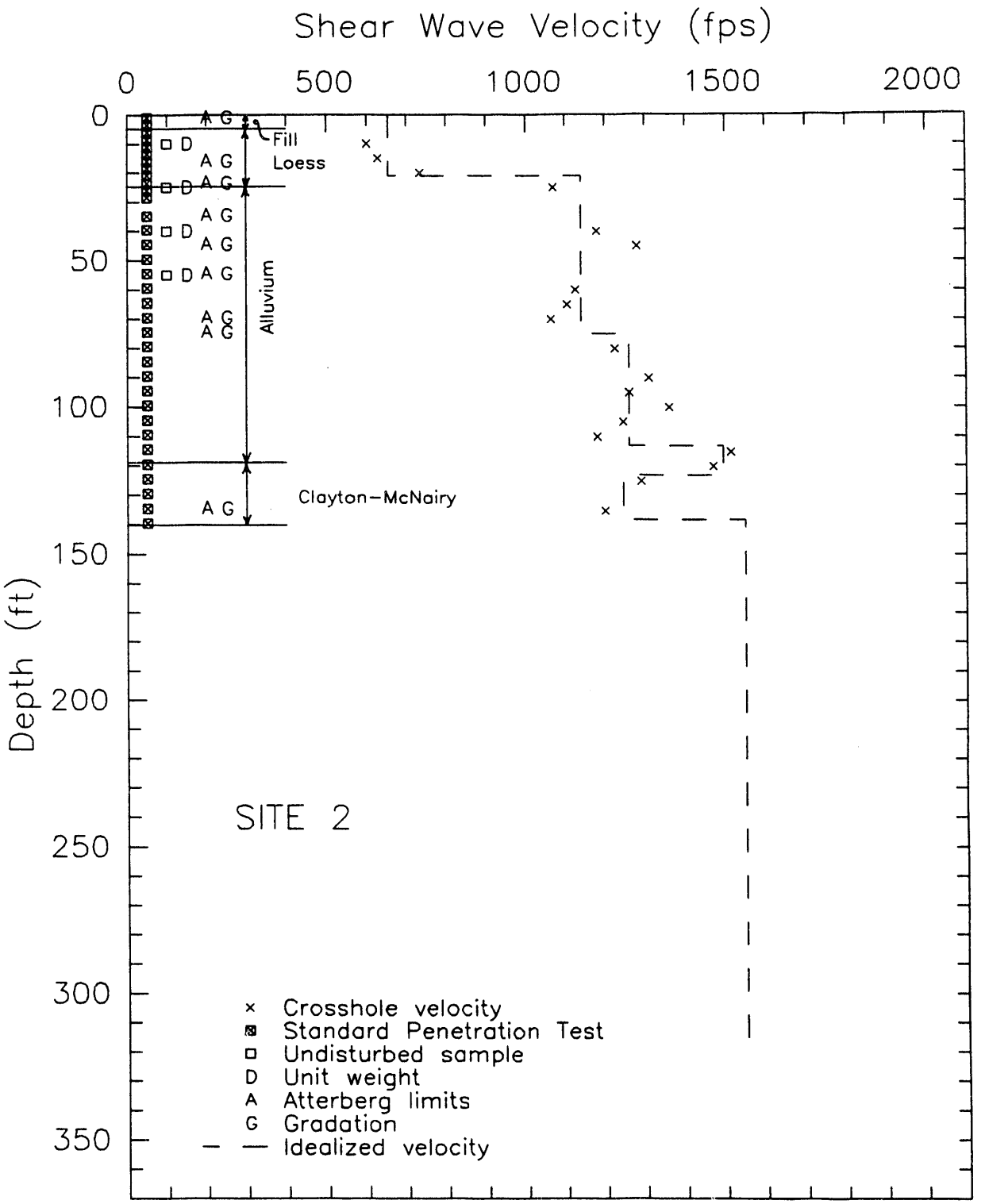

Figure 16. Depths of geotechnical testing and results of shear wave velocity measurements at Site 2

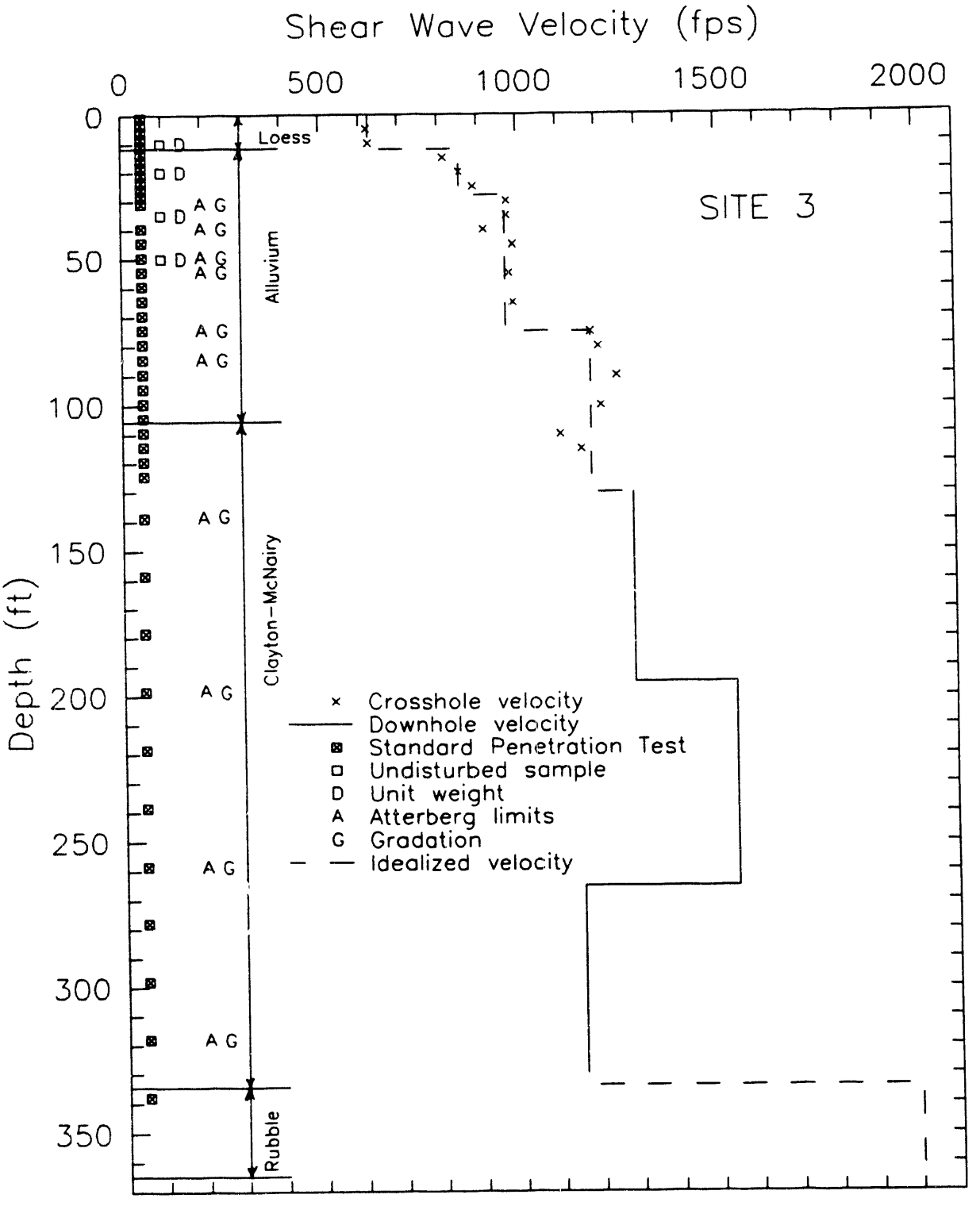

Figure 17. Depths of geotechnical testing and results of shear wave velocity measurements at Site 3

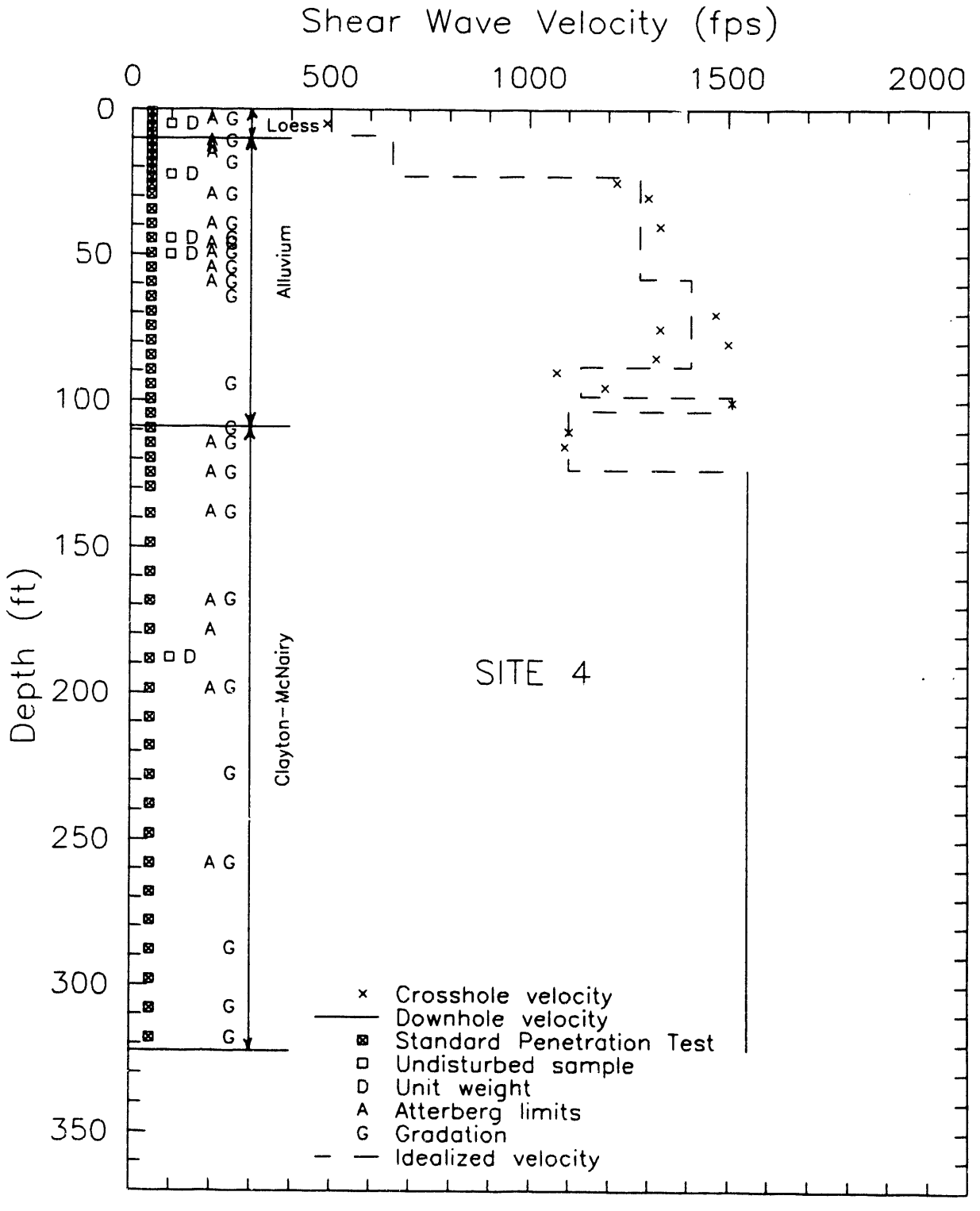

Figure 18. Depths of geotechnical testing and results of shear wave velocity measurements at Site 4

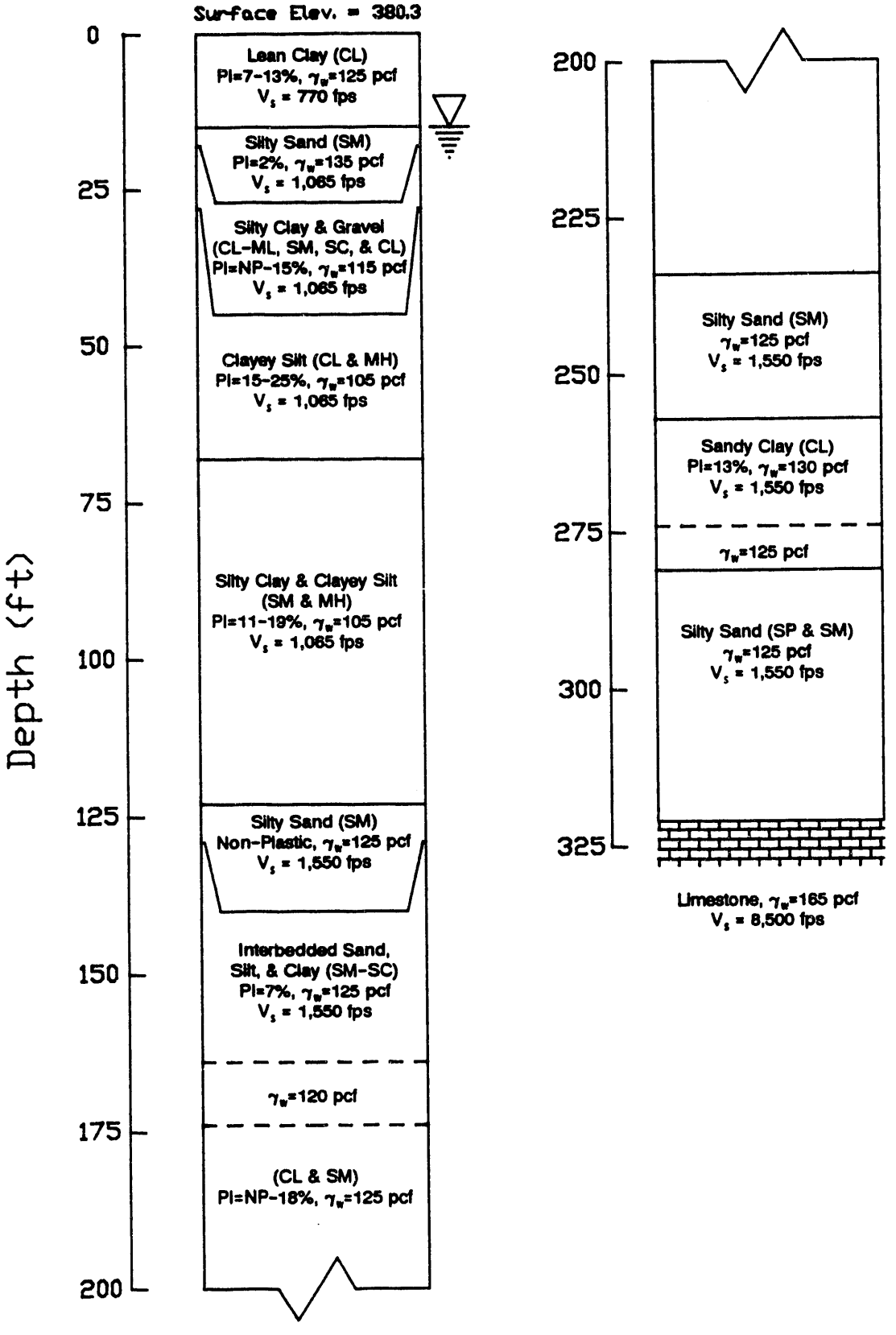

Figure 19. Soil column for Site 1

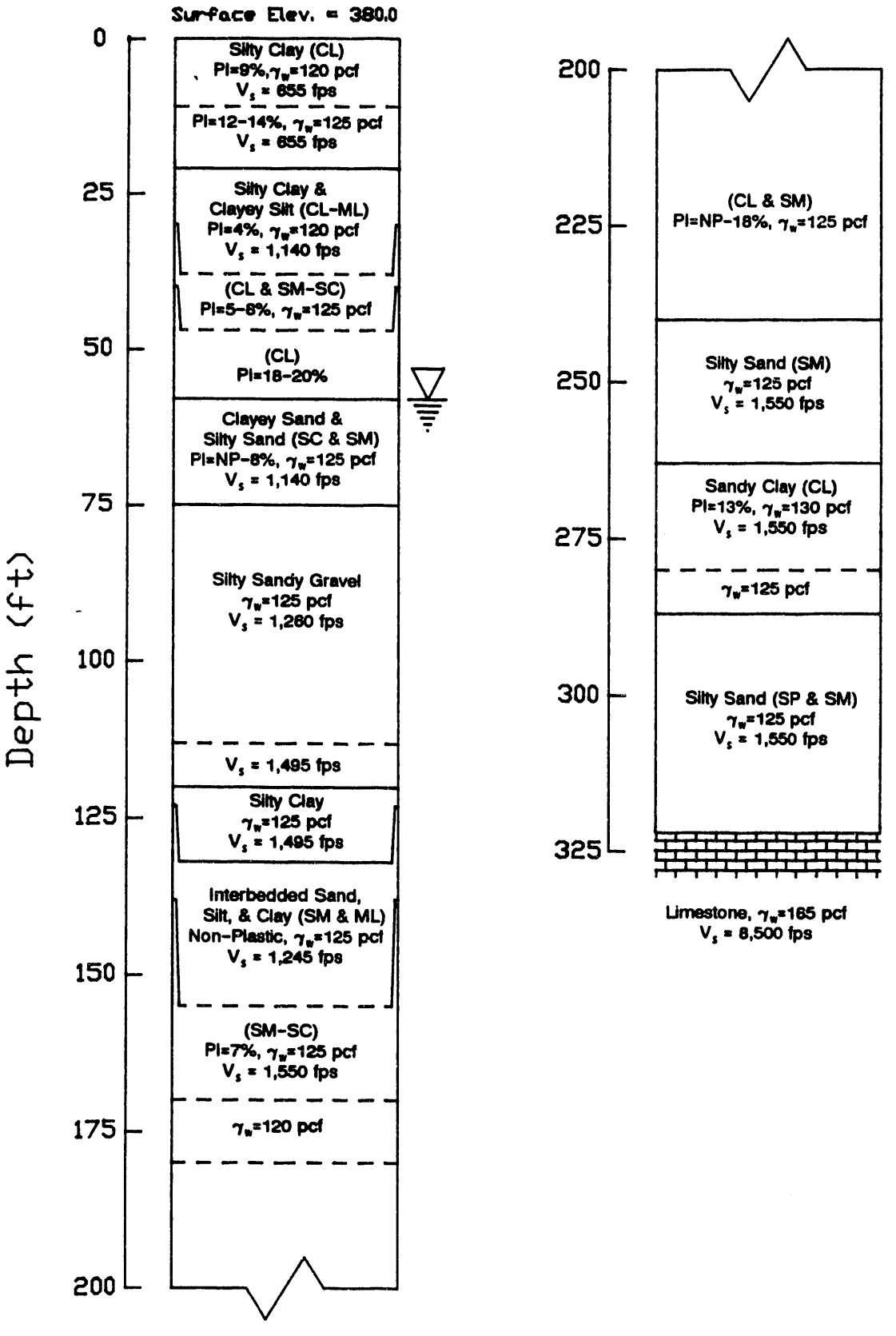

Figure 20. Soil column for Site 2

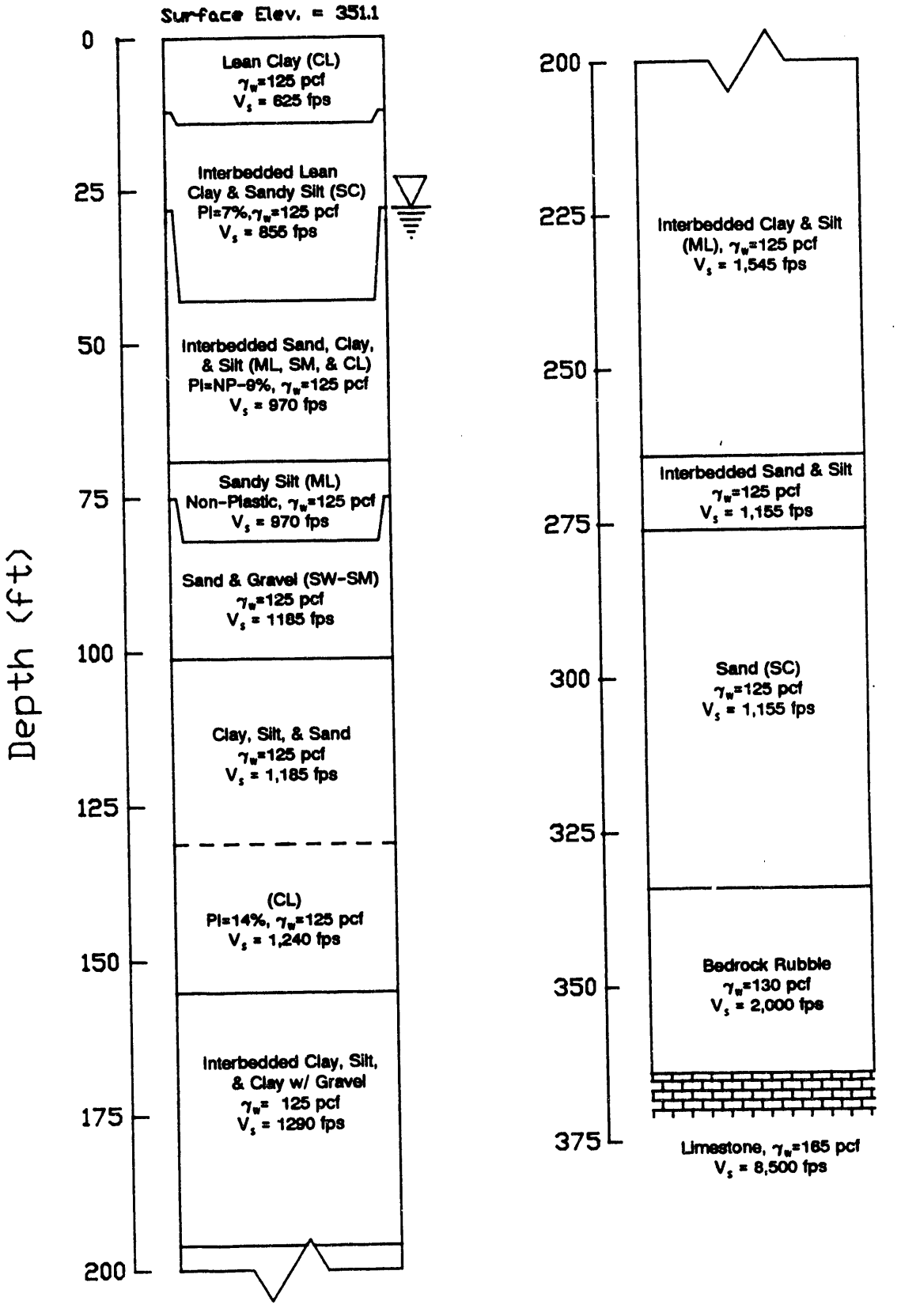

Figure 21. Soil column for Site 3

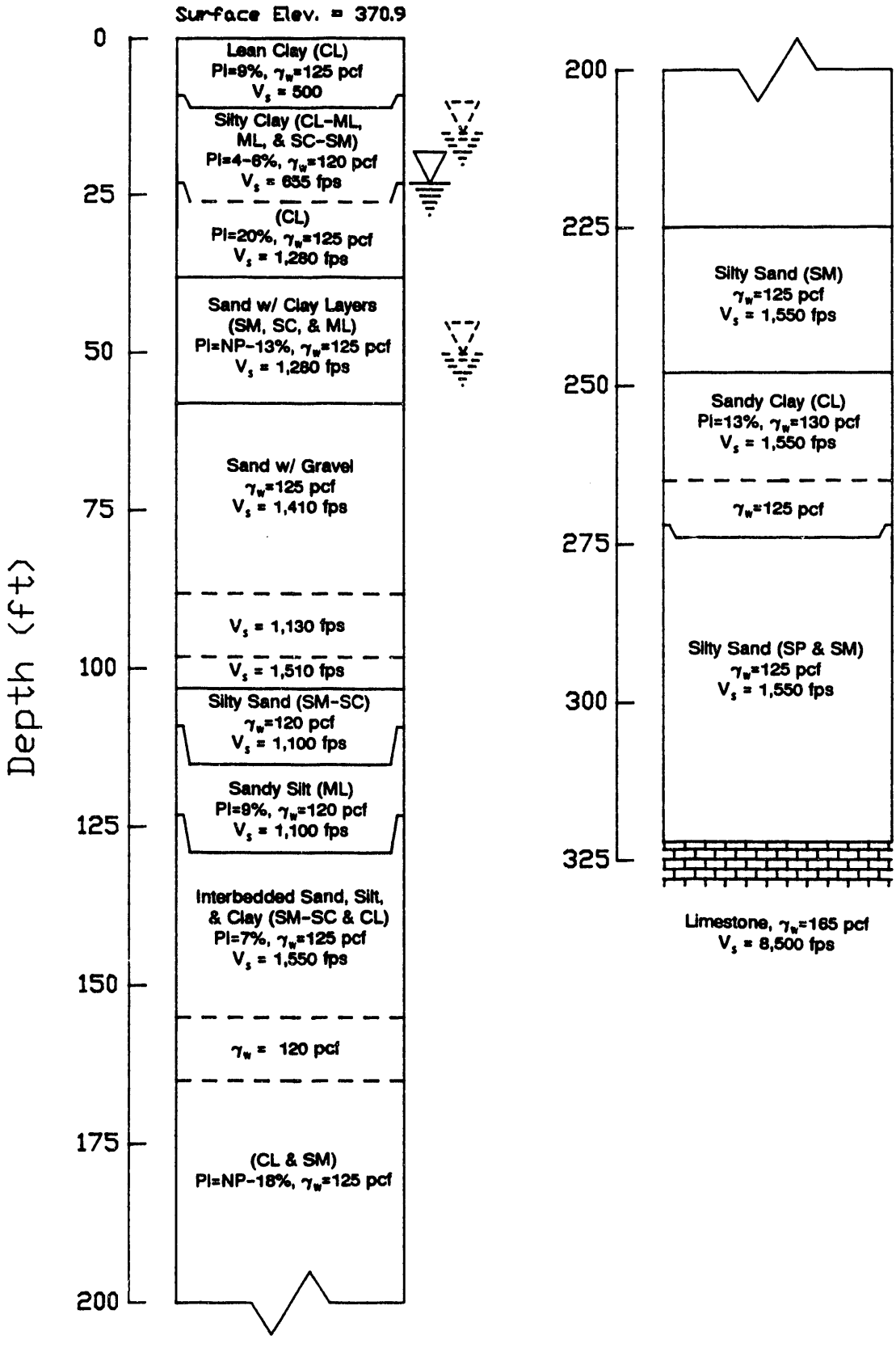

Figure 22. Soil column for Site 4

Table 4

Distances Between Sites

Site	Distance (ft)		
	Site 2	Site 3	Site 4
1	7,100	18,100	6,900
2	-	11,900	5,500
3	-	-	13,600

Geometry

43. Three or four boreholes were drilled at each of the four sites. At Sites 1 and 2, three boreholes were drilled to depths ranging from 70 to 125 ft. Boreholes were not extended to limestone bedrock at either of these sites. At Sites 3 and 4, four boreholes were drilled, three to depths of about 125 ft and the last terminated in bedrock (encountered at depths of 364 and 322 ft, respectively).

44. Soil columns for site response analysis should extend to sound bedrock. It was desirable to include information from all four sites investigated at PGDP for the site response study even though boreholes were extended to bedrock at only two sites. Therefore, Martin Marietta Energy Systems, Inc., through ERCE (1990a), interpreted soil column parameters at depth for Sites 1 and 2 based on available geologic, geophysical, and seismologic data at PGDP to allow the analysis of four (semi-) independent soil columns.

45. Soil layers within a soil column represent depths at which significant changes in material occur. This includes soil classification and material properties. The number of soil layers used for PGDP varied between 12 for Site 3 and 17 for Site 2 as shown in Figures 19 through 22.

Geotechnical engineering data

46. Geotechnical engineering data for this study refer to gradation and plasticity index (PI), the unit weights (densities), and the variations of shear modulus and damping ratio with shear strain. One of the three "shallow" holes was used as the primary source of geotechnical data at each site. Geotechnical data was also obtained from the two "deep" holes at Site 3 and

Site 4. SPT's were generally performed at 2.5-ft depth intervals in the upper strata and 5-ft intervals in continental deposits. The depth to the phreatic surface was not of importance for the site response analysis (but is for liquefaction and earthquake-induced settlement calculations subsequent to this study).

47. Gradations and Atterberg limits. A number of these tests were performed at each site, particularly in the loess and continental deposits. The gradation and Atterberg limit values were used to classify the soil to determine the appropriate number of layers and the thickness of each layer. The PI was also used to assign appropriate relationships defining the variation of shear modulus and damping ratio with shear strain as described below.

48. Unit weights. The values of unit weight for each layer of the soil columns (ERCE 1990a) were derived from measurements made in the laboratory, interpretations of downhole geophysical measurements (Automated Science Group 1991), and assumptions. All but one unit weight was measured in the laboratory on samples of loess and continental deposits at depths less than 55 ft. Measured values of moist unit weight ranged from 95 to 136 pcf. The unit weight of rock was assumed to be 165 pcf. The range of unit weights for soil column idealizations is 105 to 135 pcf.

49. The report by ERCE (1990a) indicates that some of the unit weights were measured on soil samples obtained with an SPT split-spoon sampler. This practice is not widely accepted in the geotechnical engineering profession so these values were not used for this analysis. Unit weights of samples taken using shelby tube samplers indicate that suggested values for the soil columns are representative.

50. Shear modulus and damping ratio relationships. The geotechnical study at PGDP did not include a site-specific evaluation of the variation of shear modulus and damping ratio with shear strain. Rather, standard relationships published by others were used which typically represent a best-fit of numerous compiled data from investigations conducted throughout the U.S. In the absence of site-specific data, these relationships have proven to work well in most applications for site response analyses. Upper-bound and lower-bound relationships are also considered for some applications as with this study. The results of Atterberg Limit and grain size distribution tests were used to select the best-suited relationships.

51. Nine different modulus degradation relationships and seven different damping ratio relationships were considered. The relationships representing shear modulus included the best-fit for rock (Schnabel 1973), the best-fit for gravel (Seed et al. 1986), the best-fit, upper bound, and lower bound for sand (Seed and Idriss 1970), and the best-fit for four ranges of PI for cohesive soils (Sun, Golesorkhi, and Seed 1988). The curves for soil are shown in Figures 23a and 24a. Relationships representing damping ratio include the best-fit for rock (Schnabel 1973), the best-fit, upper-bound, and lower-bound for cohesionless soils (Seed and Idriss 1970 and Seed et al. 1986), and the best-fit, upper-bound, and lower-bound for cohesive soils (Seed and Idriss 1970). The curves for soil are shown in Figures 23b and 24b. The collection of relationships are shown in Figure 25 and include the recommended cap of 15 percent for damping ratio (Nuclear Regulatory Commission 1989).

52. The initial assignments of standard modulus relationships made for each soil layer are listed in Tables 5 and 6. These assignments are based on soil classification as described above. The dotted horizontal lines in the tables show where contrasts in shear wave velocities exist for the soil columns that will be presented in the next section. Rubble (bottom of column at Site 3) was represented with the best-fit relationship for gravel. Sand and gravel deposits were represented by the lower-bound relationship for sand.

53. The assignment of standard damping ratio relationships was also made based on soil classification. Rubble and cohesionless soils were assigned the best-fit relationship for cohesionless soils. Cohesive soils were assigned the best-fit relationship for cohesive soils. The upper and lower bound damping relationships shown in Figures 23a, 24a, and 25a were only used in the parametric analyses described in Part VI.

54. Effect of confining stress. Confining pressure has been shown to affect the normalized modulus and damping ratio relationships. As the confining stress increases, the normalized modulus and damping ratio relationships shift to the right (larger shear strains required to produce same modulus or damping). At low confining stresses, the relationships shift to the left. For shear modulus, Iwasaki, Tatsuoka, and Takagi (1976) presented data for sands and Stokoe and Lodde (1978) presented data for San Francisco Bay mud. A summary of these findings are shown in Figure 26. Others have shown similar results (e.g., Zen et al. 1978, Geotechnical Engineers, Inc. 1991). In general, the effect of confining pressure on

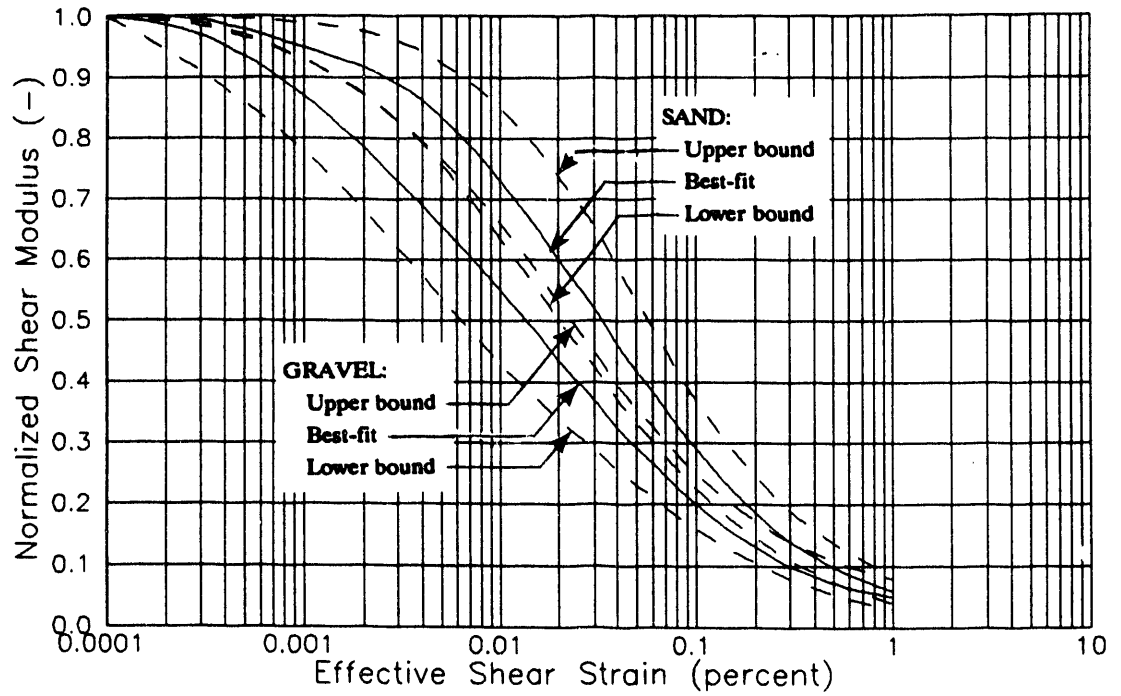

a. Shear modulus

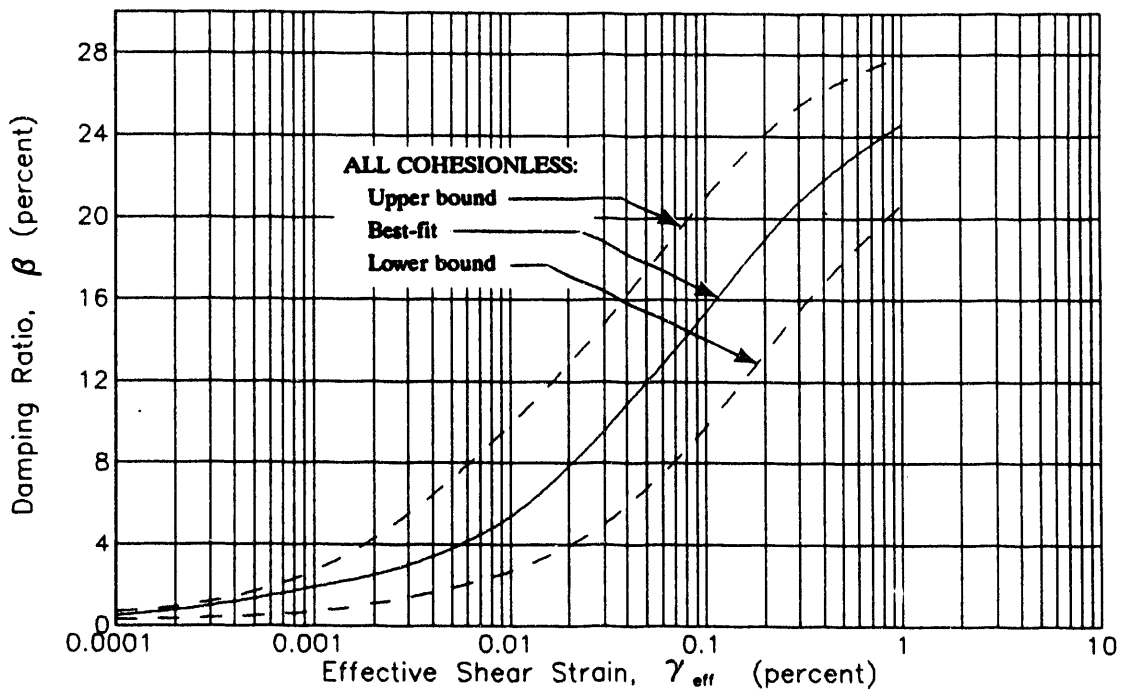

b. Damping ratio

Figure 23. Standardized relationships between shear modulus and damping ratio for cohesionless soils

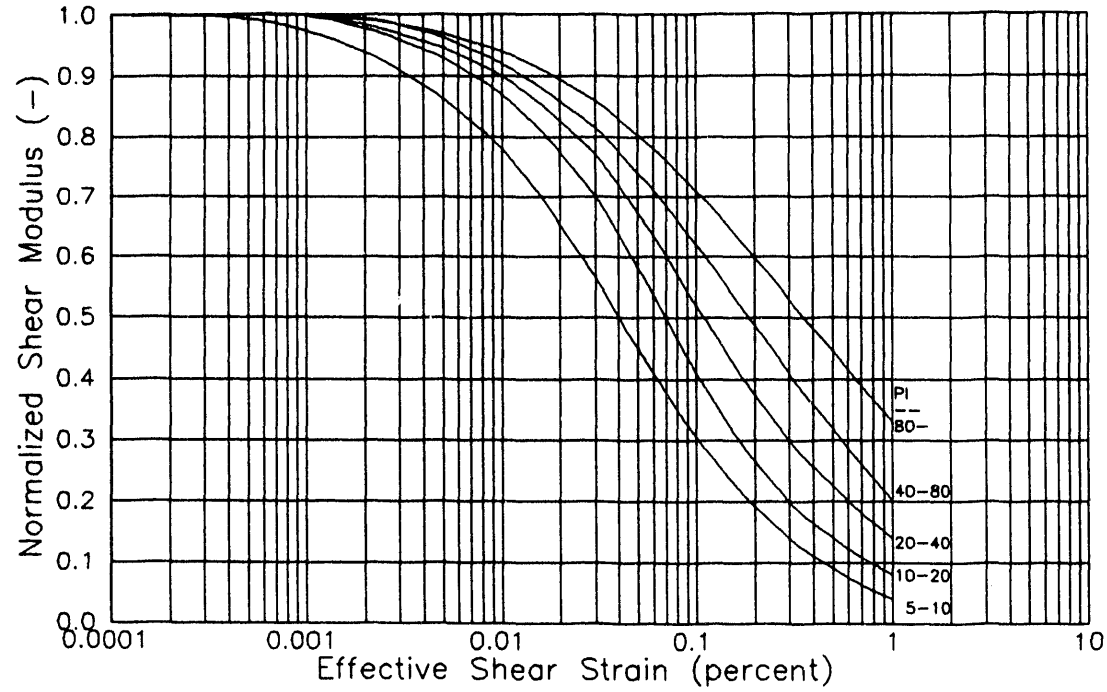

a. Shear modulus

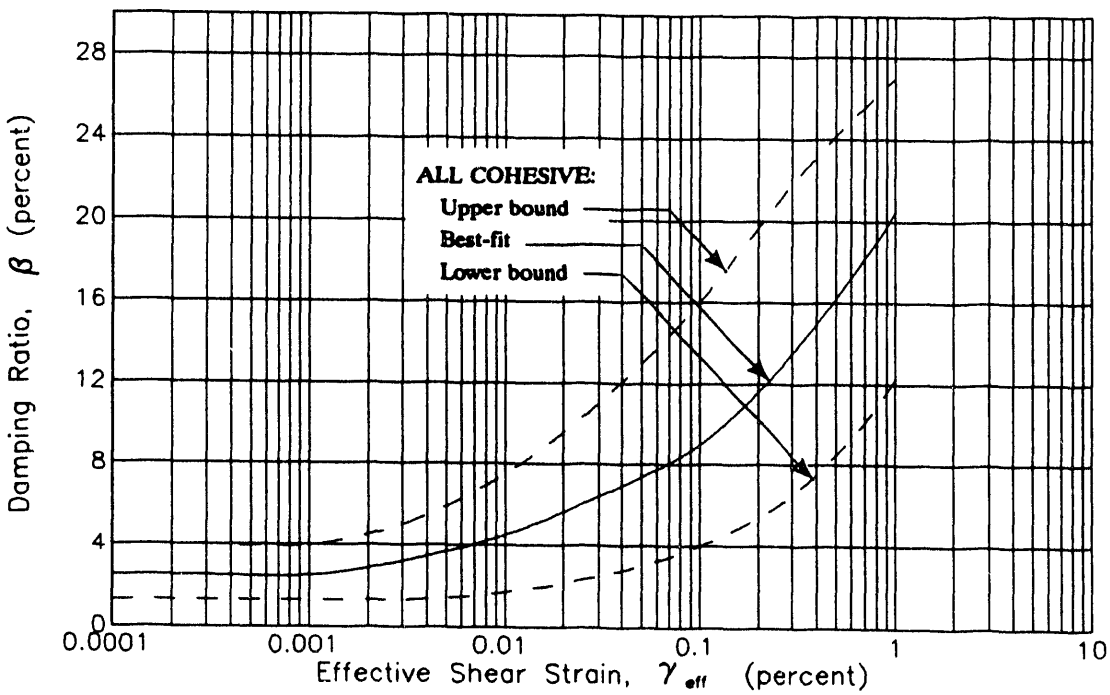

b. Damping ratio

Figure 24. Standardized relationships between shear modulus and damping ratio for cohesive soils (Sun, Golesorkhi, and Seed 1988)

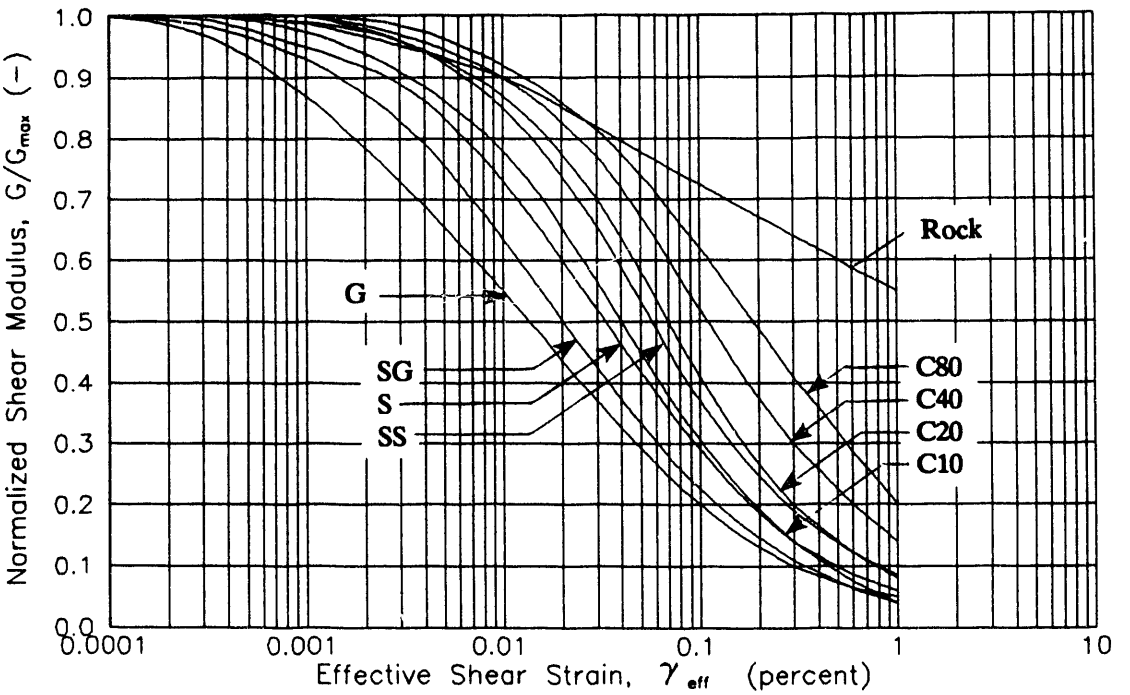

a. Shear modulus

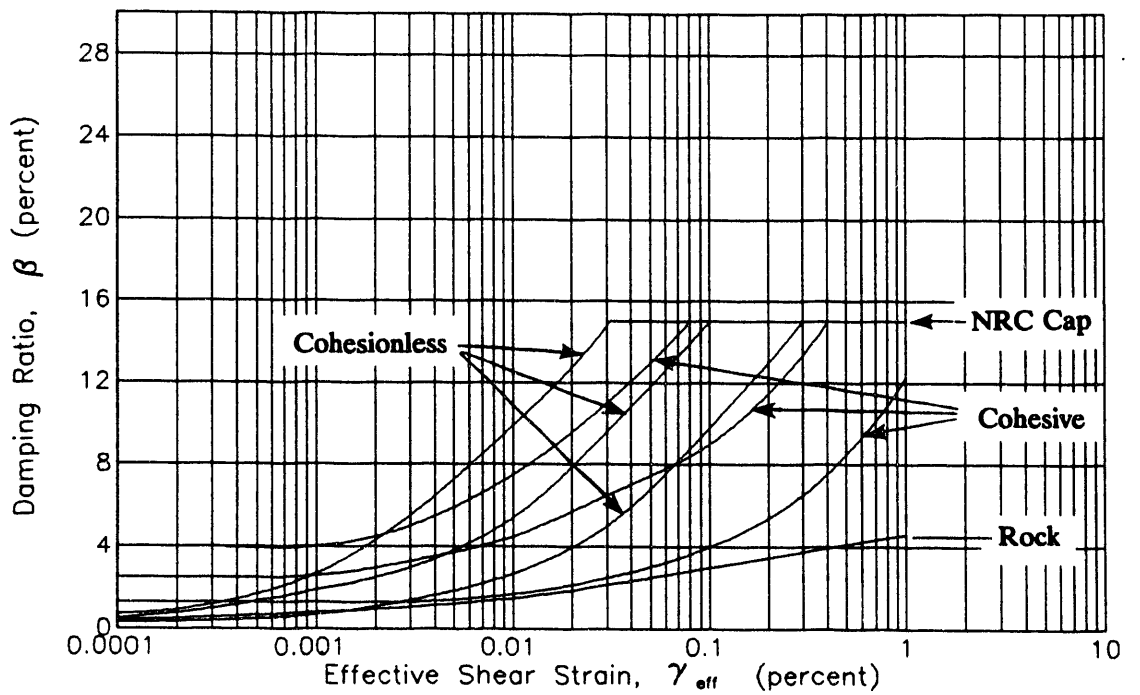

b. Damping ratio

Figure 25. Relationships between shear modulus and damping ratio versus shear strain used for this study

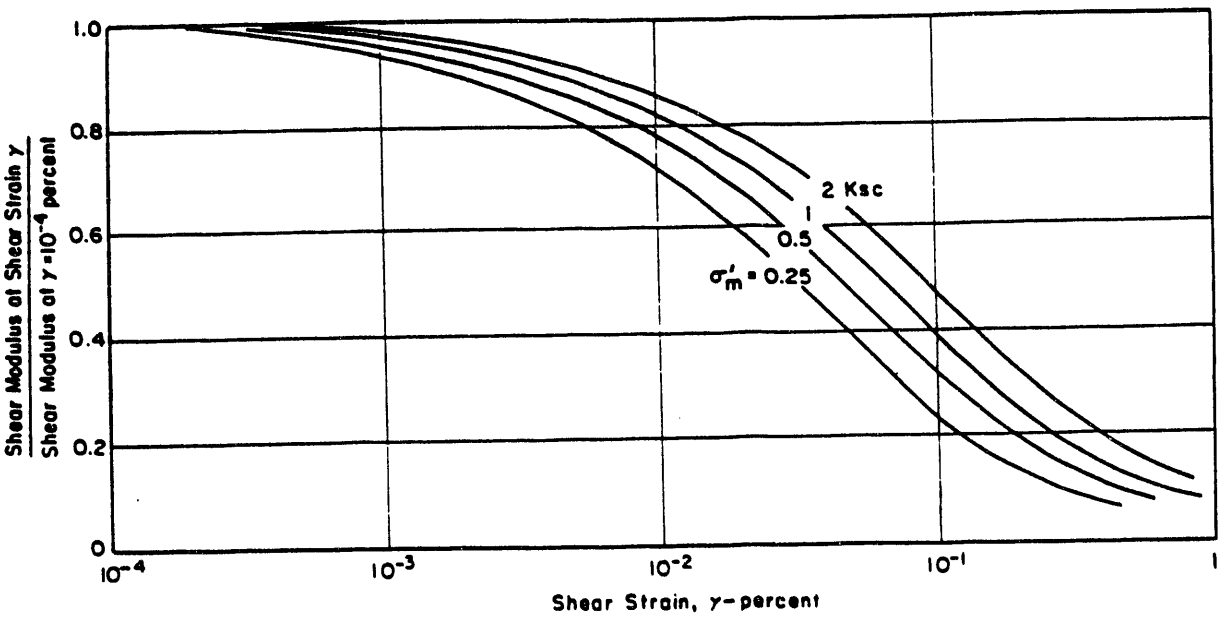

a. Cohesionless soils (Seed et al. 1986 after Iwasaki, Tatsuoka, and Takagi 1976)

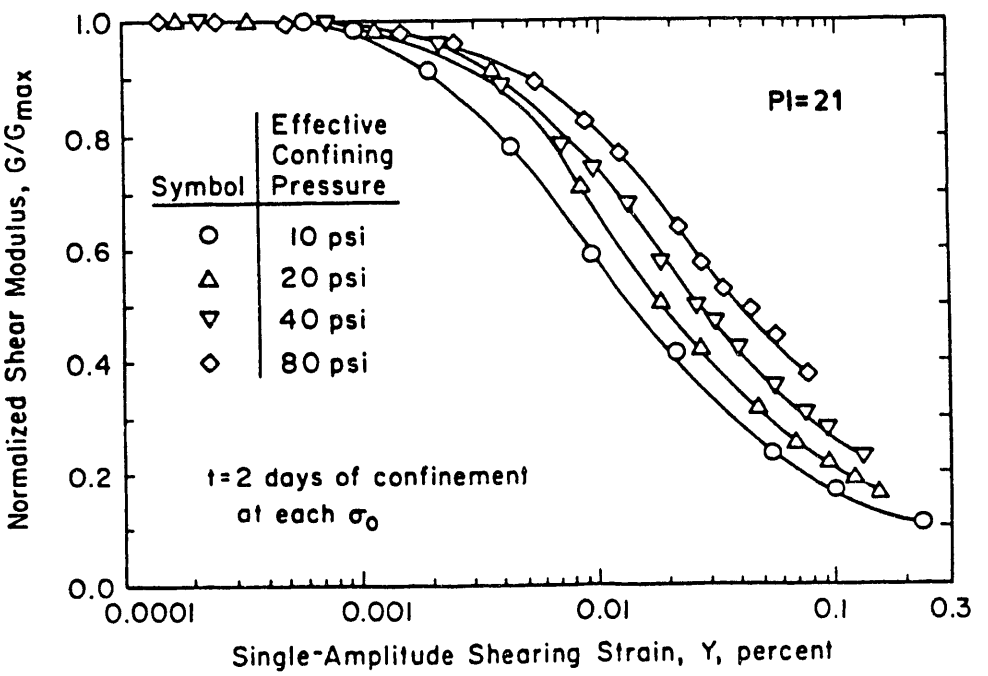

b. San Francisco Bay mud (Stokoe and Lodde 1978)

Figure 26. Effect of confining stress on normalized modulus relationships

modulus relationships increases as plasticity index decreases for cohesive soils; the effect is greatest for cohesionless soils.

Table 5

Shear Modulus Degradation Assignments Based on Soil Classification for Sites 1 and 2

Layer	Site 1		Site 2	
	Thickness (ft)	Classification Best Estimate	Thickness (ft)	Classification Best Estimate
1	15	C10	11	C10
2	3	S	10	C20
3	10	C10	9	C10
4	40	C20	10	"
5	55	"	18	C20
6	6	S	17	S
7	35	C10	38	SG
8	10	"	7	"
9	60	C20	3	C10
10	23	S	15	S
11	17	C20	32	C10
12	7	"	10	"
13	41	S	60	C20
14			23	S
15			17	C20
16			7	"
17			35	S
Total	322		322	

C10: 5 < PI < 10 S: Sand
C20: 10 < PI < 20 SG: Lower-bound sand
C40: 20 < PI < 40 G: Gravel

55. The family of curves shown in Figure 26a indicates that the best-fit relationship for sands (shown in Figure 23a) generally corresponds to a confining stress of 0.5 ksc. The upper-bound relationship for sands generally corresponds to a confining stress of 2.0 ksc. Therefore, sands confined at

stresses greater than 1 ksc may be better represented by the upper-bound sand relationship. To be consistent, sands confined at stresses less than 0.25 ksc would then be represented by the lower-bound sand relationship. This process of selecting an appropriate relationship from the proposed suite shown in Figure 25a can be applied to cohesive soils (although with less impact) and relationships can be extracted for higher stress regimes.

Table 6

Shear Modulus Degradation Assignments Based on Soil Classification for Sites 3 and 4

	Site 3		Site 4	
Layer	Thickness (ft)	Classification Best Estimate	Thickness (ft)	Classification Best Estimate
1	12	C10	9	C10
2	16	"	14	"
3	41	"	15	C20
4	6	"	20	S
5	25	SG	30	SG
6	30	C10	10	"
7	24	C20	5	"
8	41	"	6	S
9	70	C10	14	C10
10	11	S	32	"
11	58	"	10	"
12	30	G	60	C20
13			23	S
14			17	C20
15			7	"
16			50	S
Total	364		322	

C10: 5 < PI < 10 S: Sand
C20: 10 < PI < 20 SG: Lower-bound sand
C40: 20 < PI < 40 G: Gravel

56. The confining stresses likely to exist in situ at PGDP are within the range considered to affect the variation of normalized shear modulus. Therefore, modifications were made to the modulus relationship assignments to account for this influence in accordance with the aforementioned procedure. The stress-adjusted assignments are listed in Table 7.

Table 7

Shear Modulus Degradation Assignments Including Effect of Confining Stress

Layer	Site 1	Site 2	Site 3	Site 4
1	S	S	S	S
2	"	C20	C10	C10
3	C10	C10	"	C20
4	C20	"	"	C10
5	"	C20	S	S
6	SS	SS	C20	SS
7	C20	S	C40	"
8	"	"	"	C20
9	C40	C20	C20	"
10	C10	"	"	"
11	C40	"	"	"
12	"	"	S	C40
13	C10	C40		C10
14		C10		C40
15		C40		"
16		"		C10
17		C10		

C10: 5 < PI < 10
C20: 10 < PI < 20
C40: 20 < PI < 40

S: Sand
SS: Upper-bound sand
G: Gravel

57. The results for damping ratio are less conclusive. This finding does not appear to be applied as often in analyses by the profession. The computer model used to calculate site response did not allow a large

collection of modulus and damping ratio relationships. The large suite of modulus relationships precluded a complementary collection of damping ratio relationships. Therefore, the effect of damping ratio relationships was evaluated through parametric analysis.

Seismic geophysical data

58. Compression and shear wave velocities of materials were measured in situ using crosshole and downhole seismic geophysical techniques. Compression wave velocities were not of interest for this study and are, therefore, not reported. In general, shear wave velocities of loess and continental deposits were measured using the more accurate crosshole technique with the three "shallow" holes at each site. Shear wave velocities of Tertiary deposits were made with downhole measurements in deep holes at Site 3 and at Site 4. An evaluation of geophysical field and data processing procedures used by Automated Sciences Group, Inc. (1991) was conducted by Staub, Wang, and Selfridge (1991) and the results of their study for shear waves is the basis for this presentation.

59. Accepted values of shear wave velocity measured using crosshole and downhole techniques are presented in Figures 15 through 18. At Site 1, only seven values of shear wave velocity to a maximum depth of 65 ft are available from crosshole measurements. At the other three sites, several more values of shear wave velocity are available to greater depths (between 115 and 150 ft). Downhole measurements were made to depths of 334 ft and 322 ft at Site 3 and Site 4, respectively.

60. The shear wave velocities measured in loess range from 500 to 770 fps. Shear wave velocities in alluvium range from 800 to 1,500 fps. Measured shear wave velocities in the Tertiary deposits range between 1,000 and 1,200 fps in the Porter's Creek Formation and range between 1,070 and 1,550 fps in the Clayton-McNairy Formation. One interesting finding at Site 3 was the existence of a significant velocity inversion between depths of 265 and 334 ft. The importance of including this inversion was examined in the parametric analysis presented in Part VI.

61. The shear wave velocity for the limestone bedrock was assumed to be 8,500 fps based on reported velocities from the same formation at power plant projects in the region.++ The other data included calculated shear wave

---

++ Facsimile communications, Martin Marietta Energy Systems, Inc., Oak Ridge, Tennessee, 20 February and 5 March, 1991.

velocities (based on elastic moduli or compression wave measurements) at Browns Ferry of 8,200 fps, Watts Bar of 5,300 to 7,200 fps, and Yellow Creek of 6,900 to 9,700 fps and measured shear wave velocities using crosshole techniques at Bellefonte of 8,300 to 9,300 fps.

62. The idealized profiles of shear wave velocity used for the soil columns (Staub, Wang, and Selfridge 1991) are also plotted as a function of depth in Figures 15 through 18 using a dashed line. The idealized velocities attempt to average crosshole values and correspond to downhole velocities where available. The variation of measured crosshole values about idealized velocities is about ± 15 percent.

63. A comparison of all measured shear wave velocities, corresponding shear moduli, and idealized values are shown in Figure 27. Data from measurements using the crosshole method are available in the upper 135 ft. Data from measurements using the downhole method are available at depths between 123 and 334 ft (very little overlap with crosshole data). A shear wave velocity and unit weight had to be assumed for the rubble zone (below 334 ft). The idealized velocity profiles in the upper 135 ft envelop about 70 percent of the crosshole-measured velocities and appear to be good average representations for the project.

64. The collection of variations of idealized shear wave velocity and corresponding shear modulus with depth are shown in Figure 28. These data indicate that the upper 25 ft (loess) has a consistently low stiffness and that there is a sharp increase in stiffness at the top of the continental deposits which continues to increase slightly with increasing depth. The range in moduli is generally within ± 30 percent of a calculated average at any given depth. The velocity inversion is significant relative to the four idealized profiles.

65. Seismic velocities were reported by Yule and Sharp (1988) for the proposed USACE Olmsted Lock and Dam Project, located at river mile 964.4 of the Ohio River, near Olmsted, Illinois. This site is about 16 miles west of PGDP. Although the alluvial deposits are expected to be different than materials at PGDP, the condition of the older, buried Clayton-McNairy Formation should be similar.

66. The profiles of shear wave velocity measured using crosshole and downhole techniques at both the Illinois bank and Kentucky bank of the Ohio River are presented in Figure 29. The velocities measured in the Clayton-

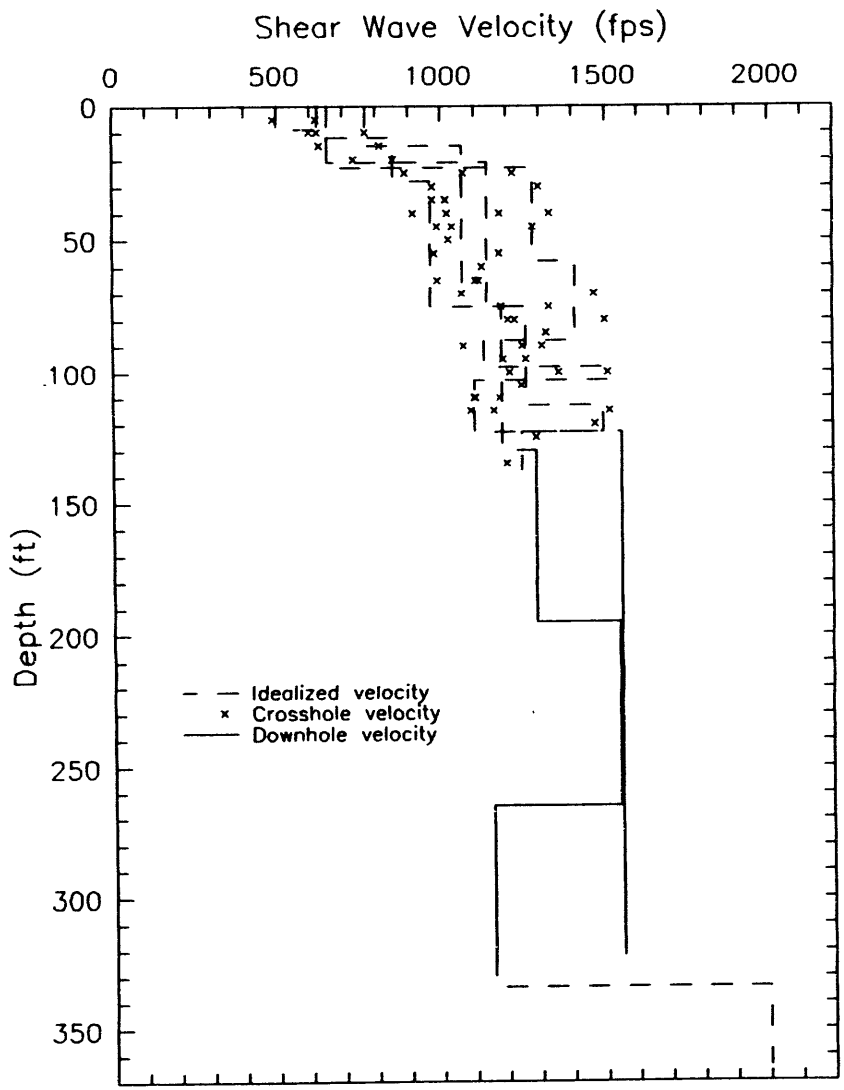

a. **Shear wave velocity**

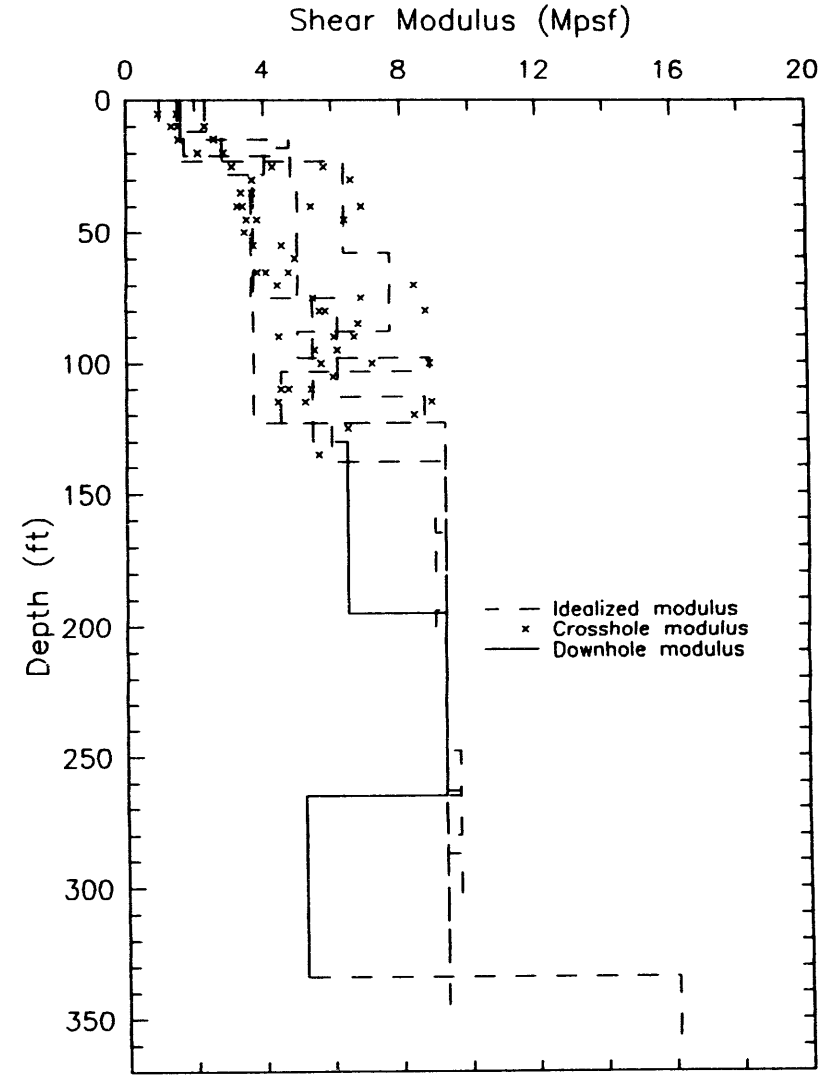

b. **Shear modulus**

Figure 27. Comparison among measured and idealized stiffnesses

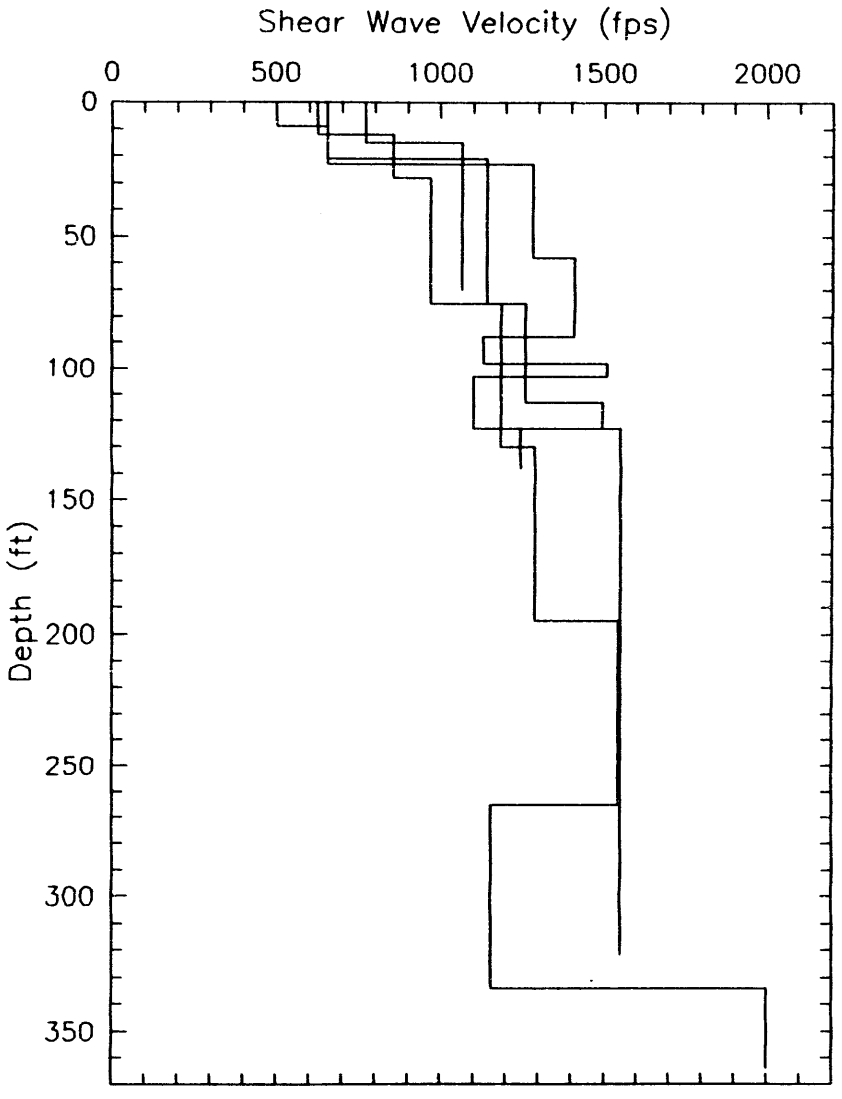

a. **Shear wave velocity**

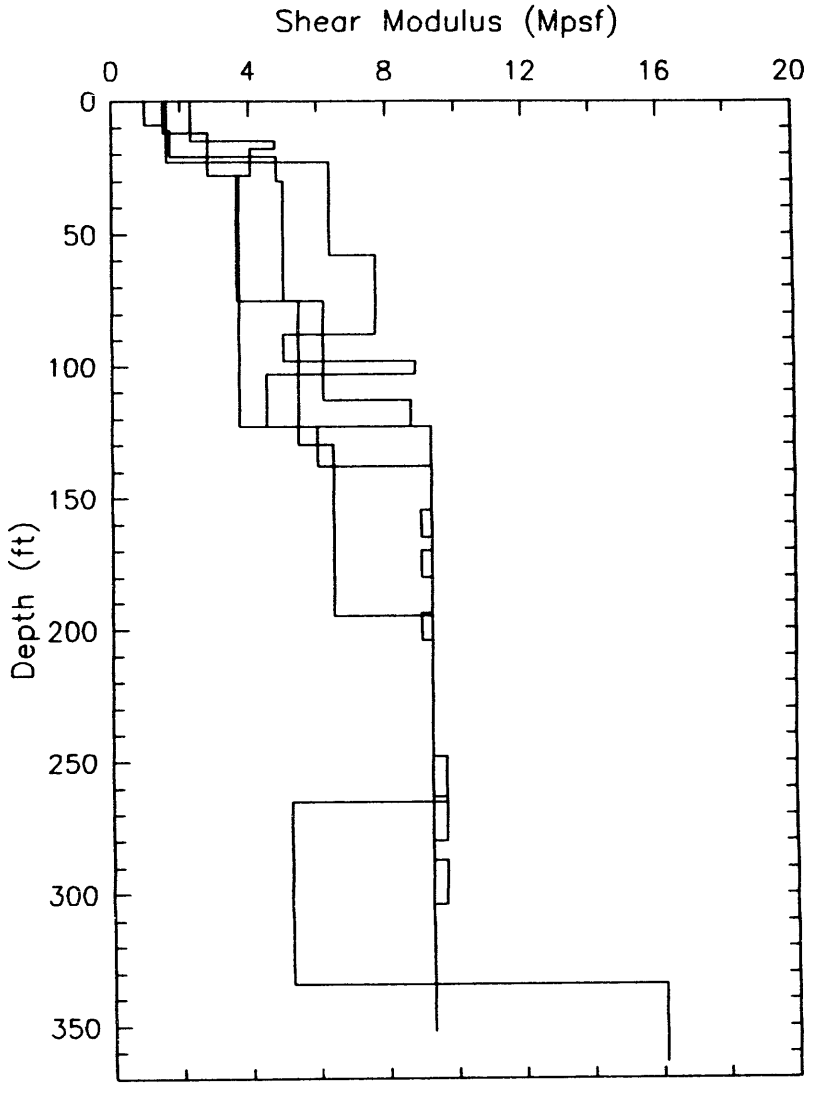

b. **Shear modulus**

Figure 28. Combined profiles of soil stiffness

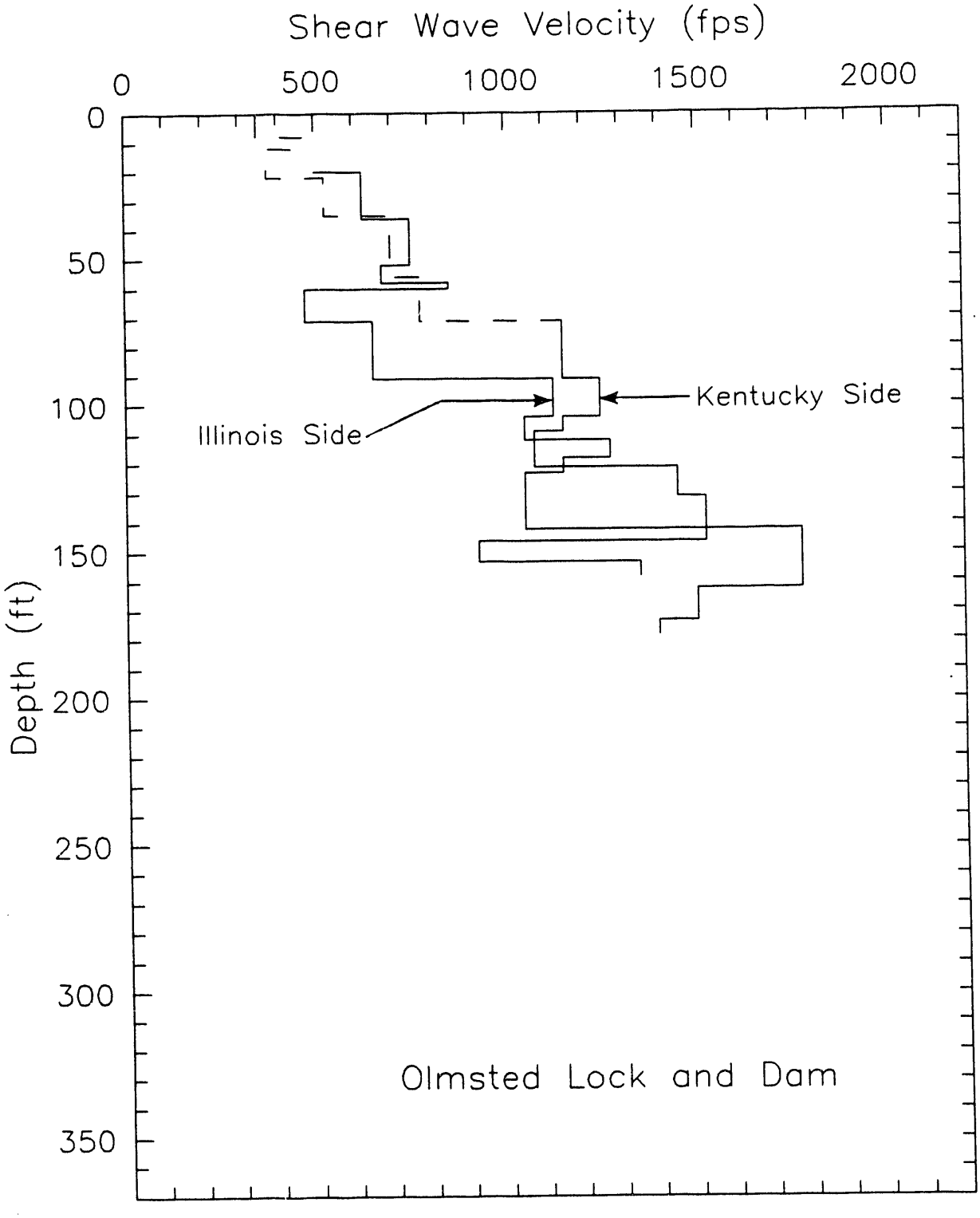

Figure 29. Measured shear wave velocities at proposed Olmsted Lock and Dam Project, Ohio River (Yule and Sharp 1988)

McNairy Formation are shown as solid lines, whereas the dashed lines represent shear wave velocities measured in alluvium. A comparison of the data shown in Figures 28a and 29 shows consistency in the range of velocities for depths between 90 and 180 ft. This similarity suggests that the measured profiles of shear wave velocity at PGDP are representative of the soils present.

Average Soil Column

67. An average column was created to conduct sensitivity studies described in Part VI and shown in Figure 30. An average column is intended to represent the overall site. An average column can be useful to evaluate the sensitivity of the analysis to various inputs. The variations of shear wave velocity and shear modulus for the average column are shown in Figure 31 along with the idealized profiles for the individual sites.

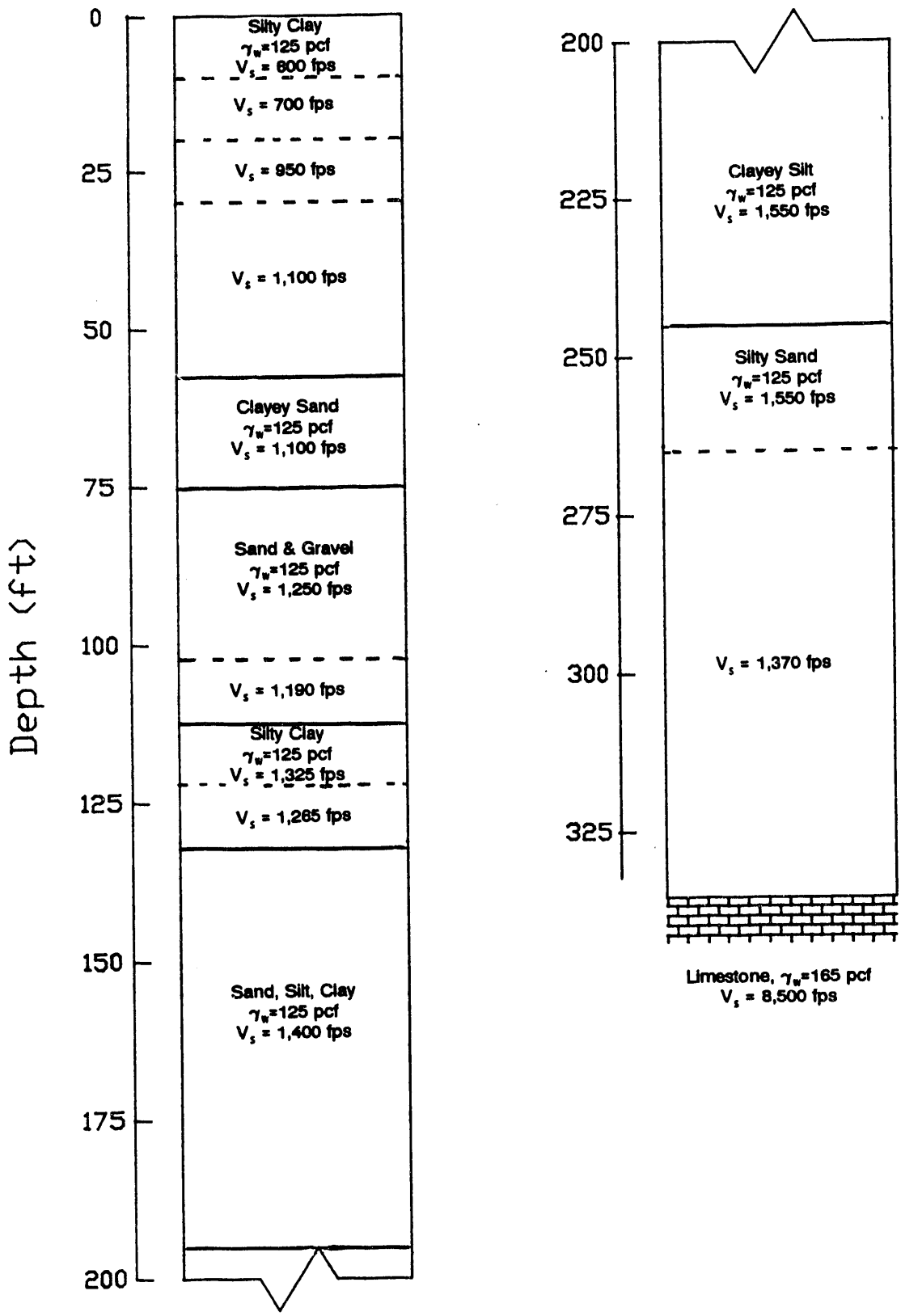

Figure 30. Average soil column

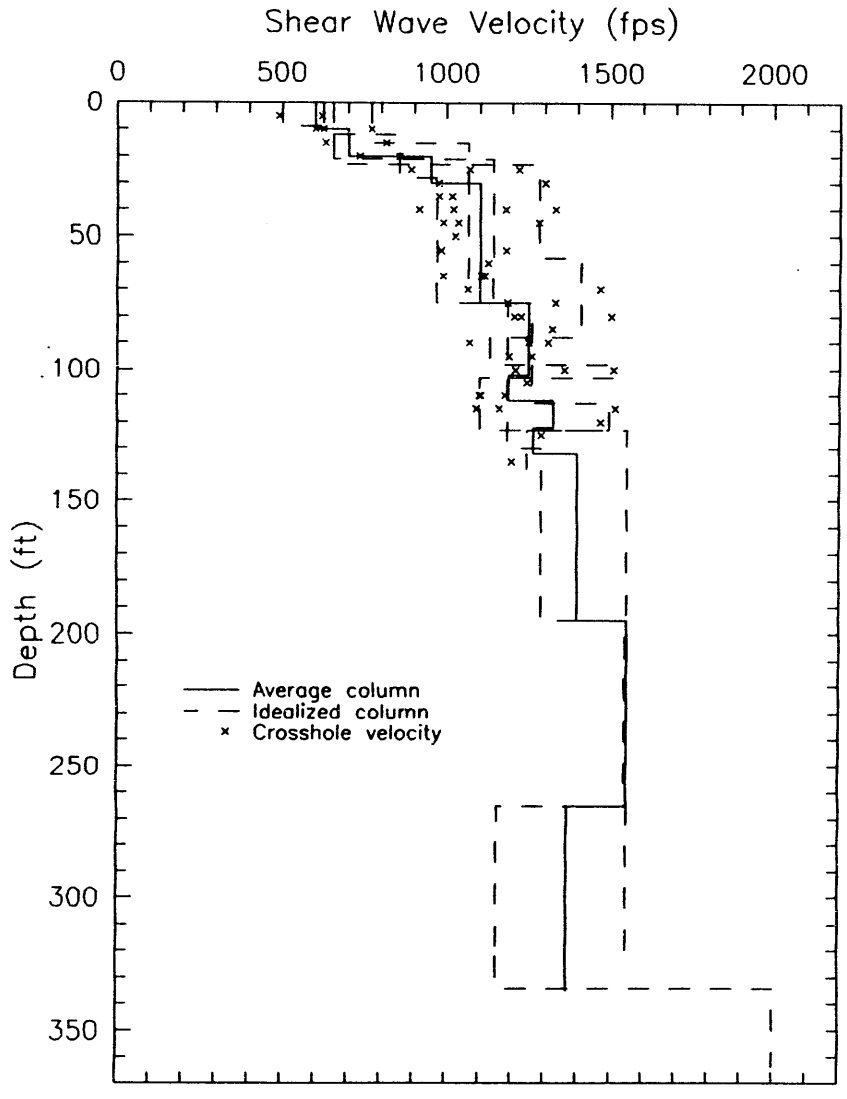

a. **Shear wave velocity**

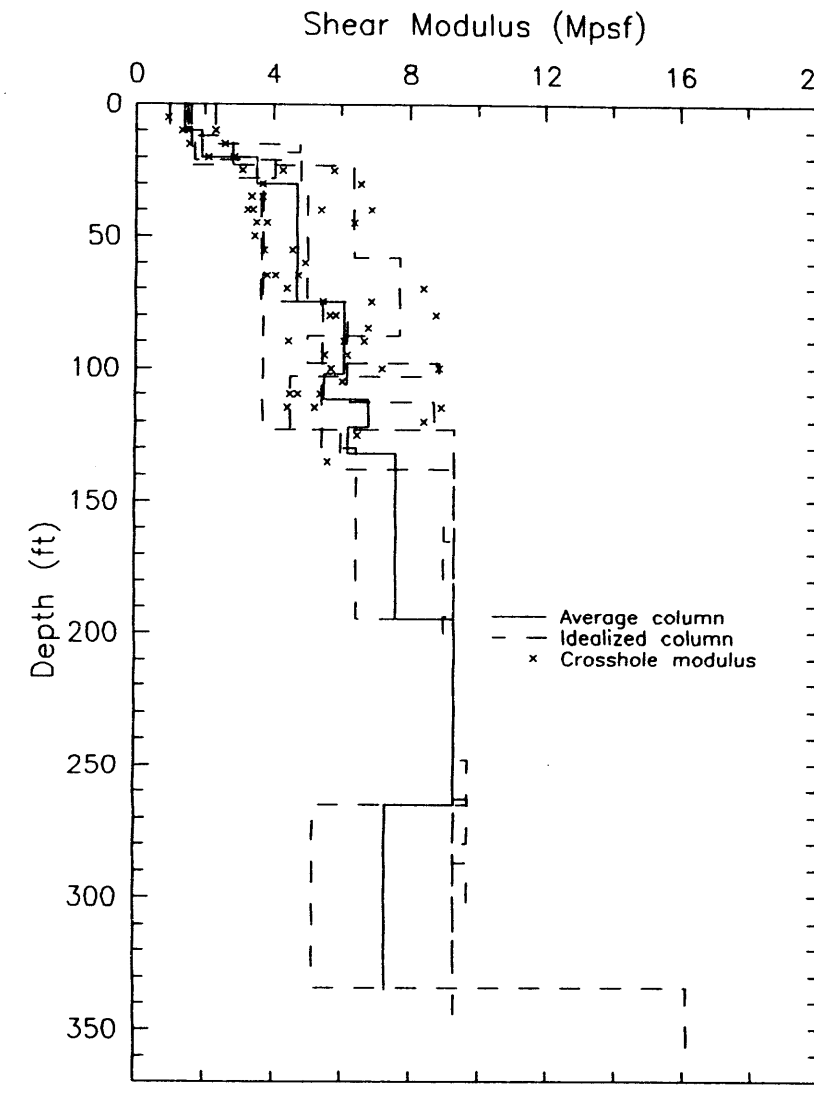

b. **Shear modulus**

Figure 31. Variation of stiffness for average column

PART IV: SITE RESPONSE CALCULATIONS

68. Site response calculations and analysis of the results comprise the third step of a site-specific earthquake response analysis. Site response calculations are presented below; the presentation of results and analysis is made in later parts of this report. Different mathematical formulations can be used to calculate site response including the solution of the wave equation and use of a shear beam analogy (both continuous solutions) and lumped mass (discrete). Initial formulations for site specific calculations were reported in the U.S. by Roesset and Whitman (1969) and Roesset (1970) and have been enhanced since. A number of computer programs are presently available to calculate site response analyses including two- and three-dimensional formulations.

Method of Response Calculations

69. The computer program *SHAKE* was used to calculate site-specific response caused by the synthetic earthquakes. *SHAKE* was developed at the University of California at Berkeley (Schnabel, Lysmer, and Seed 1972) and written in FORTRAN IV to run on a CDC 6400 computer. WES has developed pre- and post-processing routines and made enhancements to the program on two platforms—the personal IBM-compatible computer (Sykora, Wahl, and Wallace 1992) and the U.S. Army CRAY Y-MP at WES by Sykora. The latter platform was used for purposes of this study to take advantage of computational speed and massive file storage capabilities. The time necessary to iterate to the proper solution was about 1 sec.

Background

70. *SHAKE* was developed to calculate the horizontal response caused by an earthquake at any depth of a soil profile. The methodology and algorithms incorporated in the program are fairly simple and straight-forward and quite adequate for the purpose intended as clearly evident through the prolific publication of results and favorable comparisons with measured response (e.g., Seed et al. 1987 and Seed, Dickenson, and Idriss 1991). The simplicity associated with *SHAKE* is attributed to some basic assumptions regarding the cyclic behavior of materials and geometry of the problem. The basic assumptions of importance to this study are:

a. Soil layers are horizontal and extend to "infinity";

b. Ground surface is level;

c. Each soil layer is completely defined by the shear modulus and damping ratio as a function of strain, thickness, and unit weight;

d. The cyclic behavior of each soil (and base rock) is represented by the equivalent-linear constitutive model; and

e. The incident earthquake motions are uniform, horizontally-polarized shear waves propagating vertically.

In general, assumptions (a), (b), and (c) are consistent with site conditions at PGDP. The equivalent-linear constitutive model, assumption (d), described later in this section, is widely accepted by the geotechnical earthquake engineering profession as a simple but effective model for the dynamic response of soils. The last assumption, (e) above, narrows the focus to a simple class of problems, but, is a common assumption for this type of problem.

71. The computer program *SHAKE* has been in common use for almost 20 years. In that time, more knowledge has become available with regard to specification of inputs to the program and significant advances have been made in computer technology. As these findings have been made available, WES has updated and refined the program and method of data input. One of the most striking differences in the versions available at WES is the option to specify shear wave velocity for each soil layer as opposed to using the modulus coefficient, K_2 , or undrained shear strength, S_u . WES has also continually updated a library of soil modulus and damping relationships. Important input parameters to *SHAKE* for this study are described below.

Solution algorithm

72. The one-dimensional wave equation model (Kanai 1951) was used to develop *SHAKE*. This model has proven to be effective despite the simplicity and number of assumptions involved. The solution algorithm involves the complex response technique and the Fast Fourier Transform (Cooley and Tukey 1965). The general formulation of the wave equation is not unique to horizontally-polarized shear wave motion; the equation can also be solved for the vertical propagation of compression waves.

Constitutive model

73. In general, soil is a non-linear material that exhibits hysteretic behavior under cyclic loading. An example of the stress-strain behavior is

shown in Figure 32a. Soil is difficult to model accurately for cyclic response; exact representations are unavailable. The constitutive model incorporated into *SHAKE* is linear with simulated nonlinear effects to account for dependency of moduli on shear strain. This model, called the equivalent-linear method, was proposed by Seed and Idriss (1970) and is widely used in geotechnical earthquake engineering studies.

74. The basic components of the equivalent-linear method are the maximum shear modulus, G_{max}, moist unit weight, and ratio of critical damping, β. G_{max}, which corresponds to the linear-elastic, continuum material property (Lamé 1852), can be calculated from low-strain seismic shear wave velocity using:

$$G_{max} = \rho V_s^2 \tag{1}$$

where

ρ = mass density (moist unit weight / gravitational constant)
V_s = shear wave velocity

or from the maximum (low-strain) shear modulus coefficient, $(K_2)_{max}$, which is defined by Seed and Idriss (1970):

$$G_{max} = 1000\ (K_2)_{max}\ (\sigma_m')^{0.5} \tag{2}$$

where

σ_m' = mean effective stress, in psf
G_{max} is in psf

Shear wave velocities (using equation 1) were used exclusively for this study.

75. At a certain threshold of shear strain, generally accepted to be about 10^{-4} percent or less, the stiffness decreases to some value less that G_{max}. The equivalent-linear model uses secant shear moduli that are adjusted during each iteration to account for this. Damping is input by using complex moduli, G^*, and hysteretic damping (which is independent of frequency):

$$G^* = G\ (1-2\beta^2+2i\beta\sqrt{1-\beta^2}) \tag{3}$$

where

$i = \sqrt{-1}$

Damping increases as shear strain increases. The character of these functions of strain was first addressed in studies by Hardin and Drnevich (1972), Seed and Idriss (1970), and Schnabel (1973). Later studies include: Zen and

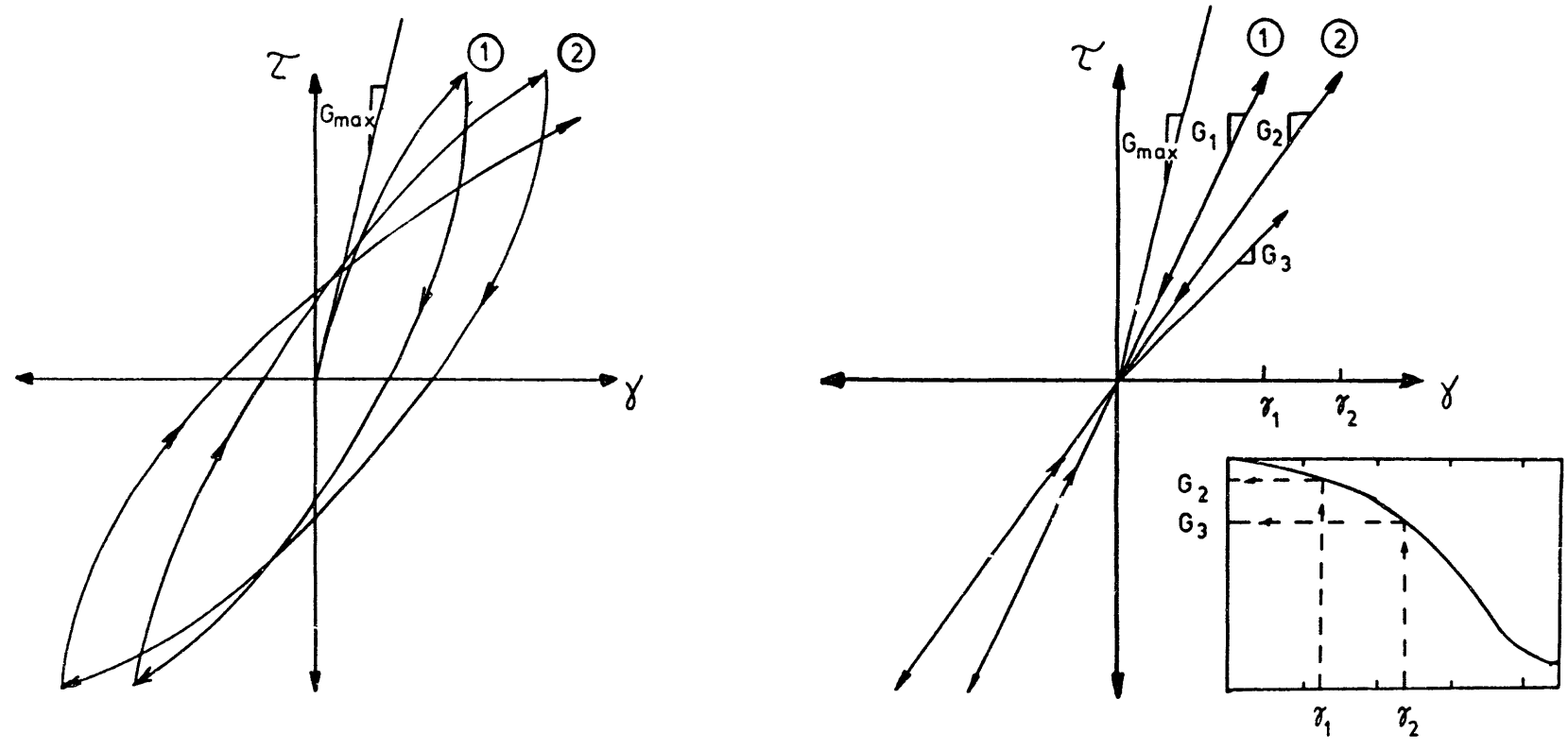

a. Ideal soil behavior

b. Equivalent linear model

Figure 32. Comparison of general cyclic behavior of soil and equivalent linear model with iterative scheme

Higuchi (1984), Seed et al. (1986), Sun, Golesorkhi, and Seed (1988), and Vucetic and Dobry (1991). A presentation of the relationships used for this study was made in Part III.

Iteration scheme

76. An example of the iterative procedure for the equivalent-linear model is shown in Figure 32b and described below. Assuming shear wave propagation, the model is initiated with an assumed value of shear modulus, G_1 , typically chosen to be slightly less than, or equal to, G_{max} . For the first cycle of loading, the stress-strain relation is linear between $\pm \tau_1$ with a slope of G_1 . The ordered pair (G_1 , τ_1) comes from the appropriate modulus degradation curve as discussed in Part III of this report and shown schematically in Figure 32b. Maximum shear strains are obtained from the solution of the wave equation. Effective shear strain, PRMUL, is some fraction of the maximum shear strain and is used to obtain a new value of shear modulus, G_2 , from the appropriate modulus curve. A new value of β is also obtained. This process is repetitive until the moduli and damping for two successive iterations are within a prescribed tolerance, ERR. A summary of system input parameters is presented in Table 8.

Table 8

Miscellaneous Parameters in *SHAKE* Used for This Study

Parameter	Description	Value
MAMAX	Maximum number of points in the Fast Fourier Transform	4096
SKO*	Lateral coefficient of earth at rest	0.45
ITMAX	Maximum number of iterations	100
ERR	Maximum acceptable difference for modulus and damping	1 %
PRMUL	Effective shear strain factor	0.65

* Did not affect the calculations for this study since G was calculated using V_s , not K_2 .

Application of Free-Field Results

77. It may not be appropriate to directly apply the free-field response to the base of the structure for a number of reasons, including:

a. The depths of the footings most likely are not at the ground surface and motions will vary with depth.

b. The weight of the structure acting on the footings will affect the motions beneath the footings.

c. The friction acting on the sides of the footing will affect the motions acting on the footing.

d. The impedance contrast between the soil and foundation is normally quite large.

The application of ground motions to the base of structures, i.e., the consideration of points such as those listed, is commonly referred to as dynamic soil-structure interaction (DSSI).

78. Basic design approaches for dynamic soil-structure interaction have recently been documented by Johnson (1980) and Veletsos, Prasad, and Tang (1988). Evaluation of simple foundation systems in the latter study suggests the following rule of thumb: at lower periods, DSSI will have no effect on the response; at higher periods, DSSI will reduce the maximum response; for intermediate periods, DSSI might increase or decrease the maximum response.

Presentation of Output

79. Although a number of output options are available using *SHAKE*, the primary focus of this study was to calculate the pseudo velocity response spectra and present the results using the tripartite representation. It was specified in the scope of work for this study that damping ratios of 2, 5, 7, 10, 12, and 15 percent be used. Other forms of data were also used to evaluate and present the results including the ratio of acceleration response spectra between free field and rock outcrop motions and the variation of ground acceleration with time as a function of depth.

80. *SHAKE* may be used to calculate spectral ordinates at periods up to 10 sec. The experience of investigators who have compared calculated free-field response using *SHAKE* with measured response from major earthquakes suggest that *SHAKE* works well at periods less than 2 sec. At periods greater than 4 sec, motions are likely to be significantly affected by two-dimensional effects and surface wave energy and are not well represented with *SHAKE* (reference in Part I). Between 2 and 3 sec, the two responses typically begin to diverge. For purposes of this study, data was presented only for periods less than 2 sec. In many cases, the response did not drop significantly enough within this range of periods to conclude unequivocally that the peak

response had been predicted. The use of other computer models may be necessary to define peak response values.

81. Six different figures and various tables are used to present different aspects of the results for each case considered. The use of different forms of results is described in the sections below and examples are presented. Each of these types of data presentation are included in appendices for each case analyzed. Care was taken to keep scales of plots consistent with respect to the earthquake event to facilitate comparisons between figures. Additional aspects of the computer code, including options not presented, are described in the program documentation. For this reason, further discussion is not included herein.

Acceleration-time records

82. The variation of particle acceleration with time was considered for this study primarily to provide insight as to the effects of various layers on wave propagation and to detect any potential anomalies. An example of the presentation of this data is shown in Figure 33. An acceleration record is plotted for each layer in the soil column, corresponding to the top of the labeled layer. The peak accelerations are also identified and labeled and are generally summarized in tables.

Shear strains

83. Shear strains corresponding to the mid-height of layers are used to update shear modulus and damping ratio from normalized relationships. The actual value used for this purpose is called the effective shear strain, γ_{eff} , which is calculated from the maximum value of shear strain, γ , as:

$$\gamma_{eff} = \text{PRMUL} * \gamma \tag{4}$$

where

PRMUL = 0.65 for this study

The variation of effective shear strain with time at different layer contacts are shown using a format similar to that for accelerations as shown in Figure 34. The top and bottom of the column are excluded since the shear strains are always zero.

Pseudo-velocity response spectrum

84. Pseudo-velocity spectrum is the response, in terms of velocity, of an equivalent damped single-degree-of-freedom (SDOF) system to the free-field motion. This spectrum is used for design and analysis by structural

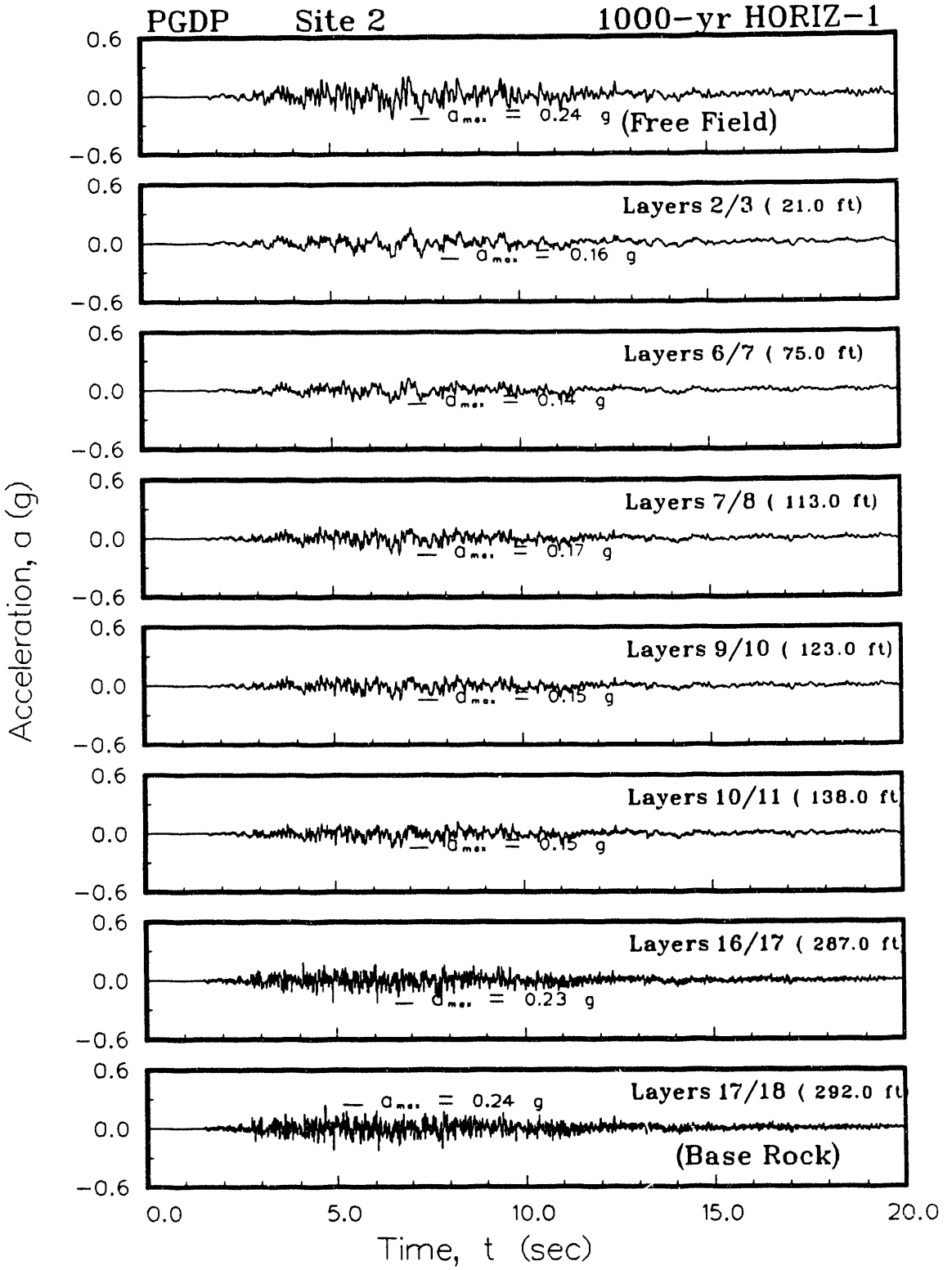

Figure 33. Example figure showing a profile of the variation of acceleration with time

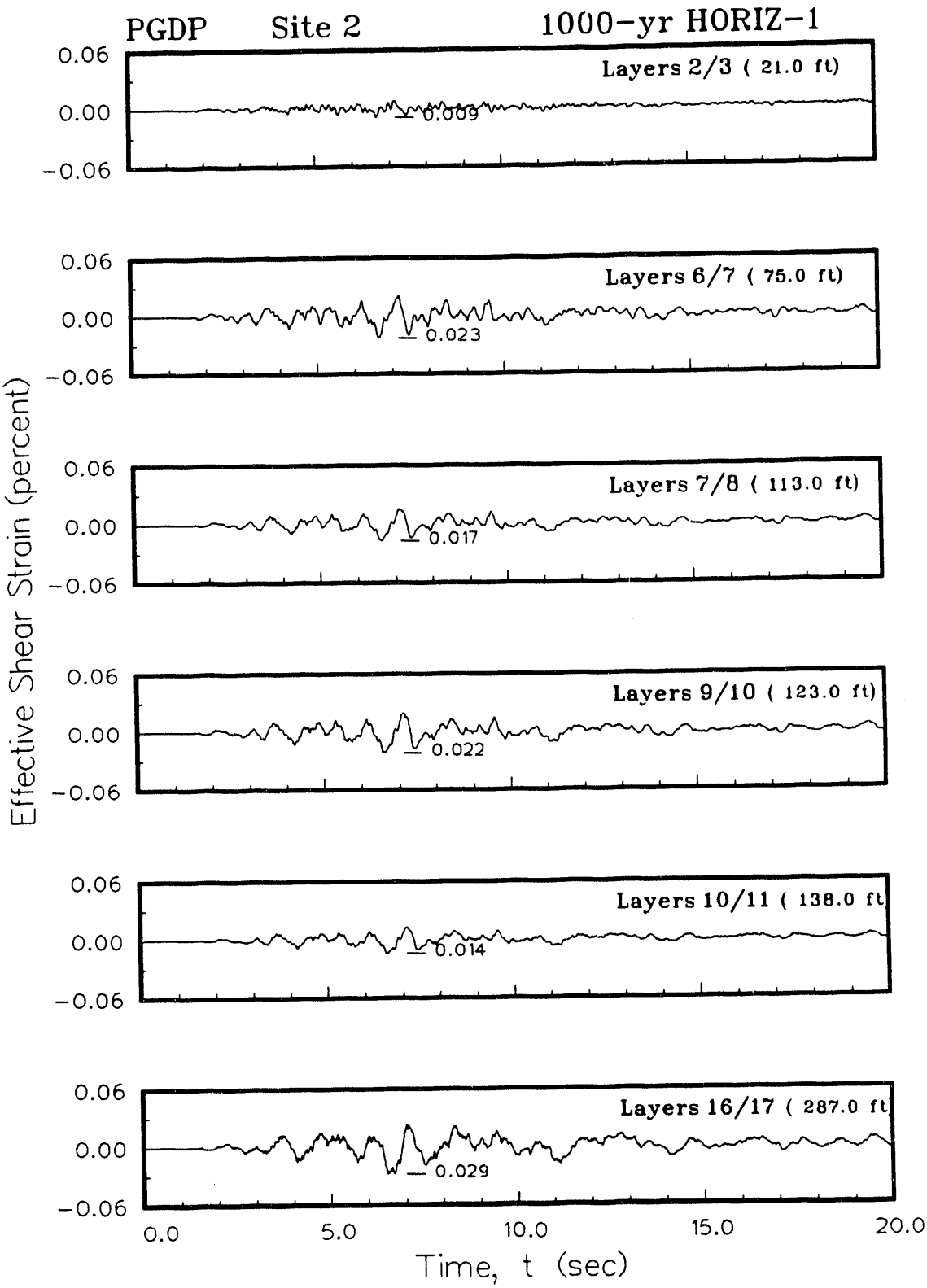

Figure 34. Example figure showing a profile of the variation of effective shear strain with time

engineers. An example of the presentation of this pseudo-velocity response spectrum at the free-field (ground surface) in tripartite form for the six levels of system damping is shown in Figure 35.

Absolute acceleration response spectrum

85. An absolute pseudo-acceleration response spectrum is the response, in terms of acceleration, of an equivalent damped single-degree-of-freedom (SDOF) system to the free-field motion. Absolute rather than relative accelerations were used for this study as recommended by Wiegel (1970). An example of the presentation of the absolute acceleration response spectrum for rock outcrop and free field motions is shown in Figure 36. The spectrum for rock outcrop is reproduced in a separate subplot using the same format for easy comparison. The peak accelerations denoted in acceleration-time records for this study generally correspond to response spectral accelerations at very low periods.

Ratios of acceleration spectra

86. The ratio of free-field ground surface acceleration spectrum to rock outcrop acceleration spectrum at each period was calculated to evaluate the periods at which motions are amplified the most and to determine the site period. The variation of this ratio with period at six levels of system damping will be used for design and seismic stability evaluations. An example of the presentation of this ratio is shown in Figure 37.

Dynamic amplification

87. Some studies of site response (e.g., Seed et al. 1974) and design manuals (e.g., Department of the Army 1986 and Uniform Building Code) use a "normalized spectra" that is calculated by dividing the acceleration response spectra by the peak horizontal acceleration. This is sometimes referred to as the dynamic amplification factor. An example figure is shown in Figure 38. Recall that the absolute response acceleration (not relative acceleration) was used in comparisons for this study.

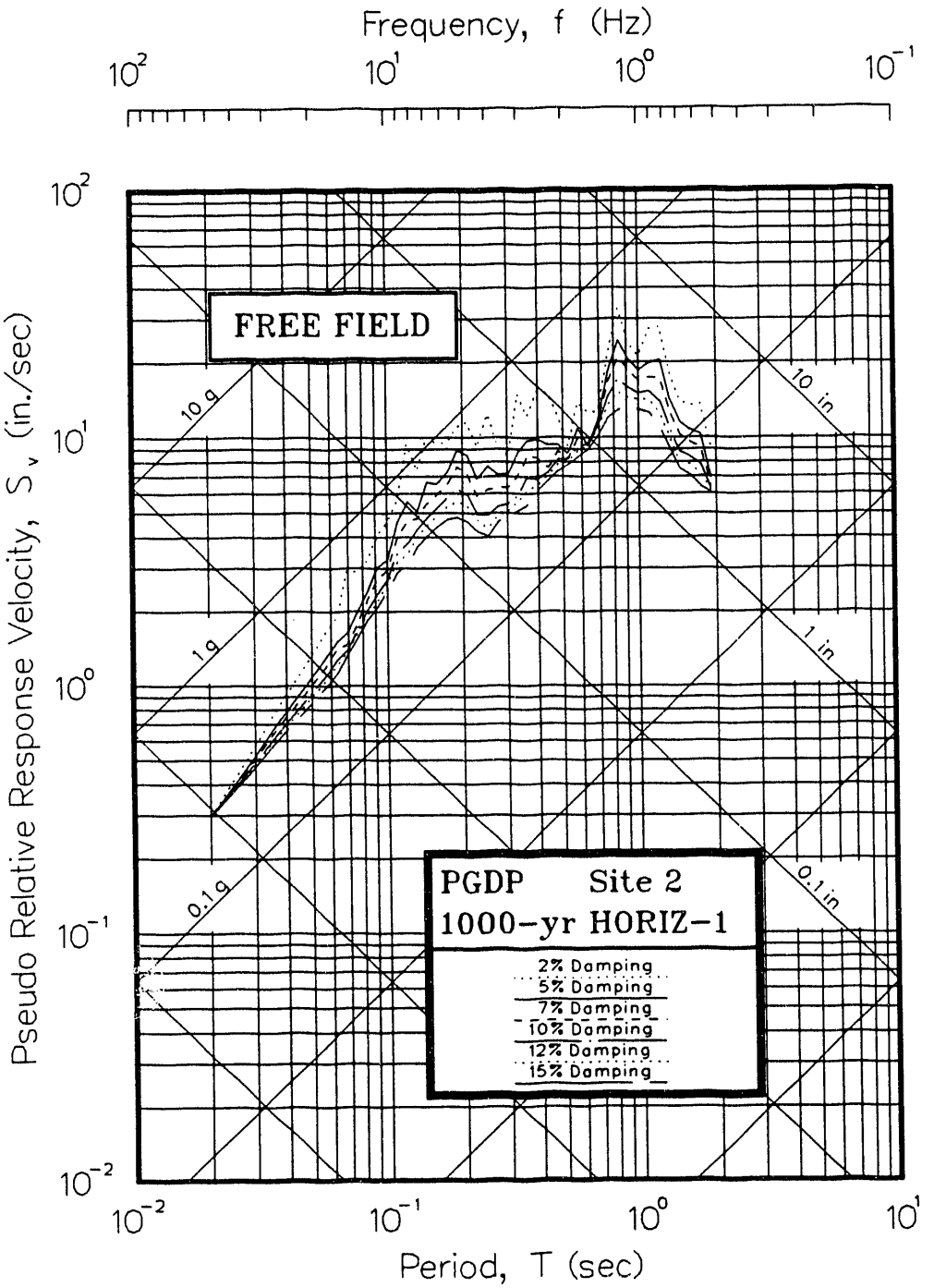

Figure 35. Example figure showing pseudo-velocity response spectra in tripartite format (5 percent damping)

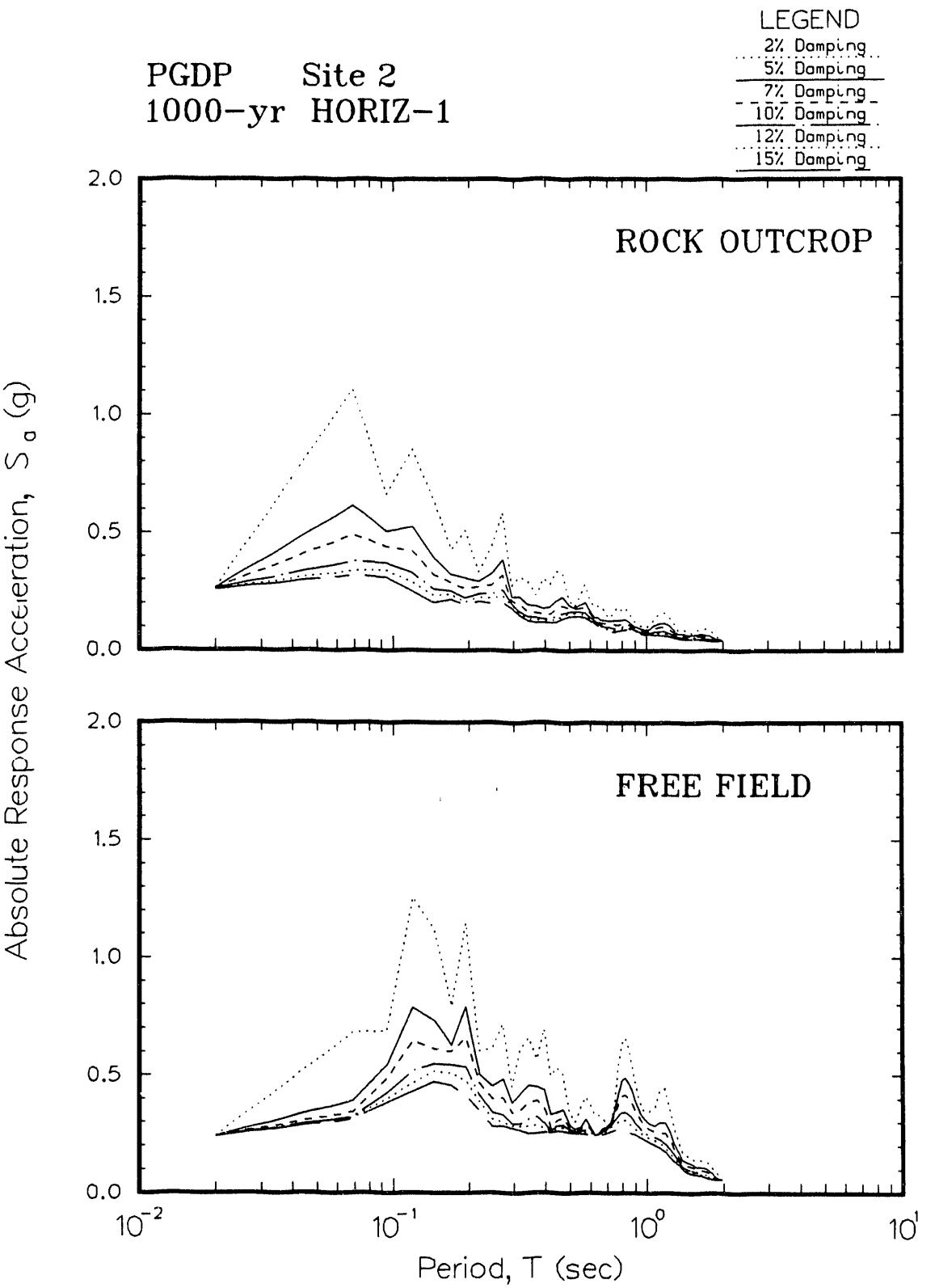

Figure 36. Example figure showing the absolute acceleration response spectra for rock outcrop and free-field motions

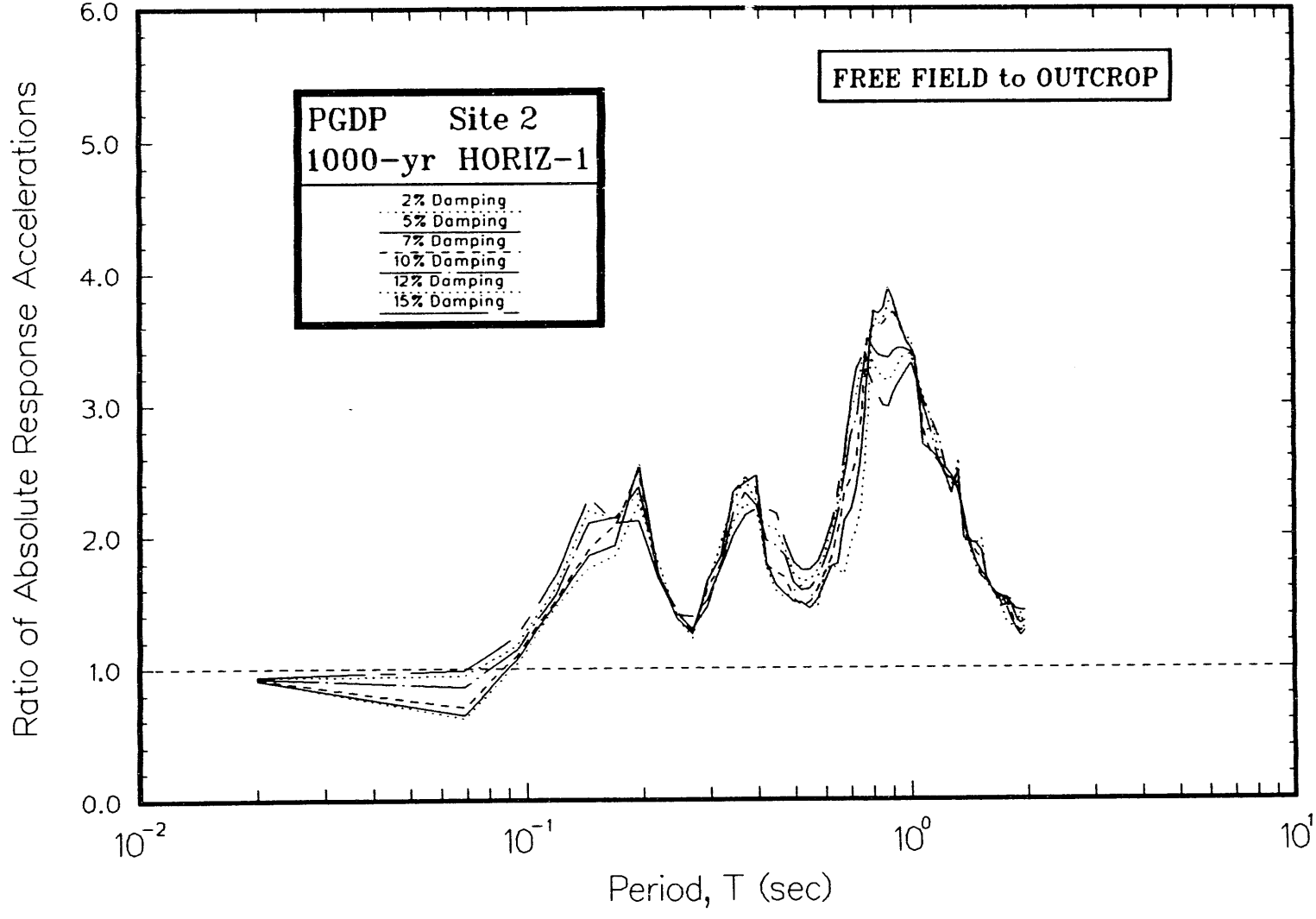

Figure 37. Example figure showing the ratio of absolute acceleration response spectra for free field to rock outcrop motions

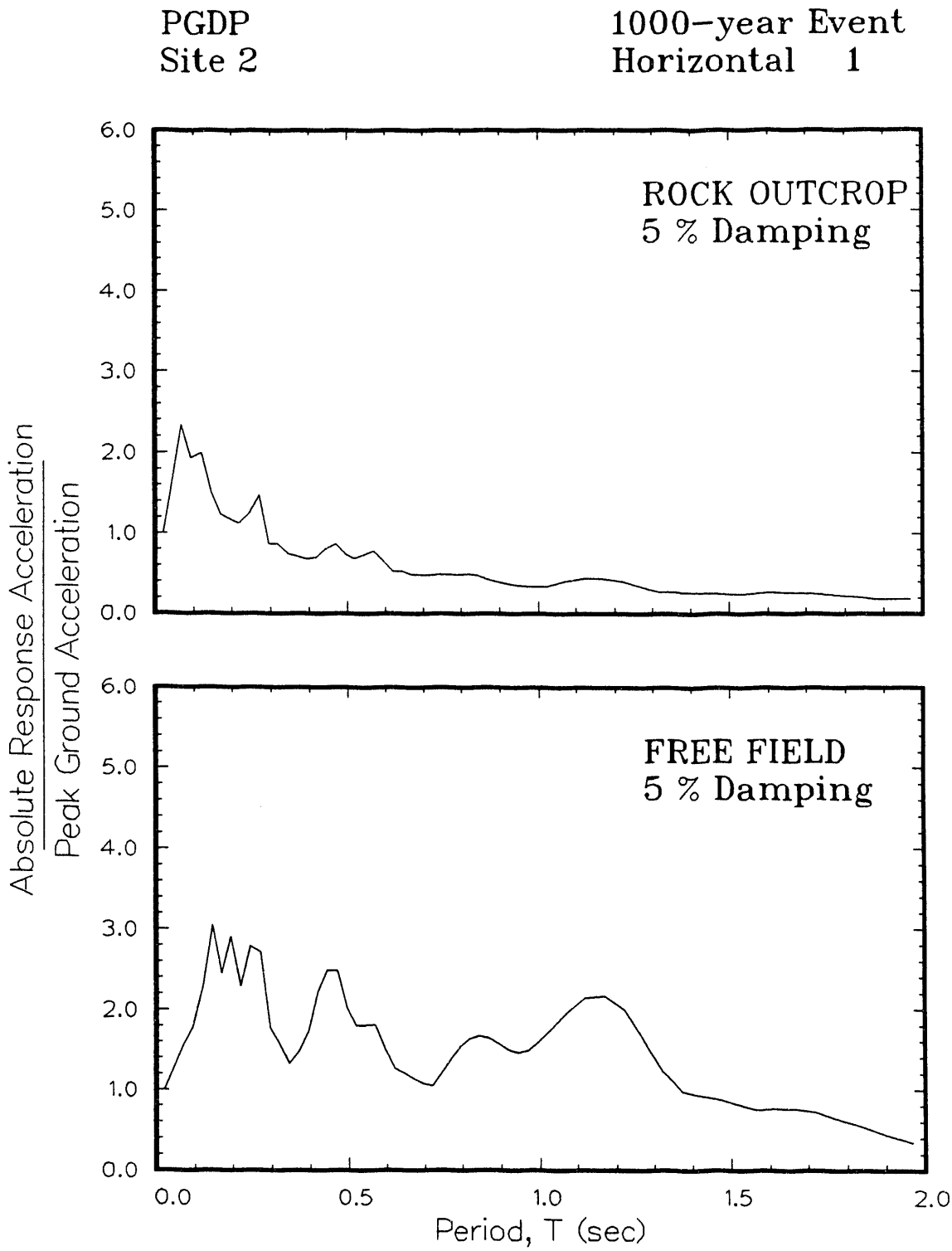

Figure 38. Example figure showing the amplification ratios (absolute acceleration response spectra normalized to peak horizontal acceleration) for rock outcrop and free field motions

PART V: RESULTS FROM COLLECTION OF INDIVIDUAL SITES

88. The results of site response calculations for individual sites are presented below respective of the three design events. Results at 5 percent system damping are presented in the formats described in Part IV. The plot scales were kept consistent, except for shear strain, to aid in comparing values among the three events. Upper and lower bounds were also interpreted to aid in these comparisons. The sensitivity of calculated response to soil column inputs using the average column is presented in Part VI.

500-Year Event

89. The 500-year event is intended to represent a large earthquake at a moderate distance. The calculated response for this event at the four sites indicates that moderate peak accelerations and moderate shear straining can be expected for this type of event. Slight de-amplification of motion at periods less than 0.08 sec and large amplification at greater periods are likely. The range of spectra for free field response is fairly narrow. Discussion of the data is presented below.

Acceleration versus time

90. The calculated motions for the top of each layer for the four sites and two horizontal input motions are presented in Appendix B. A comparison of peak accelerations is made in Table 9. The propagation of shear waves through the four soil columns with two different horizontal earthquake components produced small de-amplification of peak acceleration except in the case of the Horizontal 2 component at Site 4. The peak horizontal accelerations at free field (ground surface) range from 0.14 g to 0.20 g compared to the peak accelerations of 0.19 and 0.18 g for rock outcrop and 0.16 g and 0.17 g for base rock motions.

91. Observations of acceleration records in Appendix B indicate that, in general, the amplitude of accelerations decrease and the higher frequencies are filtered as the waves propagate upward through each layer. The spectral content seems to change the most at depths corresponding to contacts with continental deposits or the Porter's Creek Formation. Near the ground surface, additional reflections caused by the free surface cause the peak accelerations to increase. Most amplification of acceleration occurs in the

upper 25 ft of the column. There are no significant differences between the calculated responses for the two horizontal components.

Table 9

Peak Accelerations for 500-Year Event

		Peak Acceleration (g)		
	Component	Rock Outcrop	Base Rock	Free Field
Site 1	Horizontal 1	0.19	0.17	0.14
	Horizontal 2	0.18	0.16	0.17
Site 2	Horizontal 1	0.19	0.17	0.17
	Horizontal 2	0.18	0.16	0.18
Site 3	Horizontal 1	0.19	0.16	0.17
	Horizontal 2	0.18	0.16	0.14
Site 4	Horizontal 1	0.19	0.17	0.18
	Horizontal 2	0.18	0.16	0.20

Shear strains versus time

92. The calculated effective shear strains at each contact between soil layers for the four sites and two horizontal components are presented in Appendix C. The peak (effective) shear strains for each column are listed in Table 10. (Note that shear strains in Table 10 represent values calculated at mid-height of layers, whereas shear strains in Appendix C were calculated at layer interfaces.) The results listed in Table 10 are fairly consistent among sites and earthquake components, ranging from 0.015 to 0.019 percent with one value at 0.026 percent (Site 3, Horizontal 1). The peak shear strains occur in layers directly above layer contacts with large impedance contrasts. For the 500-year event, these depths range from 72 to 305 ft. Within other layers (especially near the ground surface), the peak effective shear strains are as low as 0.004 percent.

93. In general, the peak effective shear strains listed in Table 10 correspond to a moderate amount of straining. The range in shear modulus for soils corresponding to these strains is 85 to 60 percent of the small-strain

(maximum) moduli. The range in damping ratio is between 4 and 8 percent for soil layers. There are no significant differences between the calculated responses for the two horizontal components except at Site 3.

Table 10

Peak Shear Strains for 500-Year Event

	Component	Depth (ft)	Peak Effective Shear Strain (percent)
Site 1	Horizontal 1	95.5	0.018
	Horizontal 2	95.5	0.018
Site 2	Horizontal 1	304.5	0.016
	Horizontal 2	94.0	0.015
Site 3	Horizontal 1	72.0	0.026
	Horizontal 2	305.0	0.019
Site	Horizontal 1	116.0	0.018
	Horizontal 2	116.0	0.019

Pseudo-velocity spectra

94. The pseudo-velocity response spectra for the four individual sites are presented in Appendix D. The combined spectra at five percent damping for all sites and both horizontal components are shown in Figure 39. The eight spectra produce a relatively-narrow range at site periods less than 0.01 sec and a narrow to moderate range at greater periods. The peak spectral velocity is 18 in./sec at a period of 1.1 sec. The general pattern of the combined data have been characterized by tri-linear relationships representing an upper bound and a lower bound as shown in Figure 39. These three relationships are essentially parallel with transitions at 0.12 to 0.20 sec and 0.90 to 1.1 sec.

Absolute acceleration spectra

95. Absolute acceleration response spectra for the four individual sites are presented in Appendix E. The combined spectra at five percent damping for all sites and both horizontal components are shown in Figure 40. Some spectra with pronounced peaks are identified. The spectra for rock are included for comparison (refer to Figure 7). The combined spectra indicate

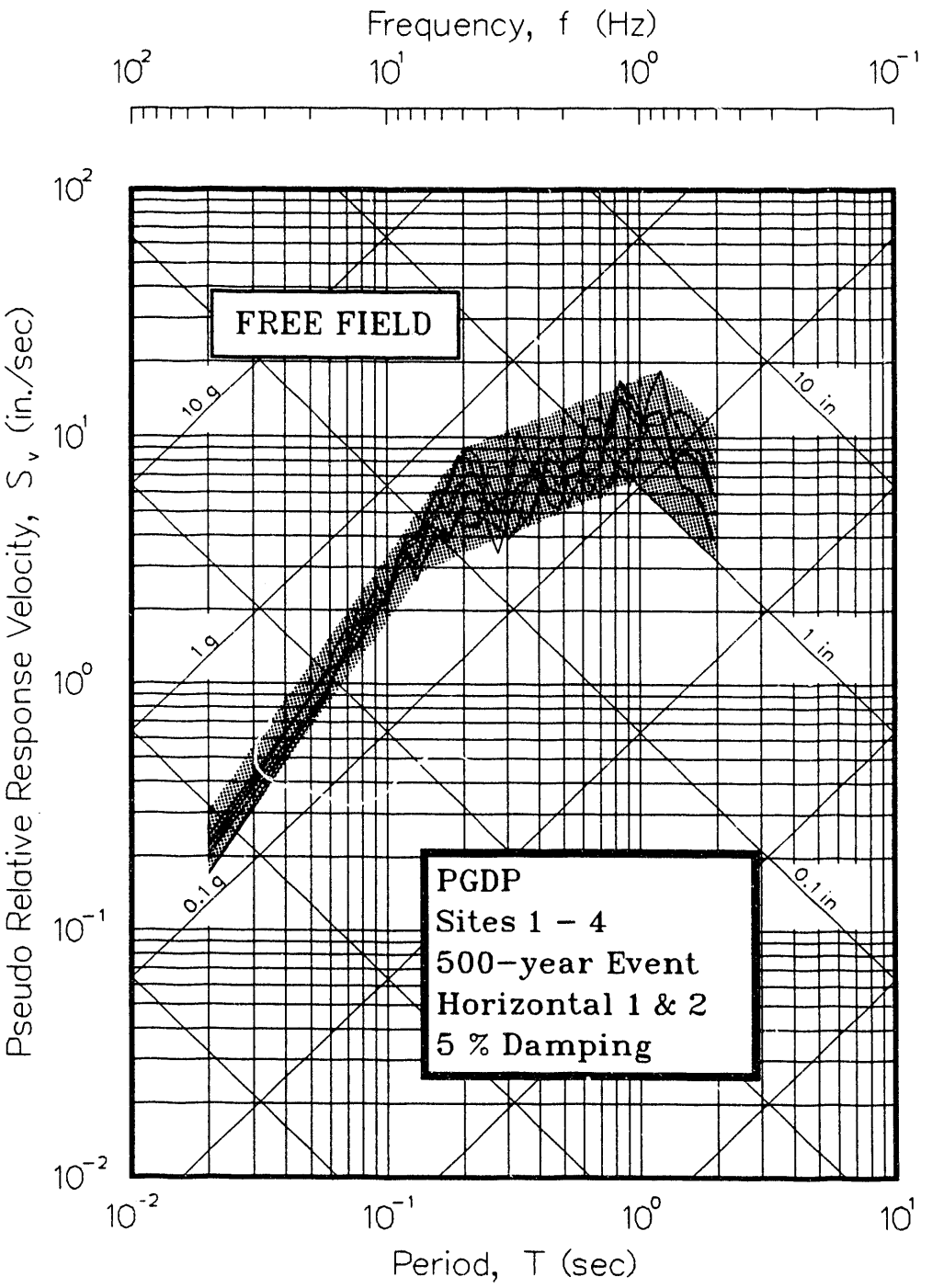

Figure 39. Pseudo-velocity response spectra for 500-year event

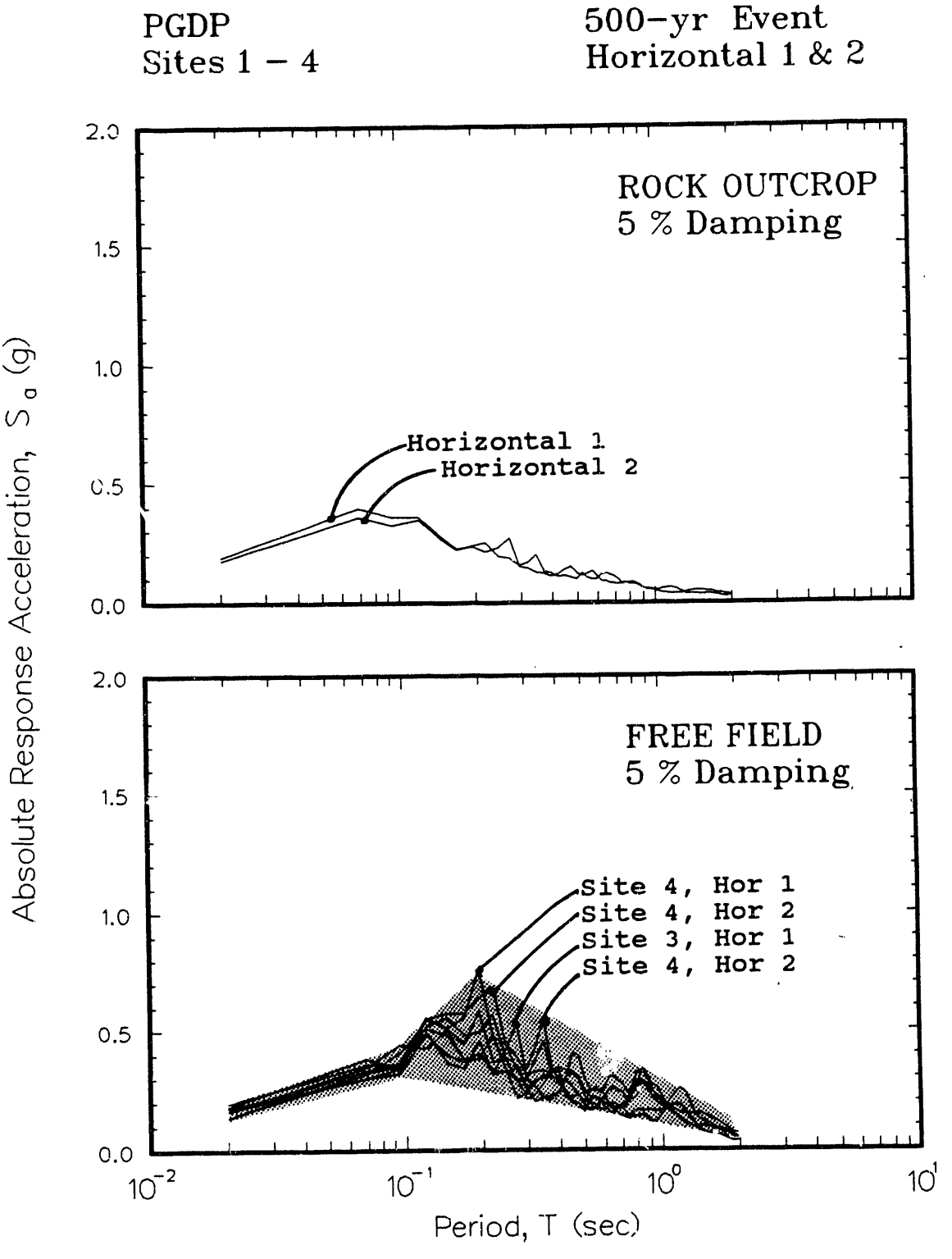

Figure 40. Absolute response acceleration spectra for 500-year event

that the largest spectral acceleration is 0.75 g at a period of 0.2 sec and was calculated for the Horizontal 1 component applied to Site 4. The peak spectral accelerations tend to occur at periods significantly greater than the predominant periods of the rock outcrop motion (0.07 sec).

96. Simple multi-linear relationships were used to represent the upper bound and lower bound of the spectral accelerations as shown in Figure 40. The trend of the peak spectral accelerations is to increase rapidly at periods between 0.09 and 0.2 sec and then decrease rapidly at periods greater than 0.2 sec compared to the spectral velocities which increase up to periods of 1.1 sec.

Ratio of acceleration spectra

97. The ratios of free field to outcrop acceleration response spectra for the four individual sites are presented in Appendix F. Combined spectra at all sites for both horizontal motions are shown in Figure 41. (The ratio for rock outcrop is 1.) Spectra with sharp peaks are identified. The eight curves shown in Figure 41 produce a wide range.

98. The predominant period of amplification is between 0.9 and 1.1 sec for all four sites. Secondary peaks occur at 0.2 and 0.4 sec. At Site 4, the amplification response at 0.2 sec approaches that at 1.0 sec for the Horizontal 1 component. The spectral ratio is generally between 1.0 and 3 at periods between 0.1 and 0.8 sec and then rises to peak values greater than 4 at periods between 0.8 sec and 1.1 sec. The amplification ratios are generally less than one for periods less than 0.08 sec.

Amplification ratio

99. The ratios of free field spectral acceleration to peak horizontal acceleration for the four individual sites are shown in Appendix G. Combined relationships at all sites for both horizontal motions are shown in Figure 42. The ratios for rock outcrop are also provided for comparison. The range of relationships is moderately-wide with peak values of 3 to 4 between 0.1 and 0.2 sec and then ratios of 1 or less at periods of about 1.5 sec and greater.

100. Simple relationships were used to bracket the collection of amplification ratio spectra as shown in Figure 42. At periods less than 0.27 sec, this ratio changes significantly, peaking at 0.2 sec. At greater periods, the upper-bound relationship shows a moderate decrease in amplification ratio as period increases; the lower bound has very little slope.

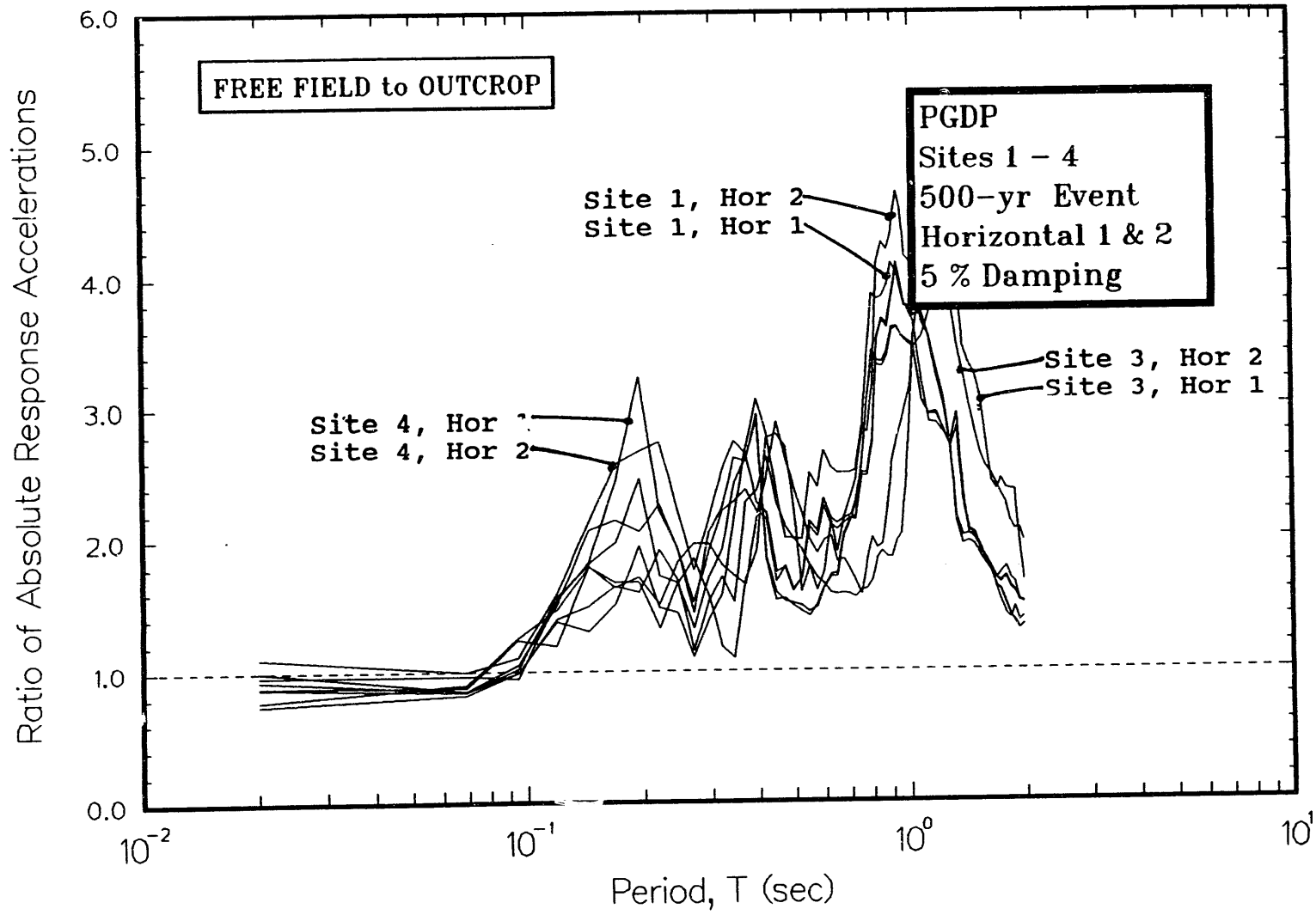

Figure 41. Ratio of free field to rock outcrop absolute acceleration response spectra for 500-year event

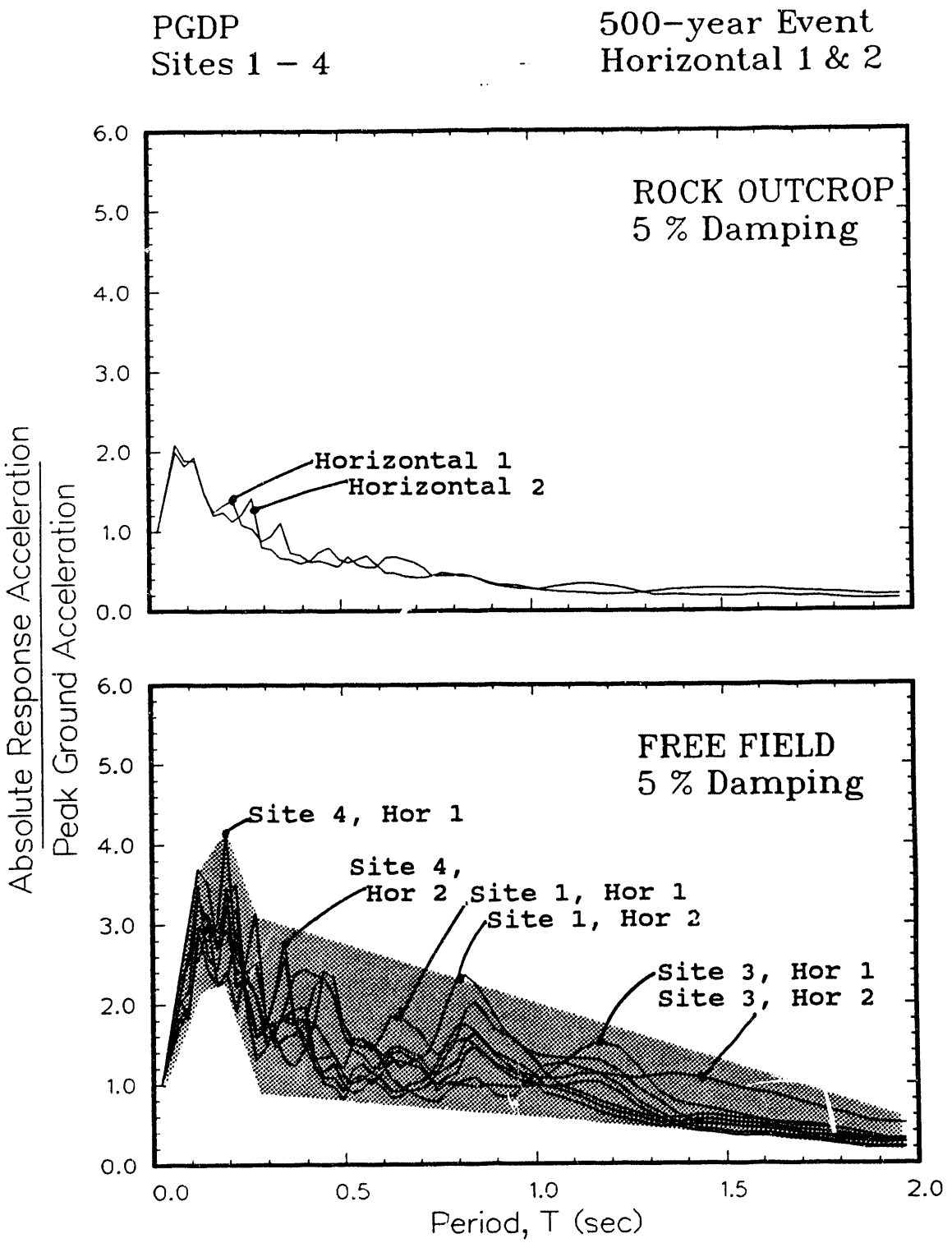

Figure 42. Amplification ratio for 500-year event

1000-Year Event

101. The 1000-year event is intended to represent a large earthquake at a moderate distance, closer than the 500-year event. The calculated response for this event at the four sites indicates that moderate peak accelerations and moderate shear straining can be expected for this type of event. Moderate de-amplification of motion at periods less than 0.1 sec and moderate to large amplification of motion at greater periods is likely. The range of spectra is narrow to moderate. Discussion of the data is presented below.

Acceleration versus time

102. The calculated motions for the top of each layer for the four sites and two horizontal input motions are presented in Appendix H. A comparison of peak accelerations is made in Table 11. The propagation of shear waves through the four soil columns with two different horizontal earthquake components produced moderate de-amplification of peak acceleration except in the case of the Horizontal 2 component at Site 4. The peak horizontal accelerations at free field (ground surface) range from 0.18 g to 0.27 g compared to the peak accelerations of 0.26 and 0.27 g for rock outcrop and 0.22 g and 0.25 g for base rock motions.

Table 11

Peak Accelerations for 1000-Year Event

		Peak Acceleration (g)		
	Component	Rock Outcrop	Base Rock	Free Field
Site 1	Horizontal 1	0.26	0.23	0.18
	Horizontal 2	0.27	0.24	0.21
Site 2	Horizontal 1	0.26	0.24	0.20
	Horizontal 2	0.27	0.24	0.24
Site 3	Horizontal 1	0.26	0.22	0.22
	Horizontal 2	0.27	0.24	0.18
Site 4	Horizontal 1	0.26	0.24	0.22
	Horizontal 2	0.27	0.25	0.27

Shear strains versus time

103. The calculated effective shear strains at each contact between soil layers for four sites and two horizontal components are presented in Appendix I. The peak (effective) shear strains at mid-heights of the layers are listed in Table 12. The peak strains are fairly consistent among sites and earthquake components, ranging from 0.025 to 0.043 percent with one value of 0.061 percent (Site 3, Horizontal 2). The peak effective strain occurs in the layer directly above the rock except for the Horizontal 2 component at Site 1 and at Site 3. Within other layers, the peak effective shear strain is as low as 0.006 percent.

Table 12

Peak Shear Strains for 1000-Year Event

	Component	Depth (ft)	Peak Effective Shear Strain (percent)
Site 1	Horizontal 1	301.5	0.033
	Horizontal 2	95.5	0.027
Site 2	Horizontal 1	304.5	0.031
	Horizontal 2	304.5	0.025
Site 3	Horizontal 1	72.0	0.043
	Horizontal 2	305.0	0.061
Site 4	Horizontal 1	297.0	0.030
	Horizontal 2	297.0	0.027

104. In general, the magnitude of calculated shear strains correspond to a moderate amount of straining. The range in shear modulus for soils corresponding to these strains is 80 to 48 percent of the small-strain moduli. The range in damping ratio is between 4 and 9 percent for soils.

Pseudo-velocity spectra

105. The pseudo-velocity response spectra for the four individual sites are presented in Appendix J. The combined spectra at five percent damping for all sites and both horizontal components are shown in Figure 43. The eight spectra produce a narrow range at site periods less than 0.015 sec and a

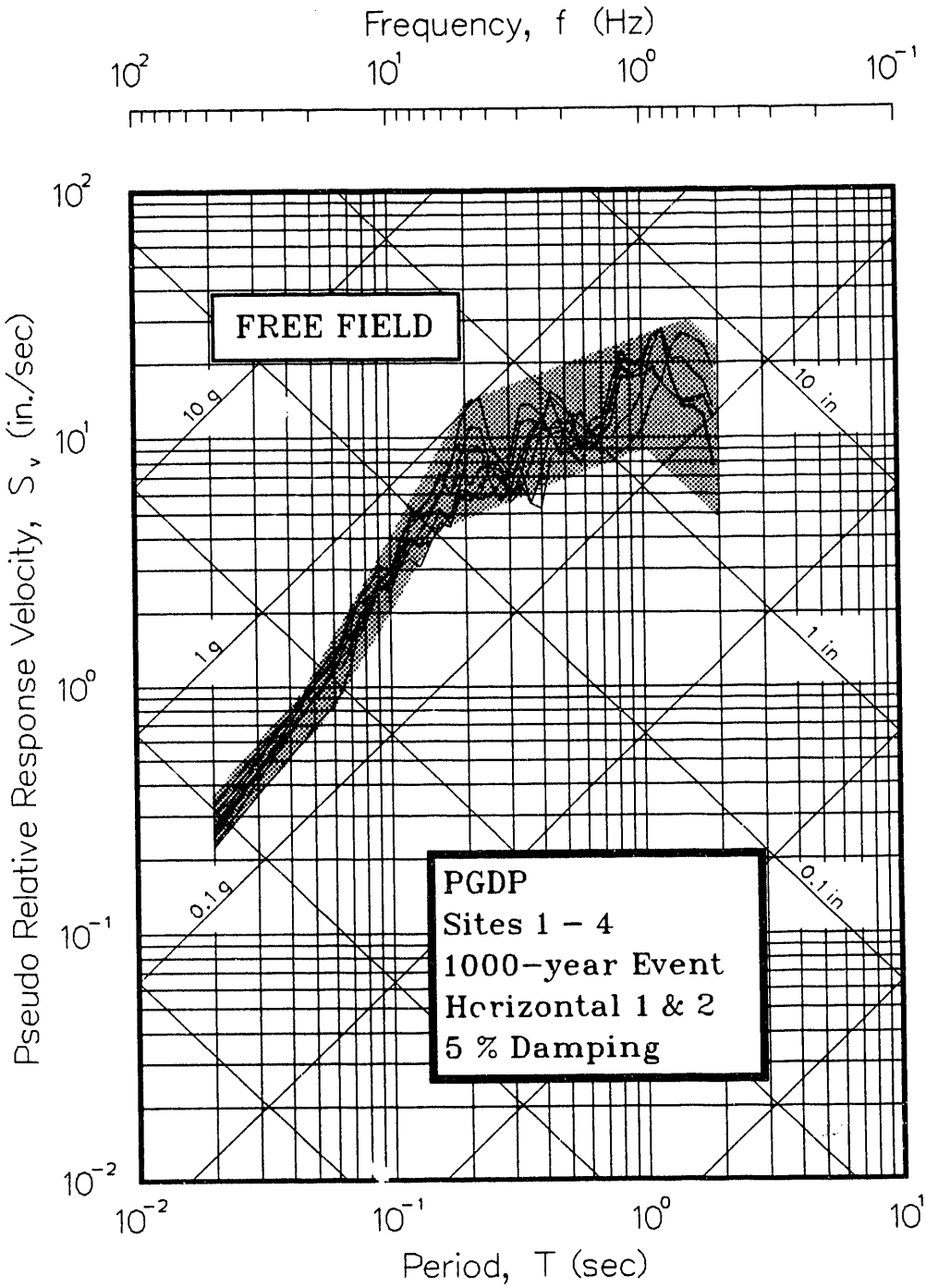

Figure 43. Pseudo-velocity response spectra for 1000-year event

narrow to moderate range at greater periods. The peak spectral velocity is 26 in./sec at a period of 1.1 sec.

106. The general pattern of the combined data can be characterized by quadra-linear relationships representing an upper bound and a lower bound as shown in Figure 43. The shape and locations of these relationships differ significantly from those developed for the 500-year event (refer to Figure 39). The results for the 1000-year event have a significant increase in spectral velocity at periods between 0.05 and 0.2 sec unlike the results for the 500-year event. The results for 1000-year event also show significantly more increase in spectral velocity with increasing period over the range of 0.2 and 1.1 sec.

Absolute acceleration spectra

107. Absolute acceleration response spectra for the four individual sites are presented in Appendix K. The combined spectra at five percent damping for all sites and both horizontal components are shown in Figure 44. The significant spectra are identified. The combined free-field spectra indicate that the largest spectral acceleration is 1.1 g at a period of 0.2 sec which corresponds to Site 4.

108. A range defined by an upper bound and a lower bound of the data are also shown in Figure 44. A comparison with similar interpretations made for the 500-year event (refer to Figure 40) shows that the most significant change has occurred in the range of periods of 0.1 to 0.3 sec. A more pronounced peak is beginning to form at these periods. For the other period ranges, the spectral accelerations are greater for the 1000-year event, but the changes in spectral accelerations with period are similar.

Ratio of acceleration spectra

109. The ratios of free field to outcrop acceleration response spectra for the four individual sites are presented in Appendix L. Combined spectra at all sites for both horizontal motions are shown in Figure 45 with some of the spectra identified. The eight curves shown in Figure 45 are again considerably different. The predominant amplification occurs at a period of 0.9 to 1.1 sec and the secondary peaks occur at 0.2 and 0.4 sec, consistent with the results for the 500-year event. The ratios are nearly always less than one for periods less than 0.1 sec and are as low as 0.6. The amplification is generally between 1.0 and 3 at periods between 0.1 and 0.8 sec and then rise to peak values between 3 and 4 at periods between

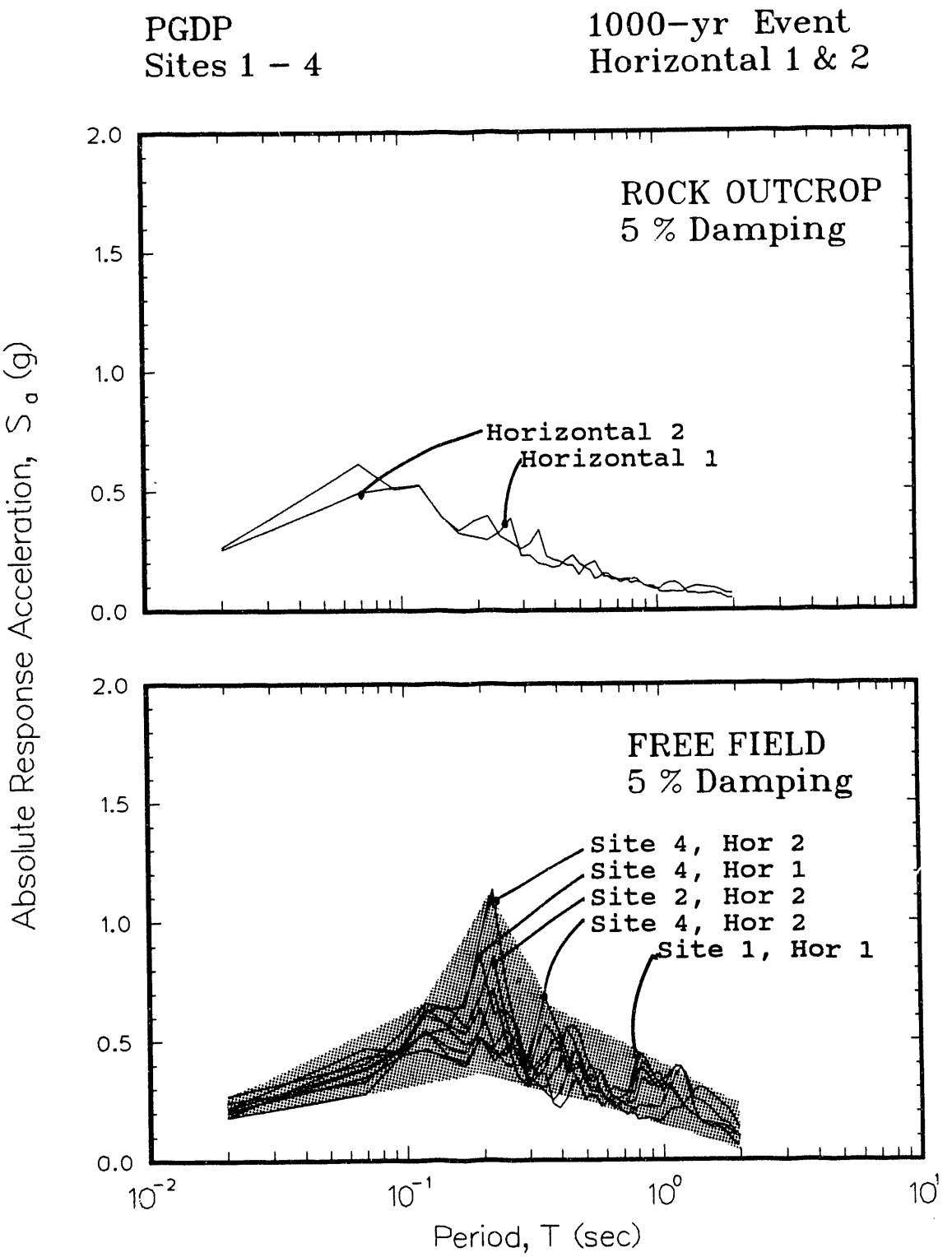

Figure 44. Absolute response acceleration spectra for 1000-year event

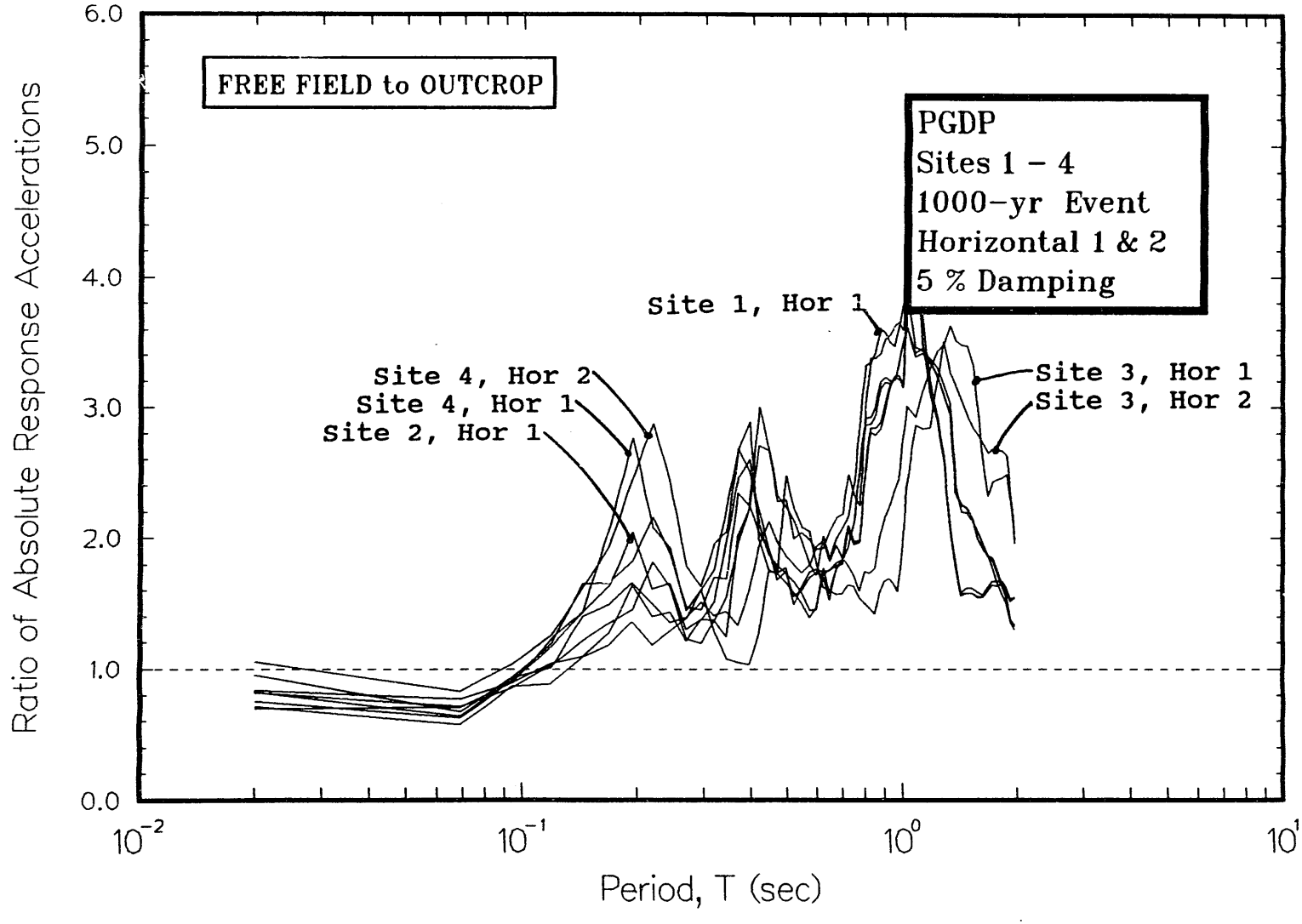

Figure 45. Ratio of free field to rock outcrop absolute acceleration response spectra for 1000-year event

0.8 sec and 1.1 sec. This ratio is generally less than that calculated for the 500-year event.

Amplification ratio

110. The ratios of free field spectral acceleration to peak horizontal acceleration for the four individual sites are shown in Appendix M. Combined relationships at all sites for both horizontal motions are shown in Figure 46. The range produced by the eight relationships is substantial and slightly wider than that calculated for the 500-year event.

111. Quadra-linear relationships describing the upper bound and lower bound of the data are also shown in Figure 46. These relationships are very similar to those drawn for the 500-year event except that the ratio of accelerations is slightly greater for the 1000-year event at periods greater than 0.2 sec.

5000-Year Event

112. The 5000-year event is intended to represent a large earthquake at a short distance. The calculated response for this event at the four sites indicates that moderate to large peak accelerations and very large shear straining can be expected for this type of event. Large de-amplification of motion at periods less than 0.2 sec and small to moderate amplification of motion at greater periods is likely. The range of spectra is typically narrow. Discussion of the data is presented below.

Acceleration versus time

113. The calculated motions for the top of each layer for the four sites and two horizontal input motions are presented in Appendix N. A comparison of peak accelerations is made in Table 13. The propagation of shear waves through the four soil columns with two different horizontal earthquake components produced large de-amplification of peak acceleration. The peak horizontal accelerations at free field (ground surface) range from 0.24 g to 0.36 g compared to the peak accelerations of 0.54 and 0.63 g for rock outcrop and 0.46 g to 0.59 g for base rock motions.

Shear strains versus time

114. The calculated effective shear strains at each contact between soil layers for four sites and two horizontal components are presented in Appendix O. The peak (effective) shear strains for each column are listed in

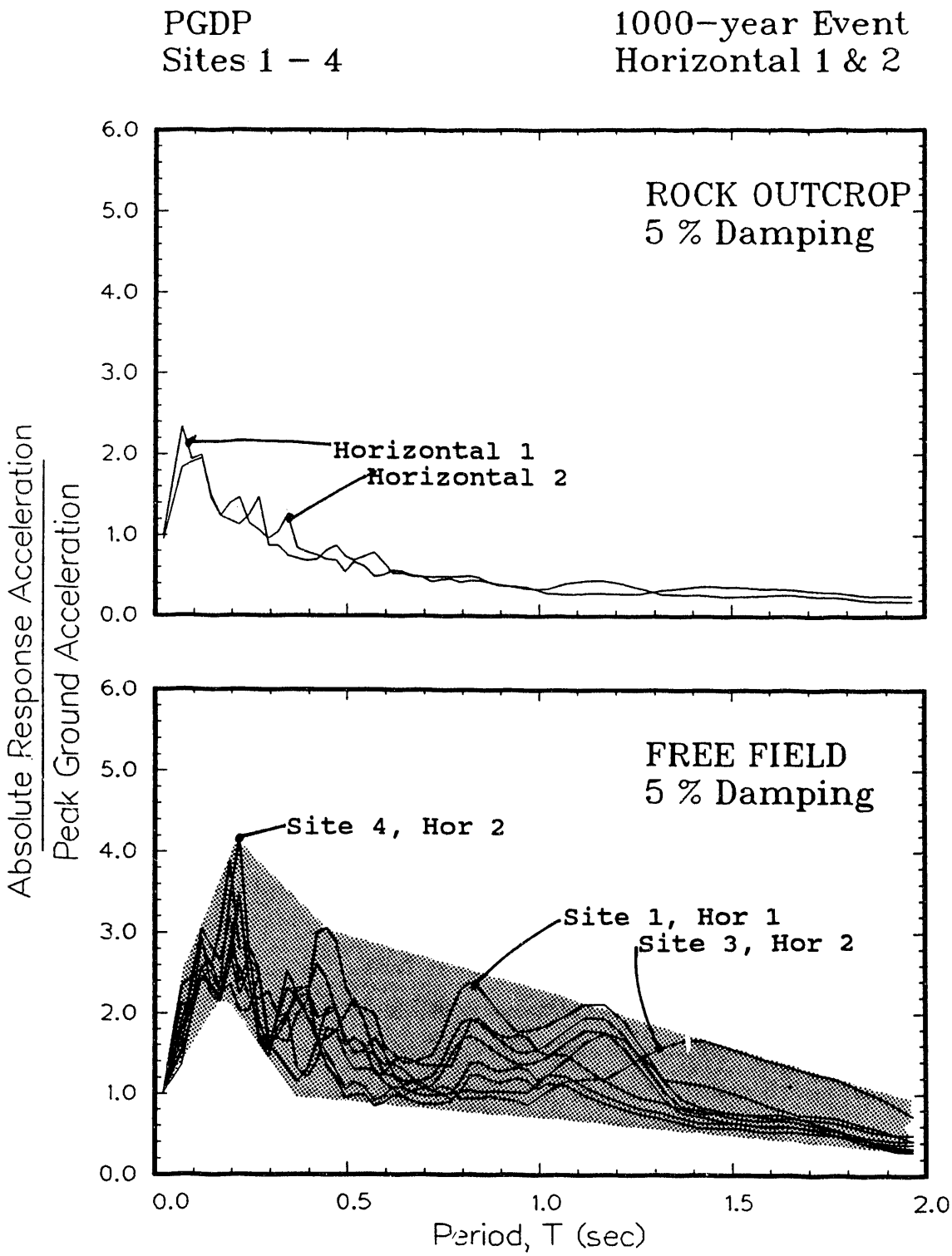

Figure 46. Amplification ratio for 1000-year event

Table 14 and are fairly consistent among sites and earthquake components, ranging from 0.18 to 0.23 percent with one value at 0.33 percent. The peaks occur in the lowest layer except at Site 3 where they occur in the layer above the rubble zone. The peak shear strains in other layers are as low as 0.010 percent.

Table 13
Peak Accelerations for 5000-Year Event

		Peak Acceleration (g)		
	Component	Rock Outcrop	Base Rock	Free Field
Site 1	Horizontal 1	0.54	0.50	0.30
	Horizontal 2	0.63	0.58	0.31
Site 2	Horizontal 1	0.54	0.50	0.30
	Horizontal 2	0.63	0.59	0.30
Site 3	Horizontal 1	0.54	0.46	0.26
	Horizontal 2	0.63	0.56	0.24
Site 4	Horizontal 1	0.54	0.50	0.30
	Horizontal 2	0.63	0.59	0.36

115. In general, the magnitudes of calculated shear strains correspond to a very large amount of straining. The range of shear modulus for soils corresponding to these strains is 73 to 13 percent of the small-strain modulus. The range in damping ratio is between 11 and 14.7 percent (NRC cap not enacted) for soils.

Pseudo-velocity spectra

116. The pseudo-velocity response spectra for the four individual sites are presented in Appendix P. The combined spectra at five percent damping for all sites and both horizontal components are shown in Figure 47. The eight spectra produce a fairly narrow range at site periods less than 0.13 sec and a narrow to moderate range at greater periods. The peak spectral velocity is 70 in./sec at a period of 1.2 sec.

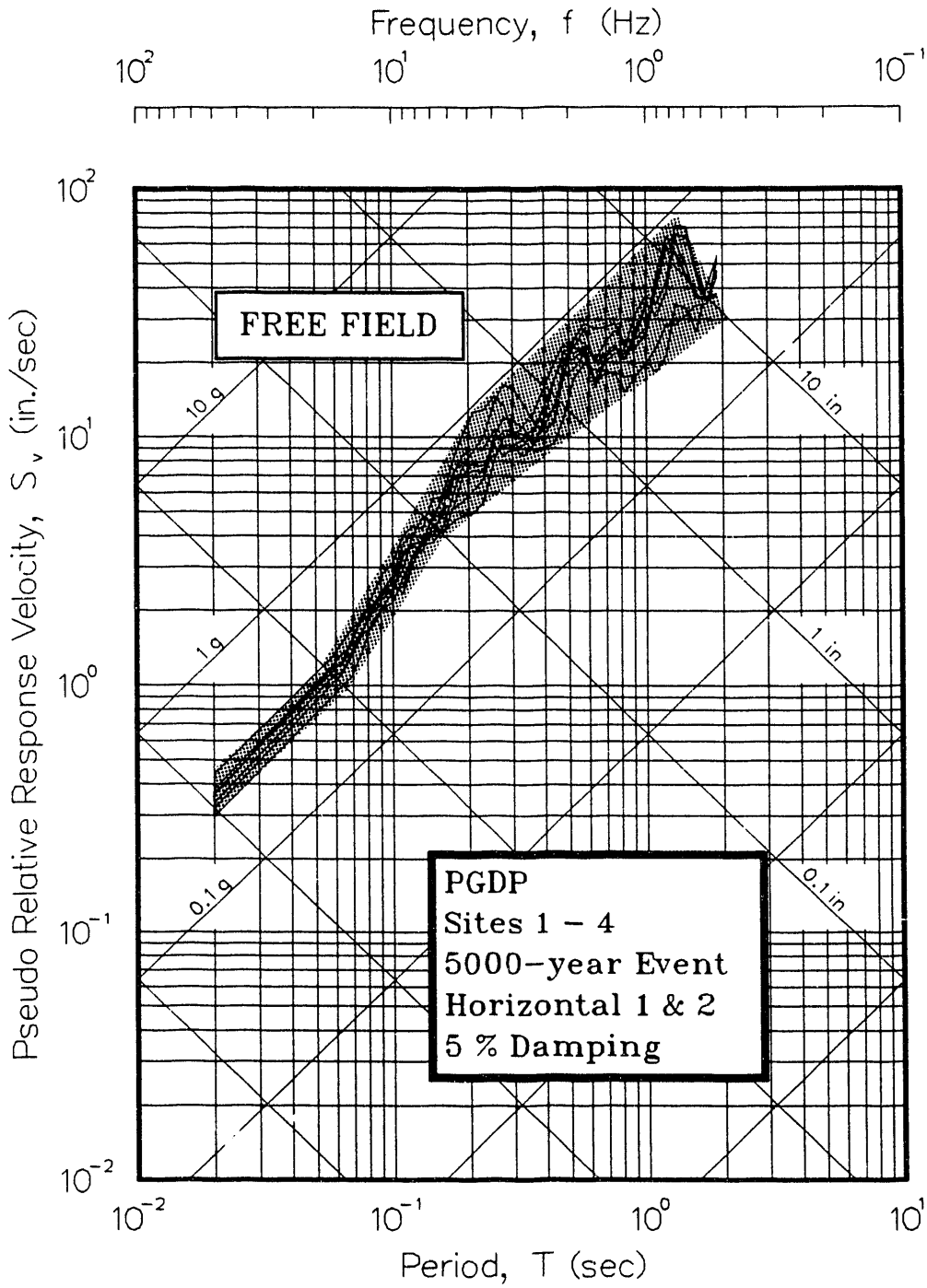

Figure 47. Pseudo-velocity response spectra for 5000-year event

117. Tri-linear relationships representing an upper bound and a lower bound are shown in Figure 47. The shape and locations of these relationships differ significantly from those developed for the 500-year and 1000-year events at periods greater than 0.2 sec. The spectra between periods of 0.07 and 0.2 sec are very similar for the 1000-year and 5000-year events. At greater periods, however, the spectra rapidly increase in velocity. The upper bound is at a constant spectral acceleration (0.9 g).

Table 14

Peak Shear Strains for 5000-Year Event

	Component	Depth (ft)	Peak Effective Shear Strain (percent)
Site 1	Horizontal 1	301.5	0.22
	Horizontal 2	301.5	0.22
Site 2	Horizontal 1	304.5	0.22
	Horizontal 2	304.5	0.21
Site 3	Horizontal 1	305.0	0.22
	Horizontal 2	305.0	0.33
Site 4	Horizontal 1	297.0	0.19
	Horizontal 2	297.0	0.18

Absolute acceleration spectra

118. Absolute acceleration response spectra for the four individual sites are presented in Appendix Q. The combined spectra at five percent damping for all sites and both horizontal components are shown in Figure 48 with some spectra identified. The combined free-field spectra indicate that the largest spectral accelerations is 1.0 g at a period close to 0.2 sec corresponding to Site 4. These accelerations are actually slightly less than those calculated for the 1000-year event. Large spectral accelerations also occur at periods of 1.0 to 1.1 sec. The range of relationship representing the upper bound and lower bound of data are is shown in Figure 48. The large spectral accelerations at high periods cause the upper bound to change very little with period.

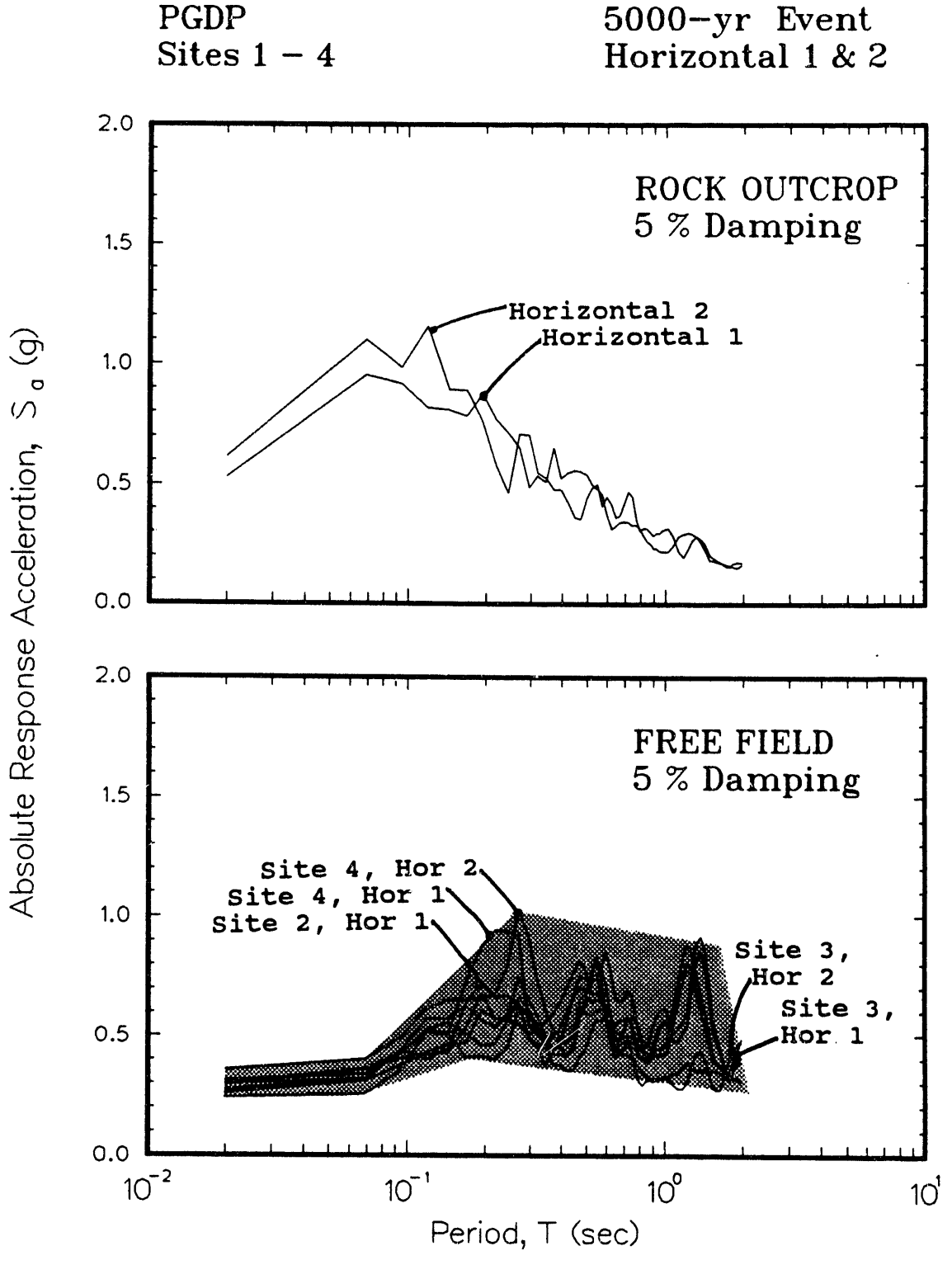

Figure 48. Absolute response acceleration spectra for 5000-year event

Ratio of acceleration spectra

119. The ratios of free field to outcrop acceleration response spectra for the four individual sites are presented in Appendix R. Combined spectra at all sites for both horizontal motions are shown in Figure 49 with some notable spectra identified. The eight spectra show much more similarity than the same presentation for the 500-year and 1000-year events. The response for Site 3 is notably different at periods greater than 0.8 sec, however. This difference is attributed to the effect of the rubble layer. For all sites, large de-amplification is expected at periods less than 0.2 sec. In general, small amplification is expected at periods between 0.2 and 0.8 sec, and moderate amplification is expected at greater periods.

Amplification ratio

120. The ratios of free field spectral acceleration to peak horizontal acceleration for the four individual sites are shown in Appendix S. Combined relationships at all sites for both horizontal motions are shown in Figure 50. The ratios for rock outcrop are also provided for comparison. The range of relationships is moderately-wide.

121. The amplification ratios for the 5000-year event are very different from those corresponding to the 500-year and 1000-year events as seen by the shape of the range shown in Figure 50 (refer to Figures 42 and 46). In general, the ratio for the 5000-year event shows a significant decrease at periods less than 1 sec and a significant increase at greater periods. The peak value is reduced from about 4 to 3.

Conclusions

122. The four sites respond similarly for a given event for a system damping of 5 percent even though the subsurface geology is different at Site 1. The response at Site 1 was notable in only a few instances. The general shape of the variation of acceleration and shear strain with time as the shear waves propagate upwards through the column is also similar among sites and events. However, the peak accelerations at Site 4 with the Horizontal 2 component and the shear strains at Site 3 tend to be significantly larger. There appears to be only minor differences between the responses calculated with the two components of motion for any given event.

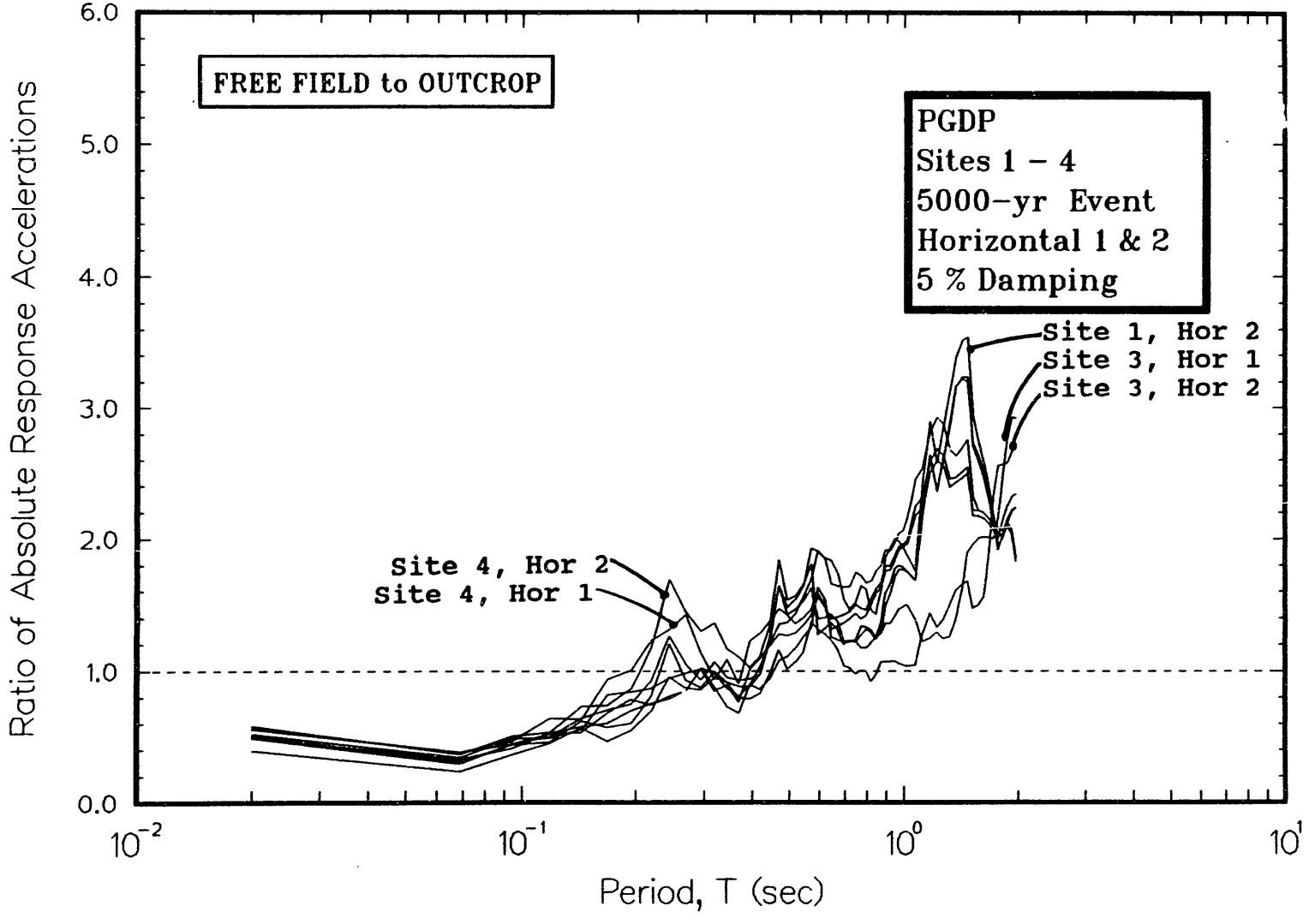

Figure 49. Ratio of free field to rock outcrop absolute acceleration response spectra for 5000-year event

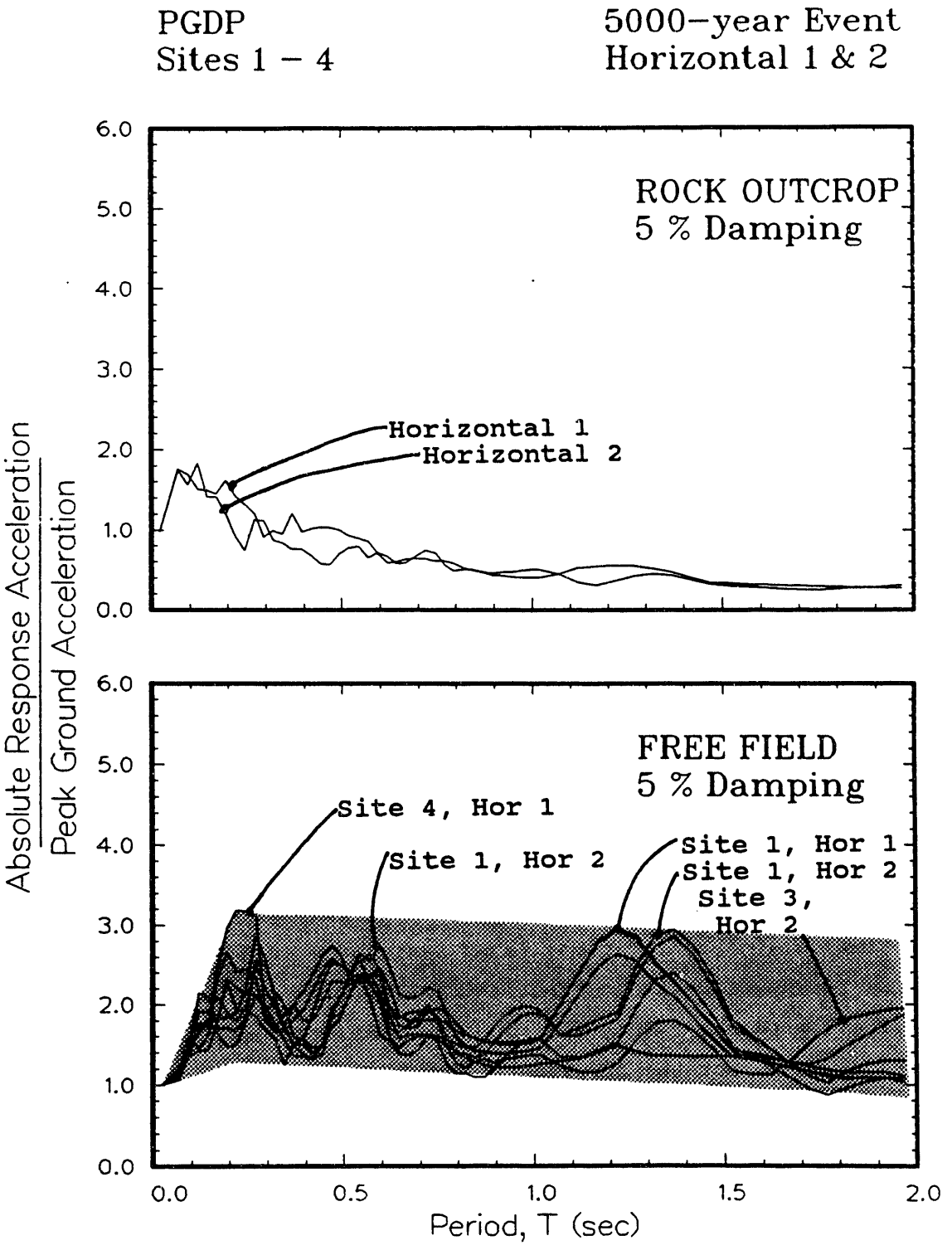

Figure 50. Amplification ratio for 5000-year event

123. The calculated peak horizontal accelerations are relatively consistent (less Site 4 and the Horizontal 2 component). The free-field peak accelerations were de-amplified for all three events. The ranges overlap somewhat: 0.14 to 0.20 g for the 500-year event, 0.18 to 0.27 g for the 1000-year event, and 0.24 to 0.36 g for the 5000-year event. The peak free field accelerations for the 5000-year event are about 45 percent greater than those calculated for the 1000-year event and 75 percent greater than those calculated for the 500-year event. The natural site period ranges from 0.9 to 1.1 sec.

124. A significant amount of modulus degradation and damping are expected because of the large shear strains. The calculated ranges of effective shear moduli for the three events are: 86 to 59 percent of maximum for the 500-year event, 80 to 48 percent for the 1000-year event, and 73 to 13 percent for the 5000-year event. Similarly, the damping ratios for the layers ranged from 4 to 8 percent, 4 to 9 percent, and 5 to 14.7 percent for the 500-year, 1000-year, and 5000-year events, respectively.

125. Some consistent trends were found in response spectral values at 5 percent system damping. Peak spectral velocities increase tremendously as the severity of motions increases. Between 0.9 and 1.1 sec, the peak velocities are 18, 26, and 70 in./sec for the 500-year, 1000-year, and 5000-year events, respectively. Conversely, peak spectral accelerations increase until shear strains become too severe. The peak spectral accelerations are 0.75, 1.15, and 1.0 g for these three events, respectively, and occur at a period of 0.2 sec. The ratio of spectral accelerations at free field over rock is as large as 4.6 at the natural period and decrease with increasing severity of motion. The amplification ratio (spectral acceleration normalized to peak time-domain acceleration) is as large as 4 at a period of 0.2 sec. The ranges in amplification ratios for the 500-year and 1000-year events are very similar, with the values for the 1000-year event being slightly greater. However, the range for the 5000-year event suggests a wide range of strong response.

PART VI: SENSITIVITY ANALYSIS USING AVERAGE COLUMN

126. An important aspect of any site response analysis is an evaluation of how various system and site parameters affect the calculated results because the site has been idealized—all the information for the site has been summarized in a finite number of soil columns. Soil and rock parameters were evaluated because of the variability and/or uncertainty associated with each as noted throughout this report. The sensitivity to system parameters (e.g., those listed in Table 8) were performed for this study and found to have negligible effect and, therefore, are not discussed further.

127. The sensitivity analysis of site parameters for this study was conducted using the average column described in Part III. Details of the average column are presented in Table 15. Stress-adjusted shear modulus and damping ratio relationships were assigned to each layer. Results for all three earthquake events using all six presentation formats are reported in Appendices T, U, and V. The best-fit, upper bound, and lower bound of moduli were considered. (Note that results are not reported for the 5000-year event using the lower bound of moduli because shear strains exceeded 1 percent.) The results for the 1000-year event using the tripartite format are presented below. Six different variations were considered: shear wave velocity inversion, depth to bedrock, impedance ratio, shear modulus relationship, damping ratio relationship, and maximum shear modulus.

128. Each of these inputs was evaluated because of uncertainties noted throughout this report. A shear wave velocity inversion was measured at Site 3 but not at Site 4. The depth to bedrock was considered because boreholes were extended to bedrock only at Sites 3 and 4. The assignment of shear modulus and damping ratio relationships was considered because "average" relationships actually represent a range of relations and site-specific measurements were not available. Furthermore, it was not possible to consider many variations in damping ratio in the analysis of individual columns. Maximum shear modulus was considered because of the idealization of shear wave velocity profiles and the lack of measured data at some depths for some sites, especially at greater depths.

129. The response of the average column to two components of the 1000-year event is shown in Figure 51 and compared with the range of individual responses (refer to Figure 43). The spectra for the average column fall

Table 15

Parameters Defining Average Soil Column

Layer	Thickness (ft)	General Soil Classification	Shear Wave Velocity (fps)			Relationships	
			Lower Bound	Average	Upper Bound	σ'-Adj. Modulus	Damping
1	10	Silty Clay	425	600	850	C10	C
2	10	"	495	700	990	"	"
3	10	"	670	950	1,345	"	"
4	28	"	780	1,100	1,555	C20	"
5	17	Clayey Sand	780	1,100	1,555	C10	S
6	27	Sand & Gravel	885	1,250	1,770	"	"
7	10	"	840	1,190	1,685	"	"
8	10	Silty Clay	935	1,325	1,875	C20	C
9	10	"	895	1,265	1,790	C40	"
10	63	Sand, Silt, Clay	990	1,400	1,980	"	"
11	50	Clayey Silt	1,095	1,550	2,190	C20	"
12	20	Silty Sand	1,095	1,550	2,190	C40	SG
13	70	"	970	1,370*	1,935	"	"
Total	335						
ROCK			6,000	8,500	12,000		

* Set equal to 1,550 fps for case of no velocity inversion.

C10: 5 < PI < 10
C20: 10 < PI < 20
C40: 20 < PI < 40

C: Average clay
S: Average sand
SG: Lower-bound sand

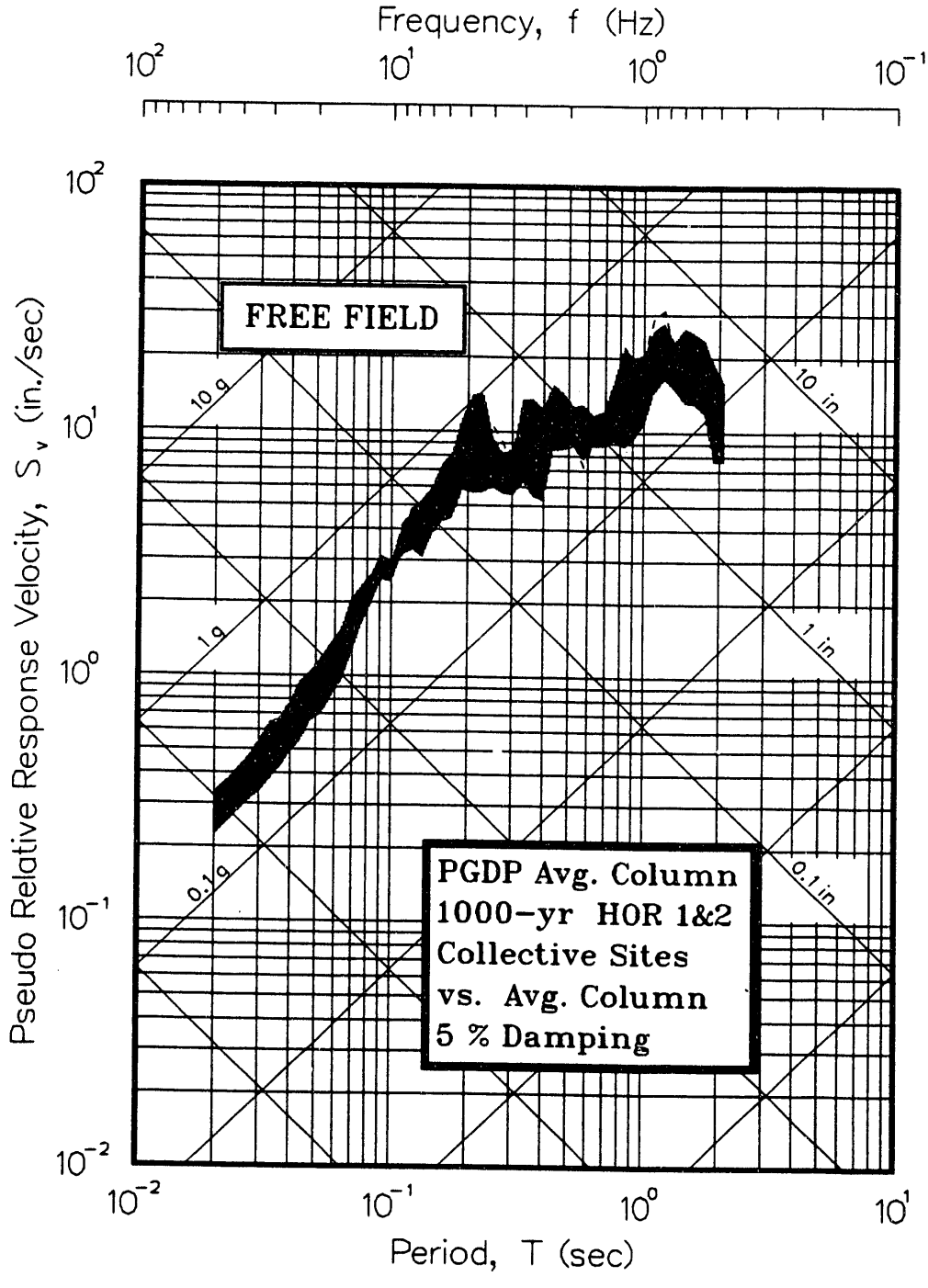

Figure 51. Comparison of results for average column and range produced from individual sites

within the range at nearly all periods. Therefore, the average column spectra are considered to be representative. The two average column spectra are used as a baseline (shown as dashed lines throughout) for comparison with sensitivity studies described below.

Velocity Inversion

130. As noted in Part III, an inversion in the shear wave velocity profile was measured at Site 3 at depths between 265 and 334 ft (refer to Figure 17). An inversion of lesser magnitude was proposed in the average column idealization as shown in Figure 31 and Table 15. The effect of including this inversion was evaluated by comparing the results with a profile with a constant shear wave velocity at depths below 140 ft. The alternate profiles of shear wave velocity and shear modulus are compared in Figure 52. The comparison of velocity spectra for both horizontal components corresponding to the average column with and without the velocity inversion is made in Figure 53. The differences between the spectra are small and inconsistent. The profile with the inversion tends to produce slightly greater spectral velocities at low periods and slightly lesser velocities at high periods. Given this insignificant difference, the average column with velocity inversion is included for the remaining comparisons.

Depth to Bedrock

131. The depth to bedrock was varied $\pm$ 10 percent of the total column height ($\pm$ 33 ft). The variation in the depth to bedrock should generally be within this range given the geologic setting. The variation was applied to the bottom-most layer. The response was calculated for both components of horizontal motion and the results are shown in Figure 54. The depth to bedrock has a small to negligible effect on the response at low periods and a small effect on the response at periods greater than 0.13 sec. Based on these results, the sensitivity of calculations to reasonable ranges in depths to bedrock is categorized as being low.

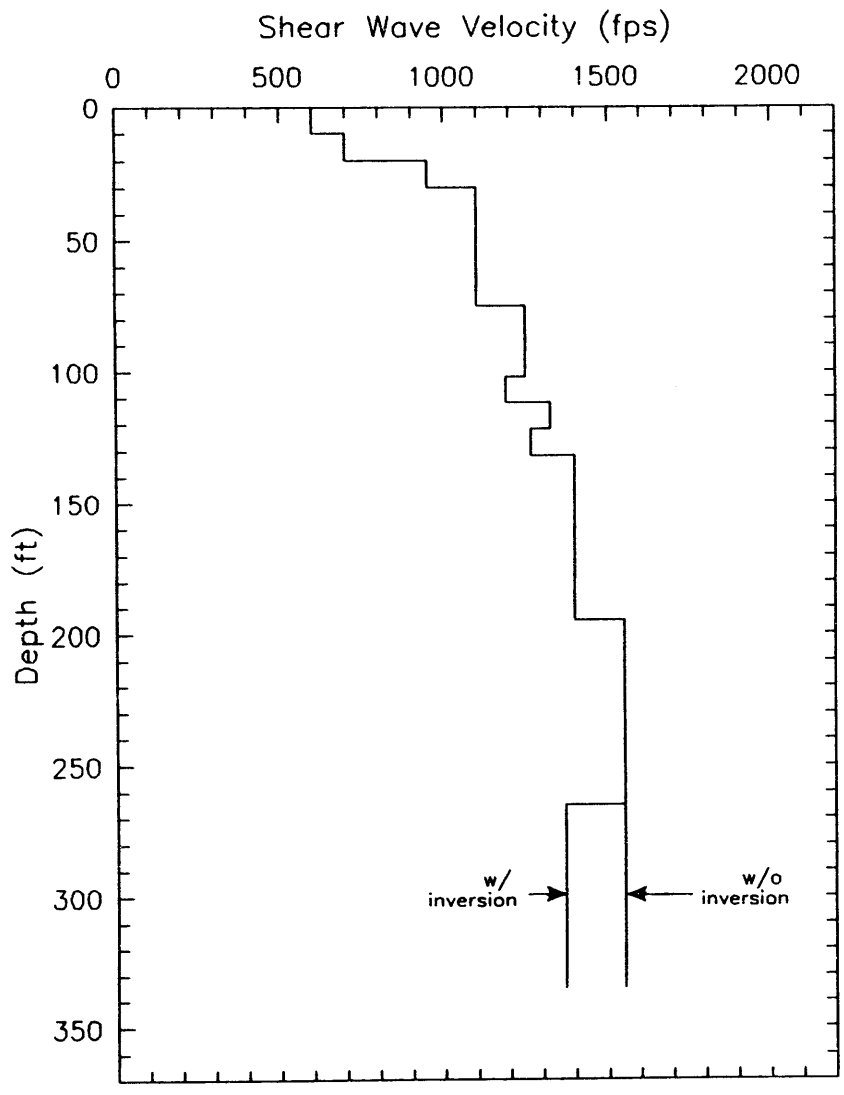

a. Shear wave velocity

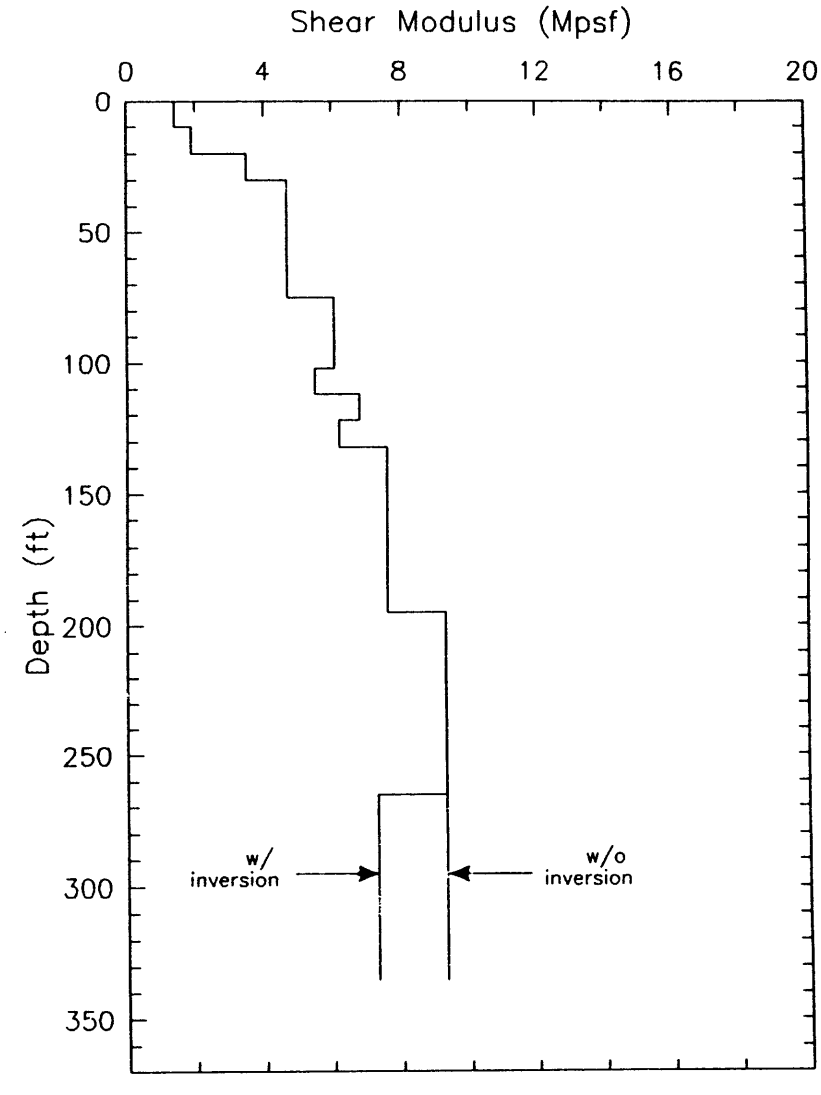

b. Shear modulus

Figure 52. Combined profiles of soil stiffness for average column with and without shear wave velocity inversion

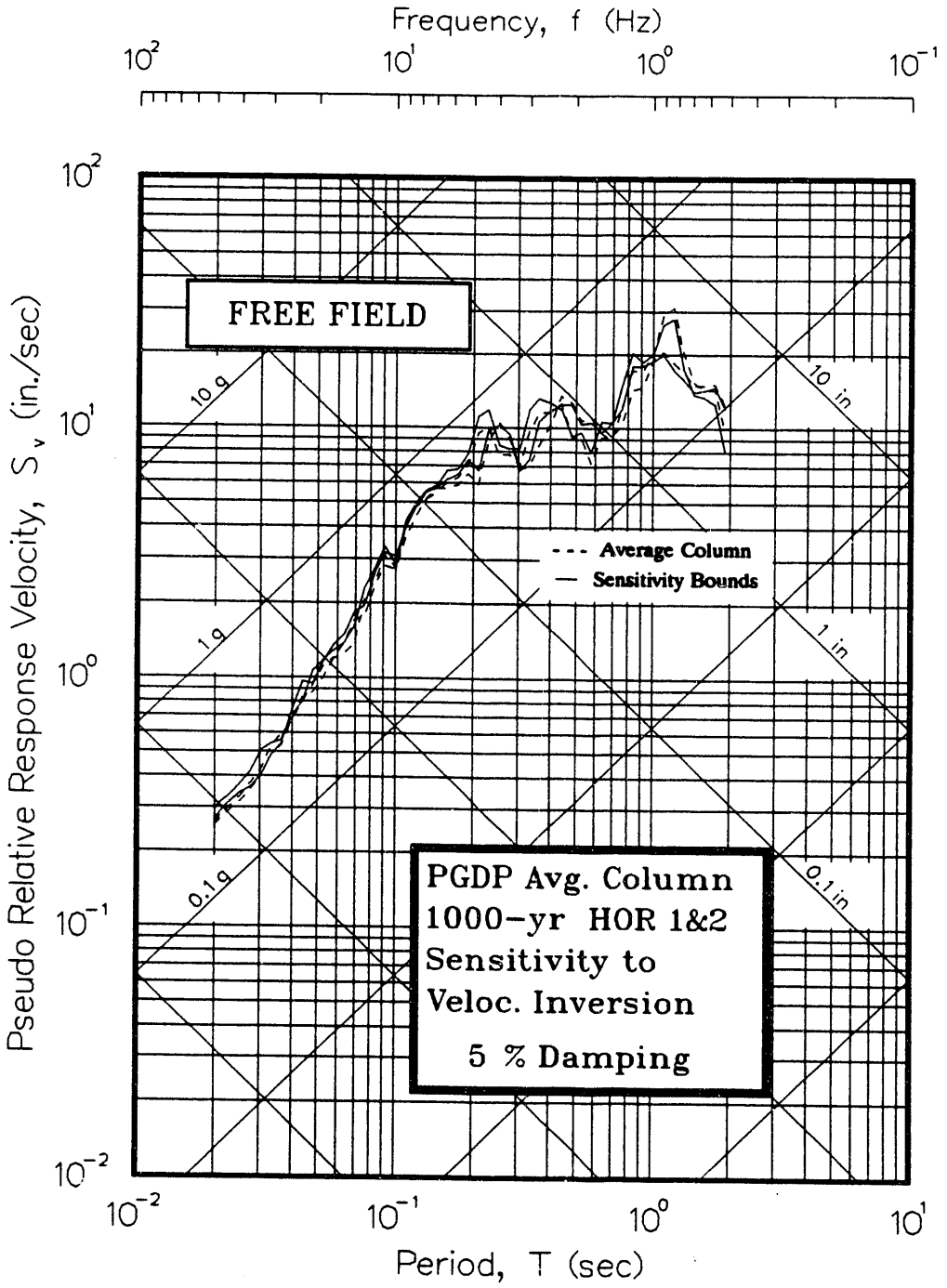

Figure 53. Pseudo-velocity response spectra showing sensitivity of results to shear wave velocity inversion

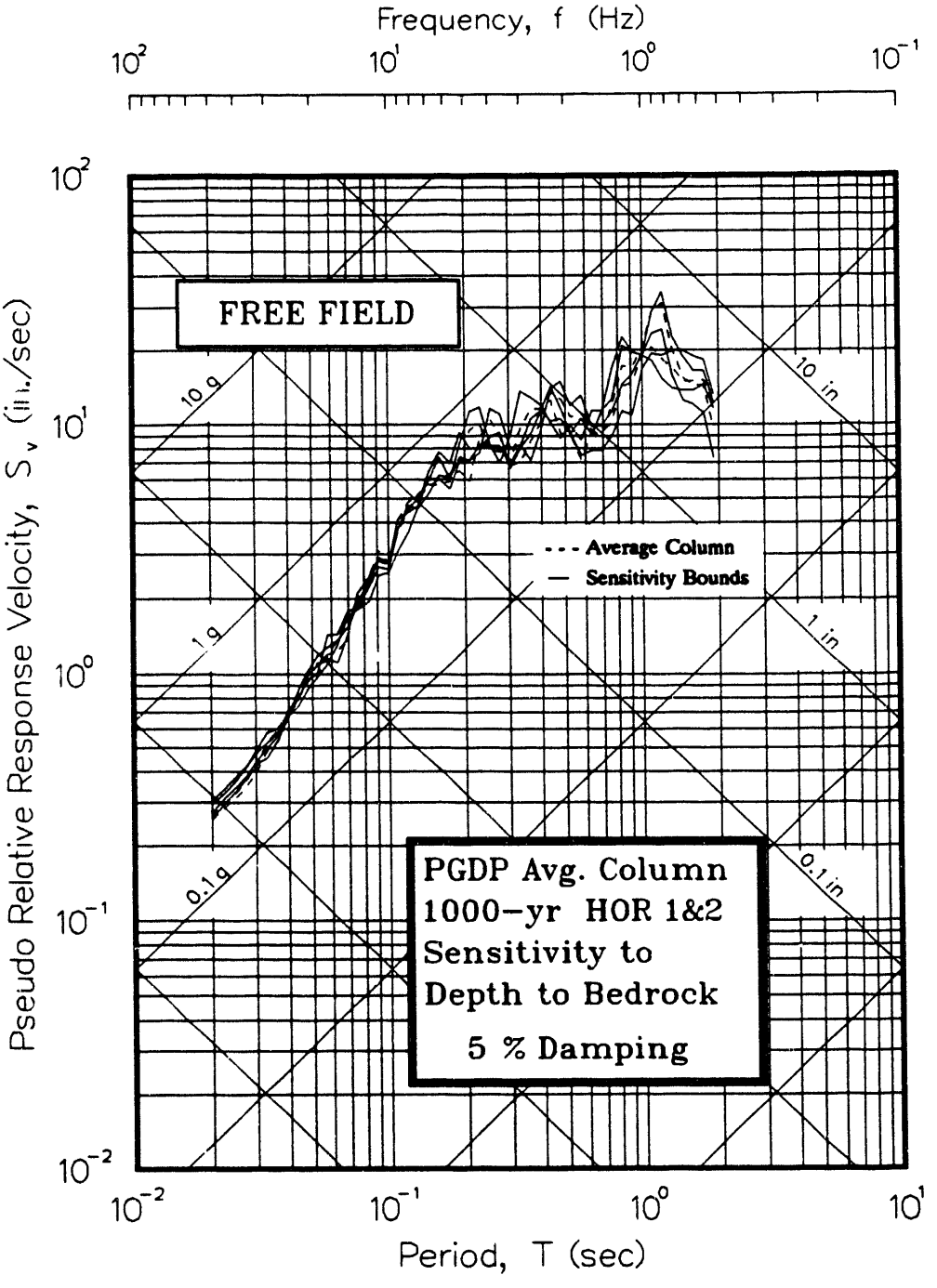

Figure 54. Pseudo-velocity response spectra showing sensitivity of results to depth of bedrock

Impedance Ratio

132. The shear wave velocity of bedrock was varied by ± 20 percent (± 1,700 fps) to evaluate the effect of impedance ratio on calculated response. This range roughly corresponds to data from investigations of similar materials at other large project sites. The pseudo-velocity response spectra for each velocity and both horizontal components are shown in Figure 55. The impedance ratio can be seen to have a negligible effect on calculated response for the stated bounds.

Modulus Relationships

133. The effect of shear modulus relationships was evaluated by reassigning each material with an adjacent curve from the family of curves shown in Figure 25a. Both cases of adjusting all curves up one and down one were used to develop the sensitivity bounds. This variation represents a reasonable bounds for this parameter and is roughly equivalent to quartile relationships for standardized relationships (refer to Figure 23a). The results of the calculations are shown in Figure 56. The impedance ratio can be seen to have only a small effect on calculated response for the stated bounds.

Damping Ratio Relationships

134. The effect of damping ratio relationships was evaluated by using the upper and lower bounds of published relationships (e.g., those shown in Figure 23 for cohesionless soils). These bounds are significantly greater than those used for the modulus relationships but was used because only three best-fit damping relationships were used in the individual site response calculations. The results are shown in Figure 57. The range of response is greatly expanded at low periods by changing the damping relationships as stated. However, at periods greater than about 0.5 sec, the effects diminish significantly. Most of the differences appear to be in amplitude of spectral velocity; there are no apparent period shifts of the predominant peaks. The lesser-damped response (upper sensitivity bounds) has spectral velocities on the order of 50 percent greater than the average column response between

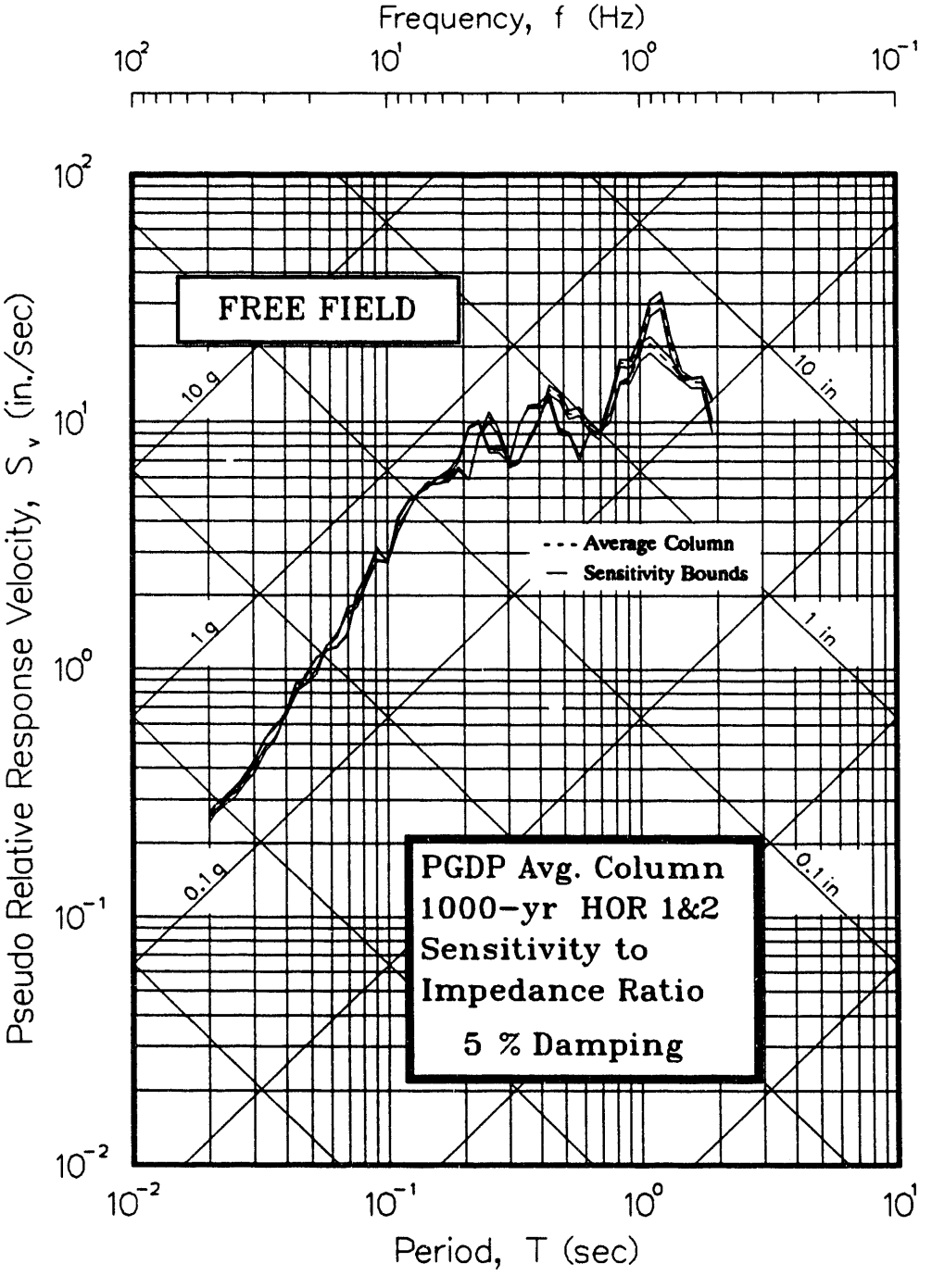

Figure 55. Pseudo-velocity response spectra showing sensitivity of results to impedance ratio

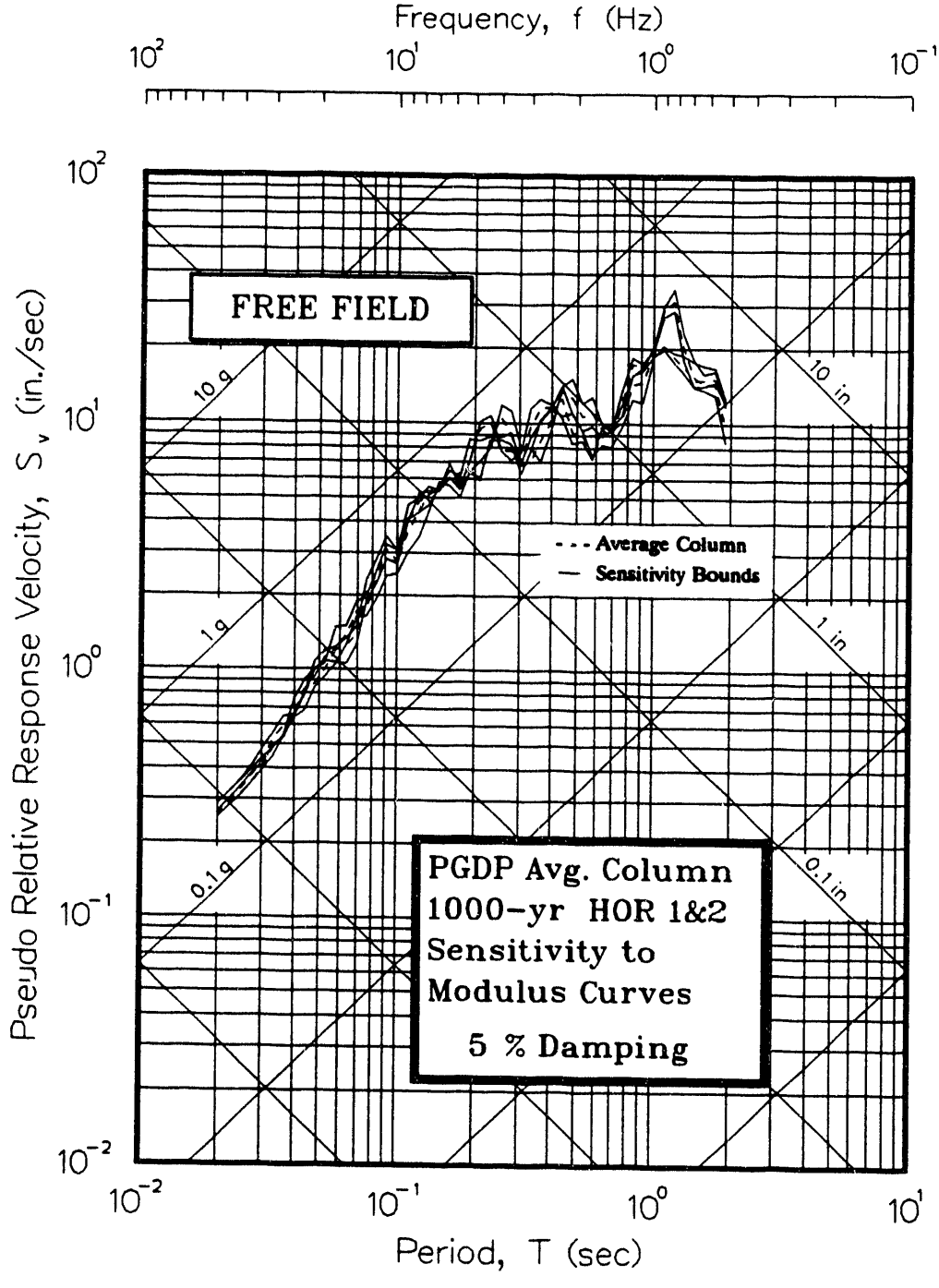

Figure 56. Pseudo-velocity response spectra showing sensitivity of results to modulus curves

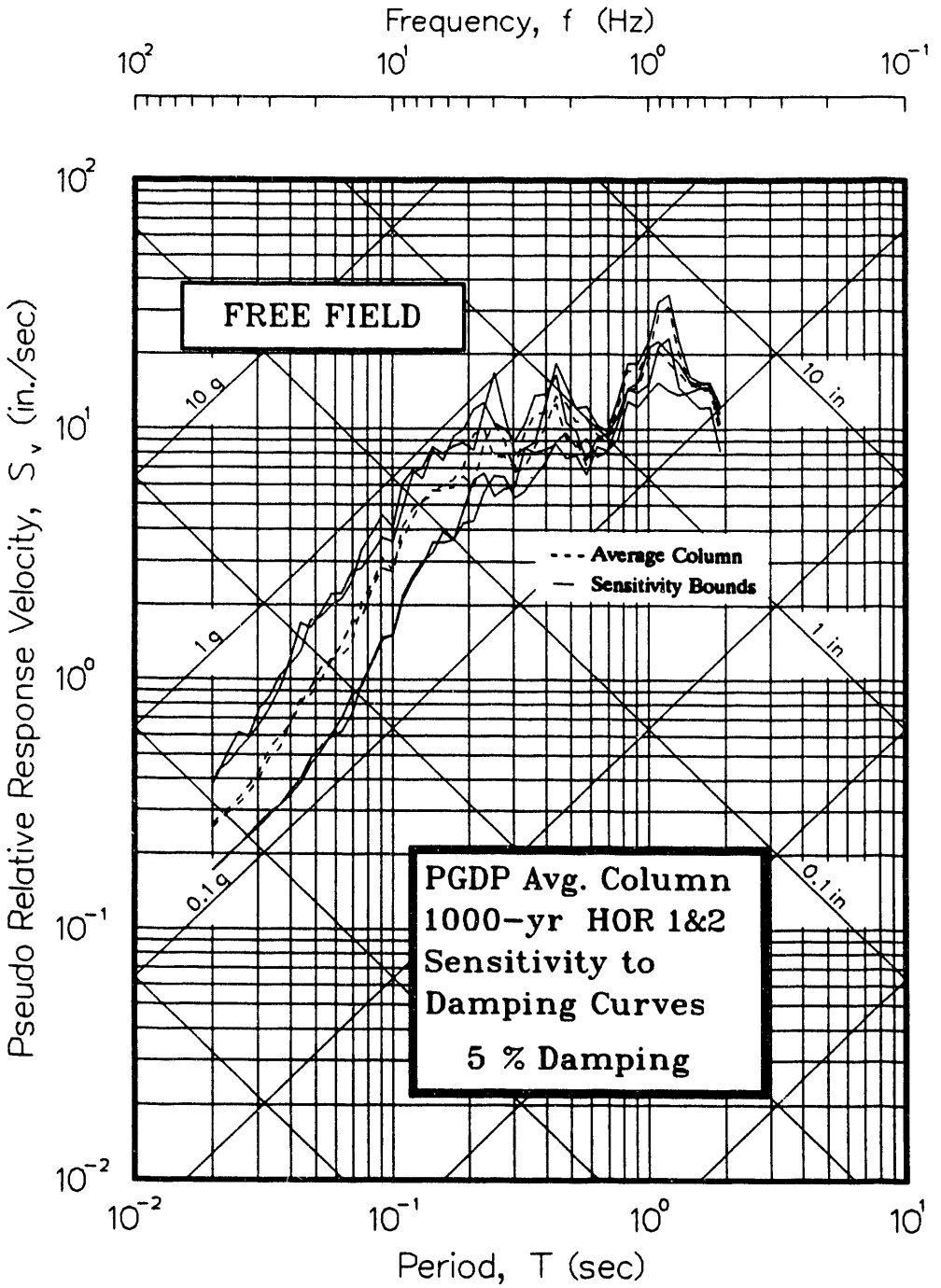

Figure 57. Pseudo-velocity response spectra showing sensitivity of results to damping ratio curves

0.02 and 0.1 sec. Notice that the upper sensitivity bounds shown in Figure 57 correspond well with the upper bound of the range defined by the collection of individual site response at periods greater than 0.2 sec (refer to Figure 51).

Maximum Shear Modulus

135. The NRC Standard Review Plan (Nuclear Regulatory Commission 1989) specifies upper and lower bounds of maximum shear modulus for use in seismic safety assessments. The bounds are defined by:

Lower bound:

$$(G_{max})^{lb} = \frac{G_{max}}{2.0} \tag{5}$$

Upper bound:

$$(G_{max})^{ub} = 2.0 \cdot G_{max} \tag{6}$$

These bounds were used to define very conservative limits to the range of shear modulus for the average column. The rock velocity was also adjusted to negate any combined effects of varying impedance ratio. A comparison of the shear wave velocity and shear modulus profiles for the average column and the corresponding lower and upper bounds is shown in Figure 58 (similar to Figure 31). The profiles for the individual columns are also shown for comparison. All measured values fall within the NRC upper and lower bounds. The shear wave velocities for the upper and lower bounds are also listed in Table 15.

136. The results for the sensitivity to shear modulus are shown in Figure 59. The maximum shear modulus has a very important effect on calculated response. The results for the lower bound moduli represent the lower sensitivity bounds at low periods and the upper sensitivity bounds at periods greater than 1.0 sec and vice versa for the upper bound moduli. Much of this difference is due to a general shifting in period of the spectra—the lower bound moduli produce an increase in natural period and vice versa. The wide range of measured velocities at the site, then, serve to create a wide range of calculated site response. The upper sensitivity bound is within the range of the collection of individual site response at periods greater than 0.12 sec.

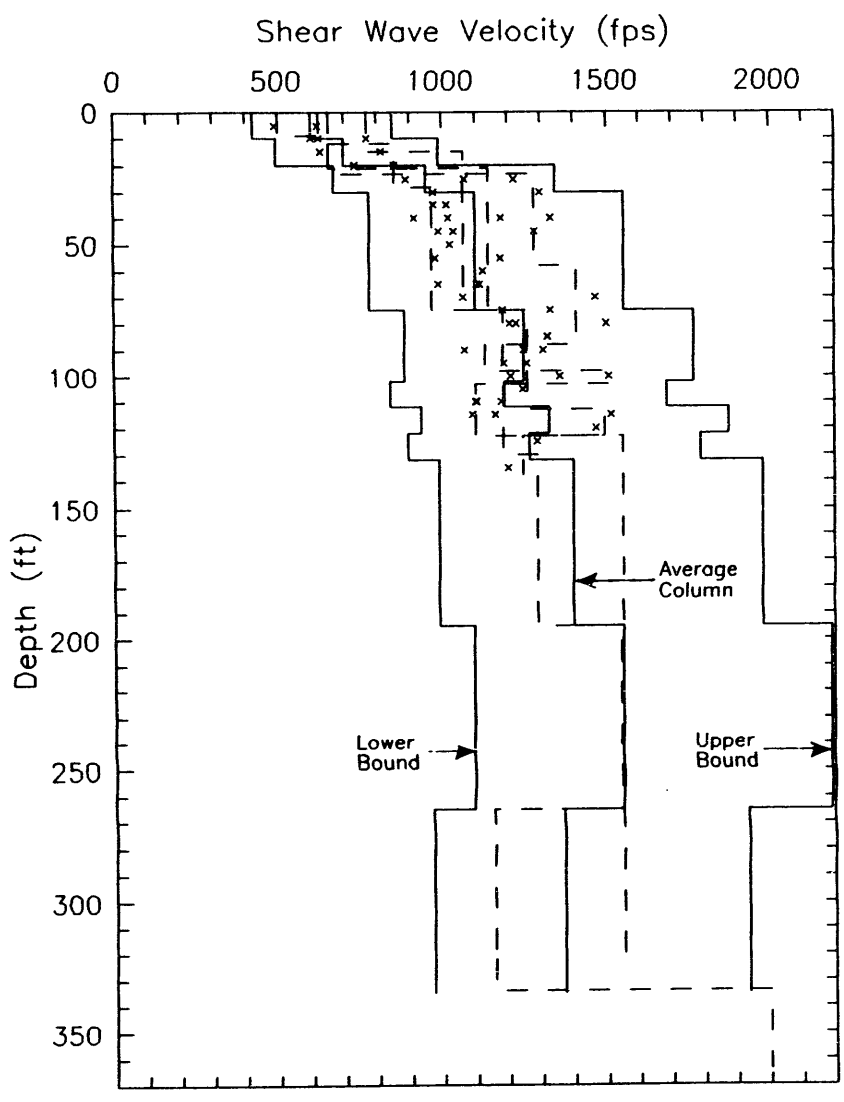

a. Shear wave velocity

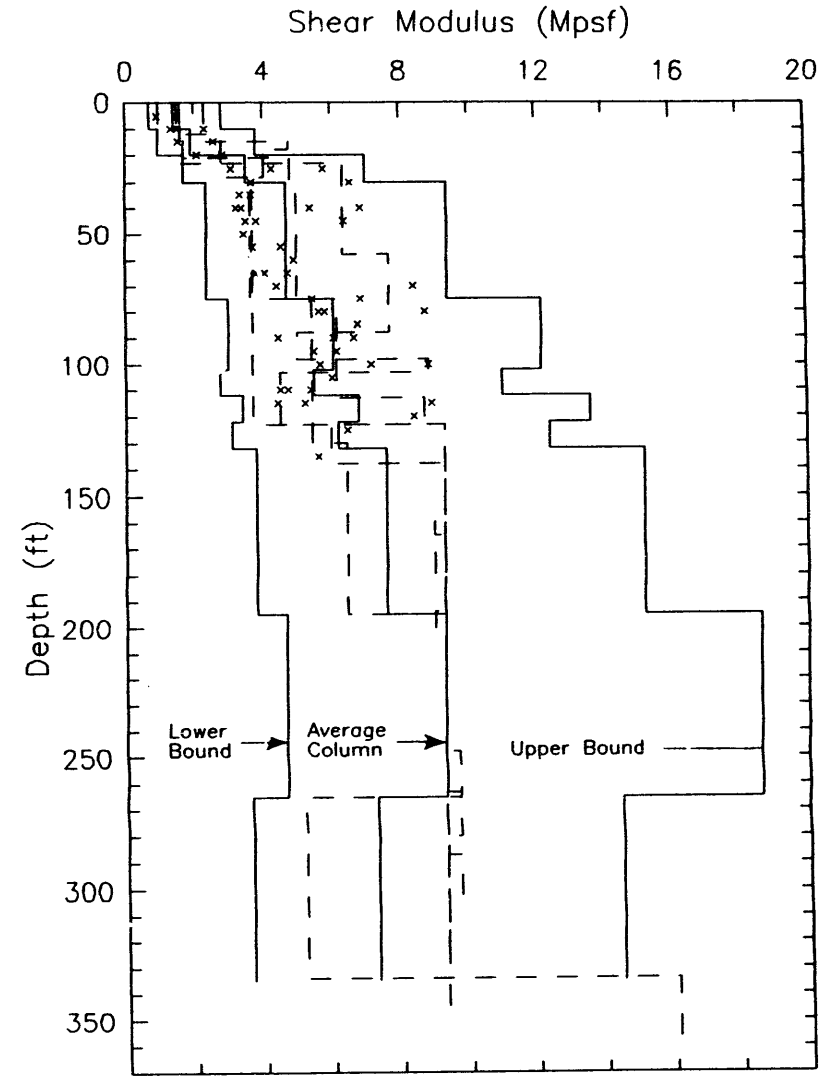

b. Shear modulus

Figure 58. Combined profiles of soil stiffness for average column with upper and lower sensitivity bounds

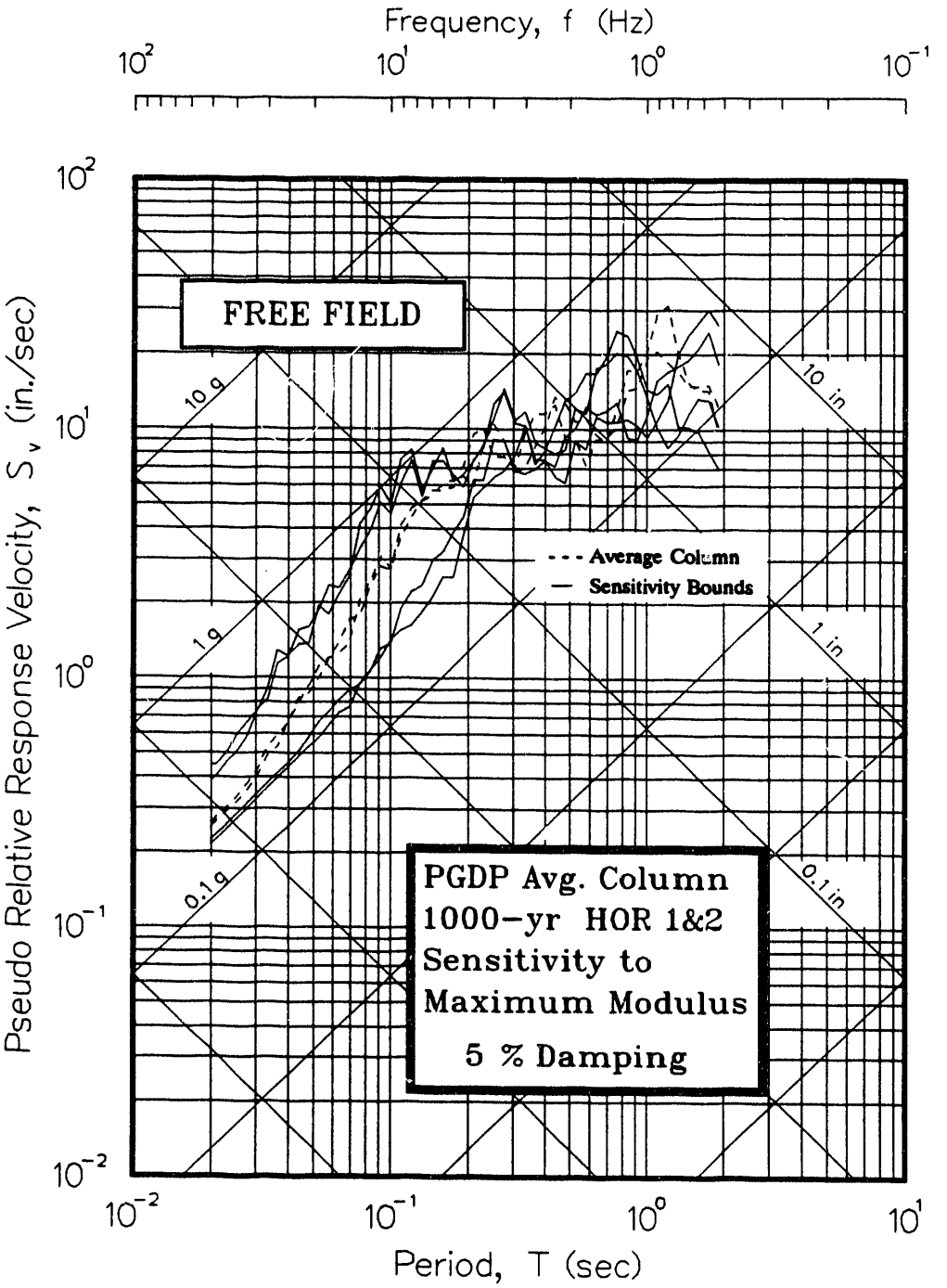

Figure 59. Pseudo-velocity response spectra showing sensitivity of results to maximum shear modulus

PART VII: SUMMARY AND CONCLUSIONS

137. The site-specific, free-field, earthquake response was calculated for four, idealized, one-dimensional soil columns at the Paducah Gaseous Diffusion Plant. Two components of three design earthquakes, a 500-year event, a 1000-year event (DBE), and a 5000-year event, were used for the analysis. The computer program *SHAKE* was used on a U.S. Army CRAY Y-MP supercomputer to perform the calculations and determine site response. *SHAKE* has been validated for horizontal response calculations at periods less than 2 sec on numerous occasions and consequently is widely accepted in the geotechnical earthquake engineering profession as a useful tool for site response analysis.

138. The results for the collection of individual columns are believed to represent reasonable expected response to vertically-propagating, horizontally-polarized shear waves. Assumptions and interpretations required to conduct the study were usually made within the bounds of reasonable values with a slight bias toward values that would produce a slightly conservative response. Potential variations across the site that could exist beyond values adopted for soil columns were evaluated through sensitivity analyses.

139. In general, the eight spectra calculated for each earthquake (using the four sites and two components of input motion) produced a fairly narrow range of response. This narrow range exists despite the separation distances between sites, noted differences in companion components of the earthquake motions, and the different geology at Site 1 (inclusion of Porter's Creek Formation); it suggests that the response is dominated by the thickness of the soil and the average shear wave velocity of the profiles.

140. Standard relationships between the normalized shear modulus and damping ratio versus shear strain were used since site-specific data were not available. Relationships were initially assigned based on soil classification and/or PI. The assignments for shear modulus were then adjusted to account for the potential effects of effective confining (overburden) stress. This procedure was considered to be appropriate because of the large confining stresses caused by thick soil deposits (322 to 364 ft). Similar adjustments were not made for damping relationships because of limitations in *SHAKE*.

141. In nearly all cases, the peak accelerations at free field were found to be de-amplified from rock outcrop values. The percentage of de-

amplification increased as the severity of motions increased. The peak accelerations were calculated to be 0.20, 0.27, and 0.36 g for the 500-year, 1000-year, and 5000-year events, respectively. The de-amplification is attributed to considerable amounts of shear straining. Peak (effective) shear strains of 0.026, 0.061, and 0.33 percent were calculated for the 500-year, 1000-year, and 5000-year events, respectively. These peak values typically occur in layers above contacts with large impedance ratios. As the shear strains increase for larger motions, the layers with the greatest straining exist at the base of the soil column (except at Site 3 where the layer with the most straining is above the rubble zone).

142. The natural site period ranges from 0.9 to 1.2 sec. Peak spectral velocities of 18, 26, and 70 in./sec for the 500-year, 1000-year, and 5000-year events, respectively, occur in this range of periods at a system damping of 5 percent. Peak spectral accelerations of 0.75, 1.1, and 1.0 g for these three events, respectively, occur at a period of 0.2 sec. The ratio of spectral accelerations at free field over rock are as large as 4.6 at the natural period and decrease with increasing severity of motion. The amplification ratio (spectral acceleration normalized to peak time-domain acceleration) are as large as 4 at a period of 0.2 sec.

143. A sensitivity analysis was conducted using an average column to represent the site and the DBE (1000-year event). The response calculated using the average column was compared with the range of response calculated using the collection of individual site responses and found to be comparable. Therefore, the average column is considered to be a suitable representation for sensitivity analysis.

144. Six different geotechnical parameters were evaluated to determine their effect on the calculated response. Four of these parameters—velocity inversion, depth to bedrock, impedance ratio, and assignment of modulus degradation relationships—were varied within reasonable bounds defined by the range of measured values. The results of these evaluations suggest that none of these parameters have an important effect. The depth to bedrock and assignment of modulus relationships are the most important of the four, but the calculated response has a low sensitivity to both of these parameters. The two other parameters—assignment of damping ratio relationships and maximum shear modulus—were varied considerably more. The results of these evaluations suggest that consideration of a maximum possible range of input values will

produce a wide range of response. The use of upper bound and lower bound damping ratio relationships significantly affected the amplitude of spectral velocities. The use of the NRC criteria for maximum shear modulus also significantly affects the amplitude as well as the periods of peak spectral velocities.

145. The calculated response for PGDP is also expected to be strongly dependent on the spectral content of the earthquake motions. The predominant periods for the earthquakes are in the range of 0.03 to 0.07 sec. The natural period of the site is in the range of 0.9 to 1.2 sec. If the period of the earthquake is closer to the natural site period, stronger ground motions are expected.

REFERENCES

Automated Science Group, Inc. 1991. "Final Data Package, Geophysical Study of Subsurface Conditions in the Vicinity of the Paducah Gaseous Diffusion Plant," Rpt. ASG/U-101, Oak Ridge, TN, 14 February.

Cooley, J. W. and Tukey, J. W. 1965. "An Algorithm for the Machine Calculation of Complex Fourier Series," Mathematics of Computation, Vol 19, No. 90, pp 297-301.

ERCE 1990a. "Recommended Soil Columns for Use in Amplification Studies, Paducah Gaseous Diffusion Plant, Paducah, Kentucky," Draft Report to Martin Marietta Energy Systems, Inc., ERCE File No. B672, Knoxville, TN, 26 November.

ERCE 1990b. "Final Safety Analysis Report, Section 3.6: Geology and Seismicity," Draft Report to Martin Marietta Energy Systems, Inc., ERCE Project No. 89-B672, Knoxville, TN, 26 November.

Geotechnical Engineers, Inc. 1991. "K-Reactor Area, Geotechnical Investigations for Seismic Issues, Savannah River Site (U)," Rpt. WSRC TR-91-47, Vol 1, March.

Hardin, B. O. and Drnevich, V. P. 1972. "Shear Modulus and Damping in Soils: Design Equations and Curves," Journ., Soil Mechanics and Foundation Engineering, ASCE, Vol 98. No. SM7, pp 667-692.

Iwasaki, T., Tatsuoka, F. and Takagi, Y. 1976. "Dynamic Shear Deformation Properties of Sand for Wide Strain Range," Report Civil Engineering Institute, No. 1085, Ministry of Construction, Tokyo, JAPAN, (in Japanese).

Johnson, J. J. 1980. "Soil-Structure Interaction: The Status of Current Analysis Methods and Research," U.S. Nuclear Regulatory Commission, NUREG/CR-1780, Washington, D.C.

Kanai, K. 1951. "Relation Between the Nature of Surface Layer and the Amplitude of Earthquake Motions," Bull., Tokyo Earthquake Research Institute, Tokyo, JAPAN, (in Japanese).

Kennedy, R. P., Short, S. A., McDonald, J. R., McCann, M. W., Jr., Murray, R. C., and Hill, J. R. 1990. "Design and Evaluation Guidelines for Department of Energy Facilities Subjected to Natural Phenomena Hazards," Lawrence Livermore National Laboratory, UCRL-15910, Livermore, CA.

Lamé 1852. "*Leçons sur la théorie mathématique de l' élasticité des corps solides*," Paris, FRANCE.

Nuclear Regulatory Commission 1989. "Standard Review Plan," NUREG-0800, Section 3.7.2, rev. 2, Office of Nuclear Reactor Regulation, Washington, D.C., August.

Risk Engineering, Inc. 1992. "Pseudo-Velocity Response Spectra and Time Histories, Paducah Gaseous Diffusion Plant," floppy disk to Martin Marietta Energy Systems, Inc., Oak Ridge, TN.

Risk Engineering, Inc. 1993. "Seismic Hazard Evaluation for the Paducah Gaseous Diffusion Plant, Paducah, Kentucky," Report K/GDP/SAR/SUB-1, Martin Marietta Energy Systems, Inc., Oak Ridge, TN.

Roesset, J. M. 1970. "Fundamentals of Soil Amplification," Seismic Design for Nuclear Power Plants, ed. R. Hansen, MIT Press, Cambridge, MA, pp. 183-244.

Roesset, J. M. and Whitman, R. V. 1969. "Theoretical Background for Amplification Studies," Research Report No. R69-15, Soils Publication No. 231, Massachusetts Institute of Technology, Cambridge, MA.

Schnabel, P. B. 1973. "Effects of Local Geology and Distance from Source on Earthquake Ground Motions," PhD Thesis, University of California, Berkeley, CA.

Schnabel, P. B., Lysmer, J., and Seed, H. B. 1972. "*SHAKE*: A Computer Program for Earthquake Response Analysis of Horizontally Layered Sites," Report EERC-72/12, Earthquake Engineering Research Center, Berkeley, CA.

Seed, H. B. and Idriss, I. M. 1970. "Soil Moduli and Damping Factors for Dynamic Response Analysis," Report EERC-70/10, Earthquake Engineering Research Center, Berkeley, CA.

Seed, H. B., Romo, M. P., Sun, J., Jaime, A., and Lysmer, J. 1987. "Relationships Between Soil Conditions and Earthquake Ground Motions in Mexico City in the Earthquake of Sept. 19, 1985," Report EERC-87/15, Earthquake Engineering Research Center, Berkeley, CA.

Seed, H. B., Wong, R., Idriss, I. M., and Tokimatsu, K. 1986. "Moduli and Damping Factors for Dynamic Analysis of Cohesionless Soils," Journ., Geotechnical Engineering Division, Vol 112, No. 11, pp 1016-1032.

Seed, R. B., Dickenson, S. E., and Idriss, I. M. 1991. "Principal Geotechnical Aspects of the 1989 Loma Prieta Earthquake," Soils and Foundations, Vol 31, No. 1, pp 1-26.

Staub, W. P., Wang, J. C., and Selfridge, R. J. 1991. "Assessment and Interpretation of Cross- and Down-hole Seismograms at the Paducah Gaseous Diffusion Plant," Report K/GDP/SAR-9, Oak Ridge National Laboratory, Oak Ridge, TN.

Stokoe, K. H., II, and Lodde, P. F. 1978. "Dynamic Response of San Francisco Bay Mud," Proc., Earthquake Engineeering & Soil Dynamics, Pasadena, ASCE, Vol 2, pp 940-959.

Sun, J. I., Golesorkhi, R., and Seed, H. B. 1988. "Dynamic Moduli and Damping Rations for Cohesive Soils," Report EERC-88/15, Earthquake Engineering Research Center, Berkeley, CA.

Sykora, D. W., Wahl, R. E., and Wallace, D. C. 1992. "*WESHAKE*: COE Personal Computer Version of SHAKE," Instructional Report GL IR-92-4, US Army Engineer Waterways Experiment Station, Vicksburg, MS, 221 pgs.

Veletsos, A. S., Prasad, A. M., and Tang, Y. 1988. "Design Approaches for Soil-Structure Interaction," Technical Report NCEER-88-0031, National Center for Earthquake Engineering Research, Buffalo, NY, 25 pgs.

Wiegel, R. L. 1970. Earthquake Engineering, Prentice-Hall, Inc., Englewood Cliffs, NJ, pg 85.

Yule, D. E. and Sharp, M. K. 1988. "Geophysical Site Investigation, Ohio River Navigation Project—Olmsted Site," Misc. Paper GL-88-15, US Army Engineer Waterways Experiment Station, Vicksburg, MS.

Zen, K. and Higuchi, Y. 1984. "Prediction of Vibratory Shear Modulus and Damping Ratio for Cohesive Soils," Proc., Eighth Int'l Conf. Earthquake Engineering, San Francisco, CA, Vol 3, pp. 23-30.

APPENDIX A: LOCATIONS OF BORINGS USED FOR SOIL COLUMN

Site	Boring No.	Coordinates (ft)		Elevation* (ft)	
		Northing	Easting	Top of Hole	Bottom of Hole
1	Z-1	S 5955.57	W 4327.82	380.3	251.3
	Z-2	S 5956.08	W 4312.61	380.4	311.9
	Z-3	S 5955.68	W 4342.33	380.1	311.6
2	Z-5	N 297.88	W 891.52	379.9	239.9
	Z-6	N 297.66	W 876.46	380.1	241.1
	Z-7	N 297.72	W 861.40	380.0	241.0
3	Z-9	N 12075.30	W 2930.84	354.6	229.6
	Z-10	N 12059.93	W 2930.41	353.7	229.7
	Z-11	N 12045.08	W 2930.60	354.2	230.2
	Z-12	N 12044.52	W 2980.58	351.1	-17.9
4	Z-13	S 385.11	W 8396.49	371.6	247.6
	Z-14	S 385.28	W 8381.33	371.5	238.0
	Z-15	S 385.15	W 8366.03	371.2	246.9
	Z-16	S 385.15	W 8436.66	370.9	14.3

* MSL

APPENDIX B: ACCELERATION-TIME RECORDS FOR 500-YEAR EVENT

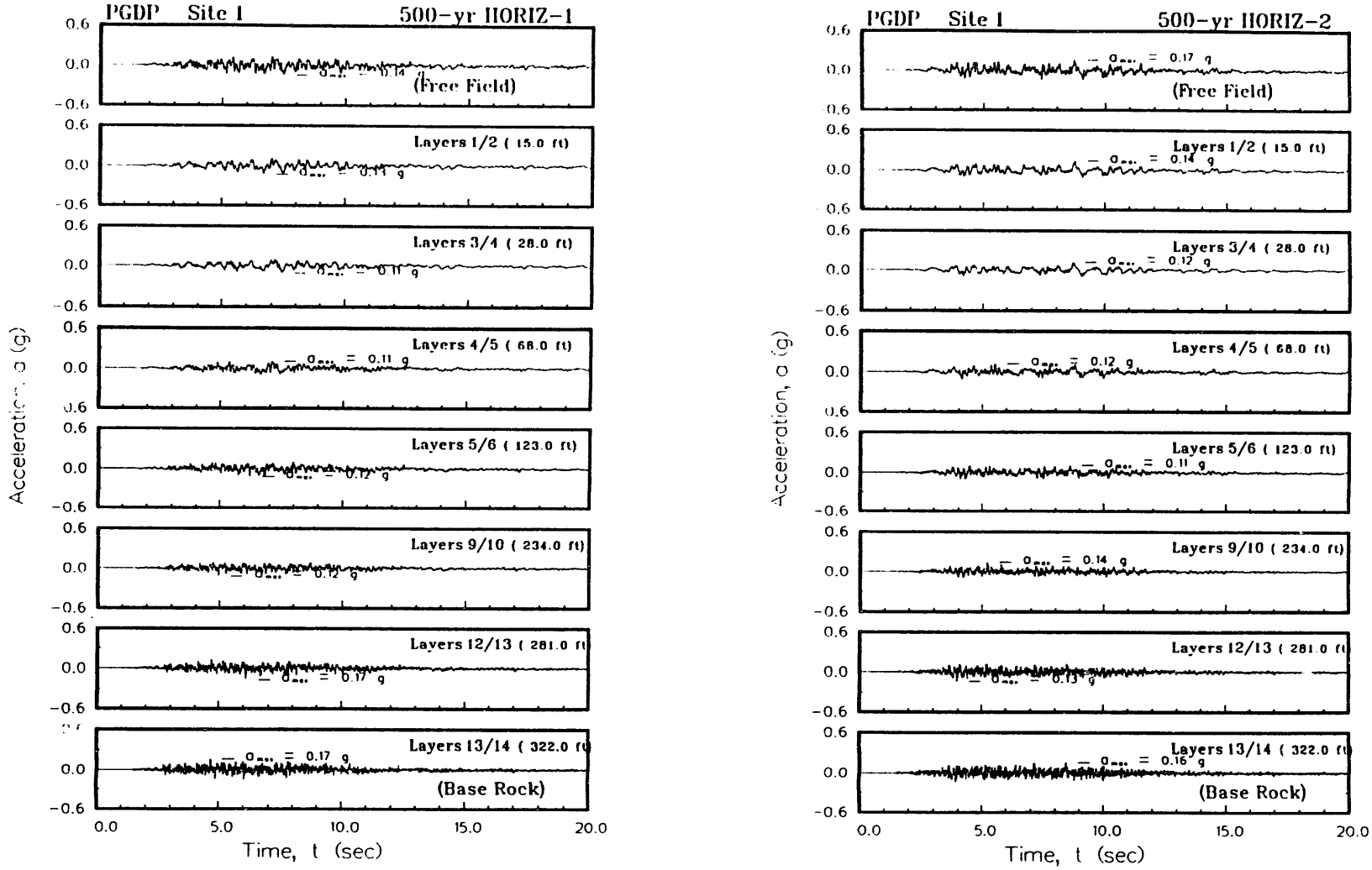

Figure B1. Variation of acceleration with time at the top of each layer for Site 1.

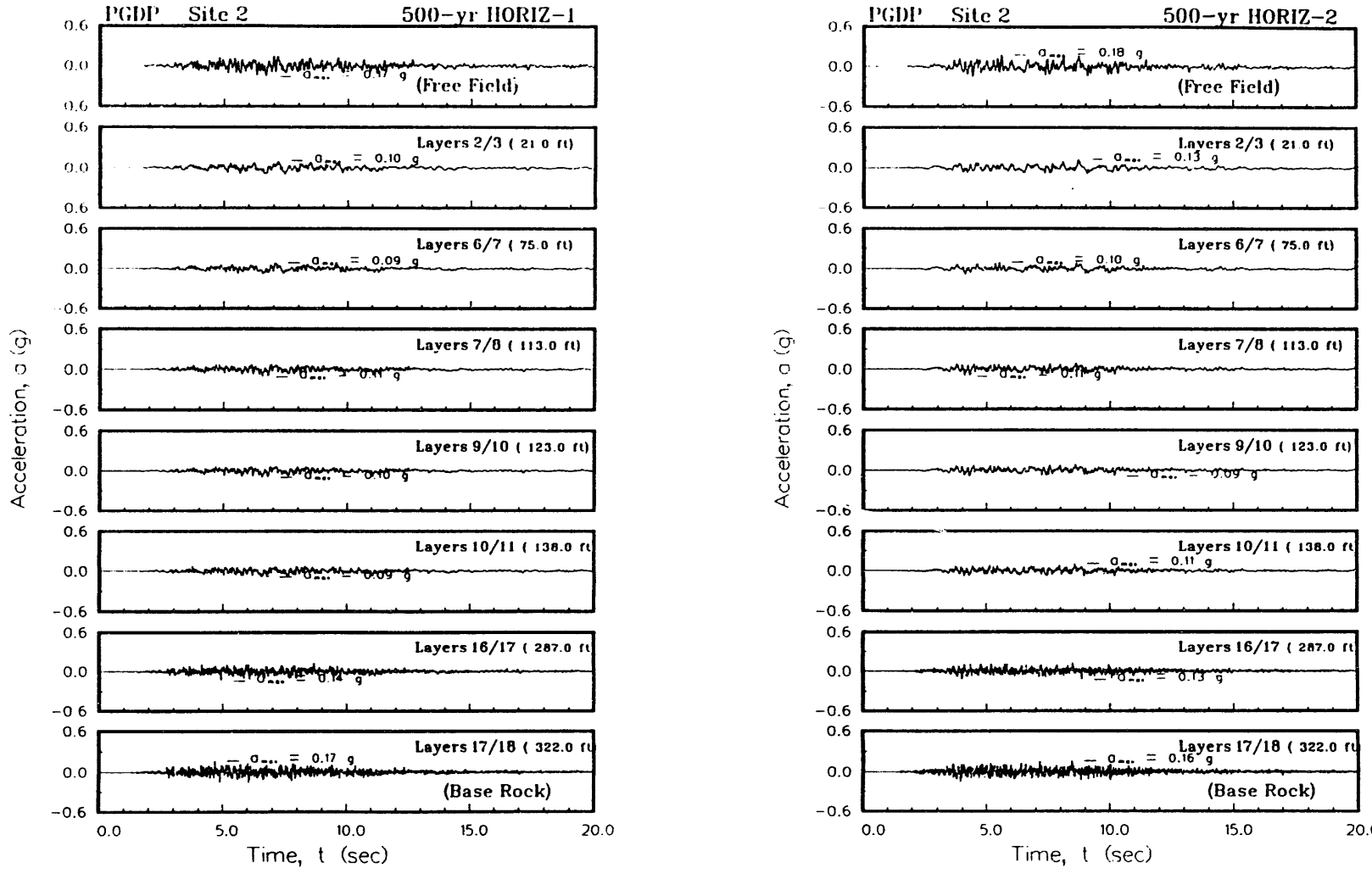

Figure B2. Variation of acceleration with time at the top of each layer for Site 2

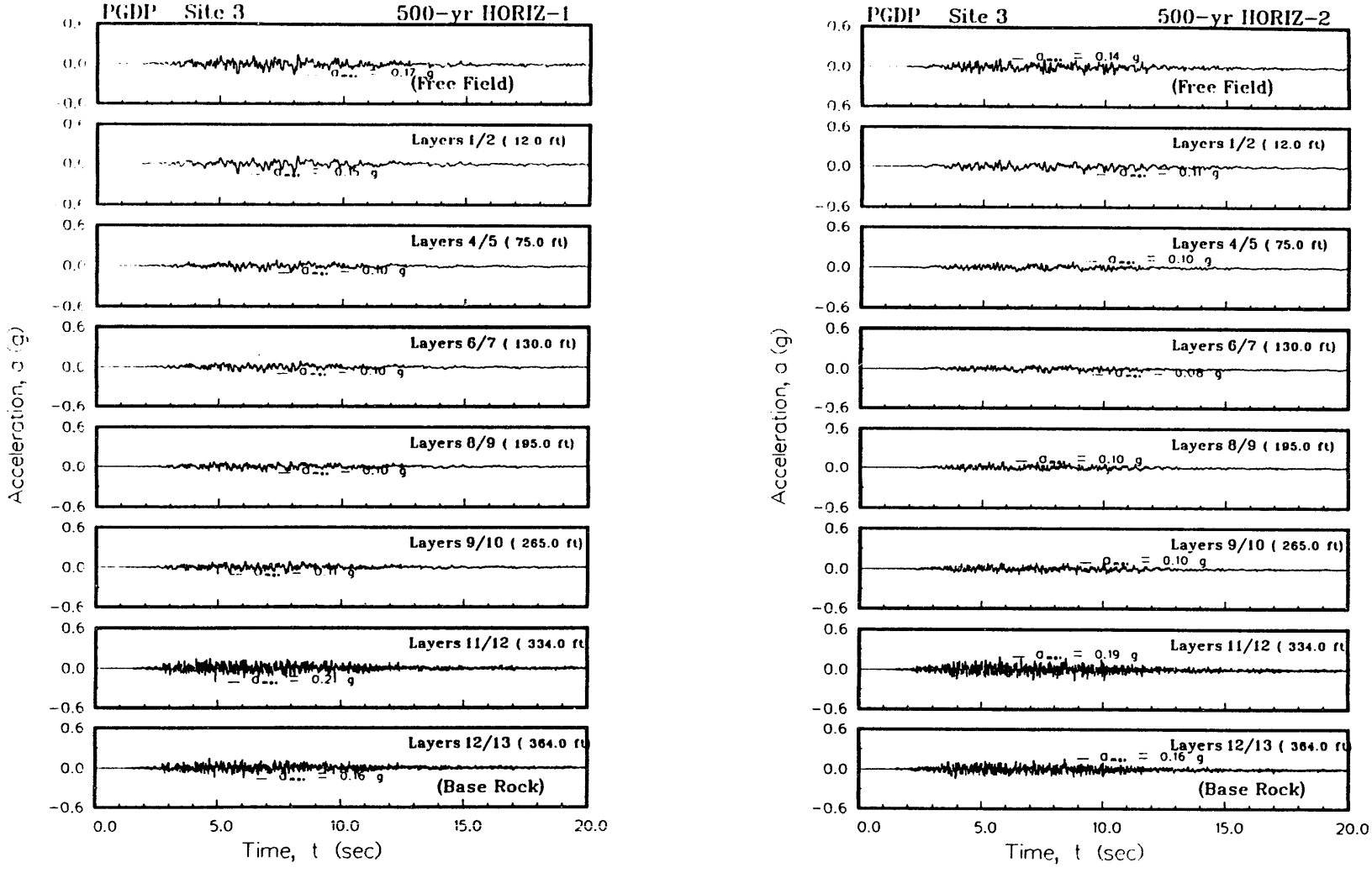

Figure B3. Variation of acceleration with time at the top of each layer for Site 3

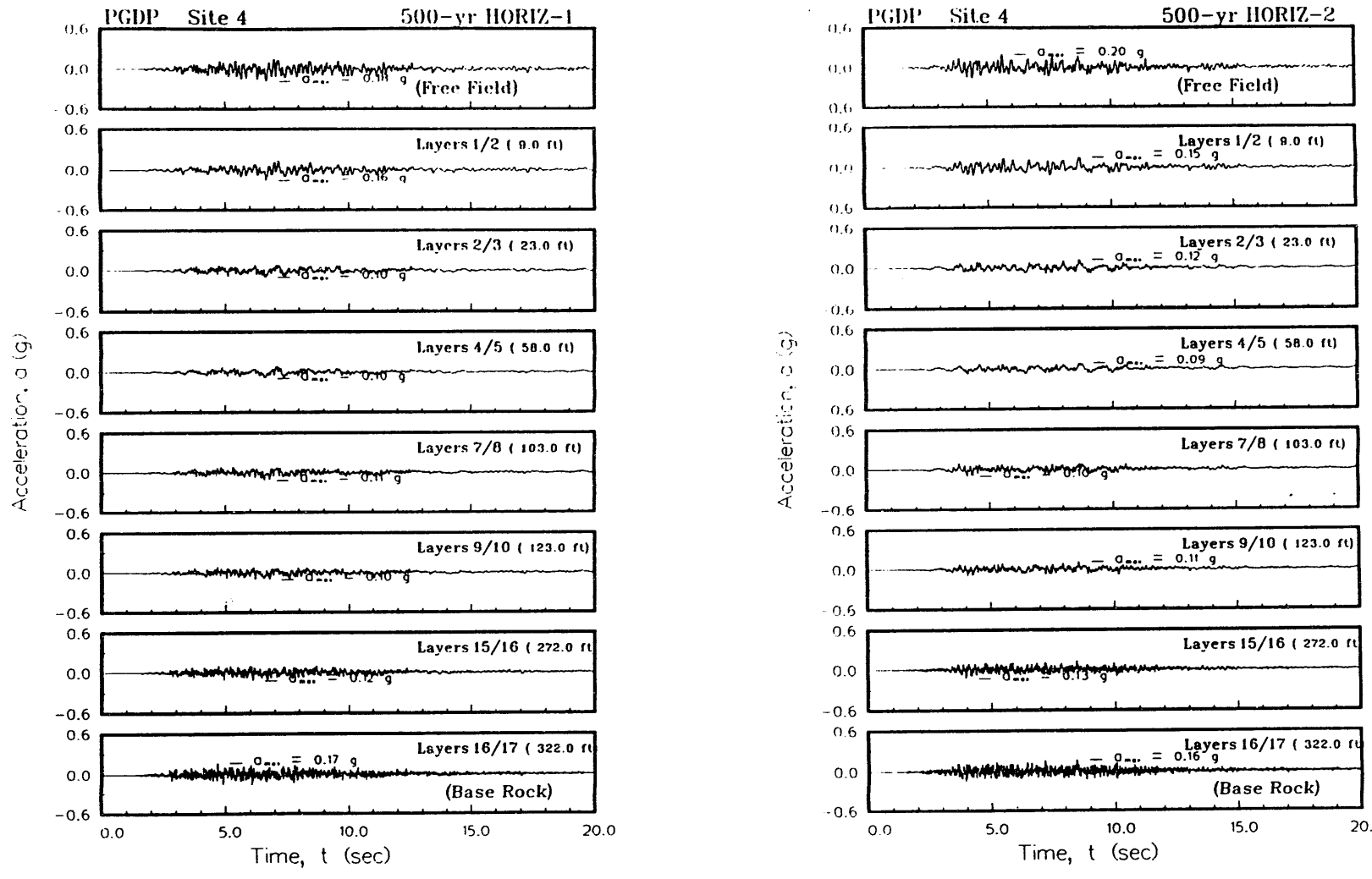

Figure B4. Variation of acceleration with time at the top of each layer for Site 4

APPENDIX C: SHEAR STRAINS FOR 500-YEAR EVENT

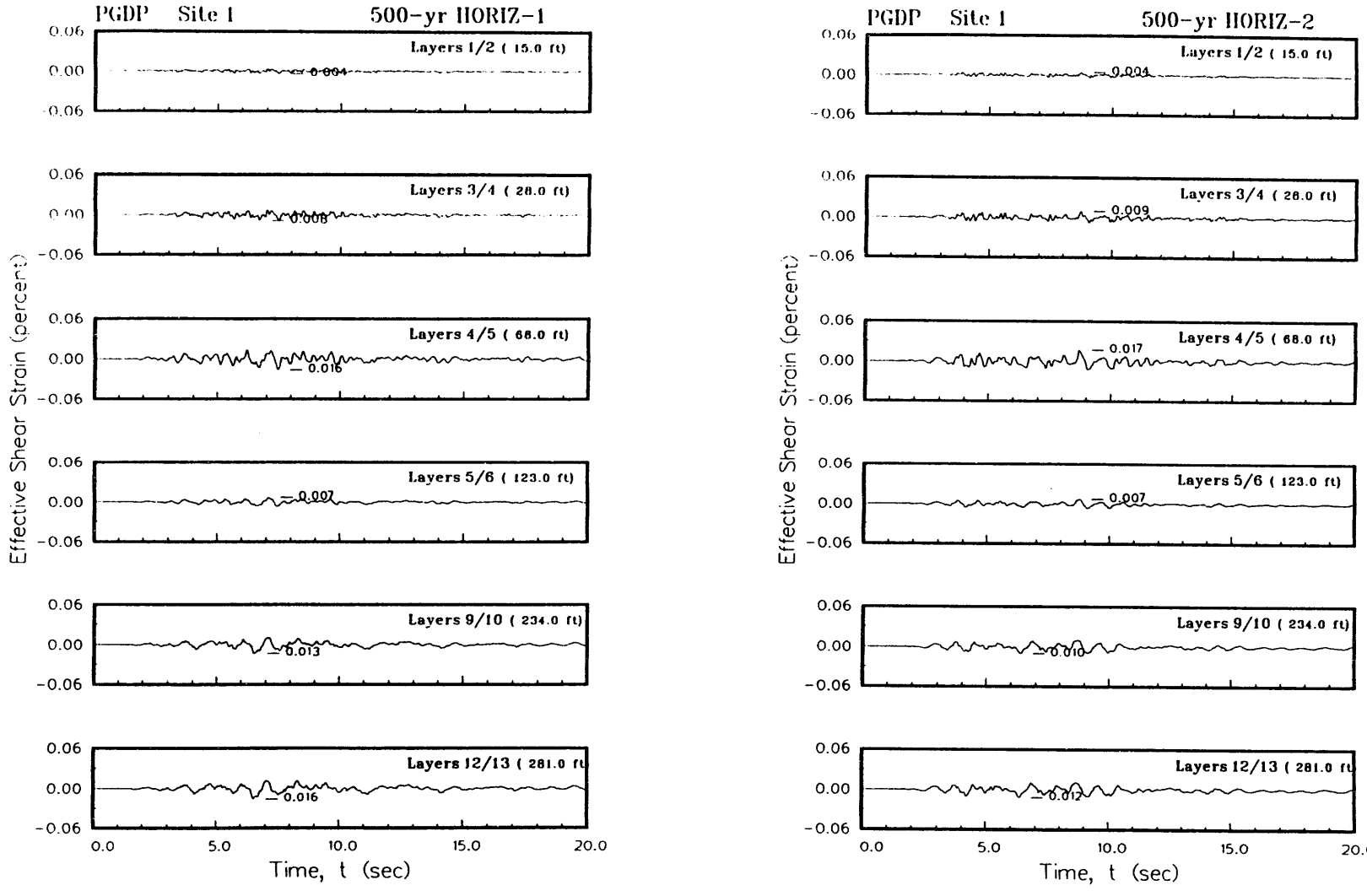

Figure C1. Variation of shear strain with time at contacts between layers for Site 1

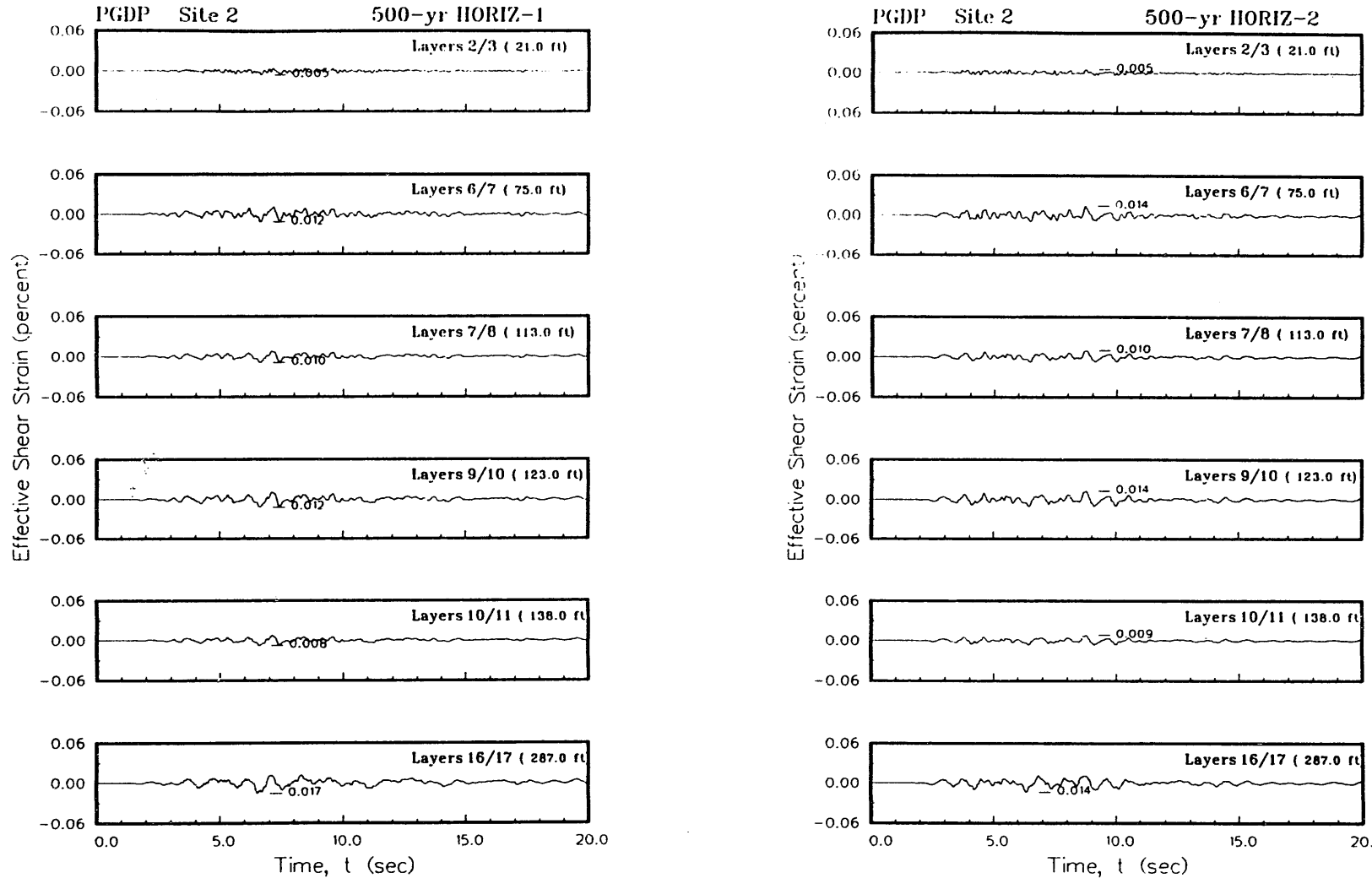

Figure C2. Variation of shear strain with time at contacts between layers for Site 2

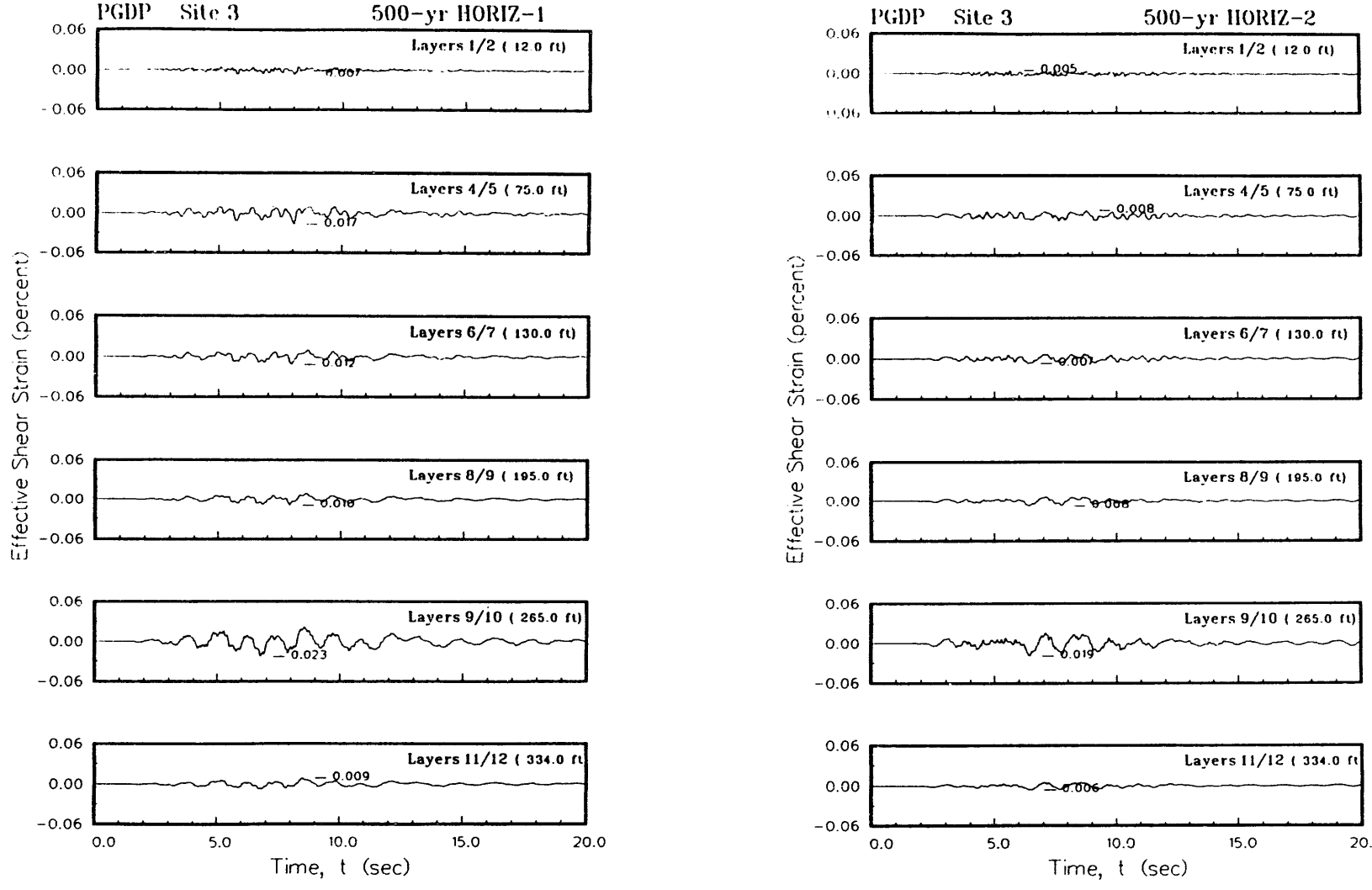

Figure C3. Variation of shear strain with time at contacts between layers for Site 3

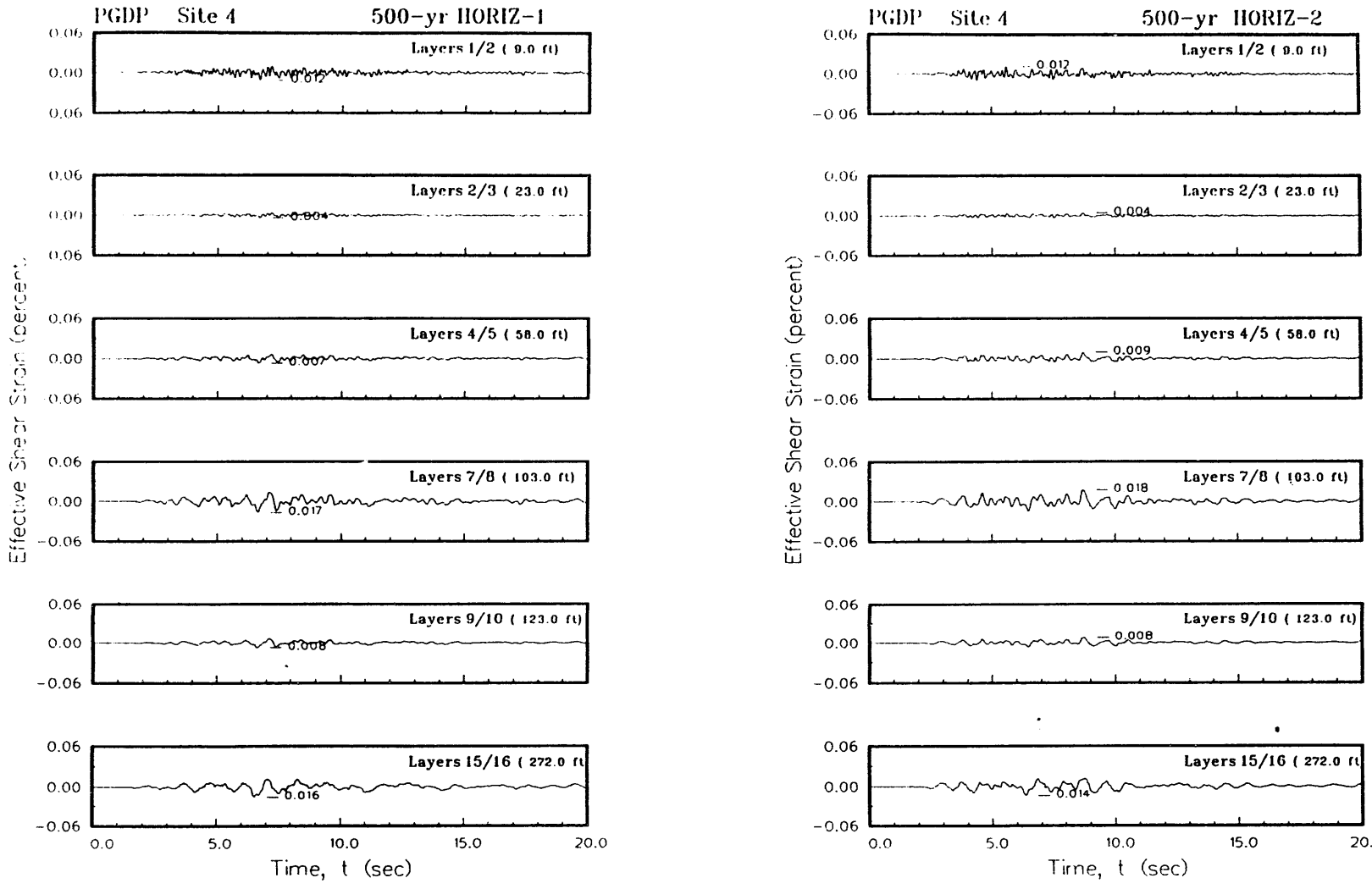

Figure C4. Variation of shear strain with time at contacts between layers for Site 4

APPENDIX D: TRIPARTITE RESPONSE SPECTRA FOR 500-YEAR EVENT

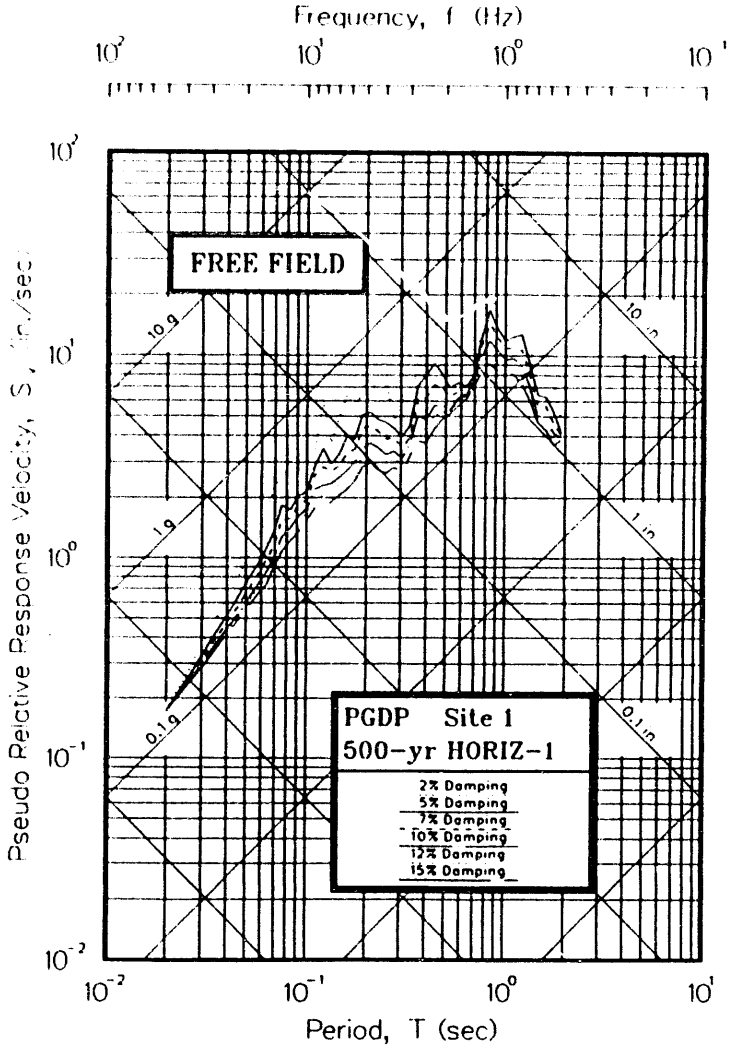

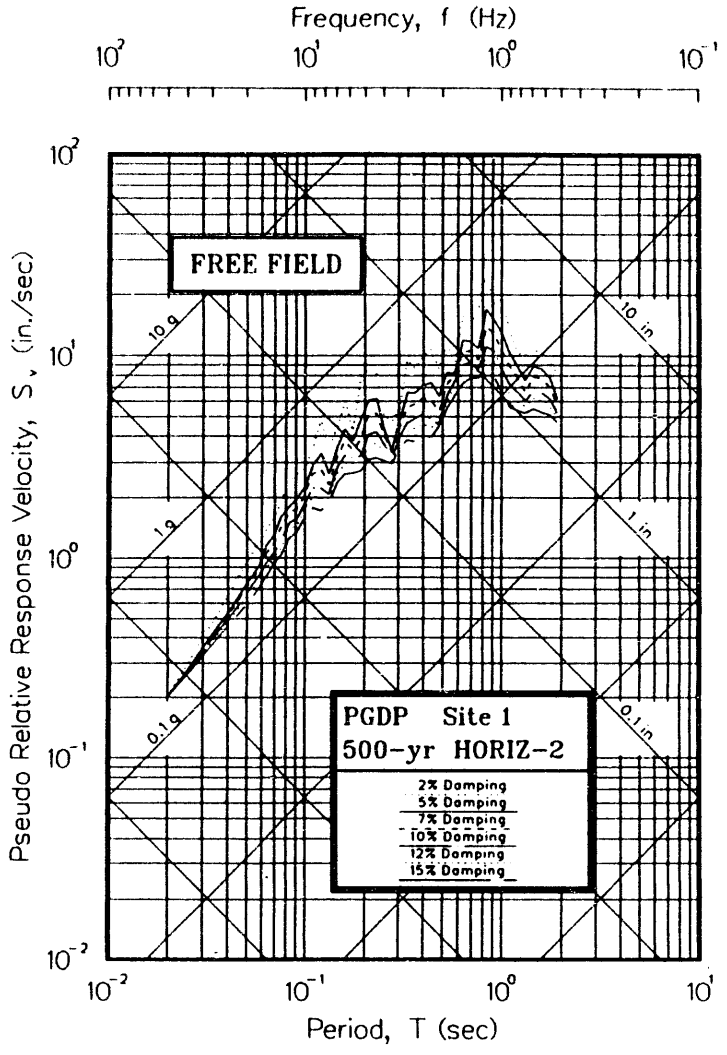

Figure D1. Psuedo-relative velocity spectra in tripartite form at free field for Site 1

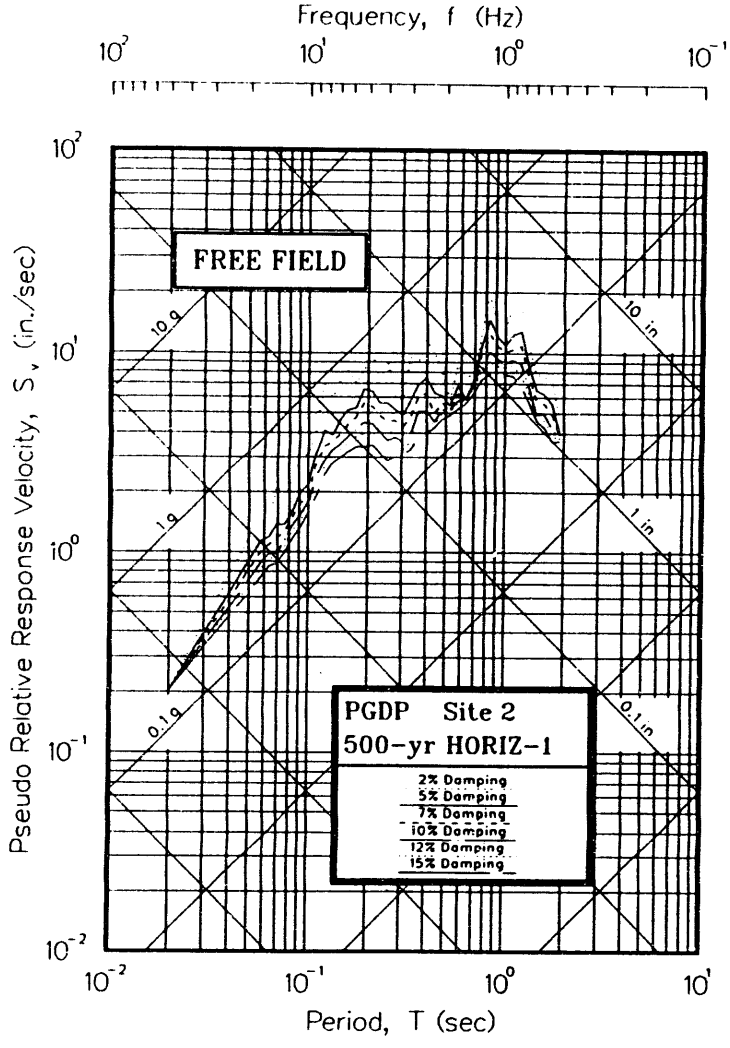

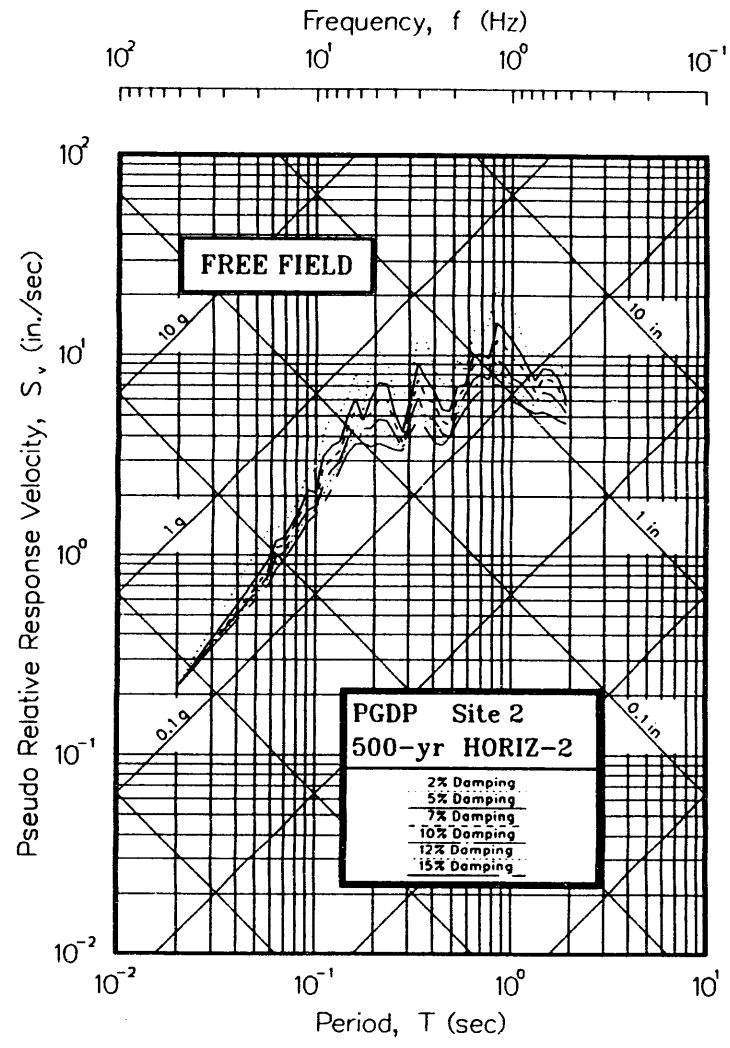

Figure D2. Psuedo-relative velocity spectra in tripartite form at free field for Site 2

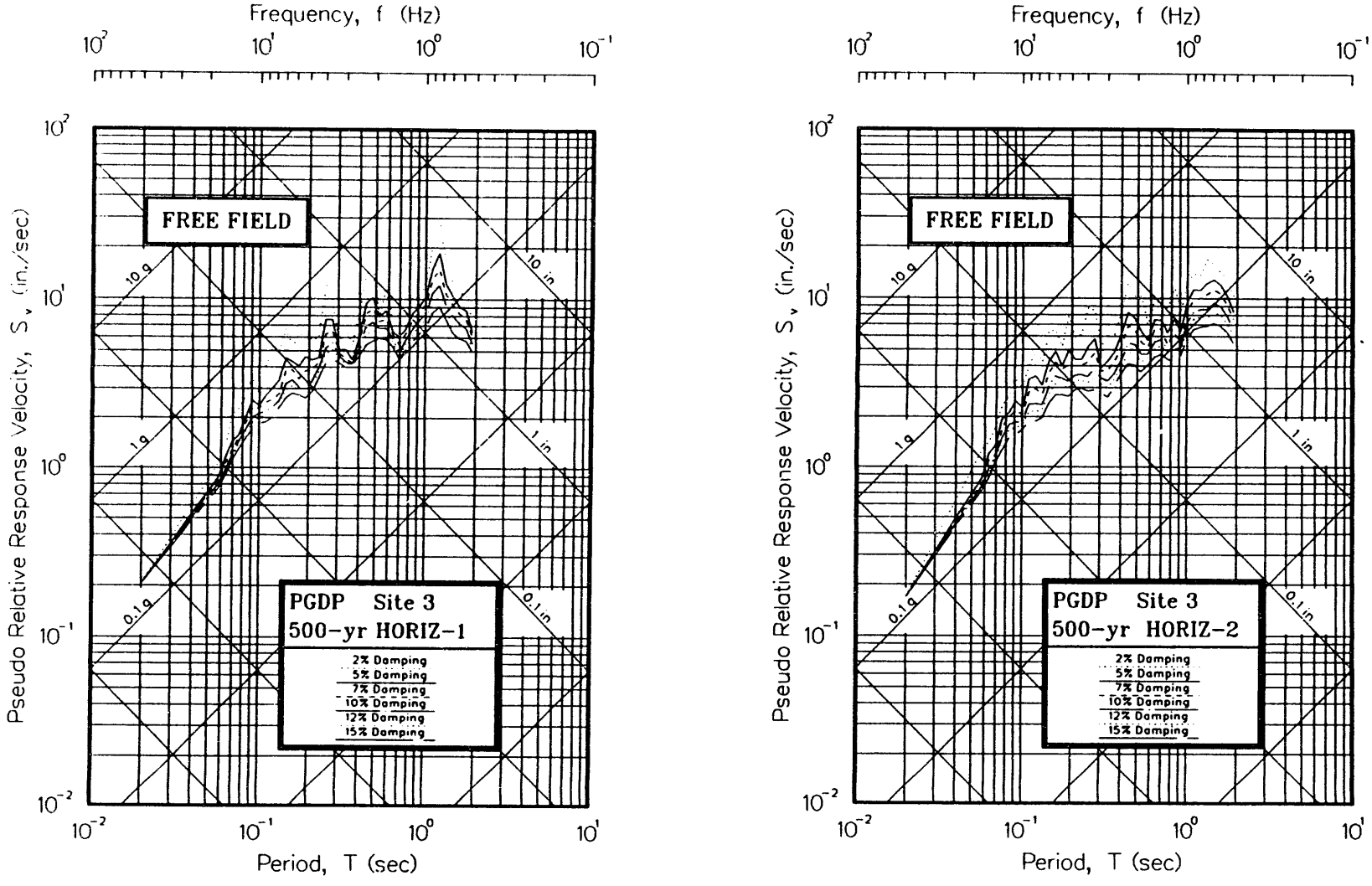

Figure D3. Psuedo-relative velocity spectra in tripartite form at free field for Site 3

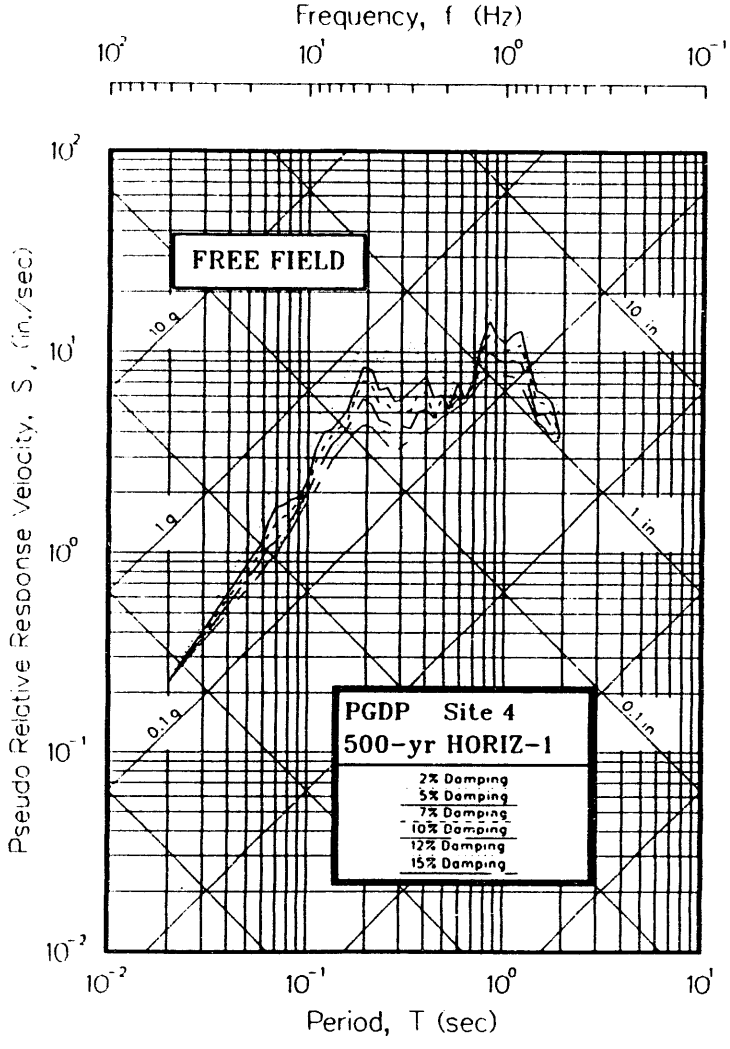

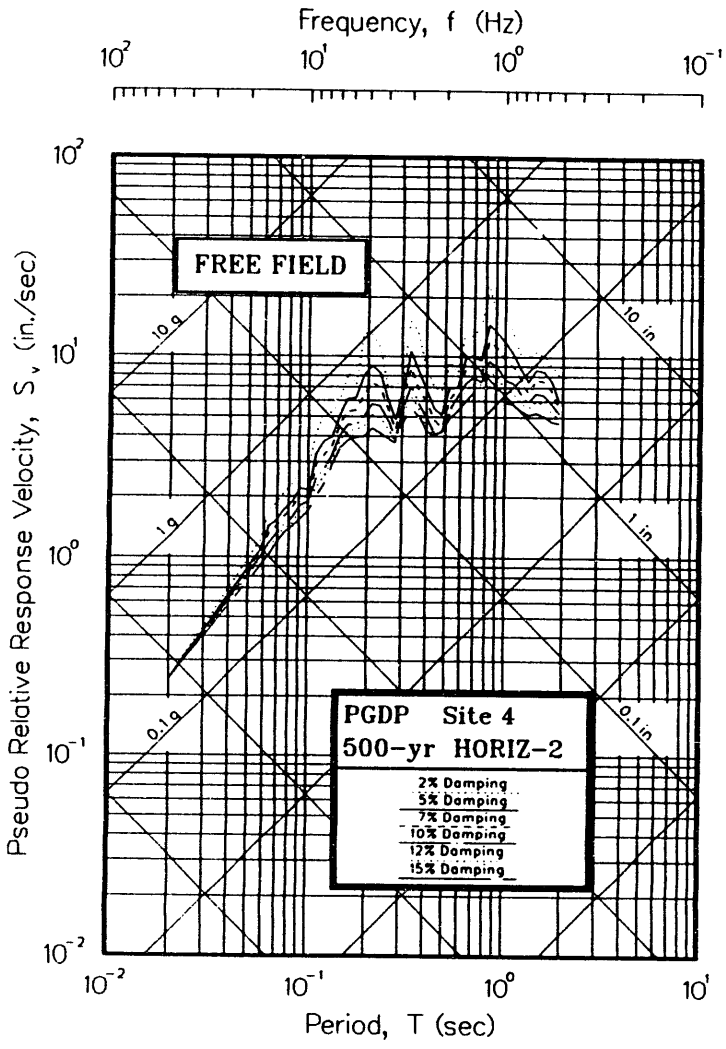

Figure D4. Psuedo-relative velocity spectra in tripartite form at free field for Site 4

APPENDIX E: ACCELERATION SPECTRA FOR 500-YEAR EVENT

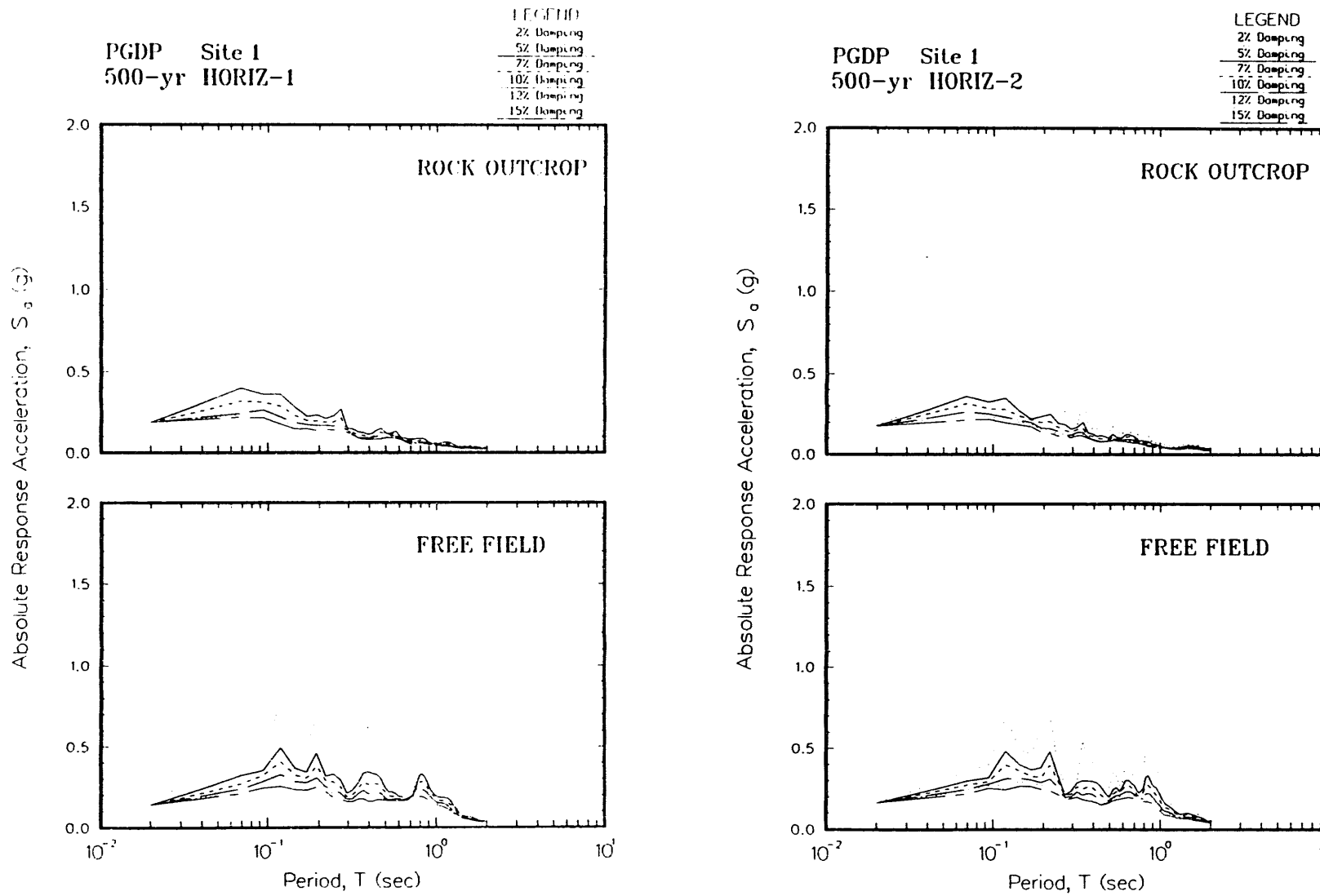

Figure E1. Absolute acceleration response spectra at free field for Site 1

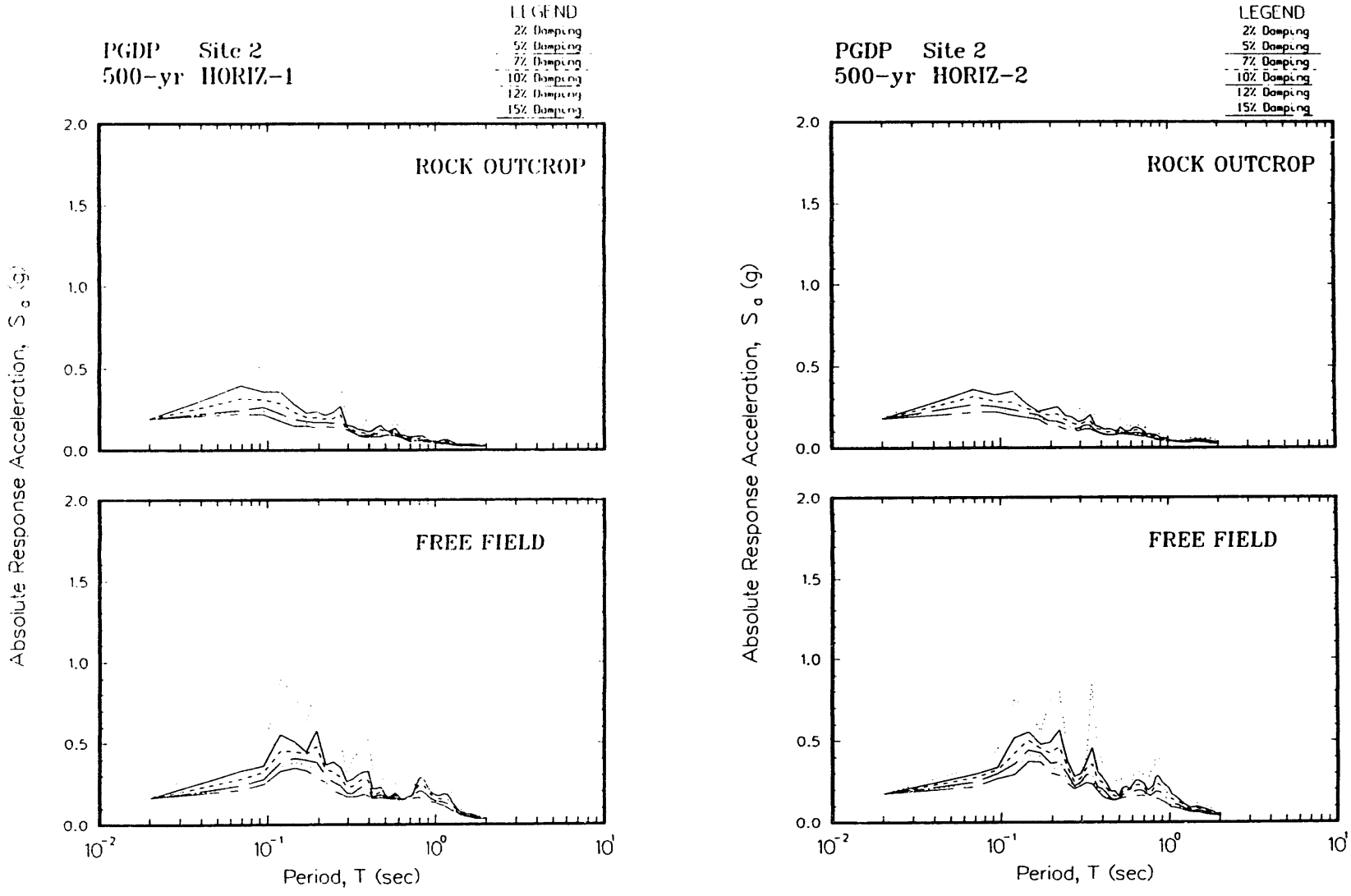

Figure E2. Absolute acceleration response spectra at free field for Site 2

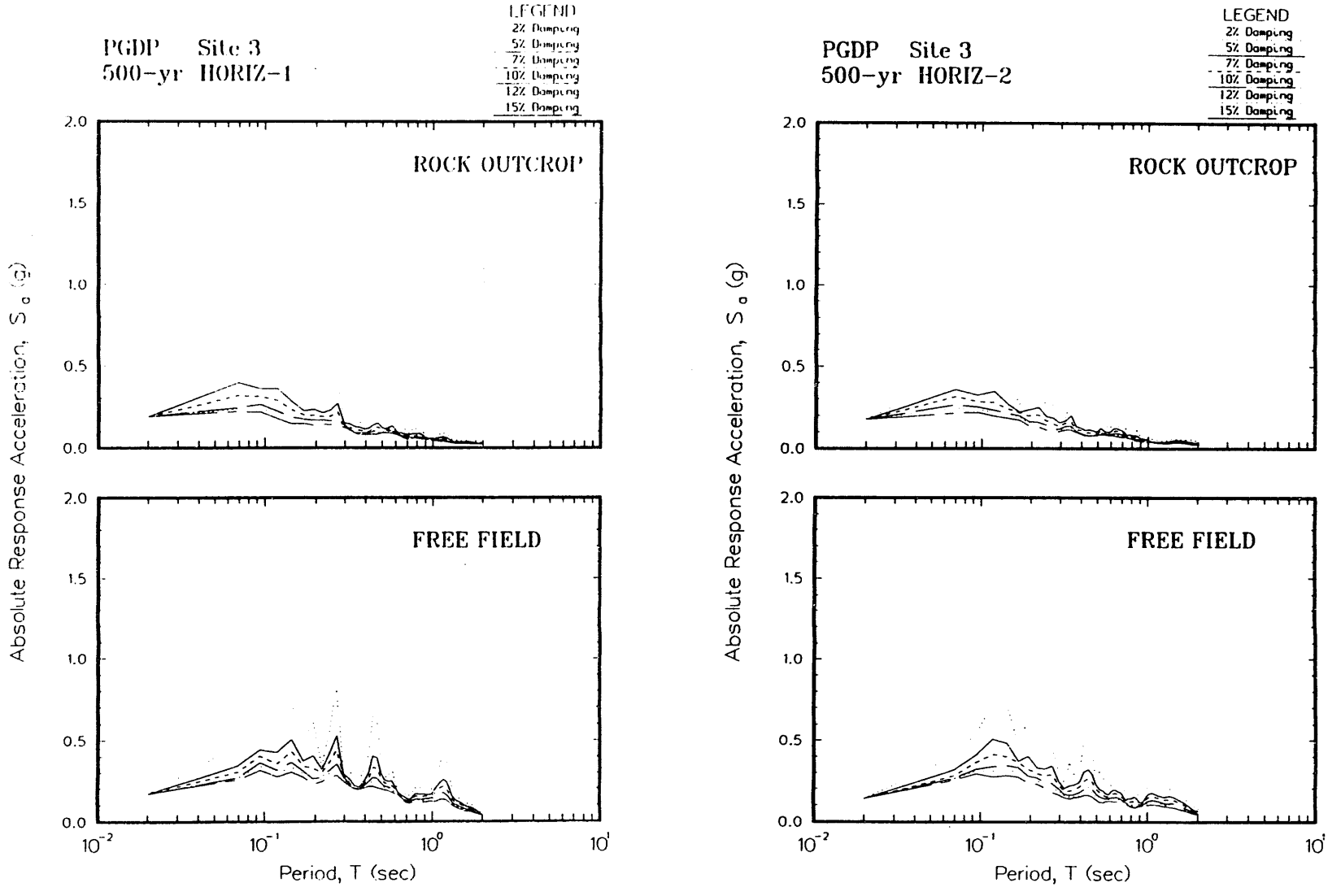

Figure E3. Absolute acceleration response spectra at free field for Site 3

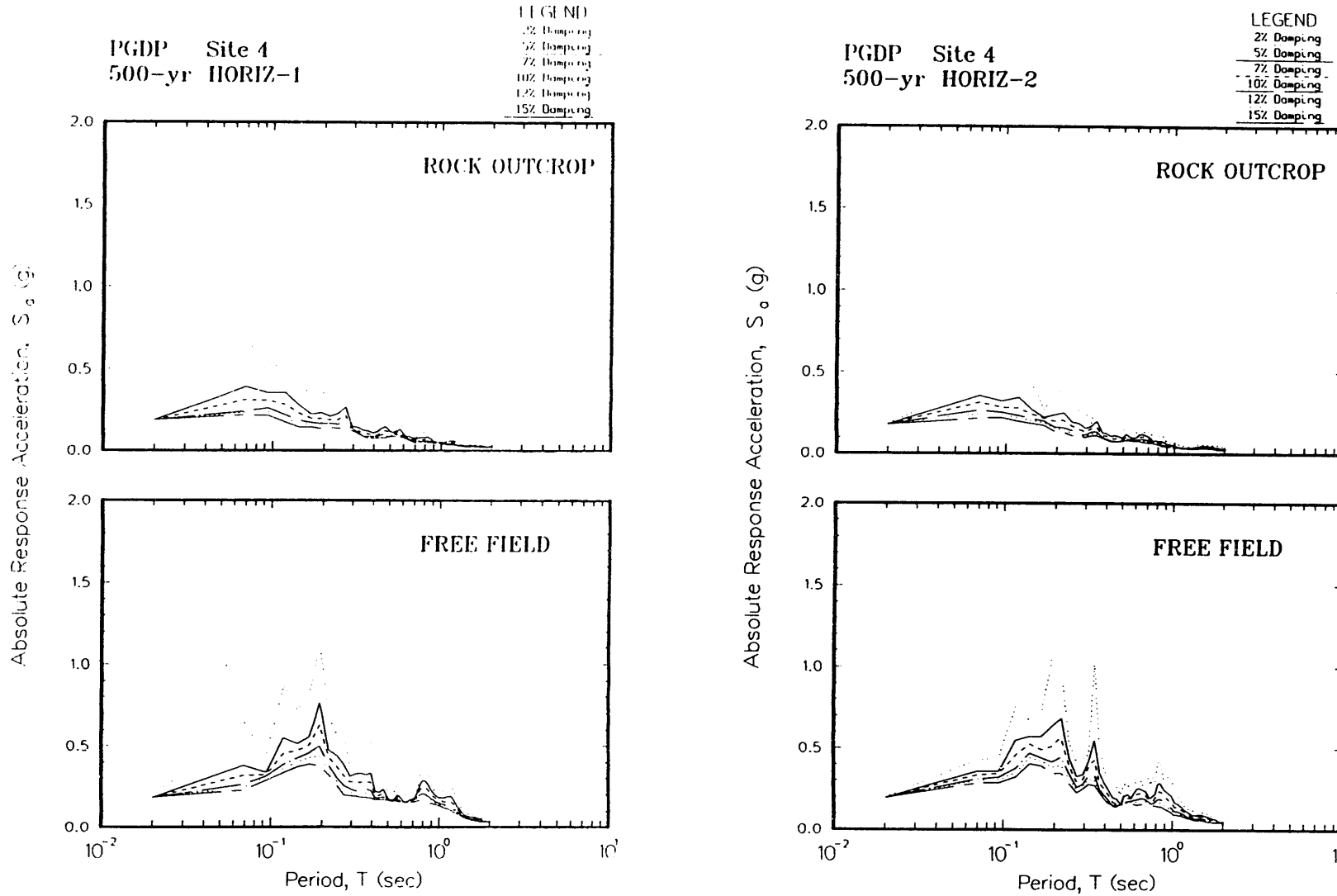

Figure E4. Absolute acceleration response spectra at free field for Site 4

APPENDIX F: RATIO OF ACCELERATION SPECTRA FOR 500-YEAR EVENT

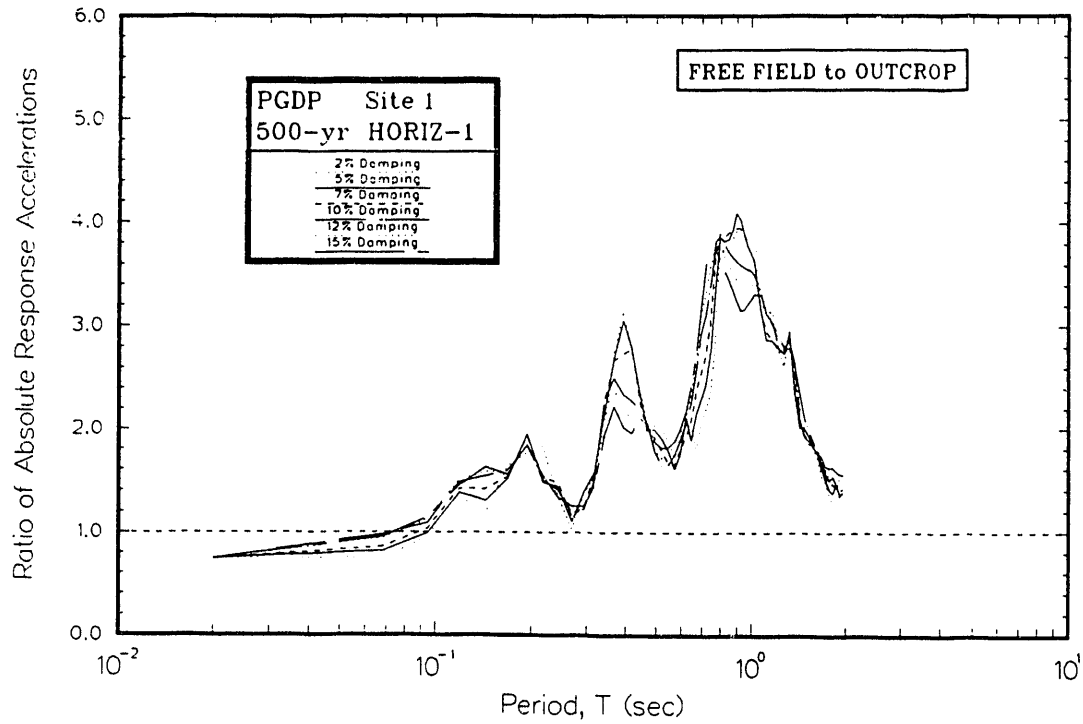

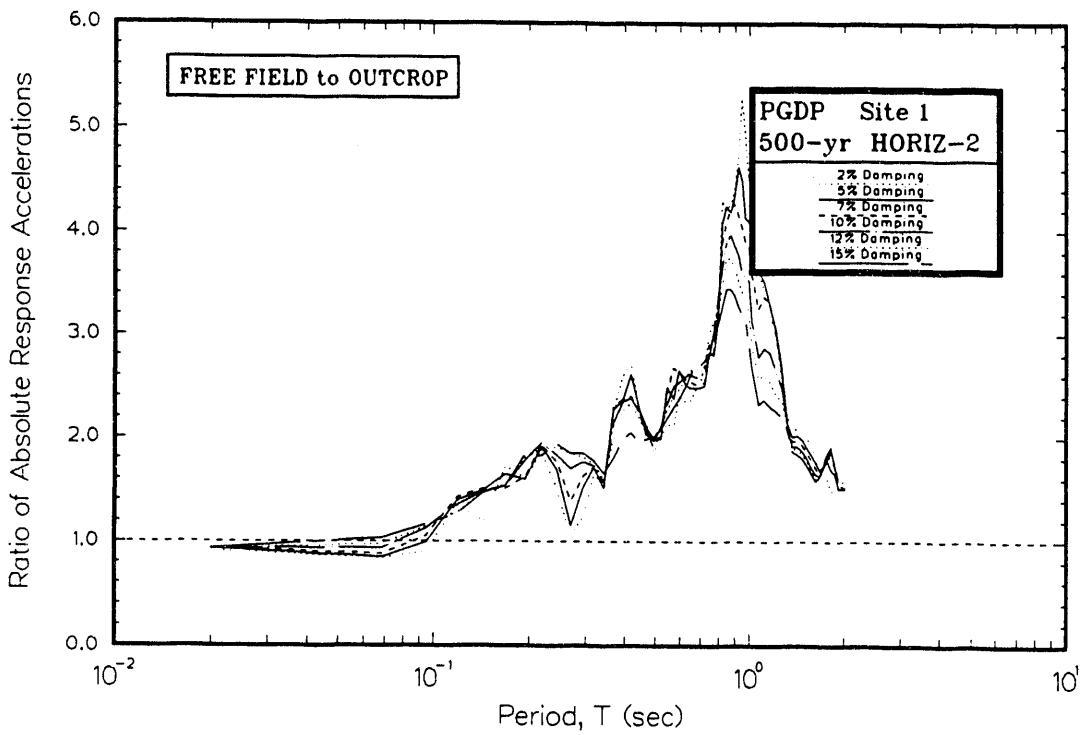

Figure F1. Ratio of absolute acceleration response spectra at free field to rock for Site 1

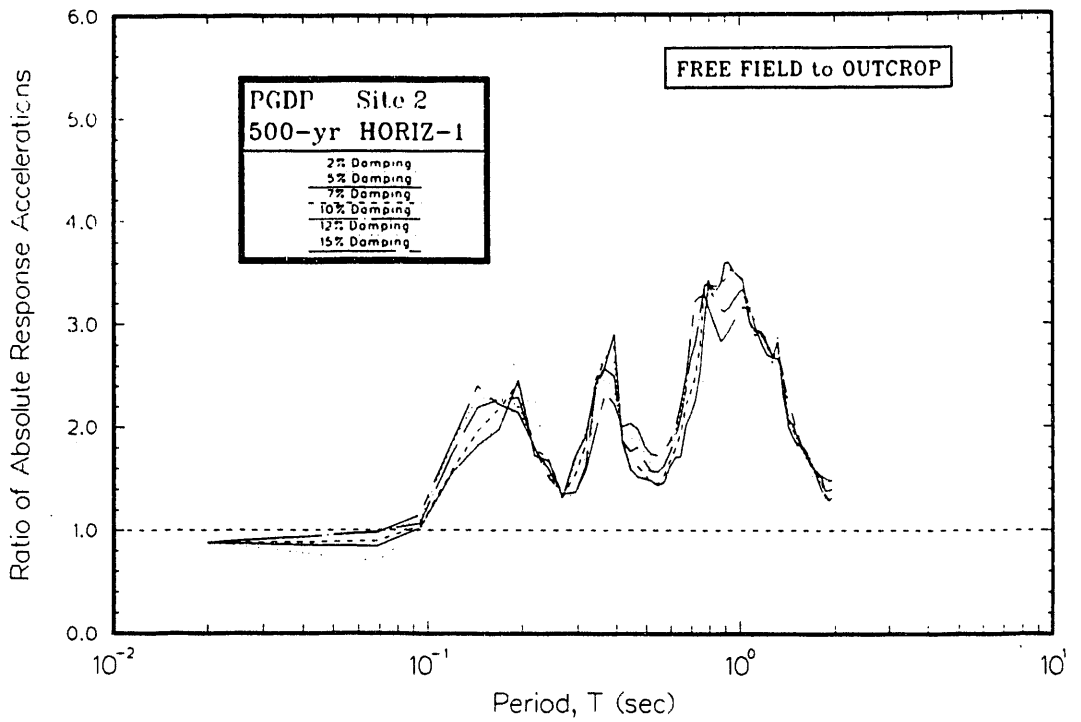

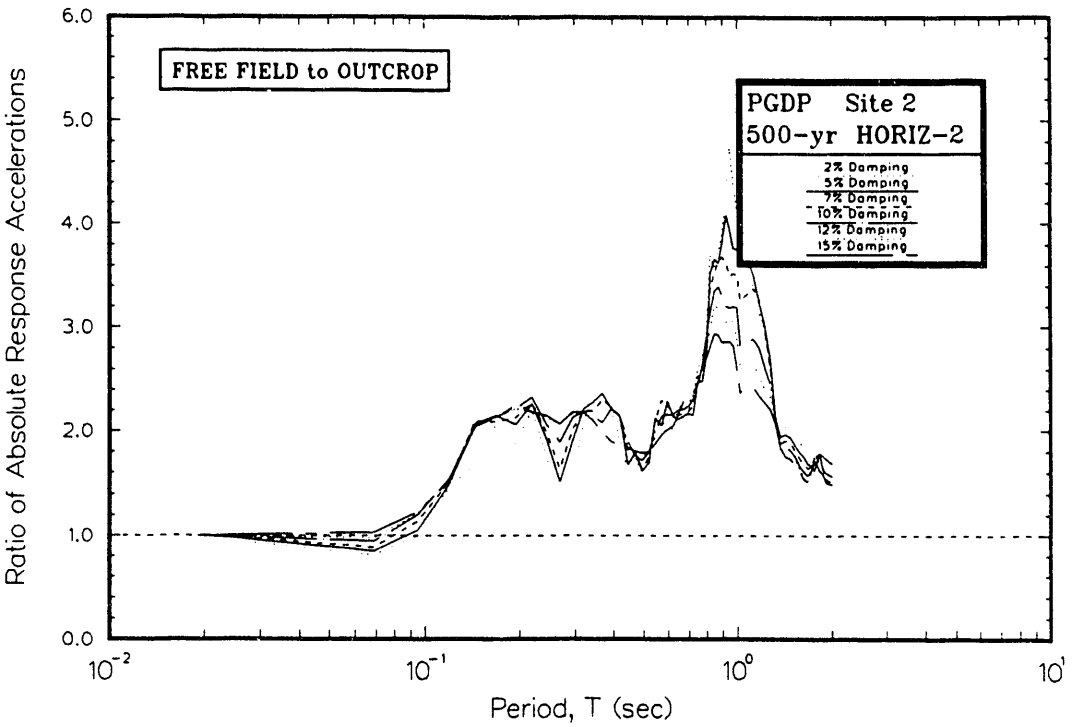

Figure F2. Ratio of absolute acceleration response spectra at free field to rock for Site 2

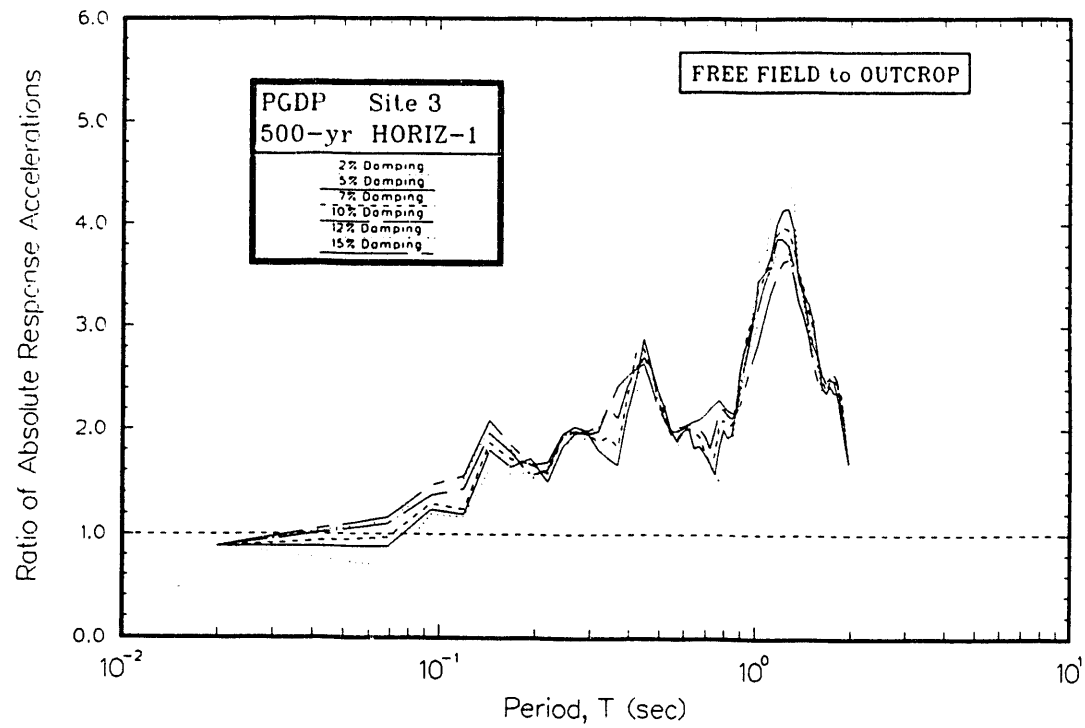

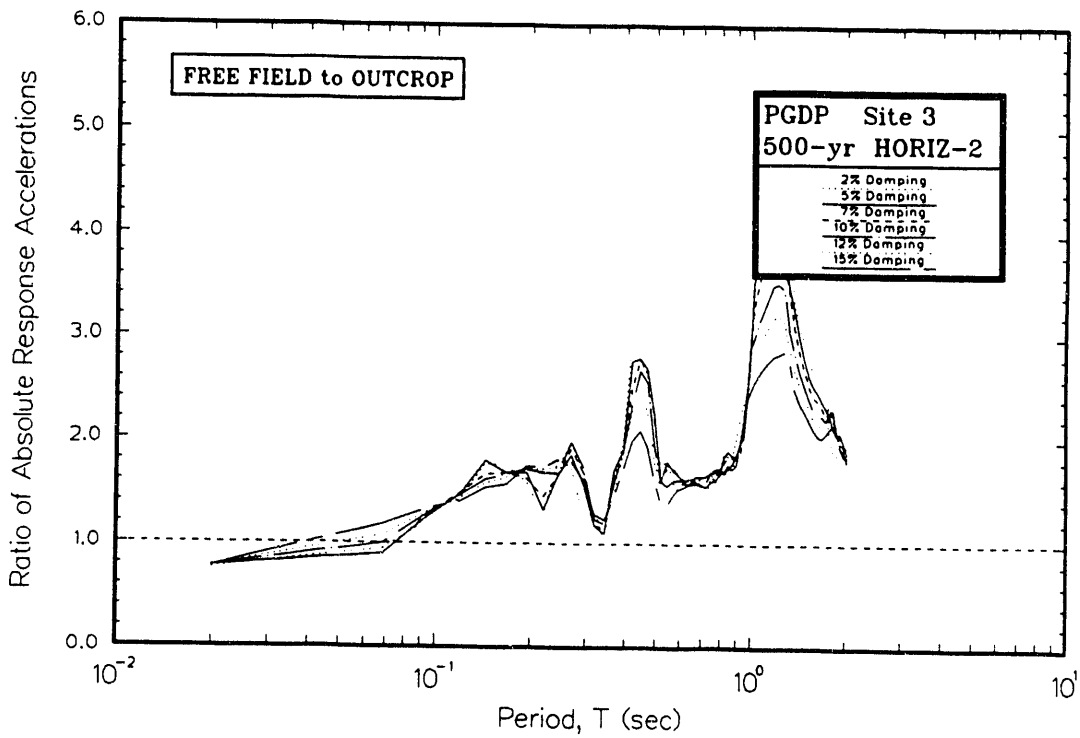

Figure F3. Ratio of absolute acceleration response spectra at free field to rock for Site 3

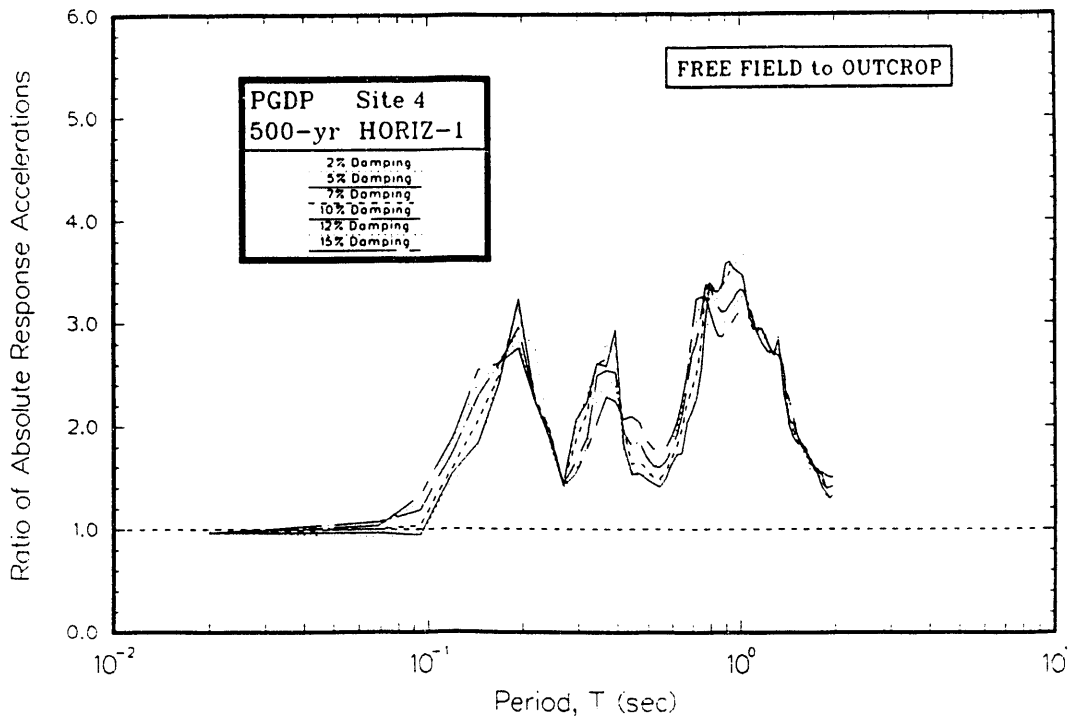

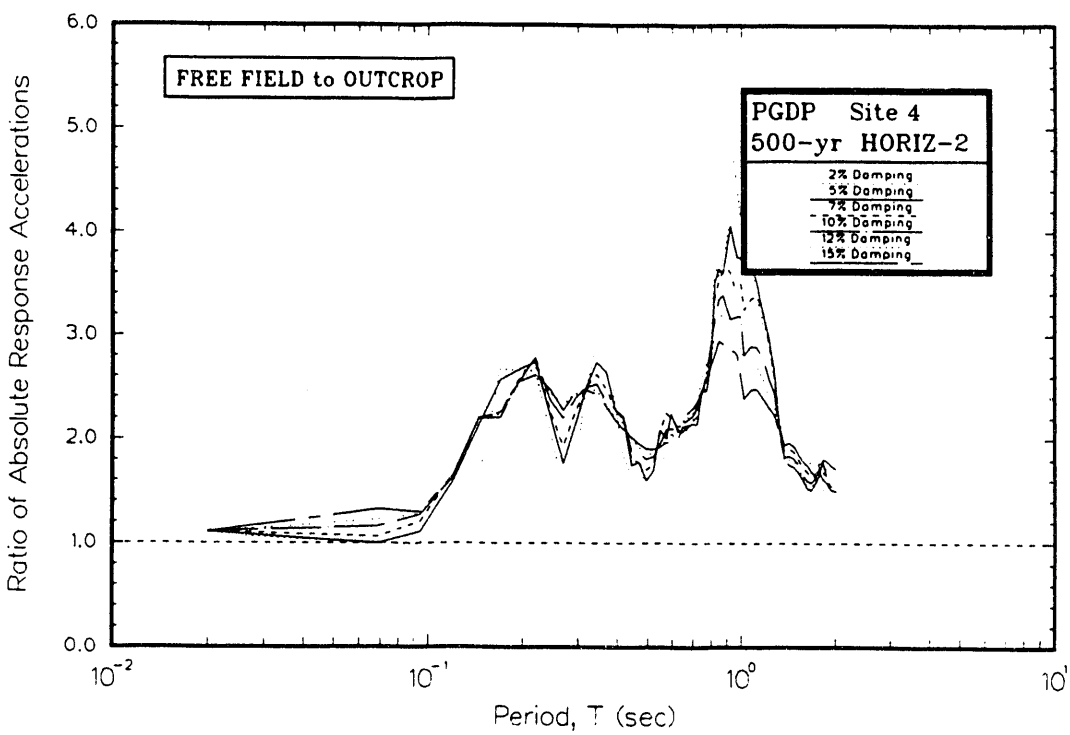

Figure F4. Ratio of absolute acceleration response spectra at free field to rock for Site 4

APPENDIX G: AMPLIFICATION RATIOS FOR 500-YEAR EVENT

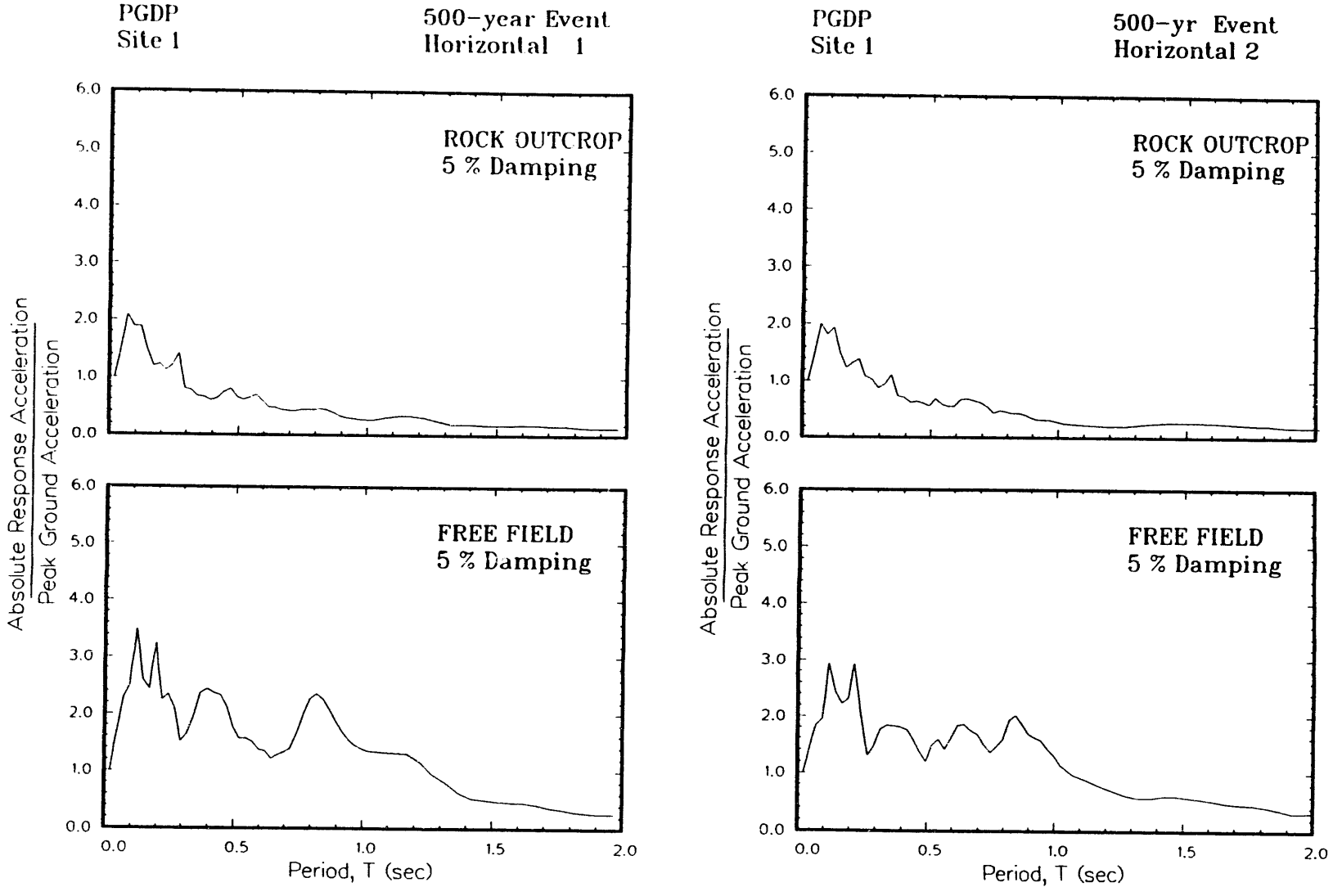

Figure G1. Ratio of amplification of absolute acceleration response spectra to peak acceleration at free field for Site 1

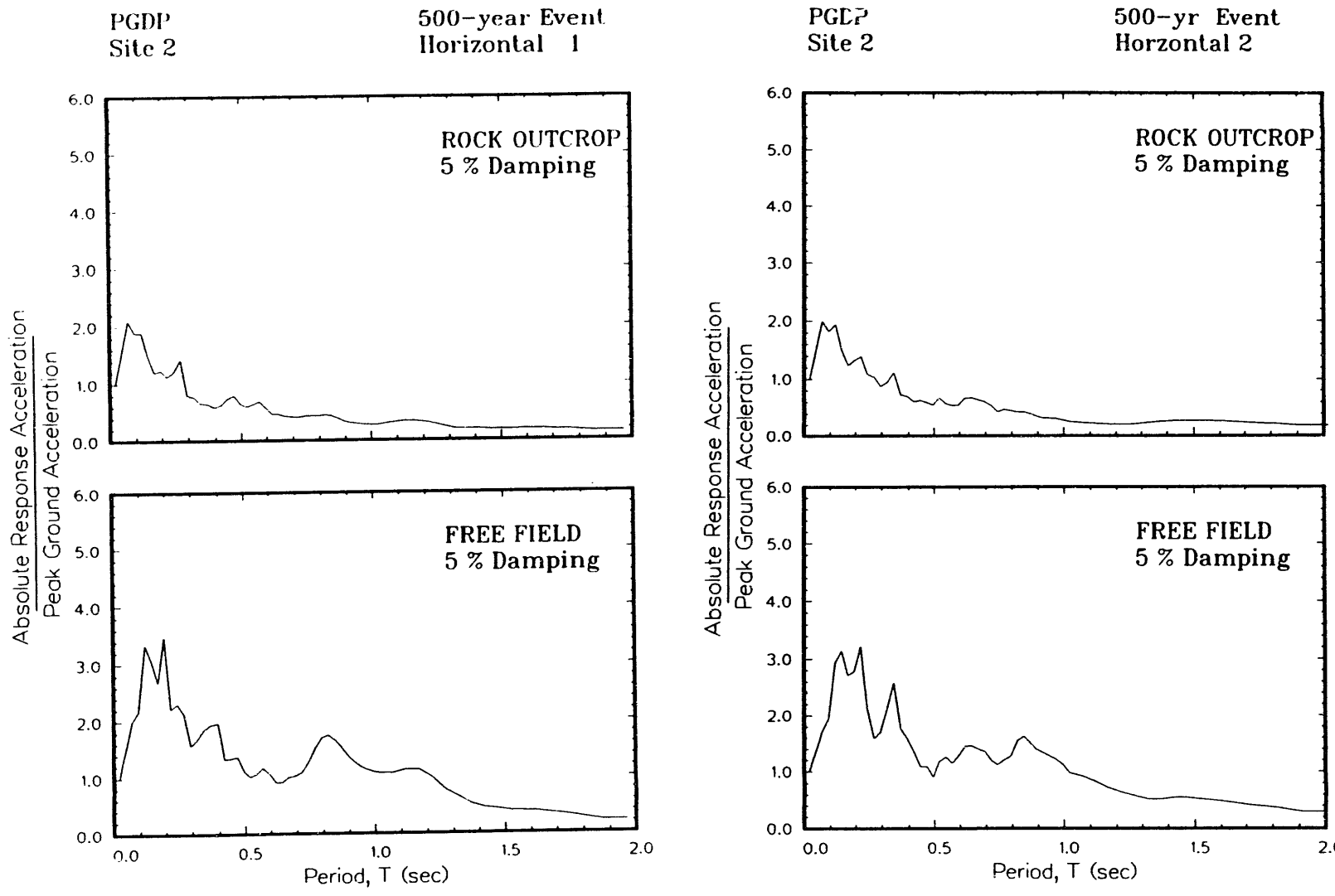

Figure G2. Ratio of amplification of absolute acceleration response spectra to peak acceleration at free field for Site 2

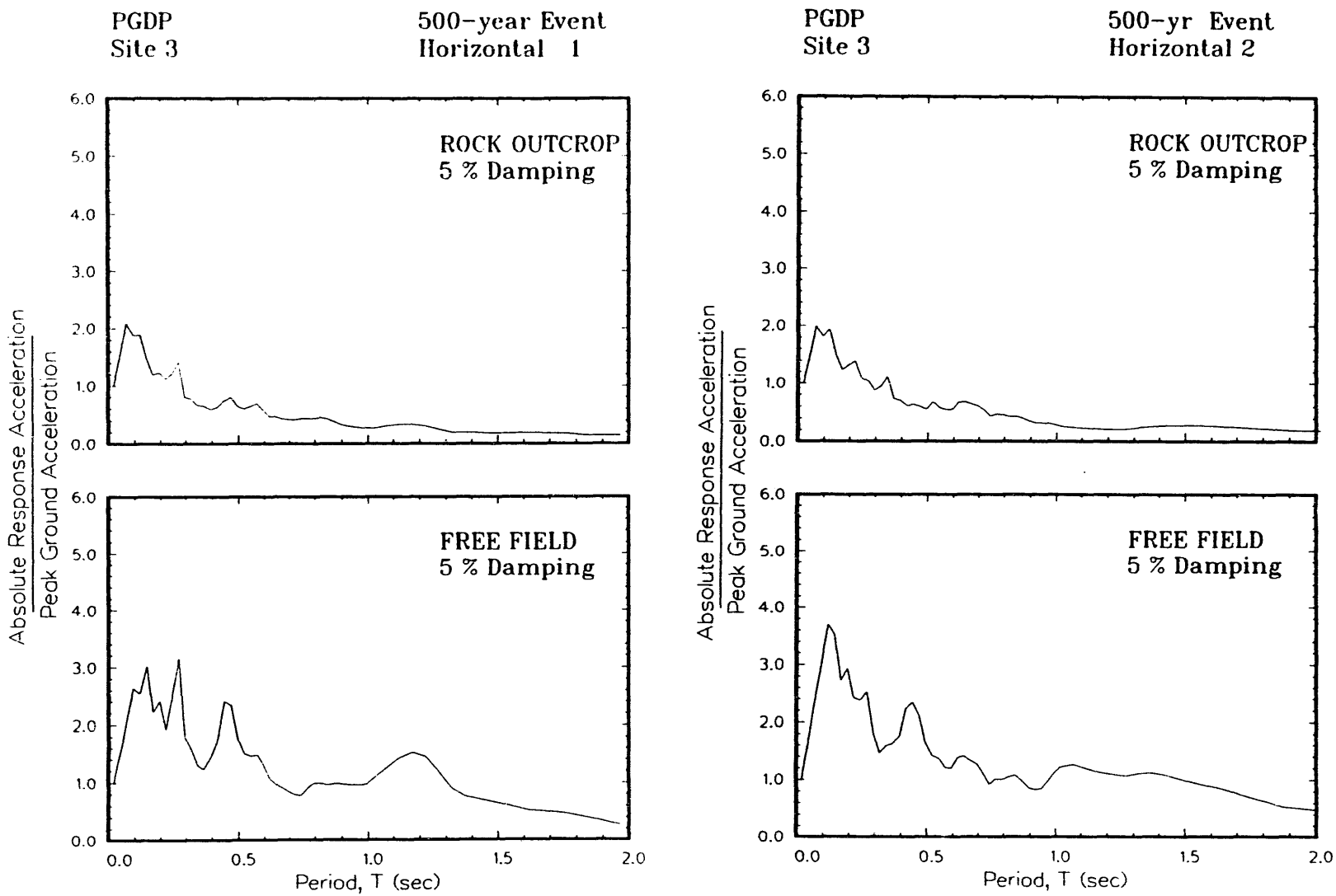

Figure G3. Ratio of amplification of absolute acceleration response spectra to peak acceleration at free field for Site 3

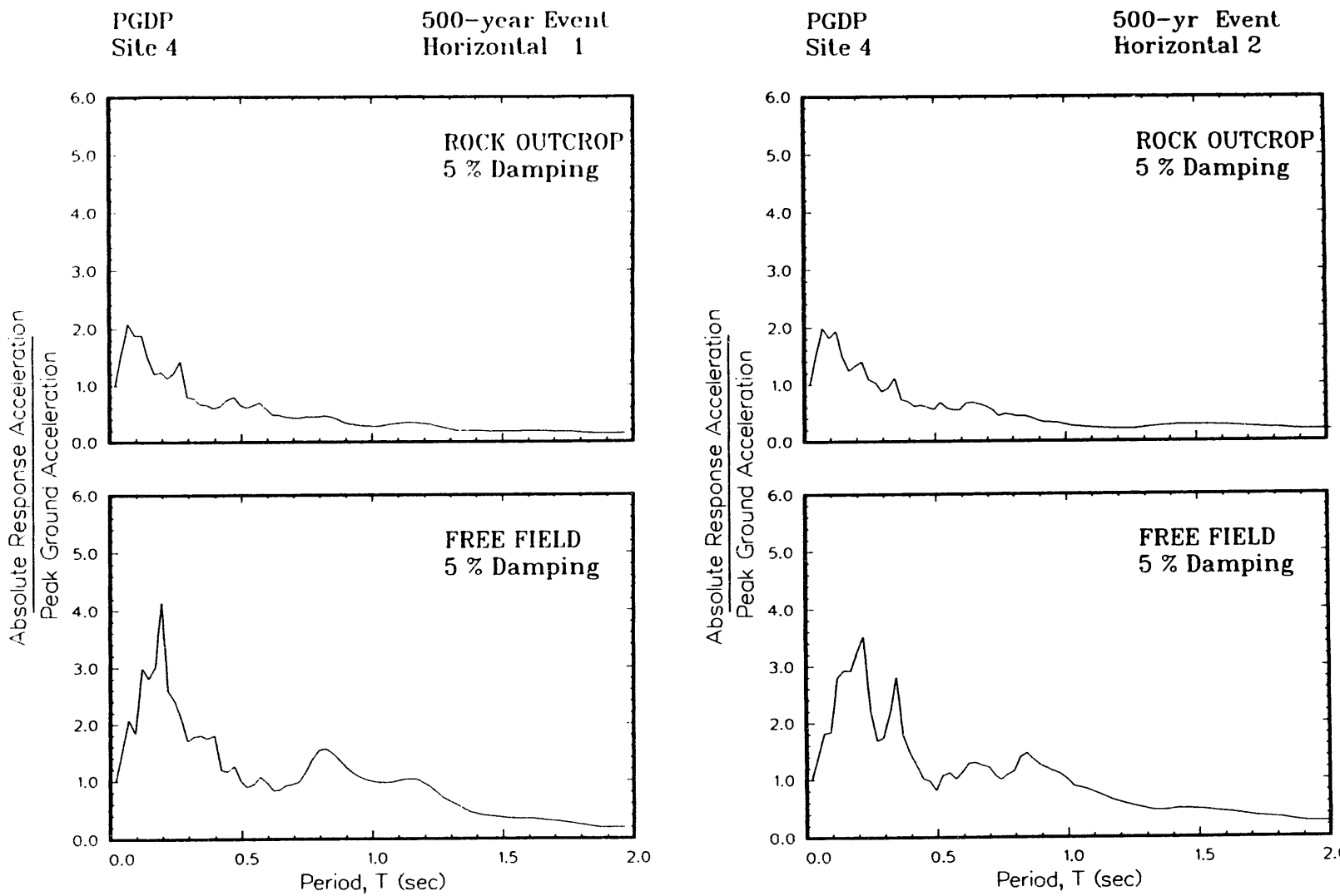

Figure G4. Ratio of amplification of absolute acceleration response spectra to peak acceleration at free field for Site 4

APPENDIX H: ACCELERATION-TIME RECORDS FOR 1000-YEAR EVENT

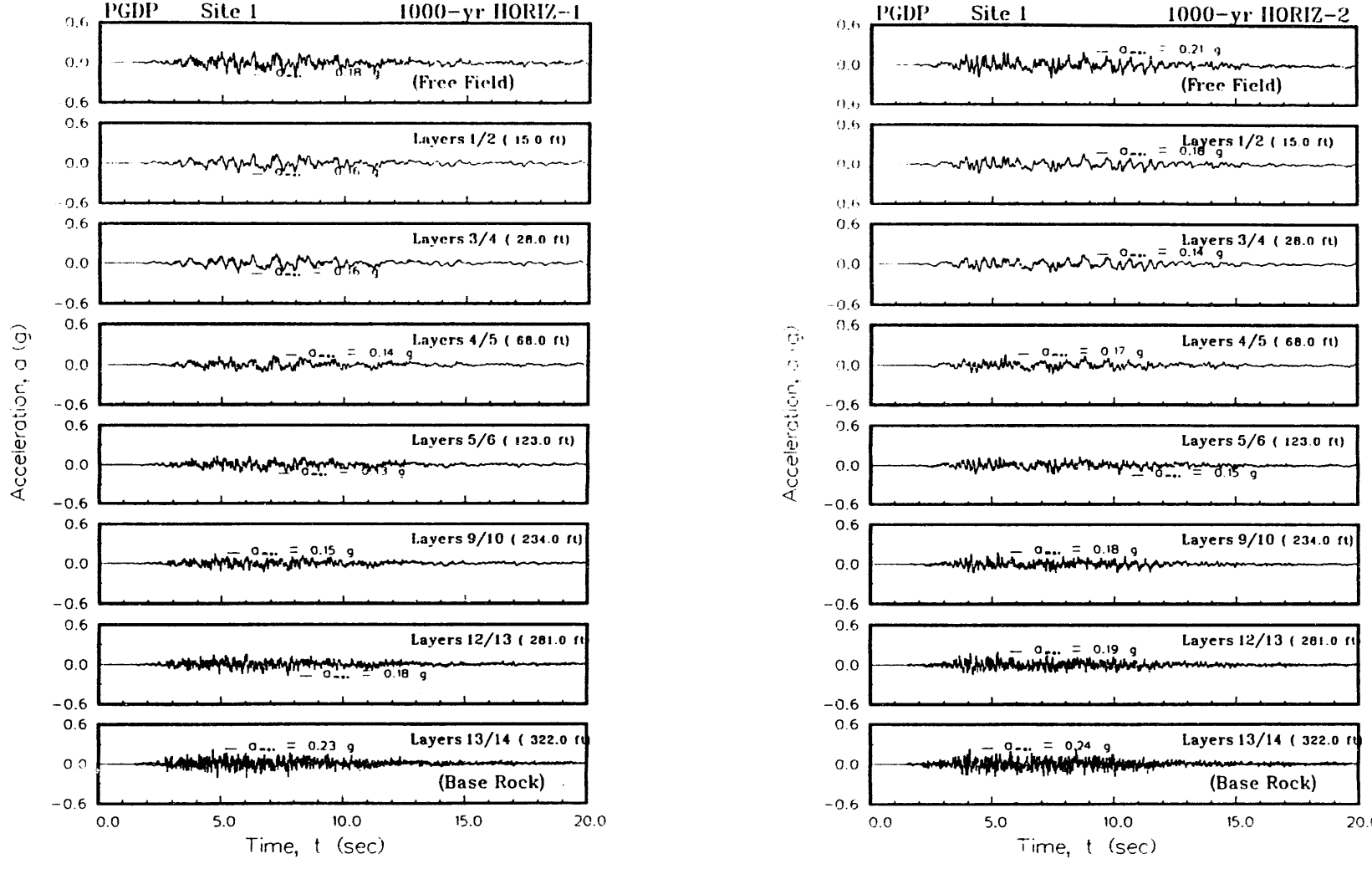

Figure H1. Variation of acceleration with time at the top of each layer for Site 1

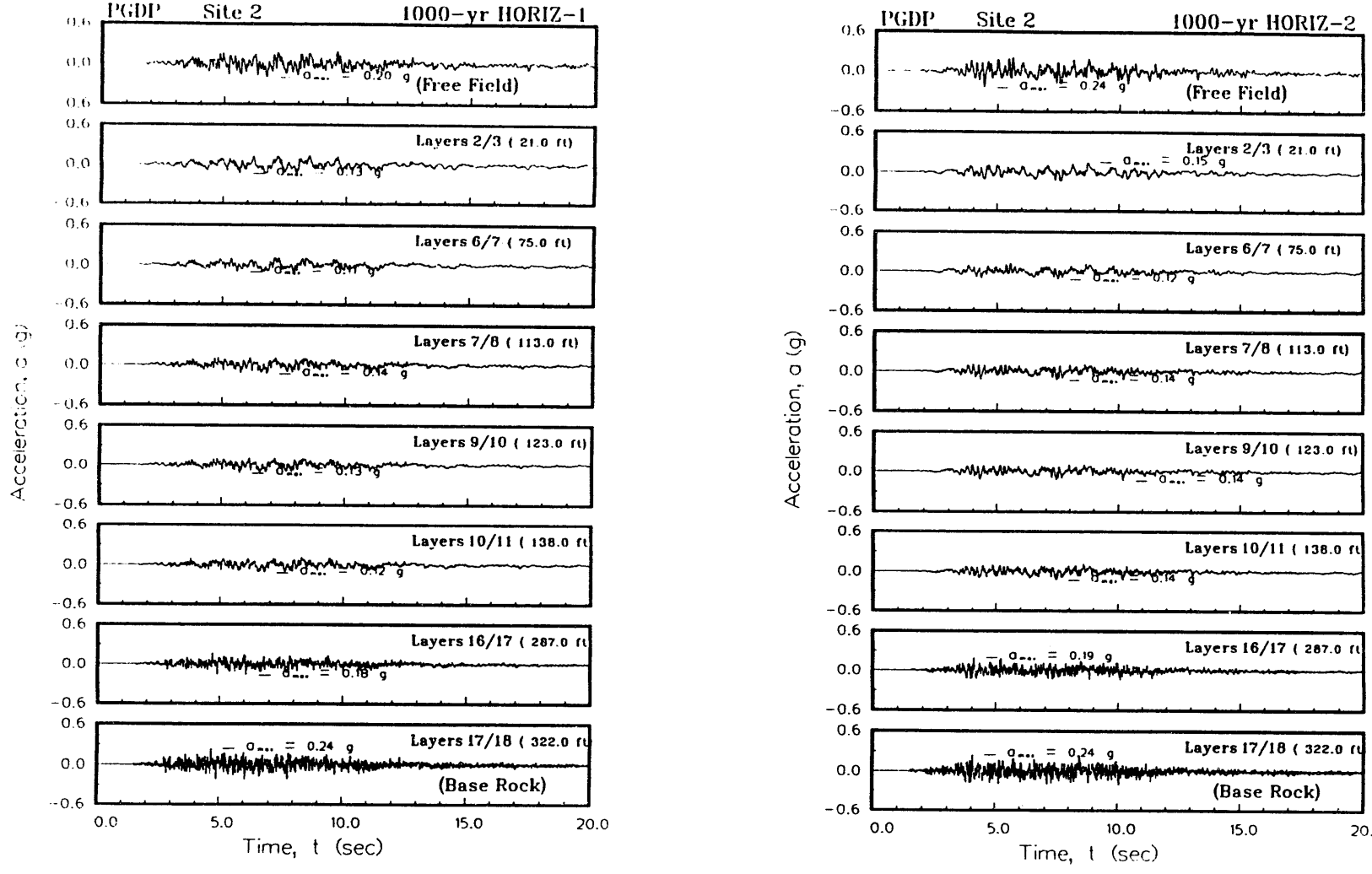

Figure H2. Variation of acceleration with time at the top of each layer for Site 2

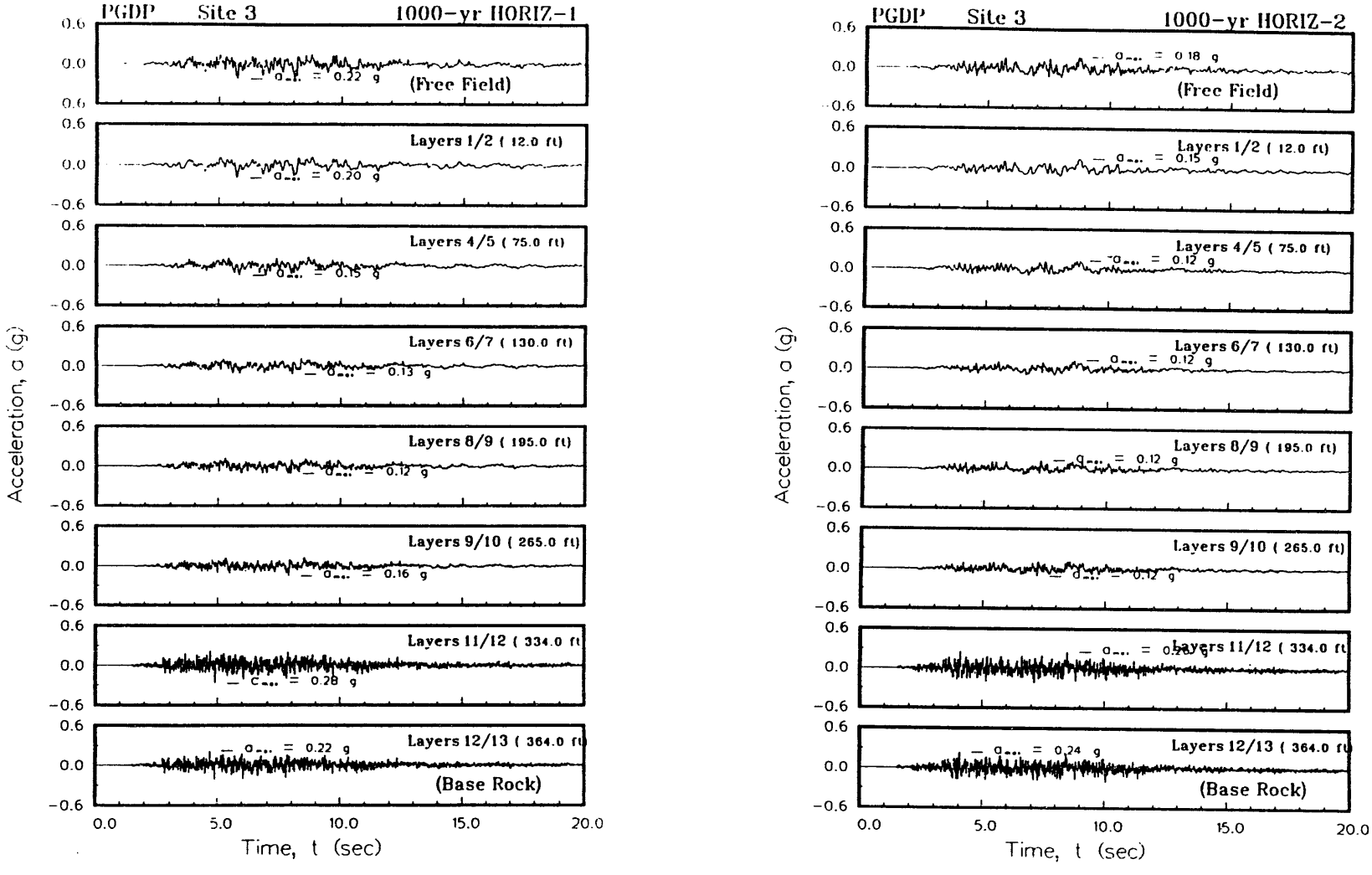

Figure H3. Variation of acceleration with time at the top of each layer for Site 3

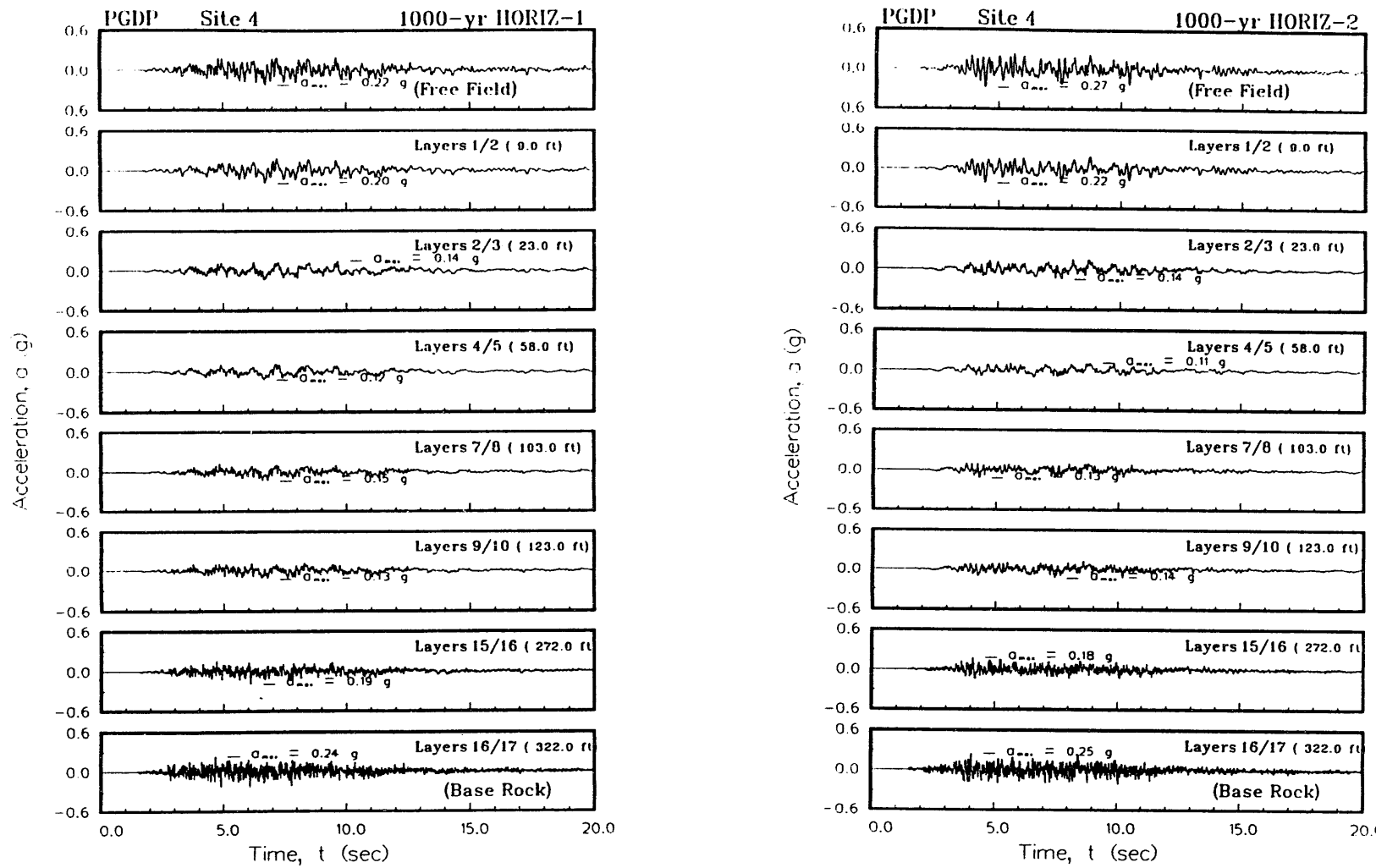

Figure H4. Variation of acceleration with time at the top of each layer for Site 4

APPENDIX I: SHEAR STRAINS FOR 1000-YEAR EVENT

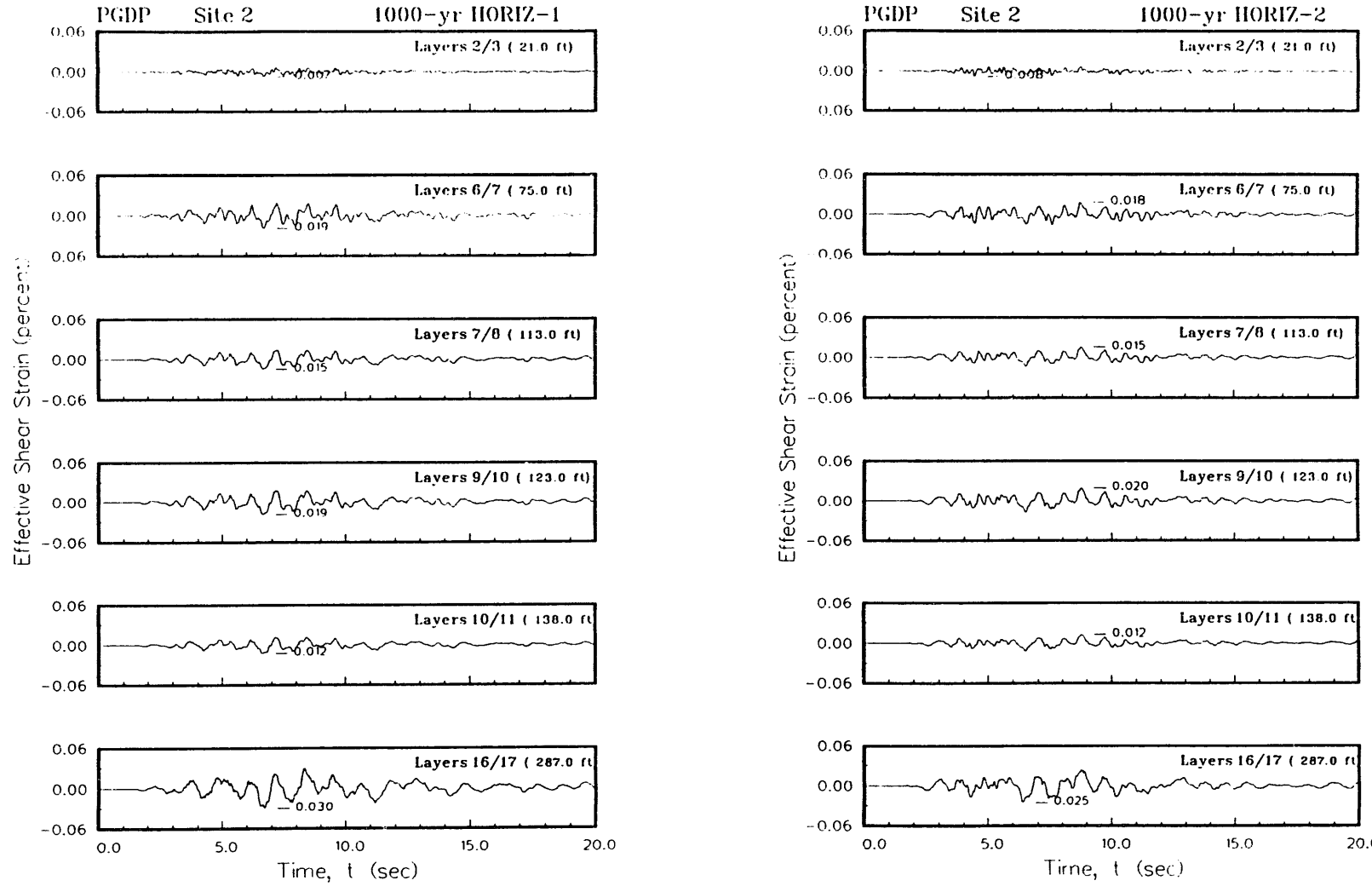

Figure I2. Variation of shear strain with time at contacts between layers for Site 2

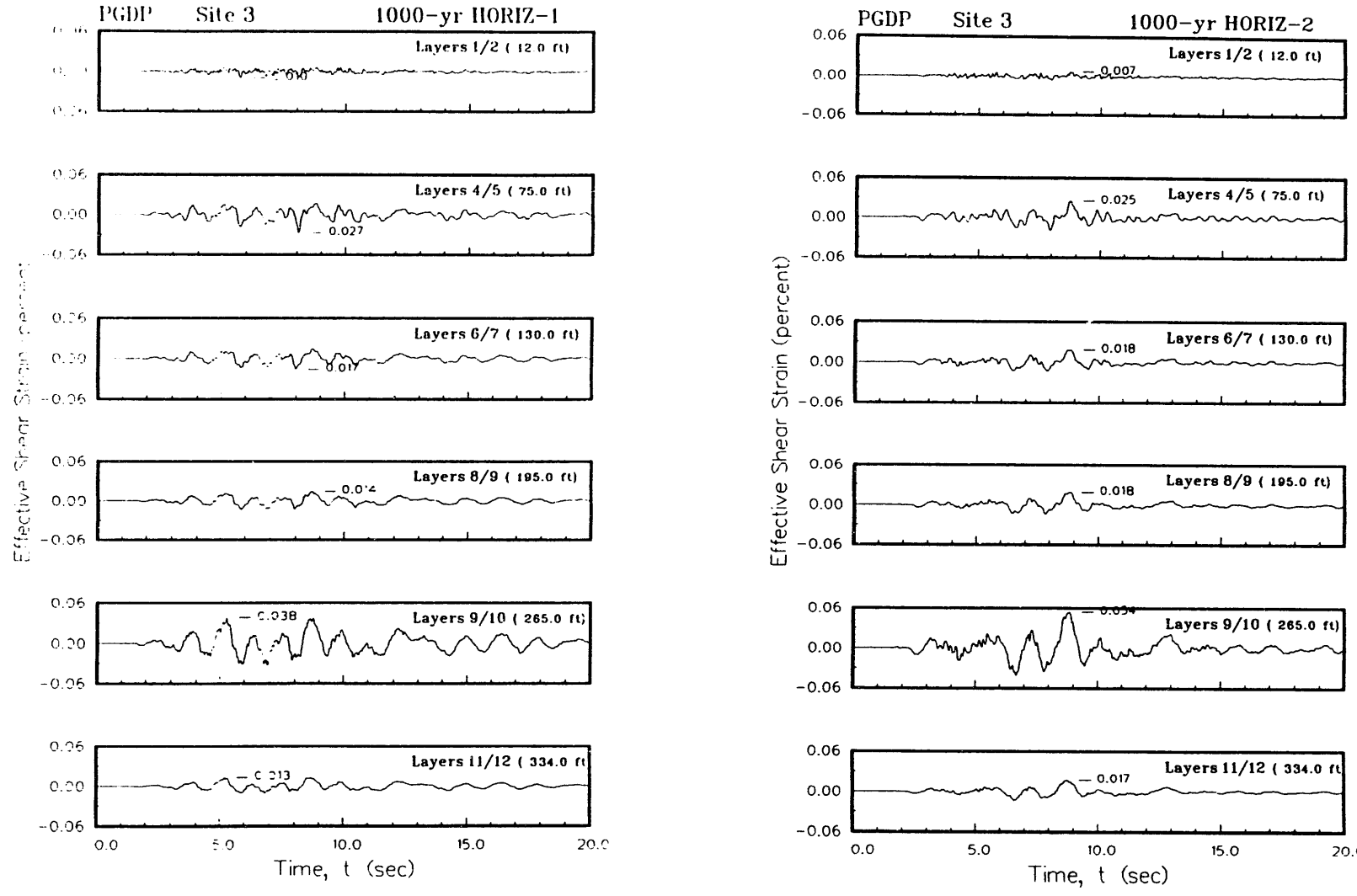

Figure I3. Variation of shear strain with time at contacts between layers for Site 3

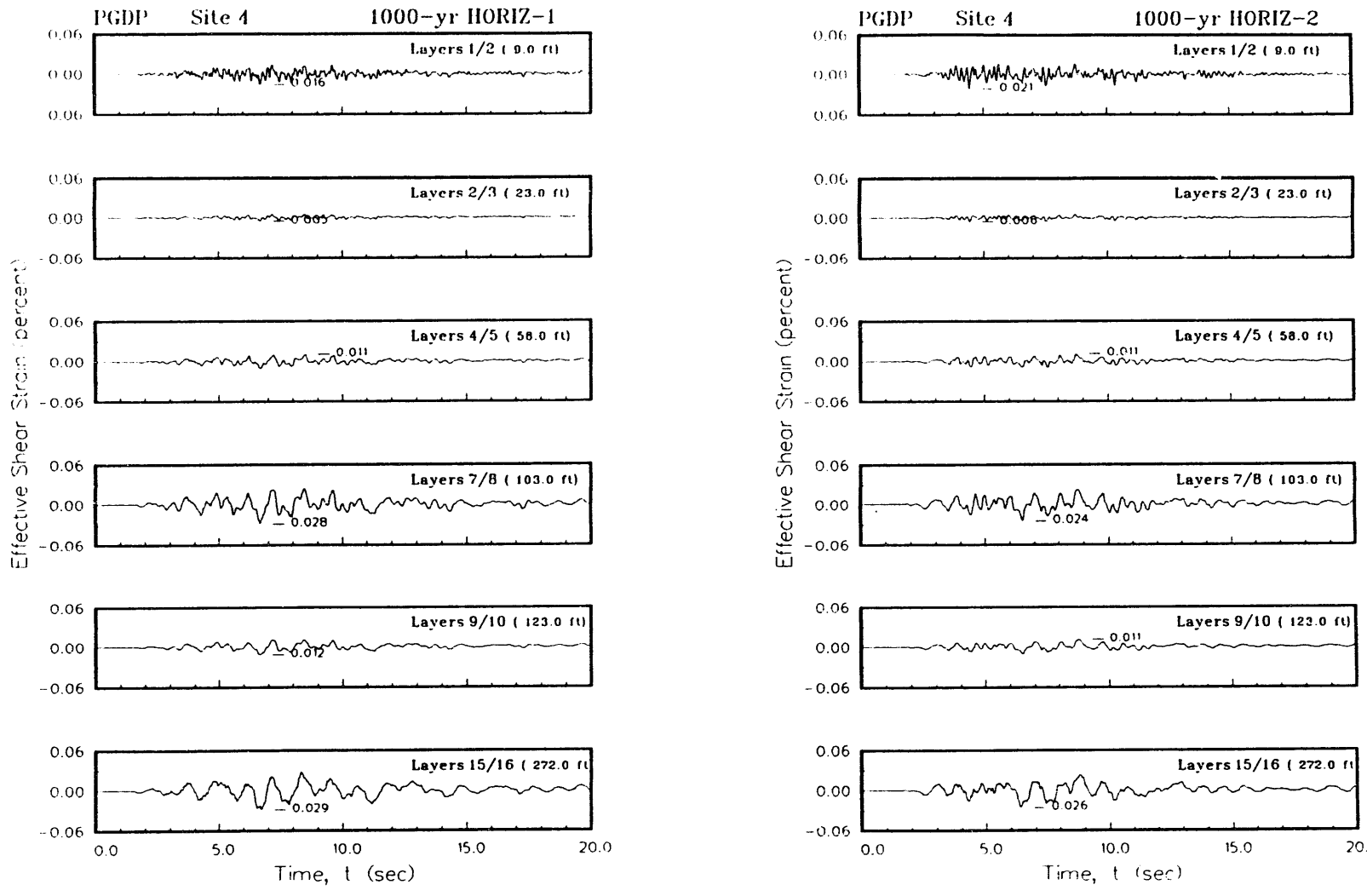

Figure I4. Variation of shear strain with time at contacts between layers for Site 4

APPENDIX J: TRIPARTITE RESPONSE SPECTRA FOR 1000-YEAR EVENT

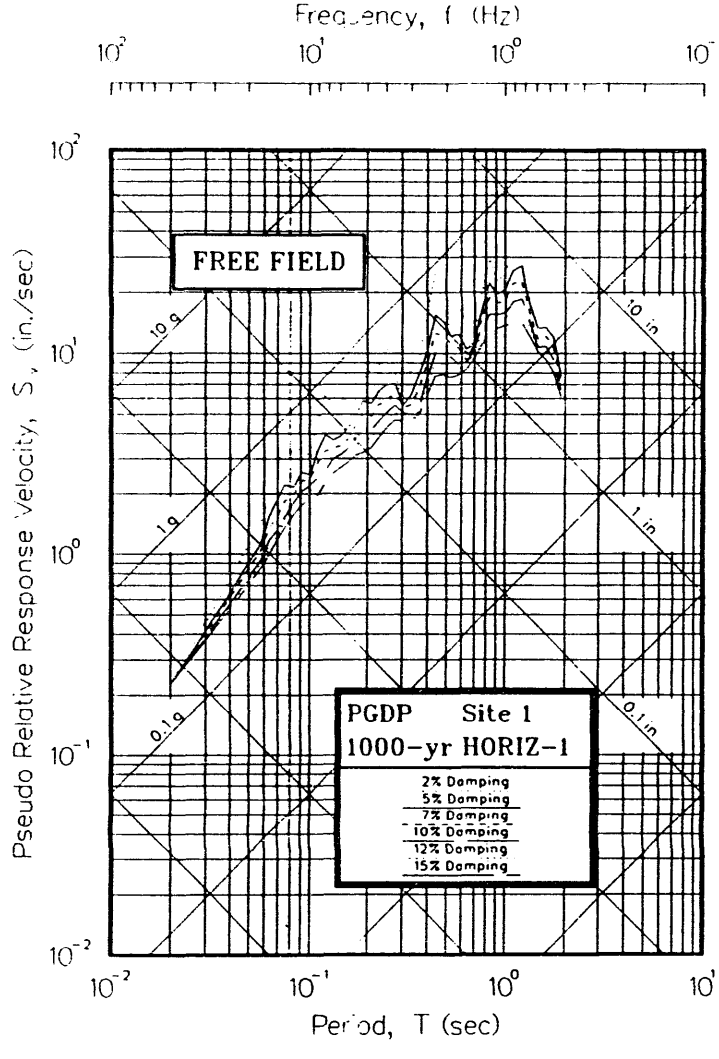

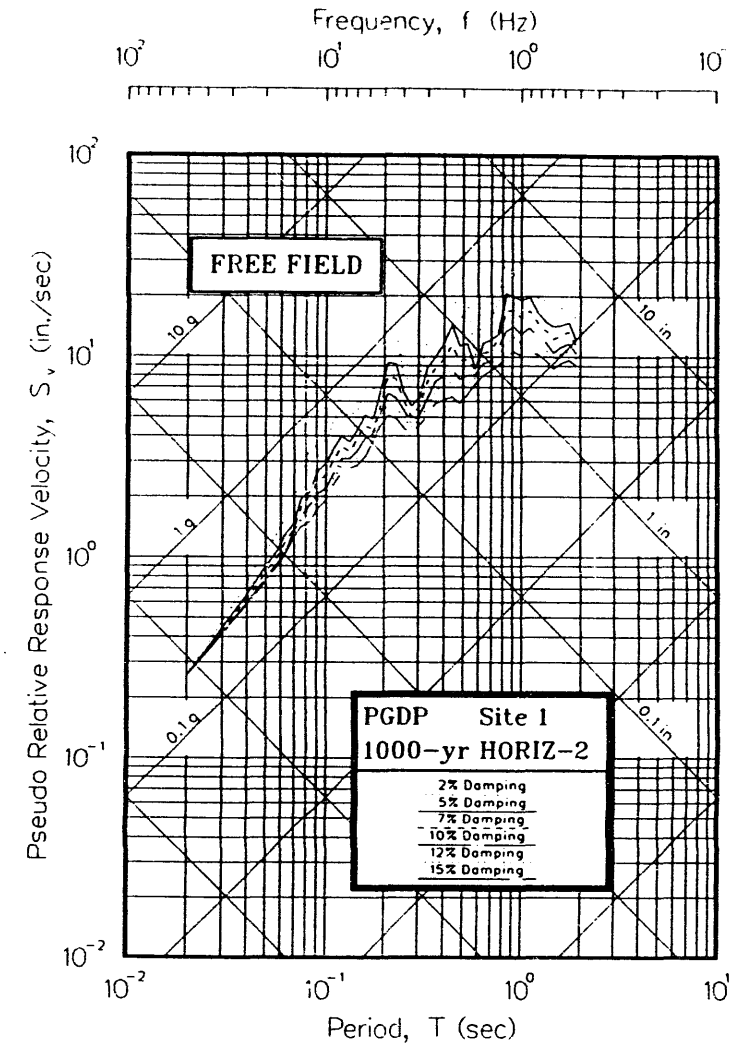

Figure J1. Psuedo-relative velocity spectra in tripartite form at free field for Site 1

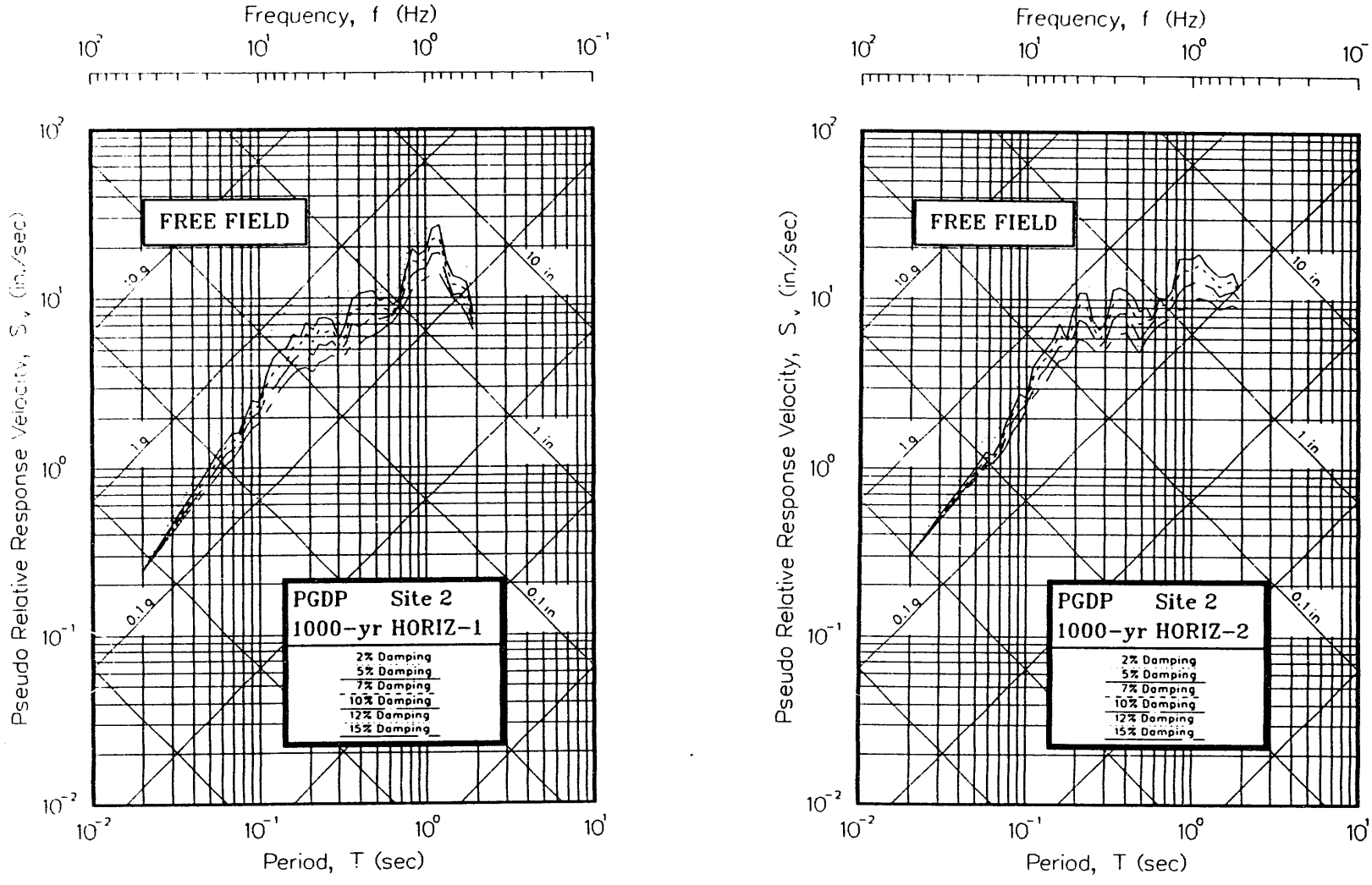

Figure J2. Psuedo-relative velocity spectra in tripartite form at free field for Site 2

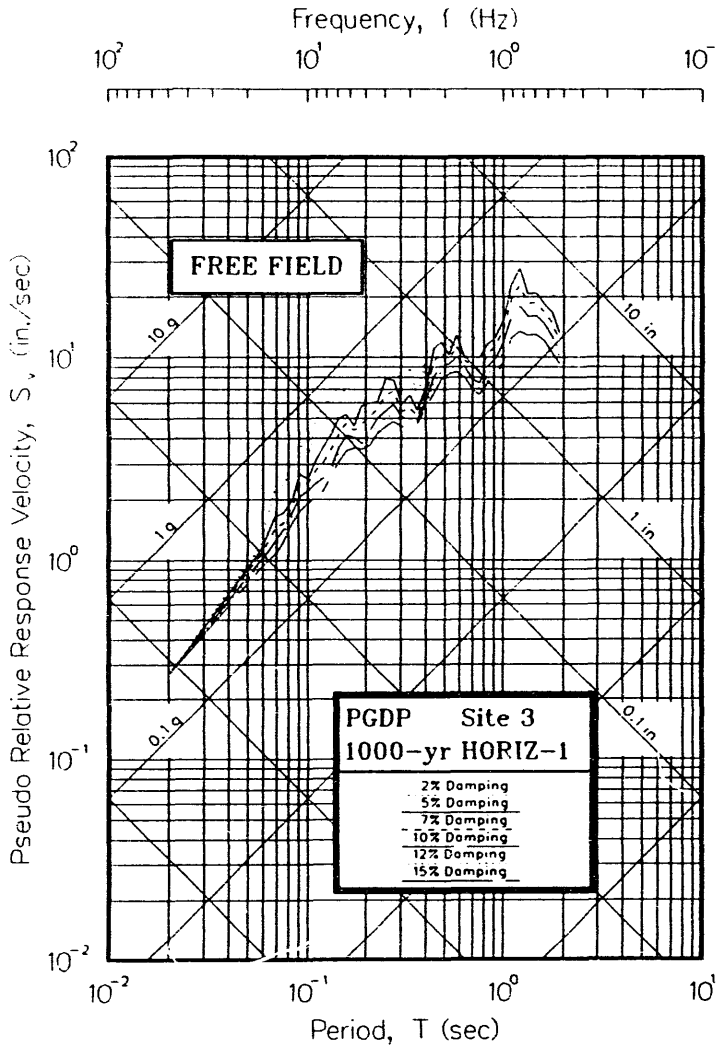

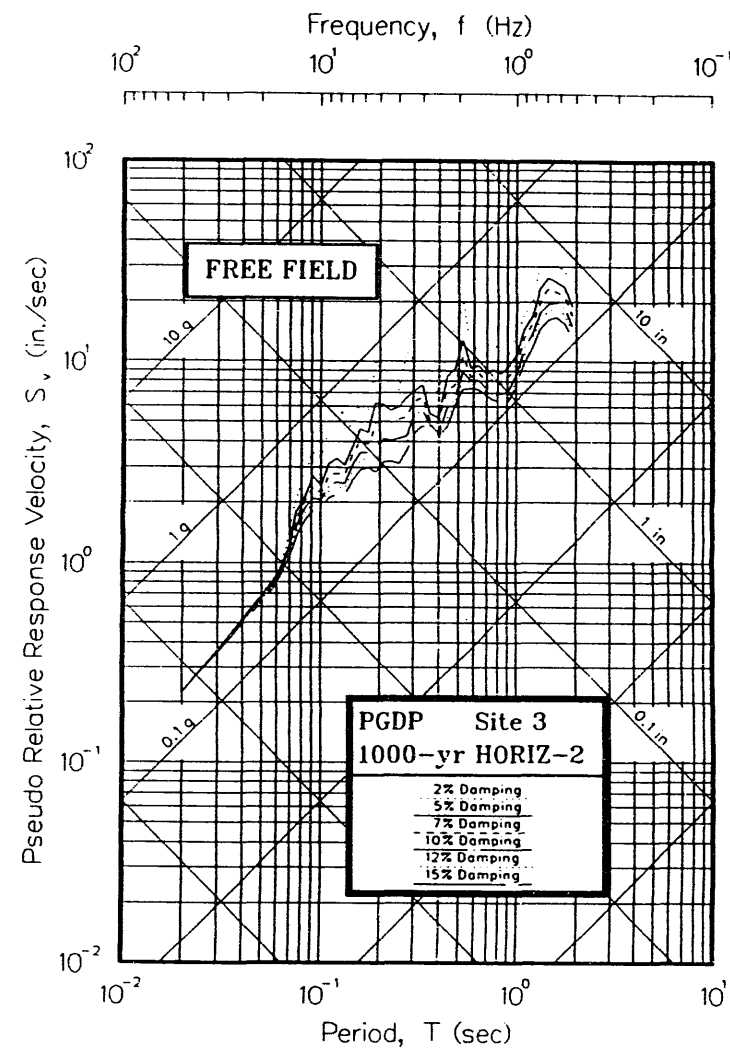

Figure J3. Psuedo-relative velocity spectra in tripartite form at free field for Site 3

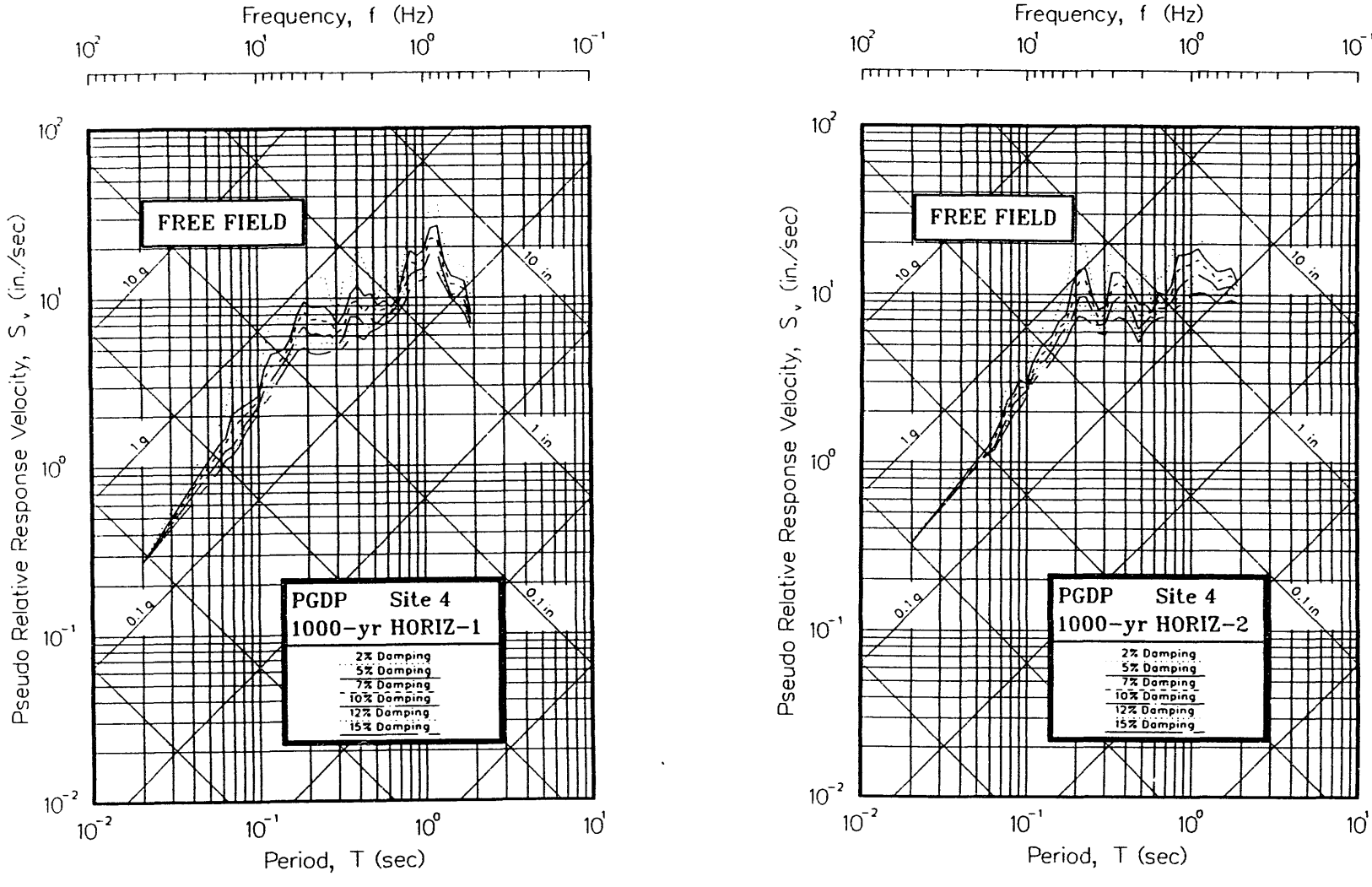

Figure J4. Psuedo-relative velocity spectra in tripartite form at free field for Site 4

APPENDIX K: ACCELERATION SPECTRA FOR 1000-YEAR EVENT

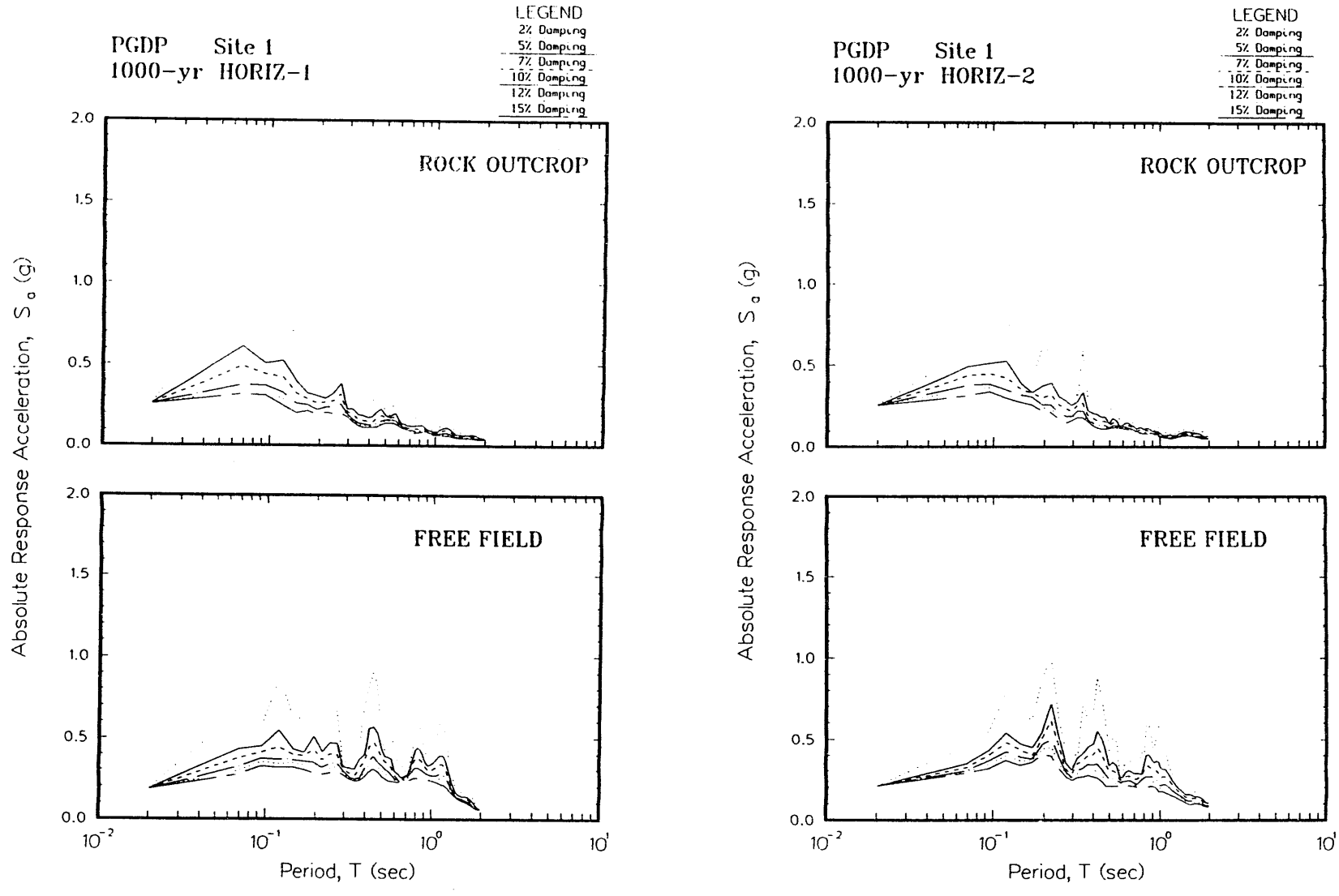

Figure K1. Absolute acceleration response spectra at free field for Site 1

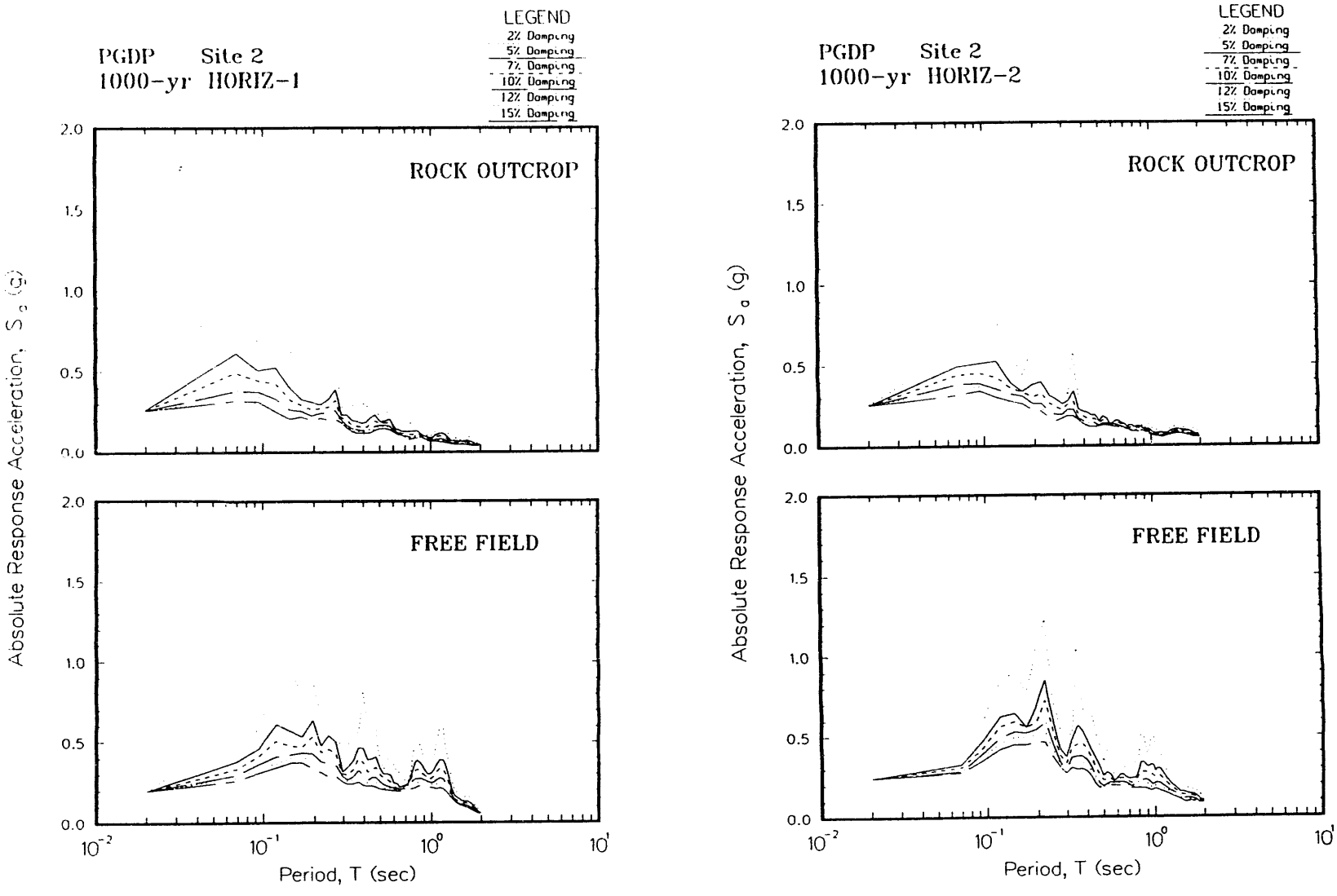

Figure K2. Absolute acceleration response spectra at free field for Site 2

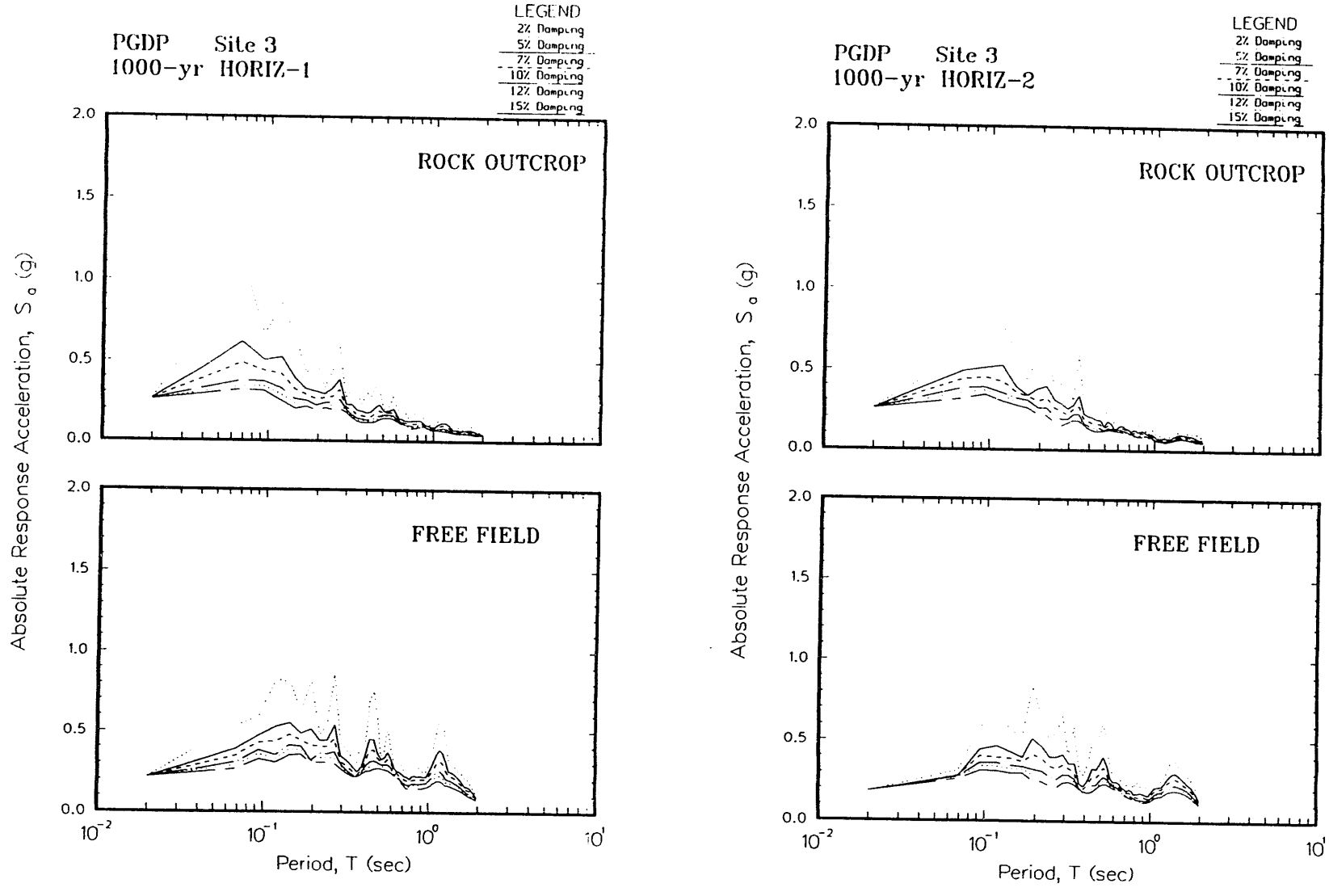

Figure K3. Absolute acceleration response spectra at free field for Site 3

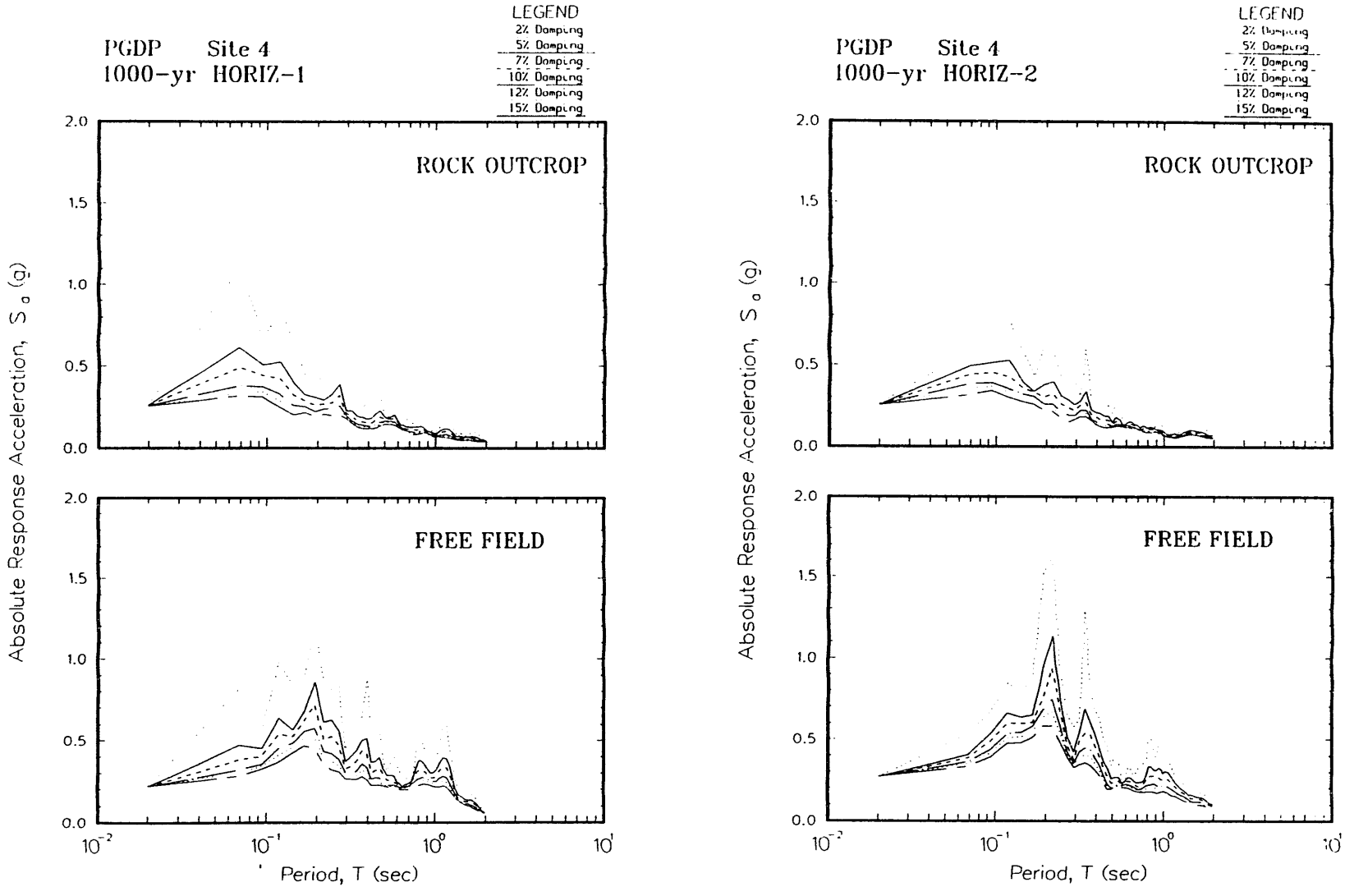

Figure K4. Absolute acceleration response spectra at free field for Site 4

APPENDIX L: RATIO OF ACCELERATION SPECTRA FOR 1000-YEAR EVENT

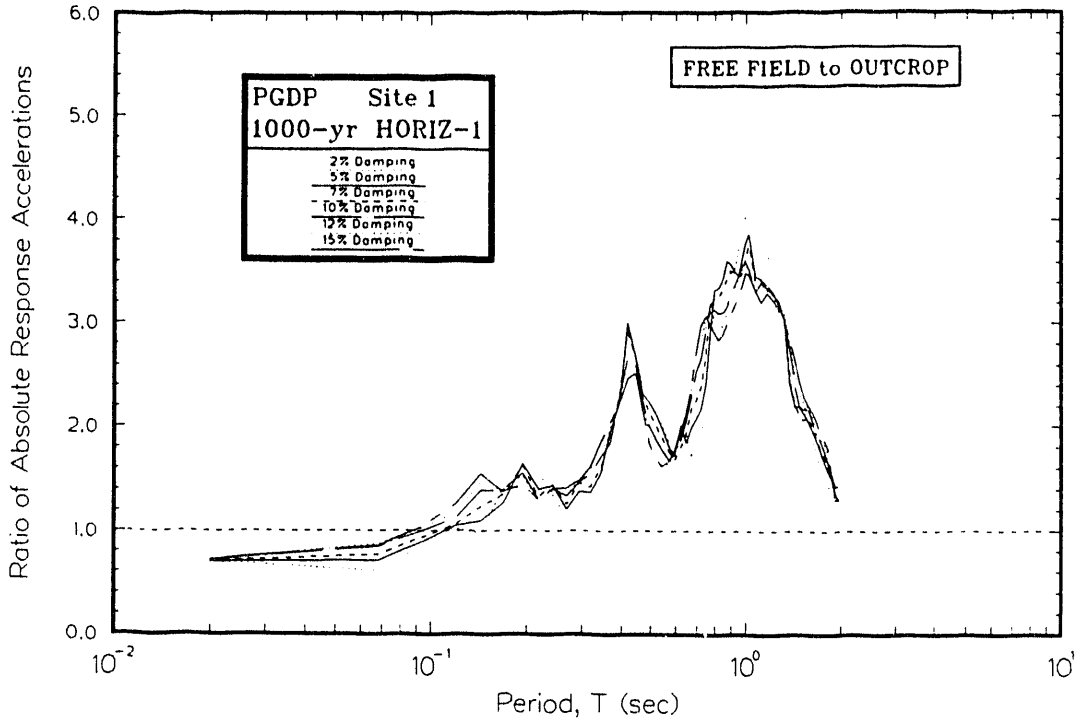

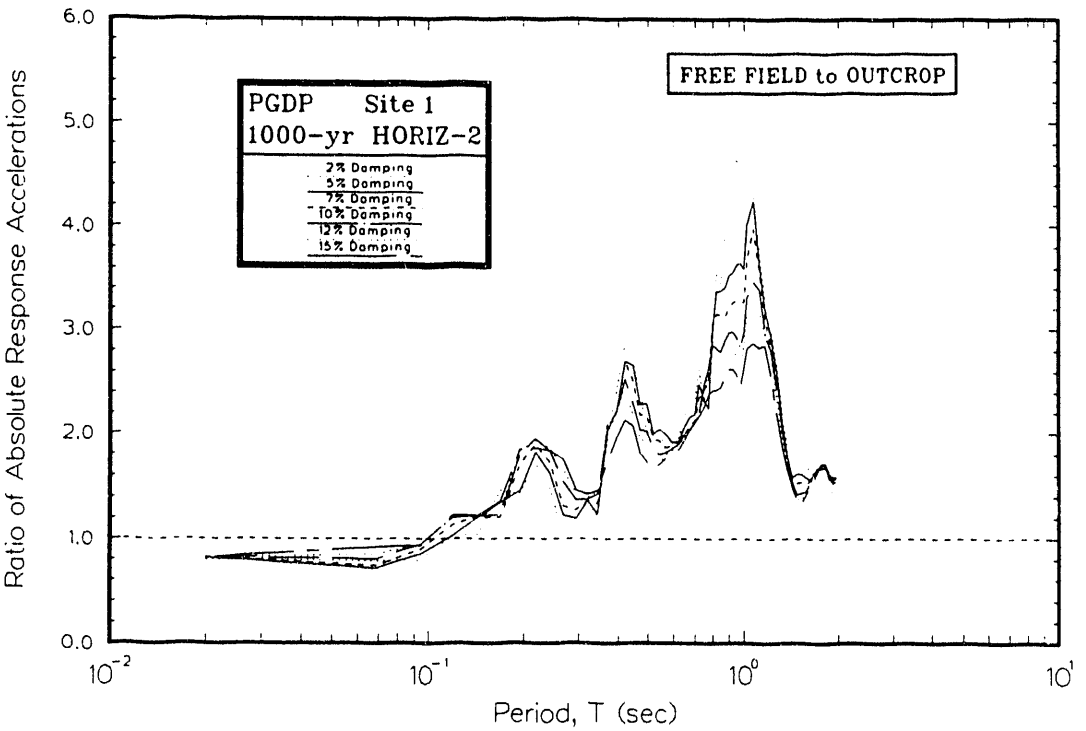

Figure L1. Ratio of absolute acceleration response spectra at free field to rock for Site 1

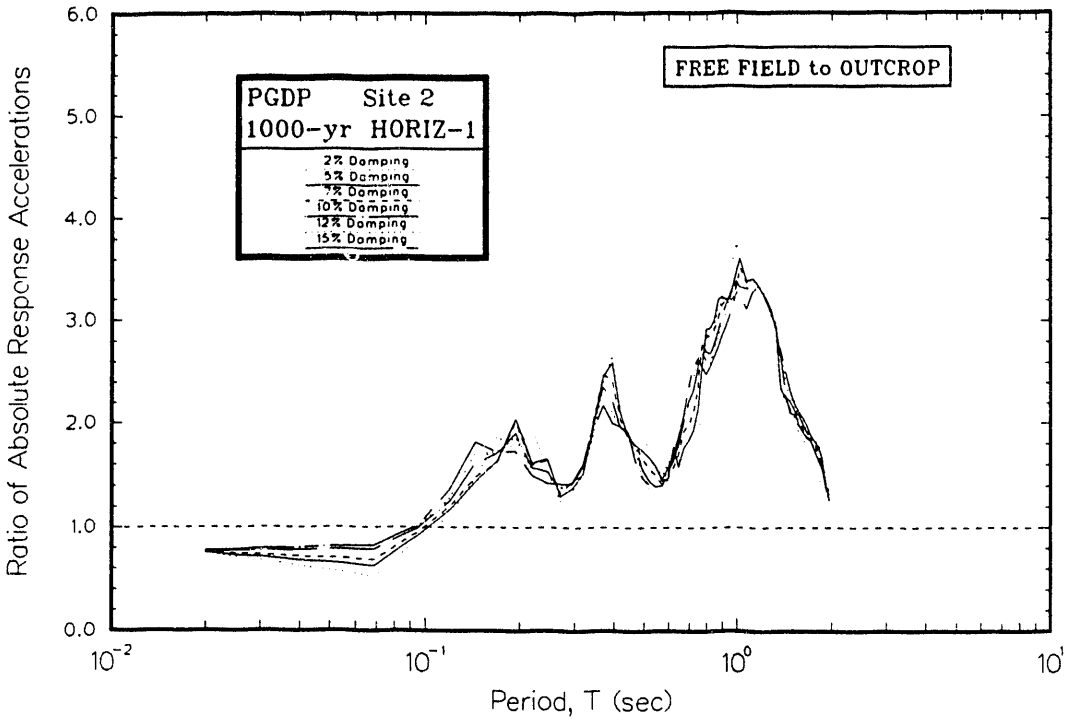

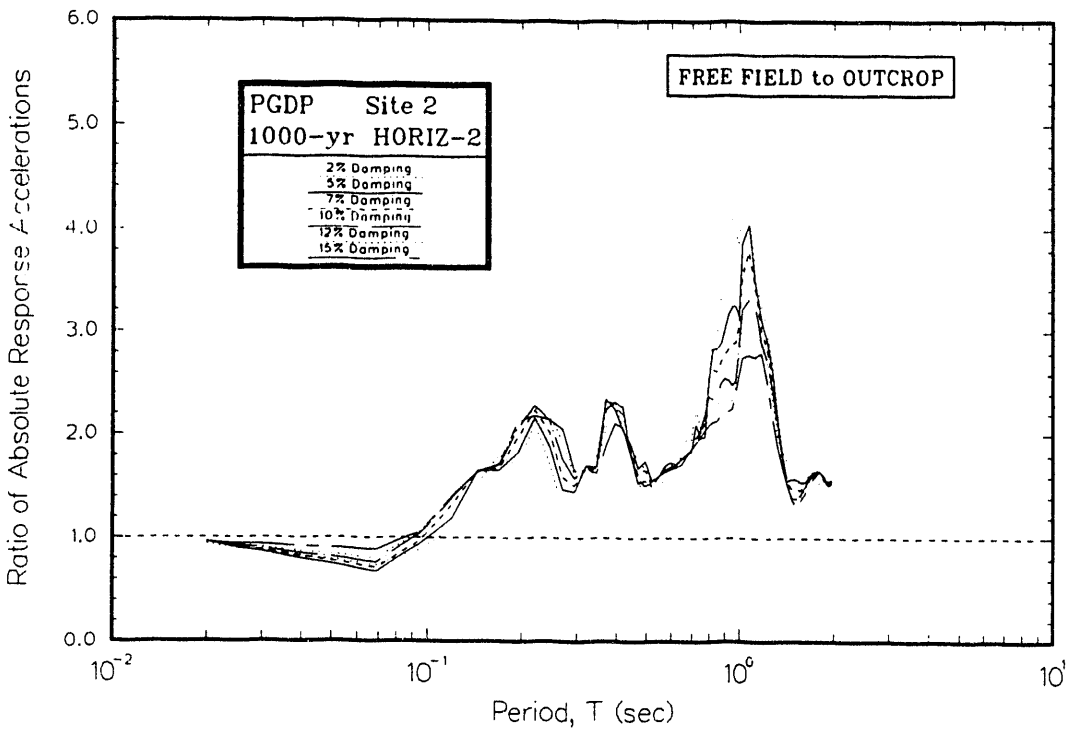

Figure L2. Ratio of absolute acceleration response spectra at free field to rock for Site 2

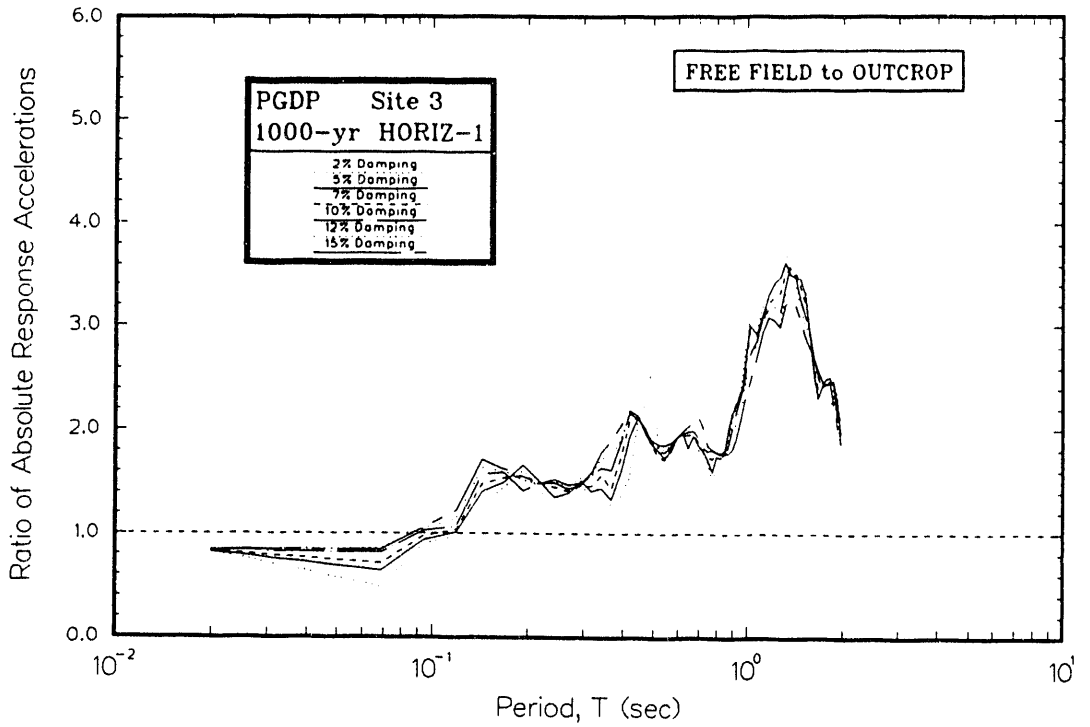

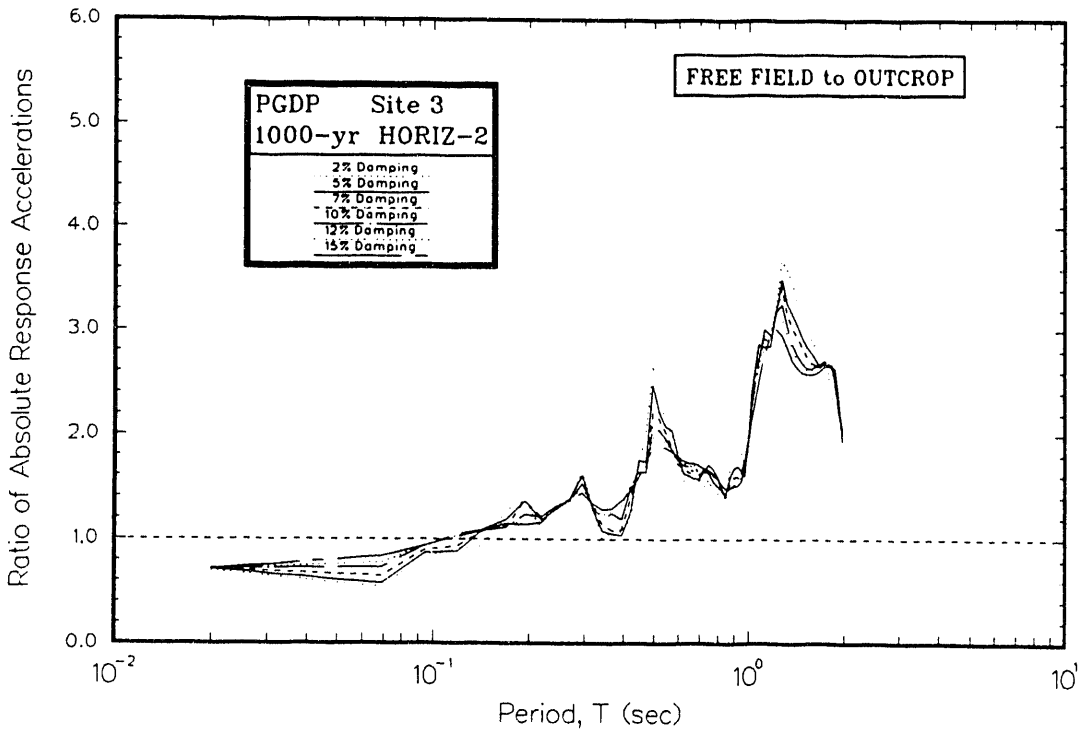

Figure L3. Ratio of absolute acceleration response spectra at free field to rock for Site 3

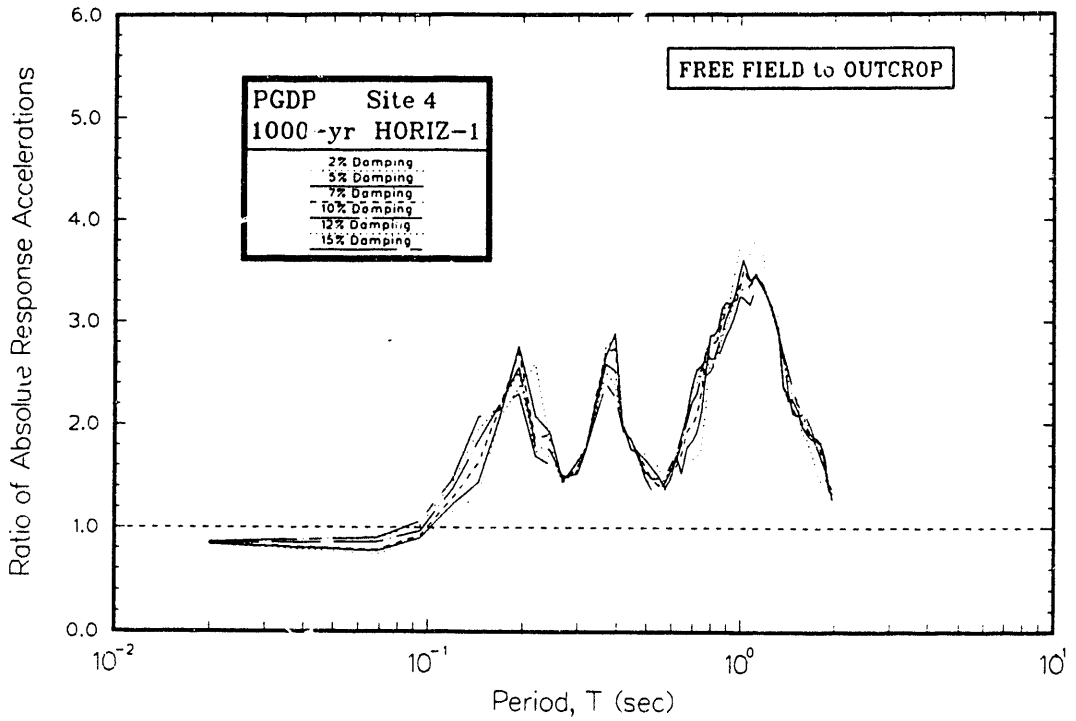

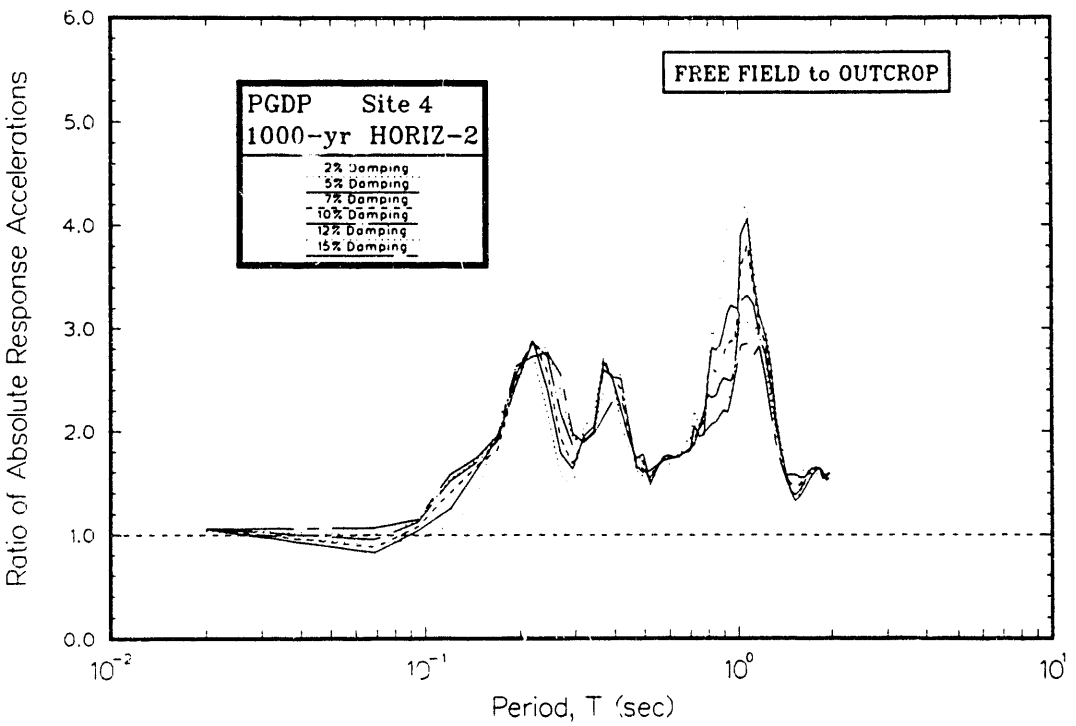

Figure L4. Ratio of absolute acceleration response spectra at free field to rock for Site 4

APPENDIX M: AMPLIFICATION RATIOS FOR 1000-YEAR EVENT

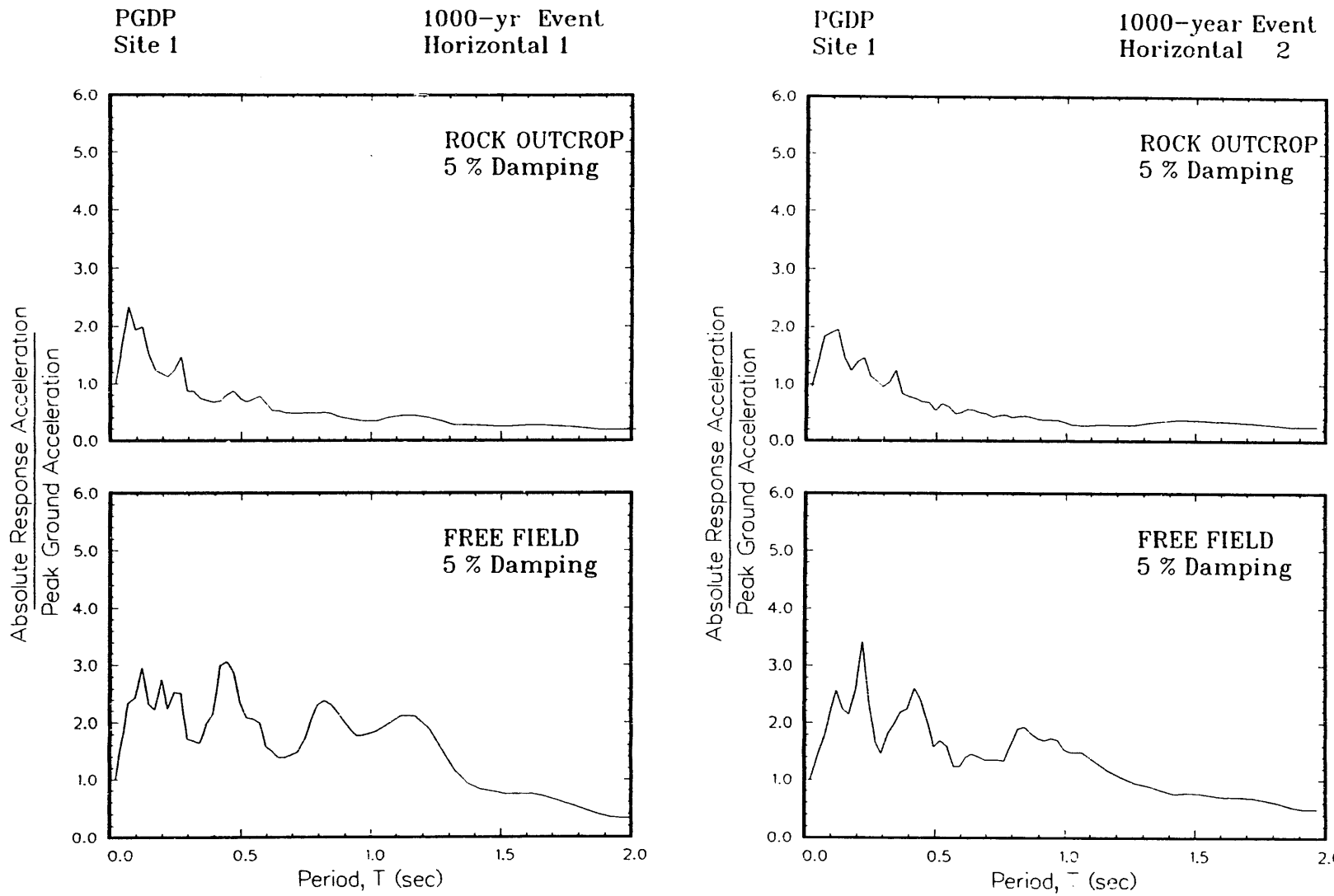

Figure M1. Ratio of amplification of absolute acceleration response spectra to peak acceleration at free field for Site 1

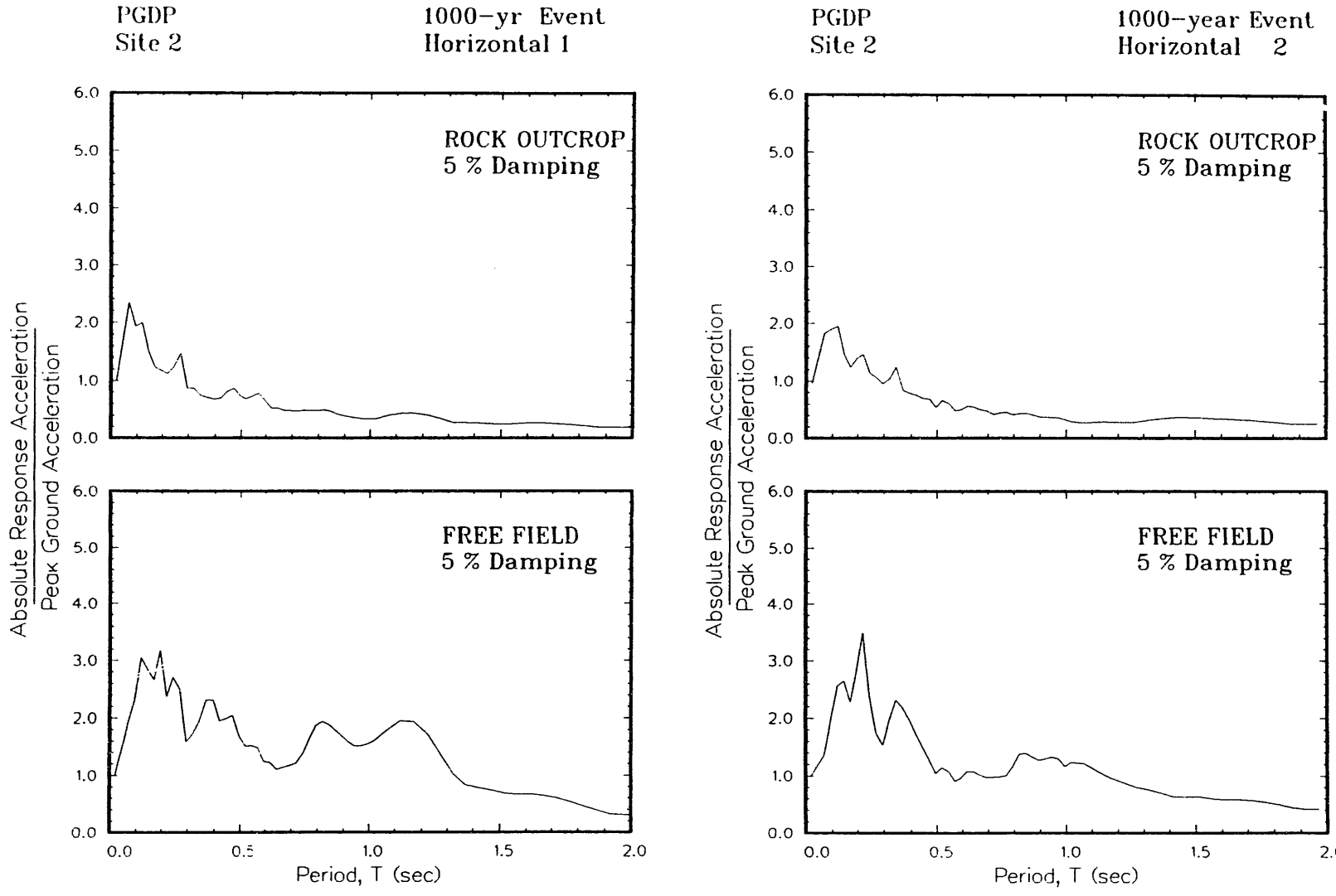

Figure M2. Ratio of amplification of absolute acceleration response spectra to peak acceleration at free field for Site 2

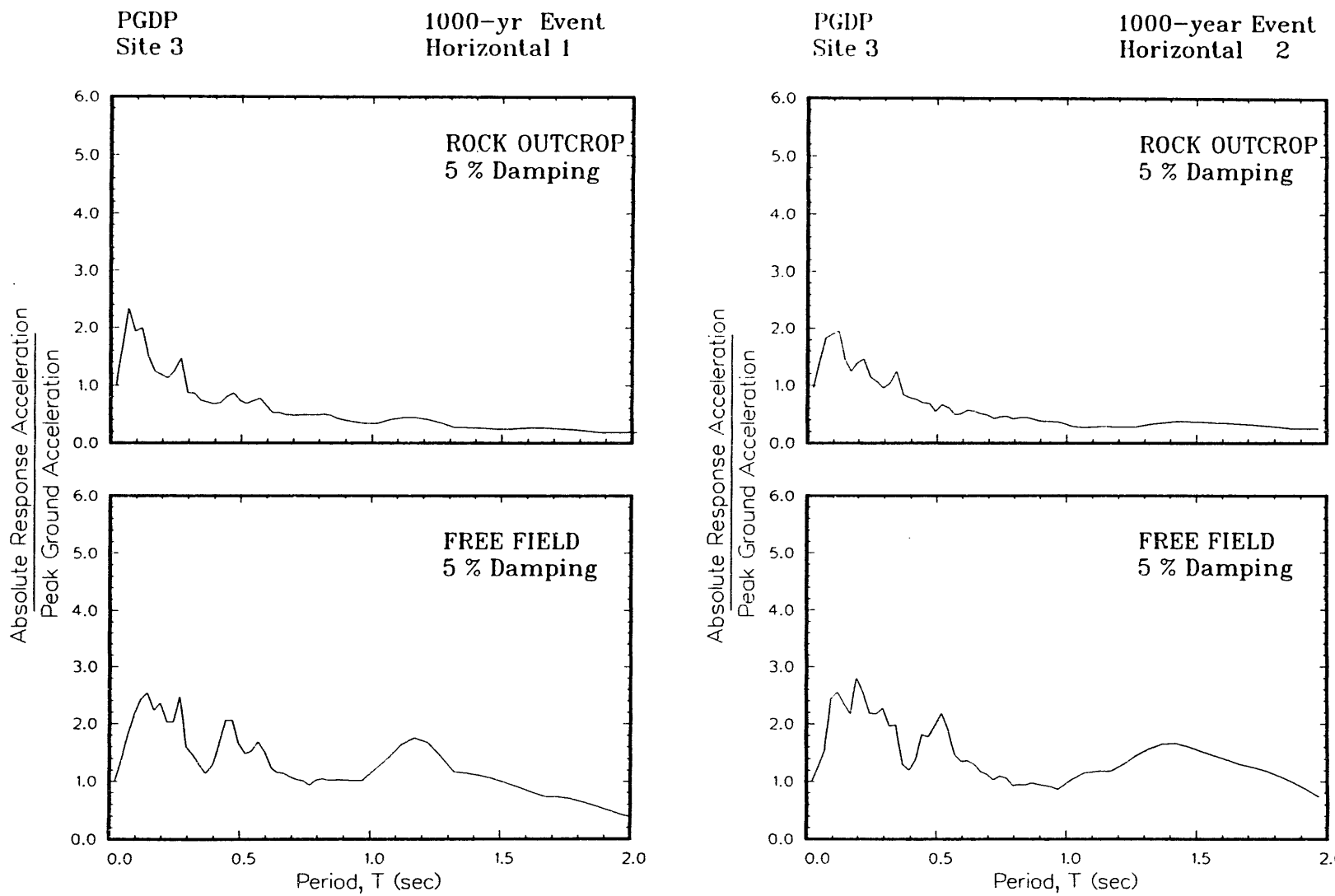

Figure M3. Ratio of amplification of absolute acceleration response spectra to peak acceleration at free field for Site 3

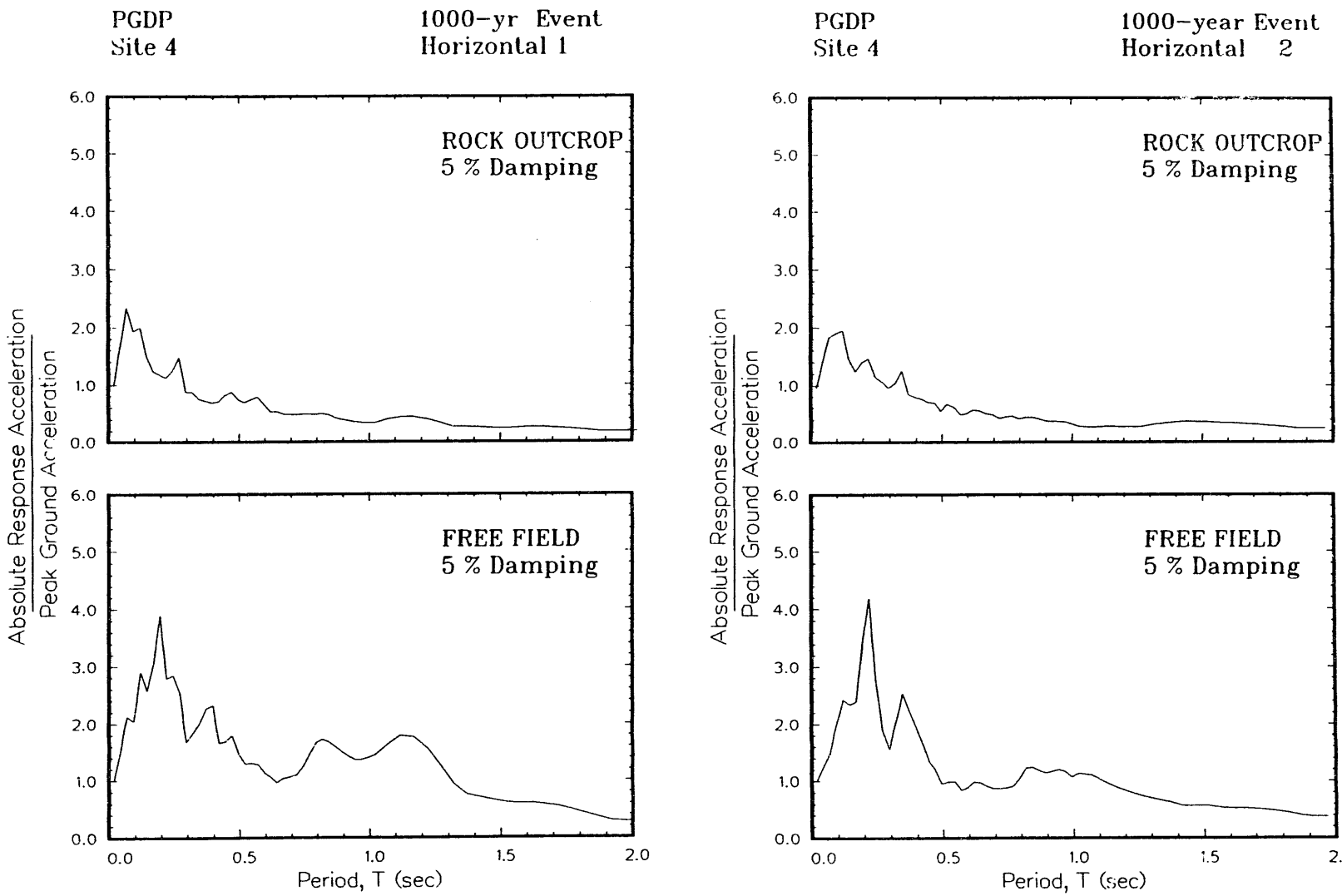

Figure M4. Ratio of amplification of absolute acceleration response spectra to peak acceleration at free field for Site 4

APPENDIX N: ACCELERATION-TIME RECORDS FOR 5000-YEAR EVENT

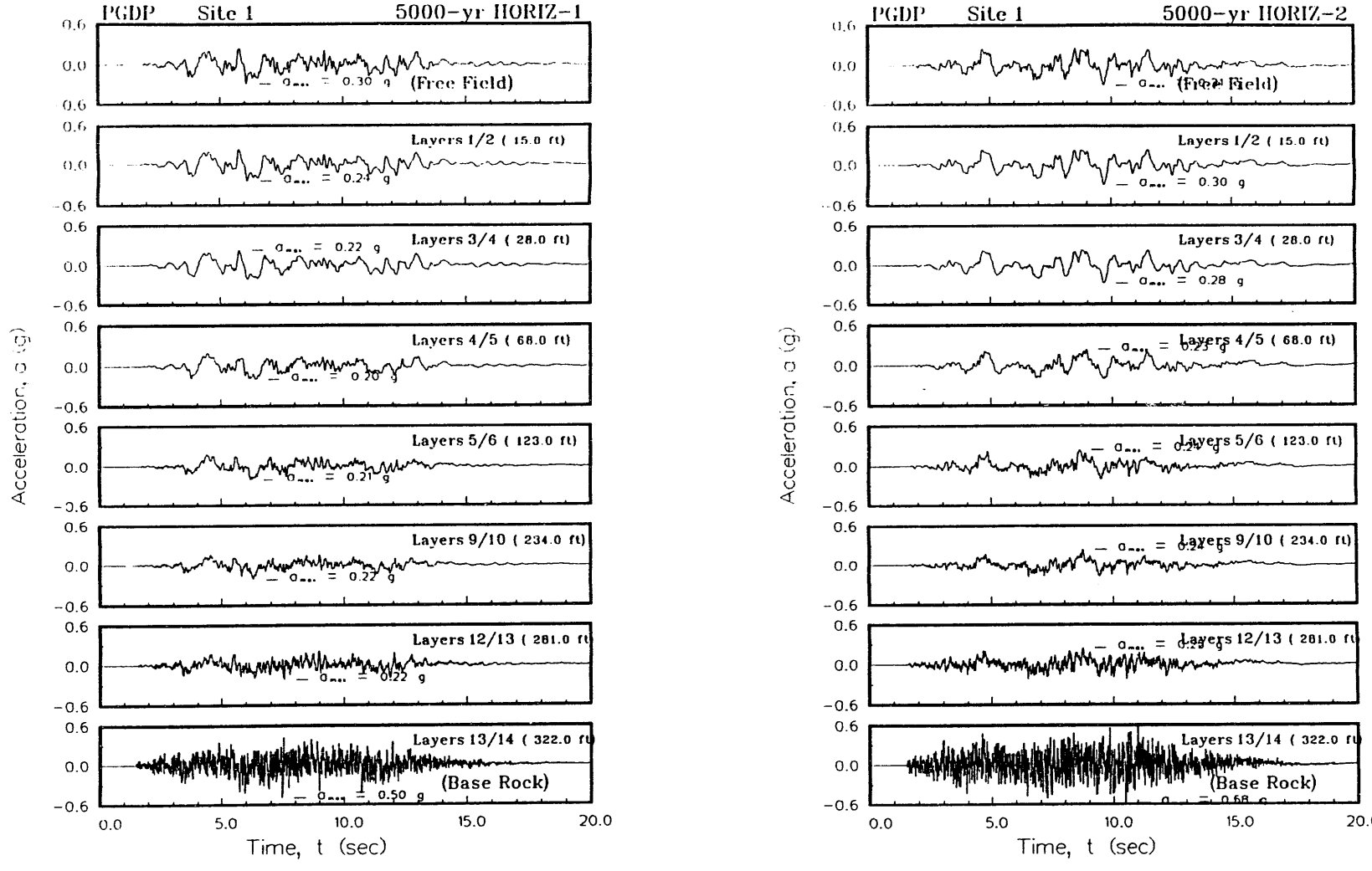

Figure N1. Variation of acceleration with time at the top of each layer for Site 1

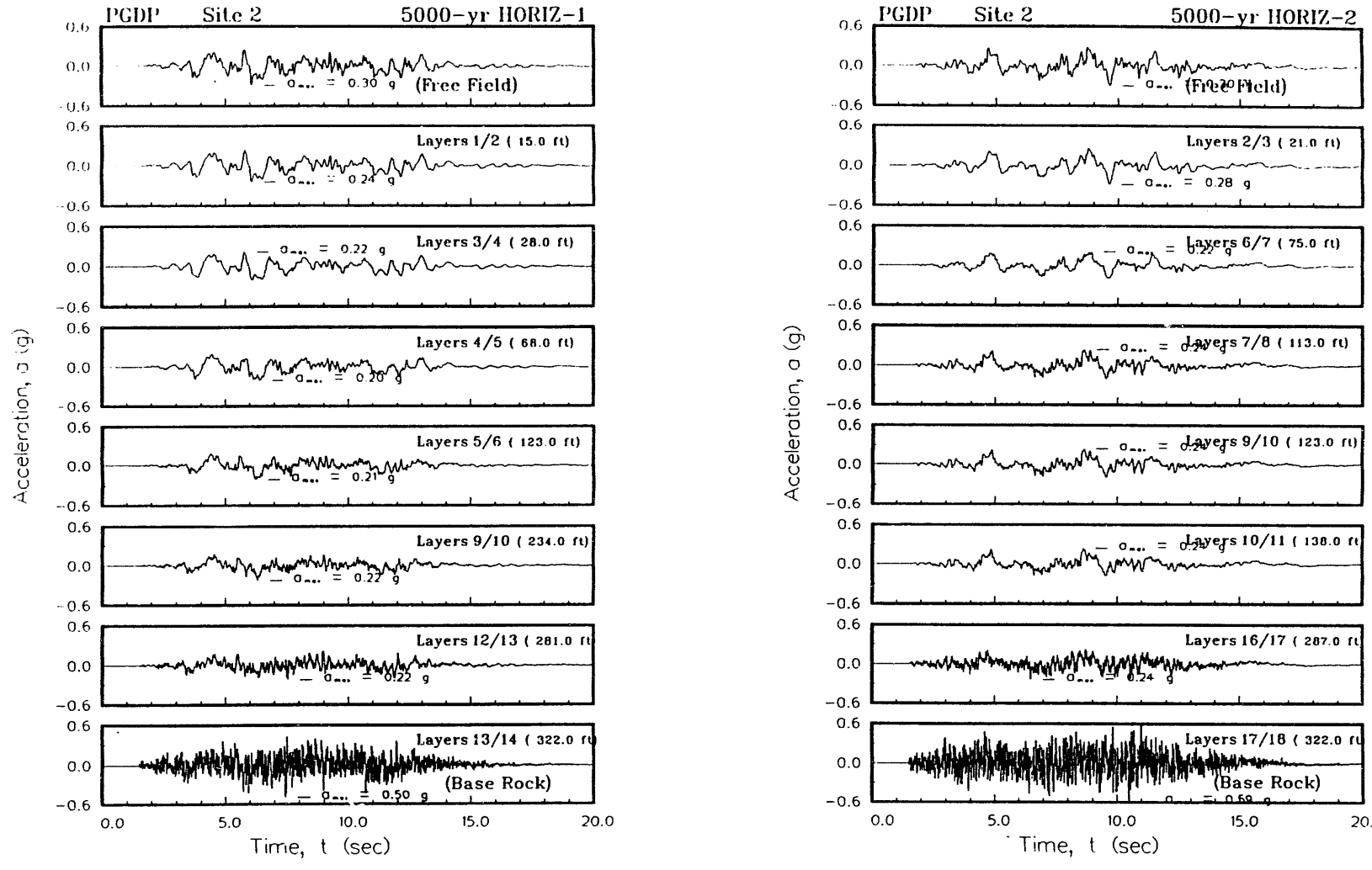

Figure N2. Variation of acceleration with time at the top of each layer for Site 2

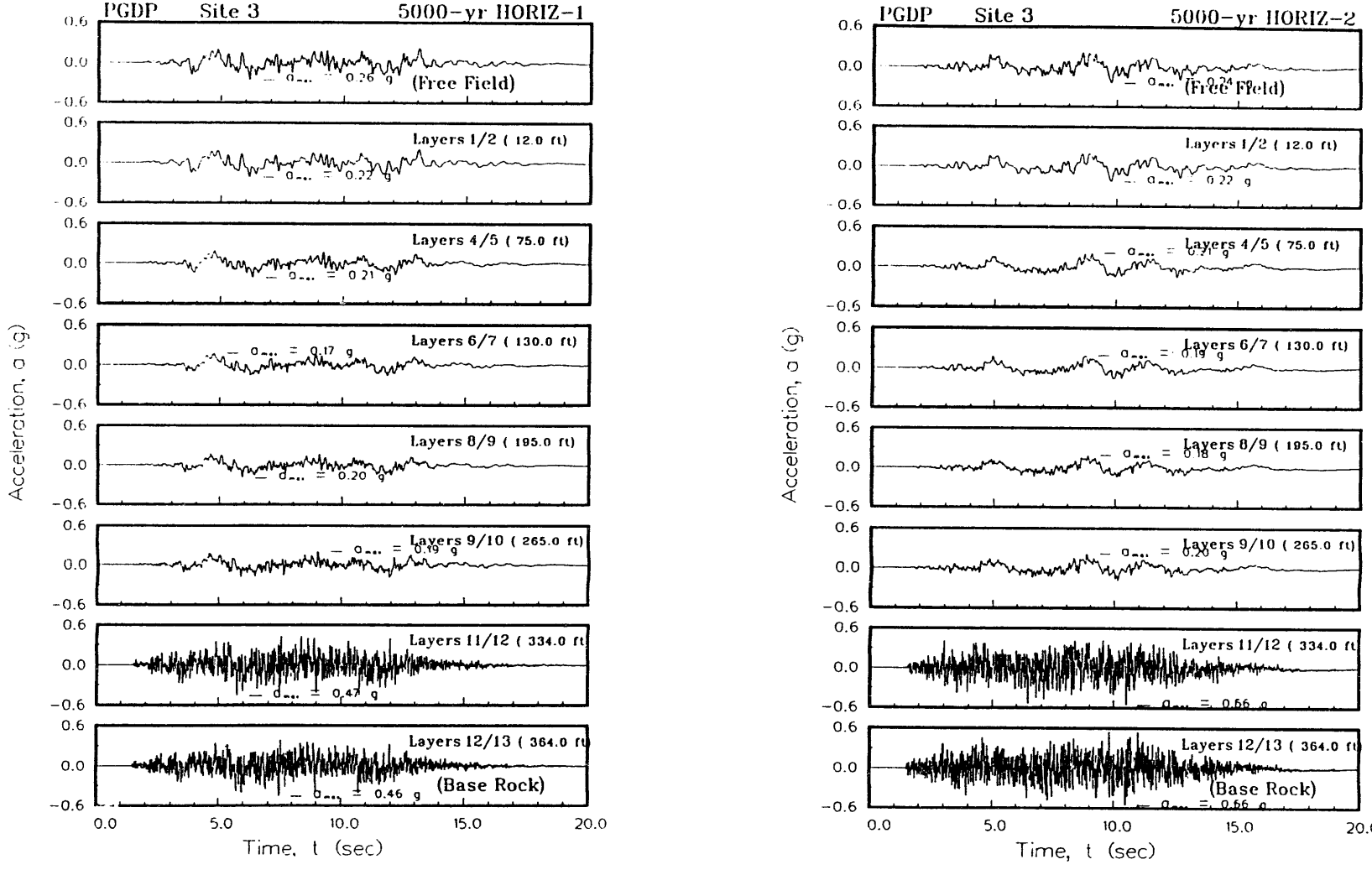

Figure N3. Variation of acceleration with time at the top of each layer for Site 3

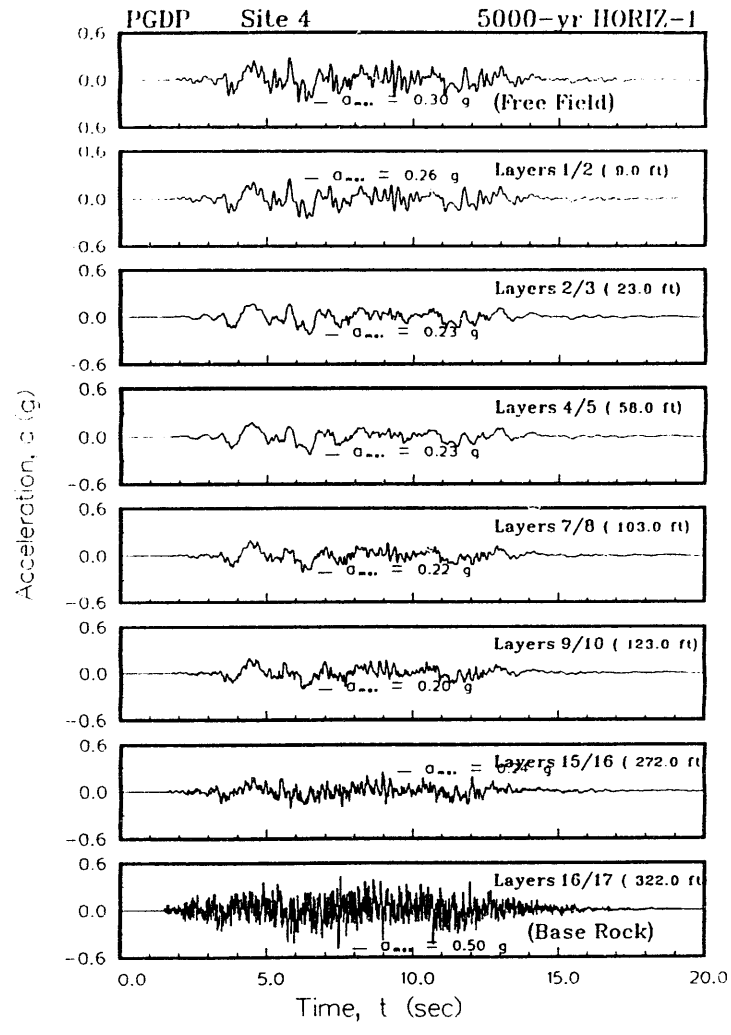

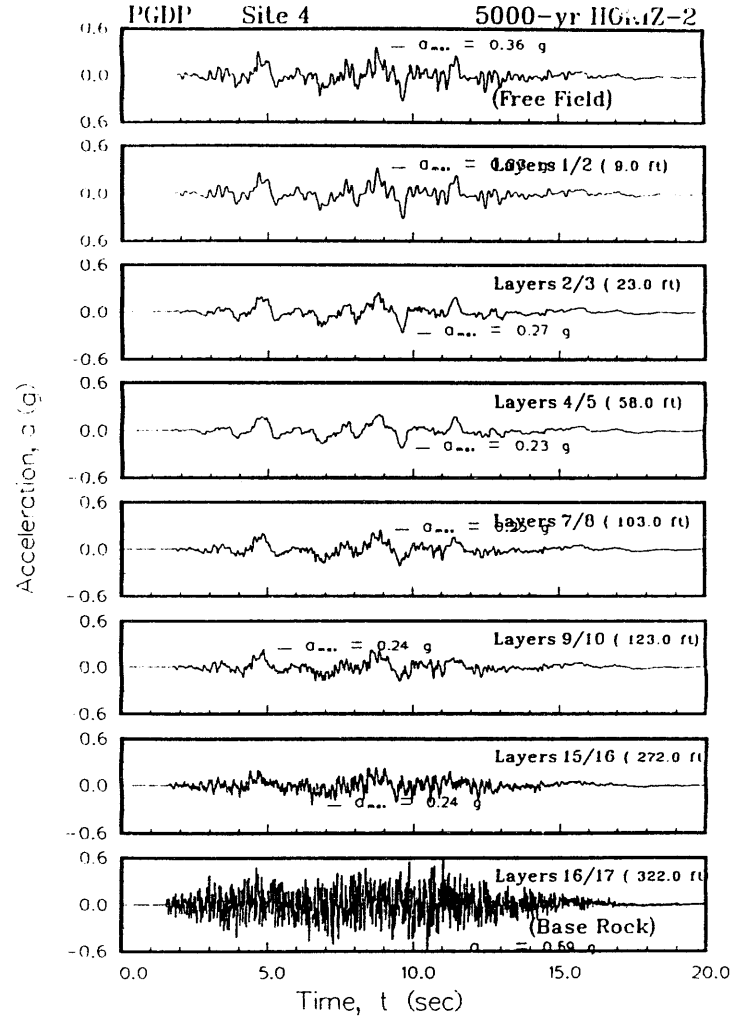

Figure N4. Variation of acceleration with time at the top of each layer for Site 4

APPENDIX O: SHEAR STRAINS FOR 5000-YEAR EVENT

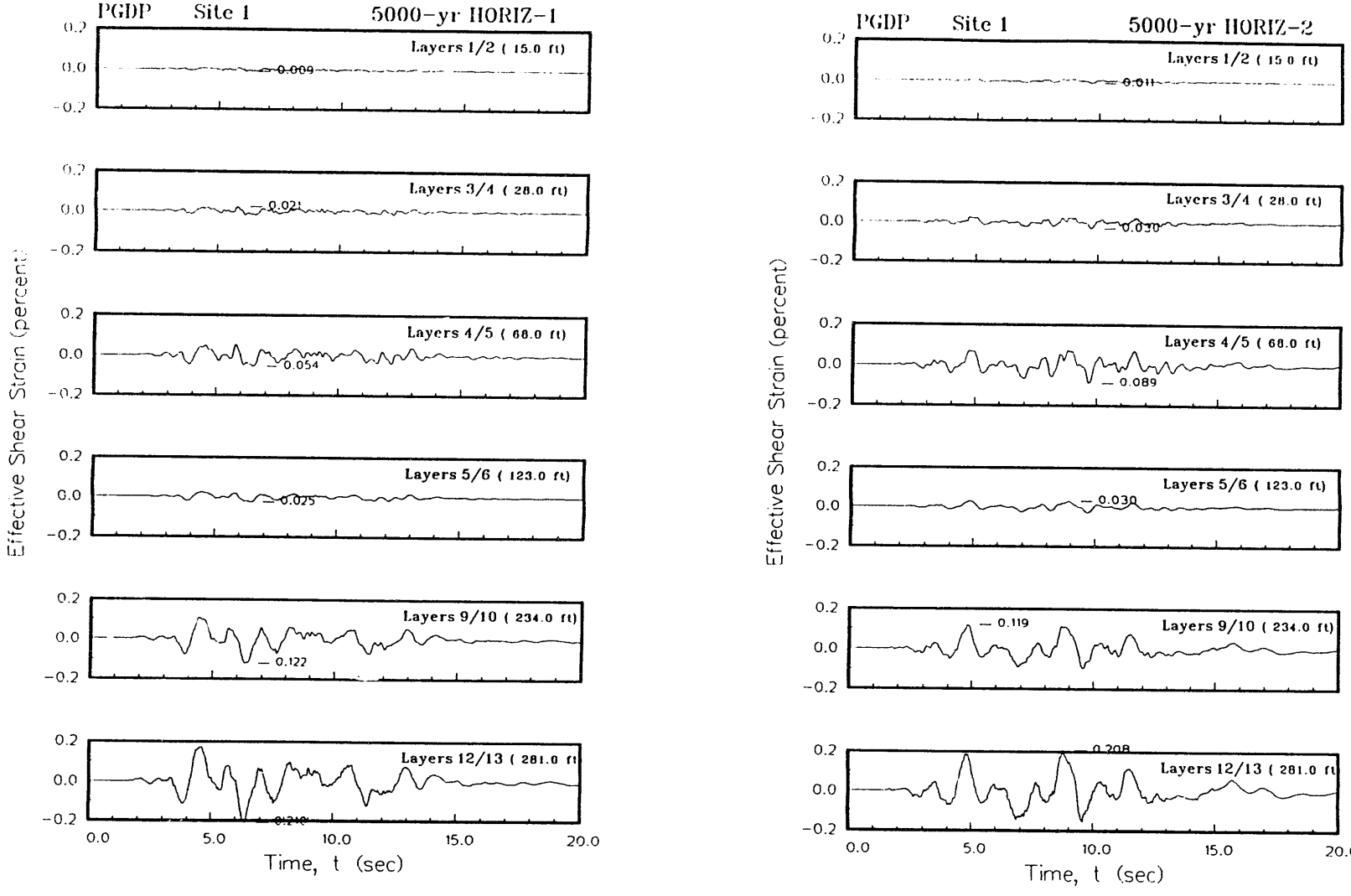

Figure 01. Variation of shear strain with time at contacts between layers for Site 1

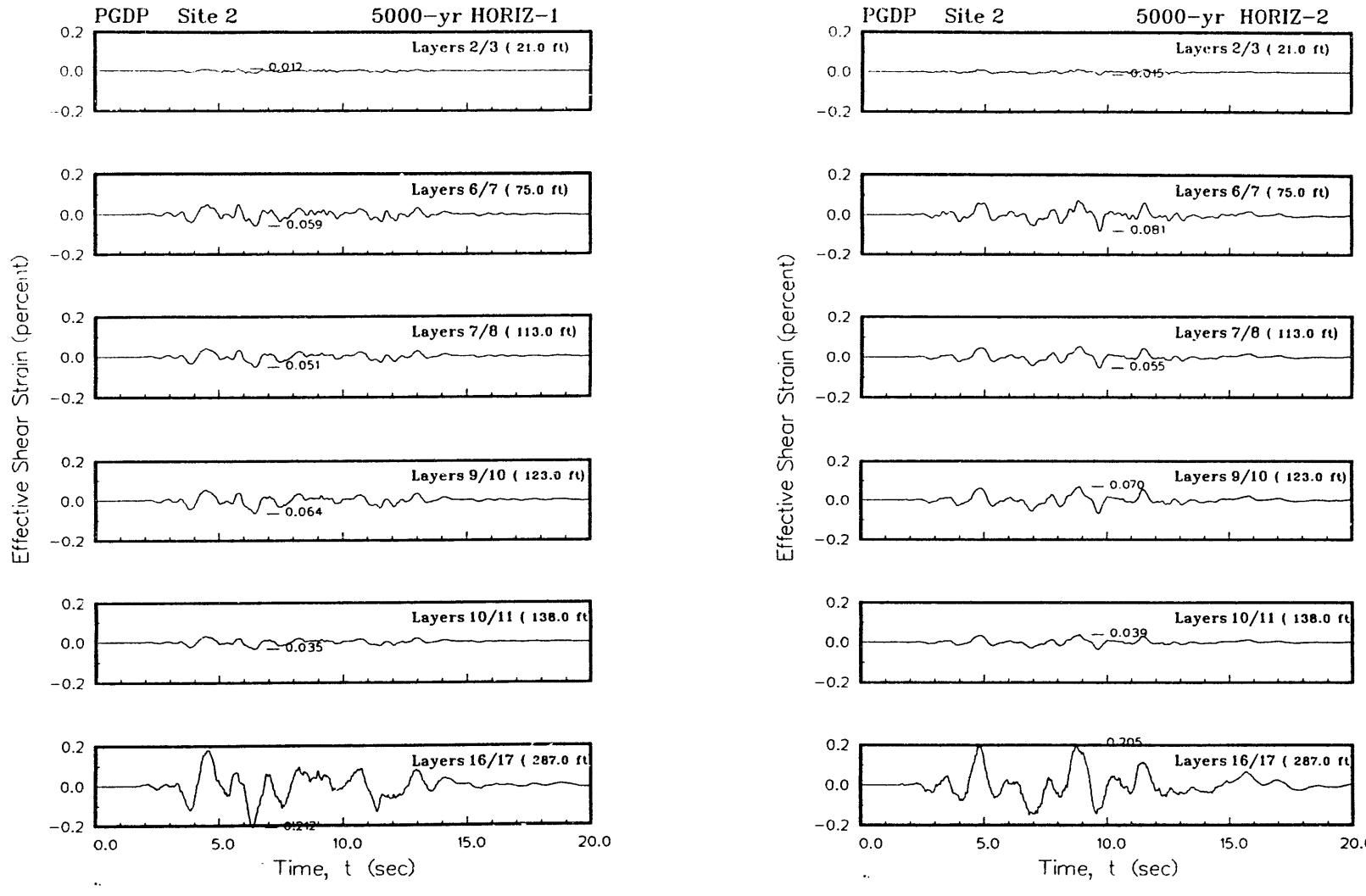

Figure 02. Variation of shear strain with time at contacts between layers for Site 2

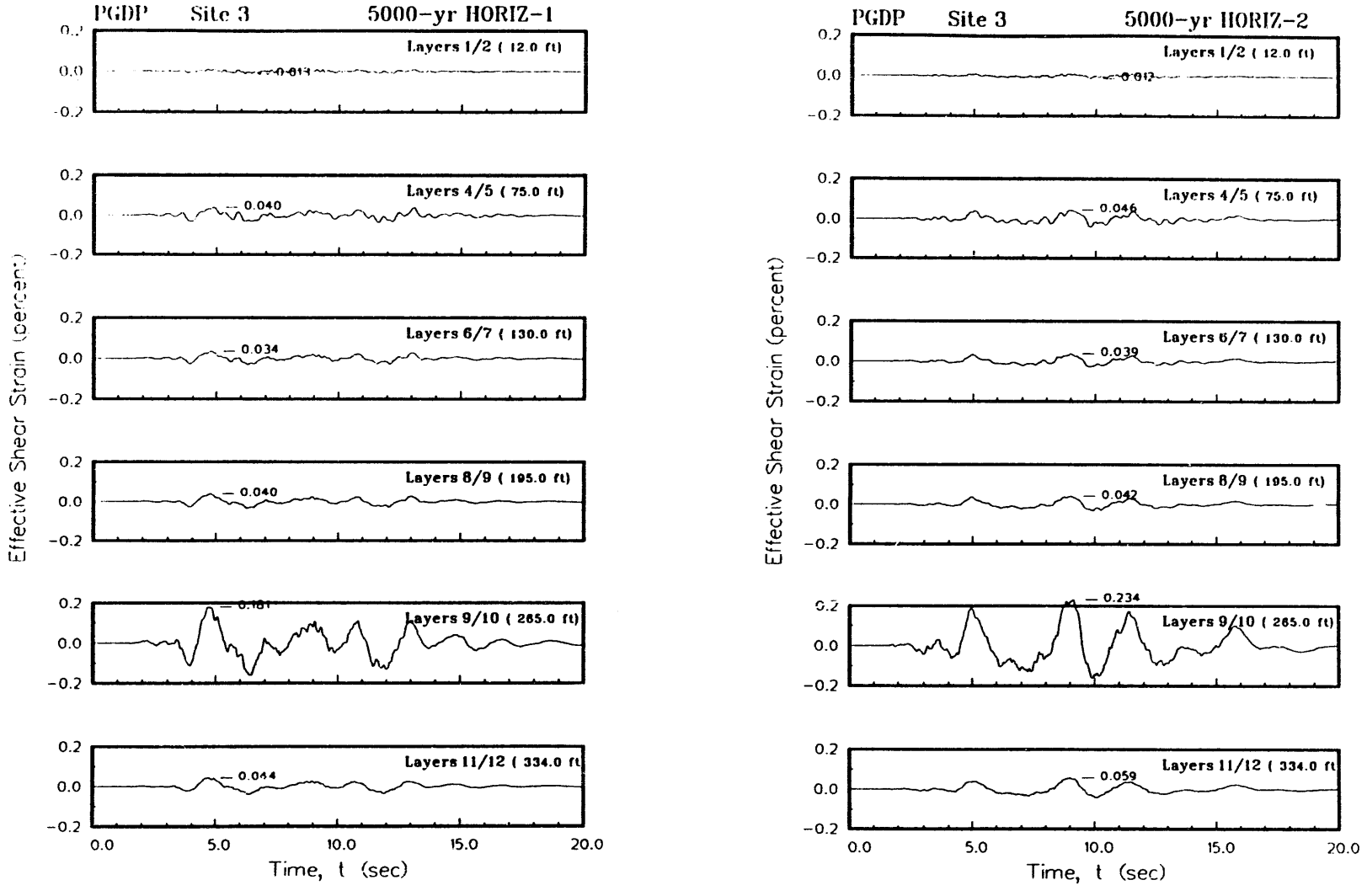

Figure 03. Variation of shear strain with time at contacts between layers for Site 3

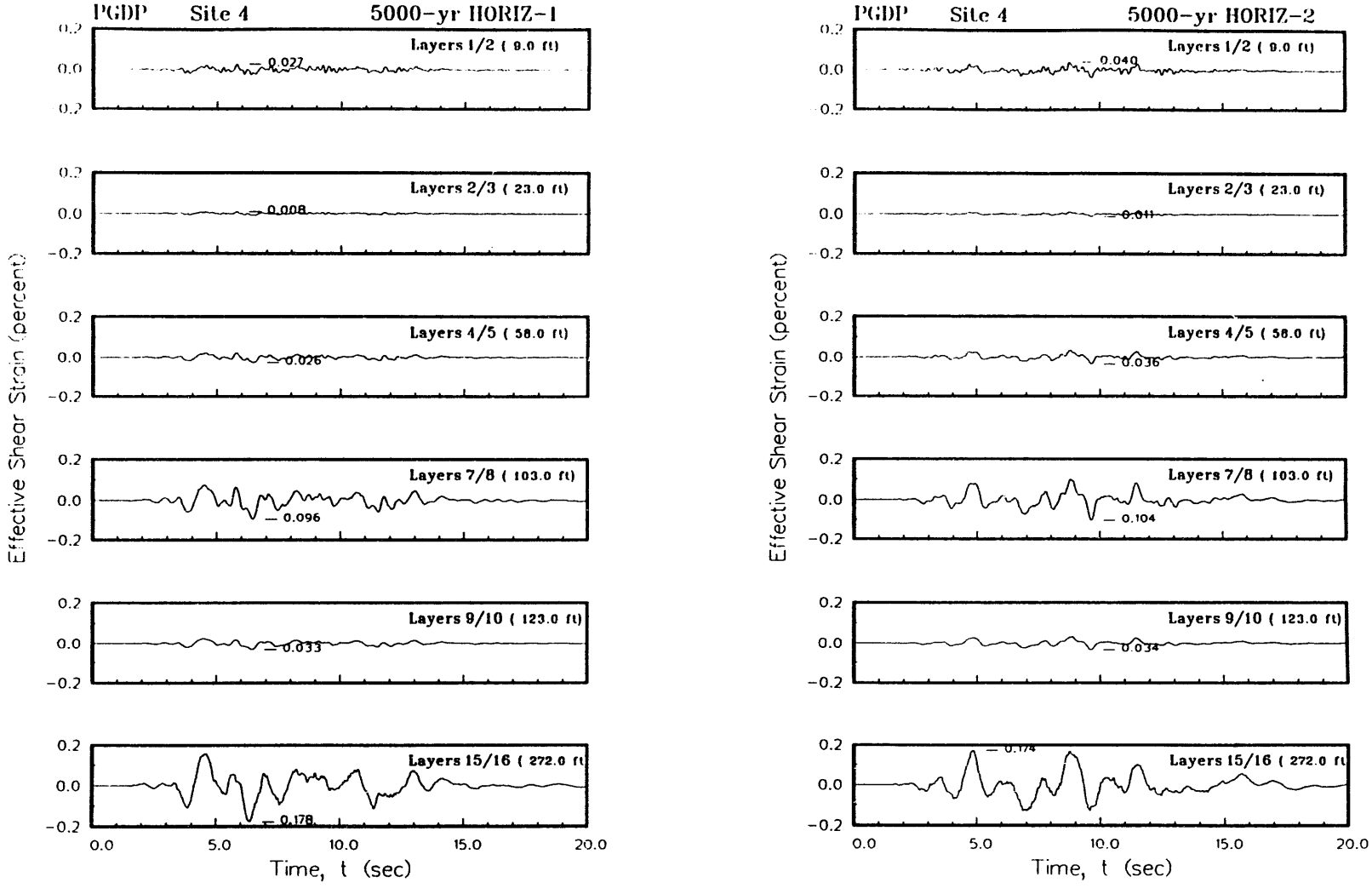

Figure 04. Variation of shear strain with time at contacts between layers for Site 4

APPENDIX P: TRIPARTITE RESPONSE SPECTRA FOR 5000-YEAR EVENT

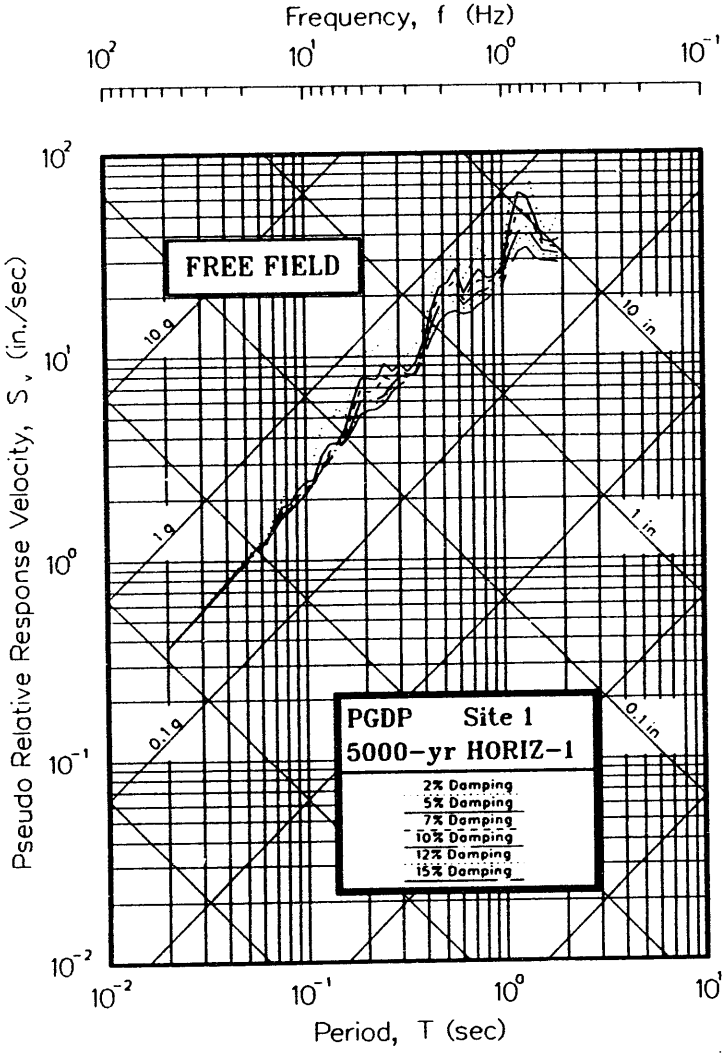

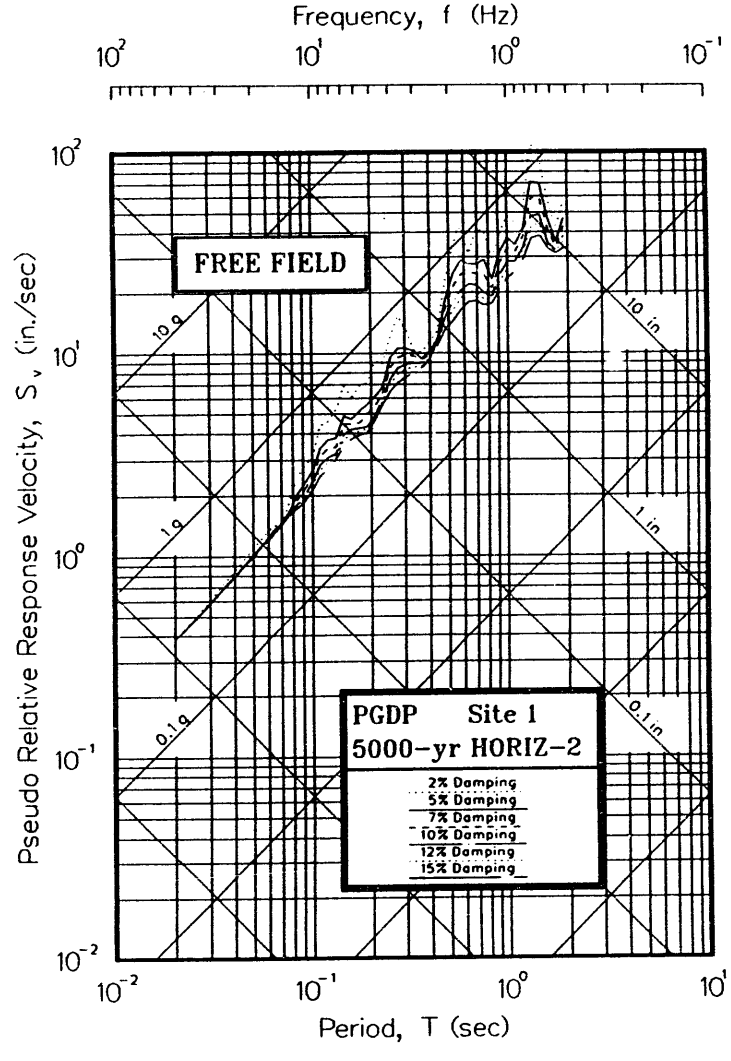

Figure P1. Psuedo-relative velocity spectra in tripartite form at free field for Site 1

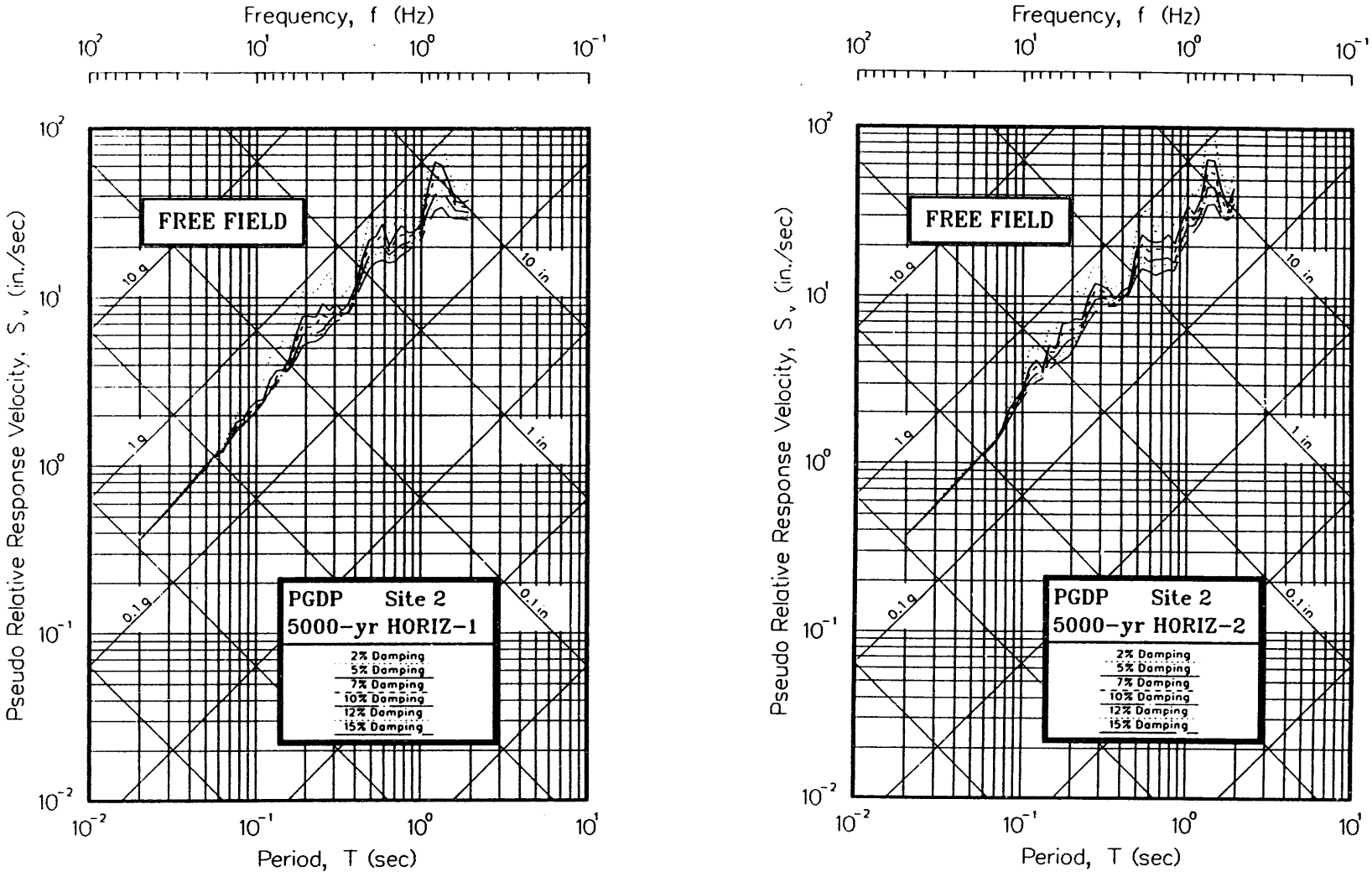

Figure P2. Psuedo-relative velocity spectra in tripartite form at free field for Site 2

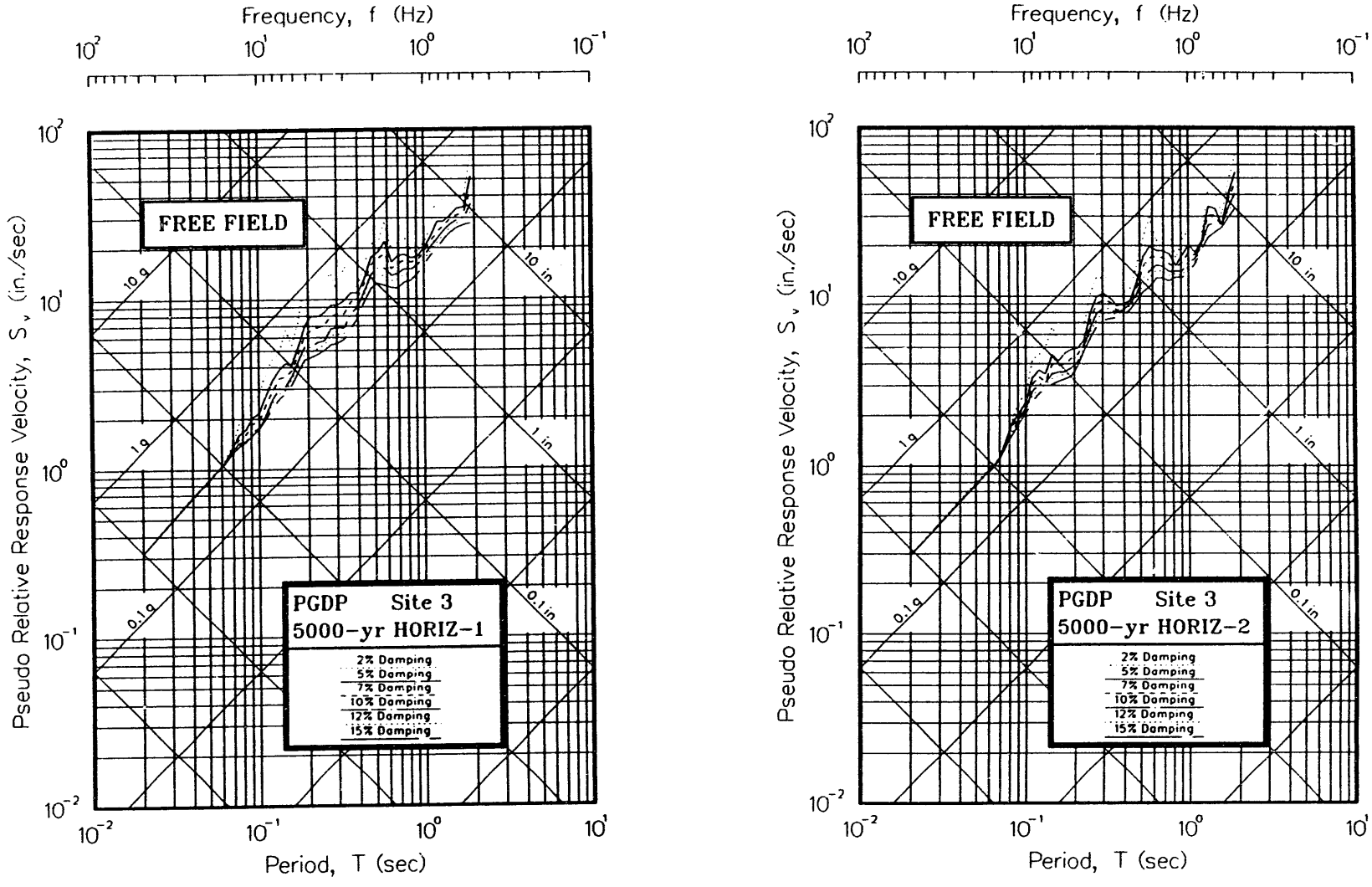

Figure P3. Psuedo-relative velocity spectra in tripartite form at free field for Site 3

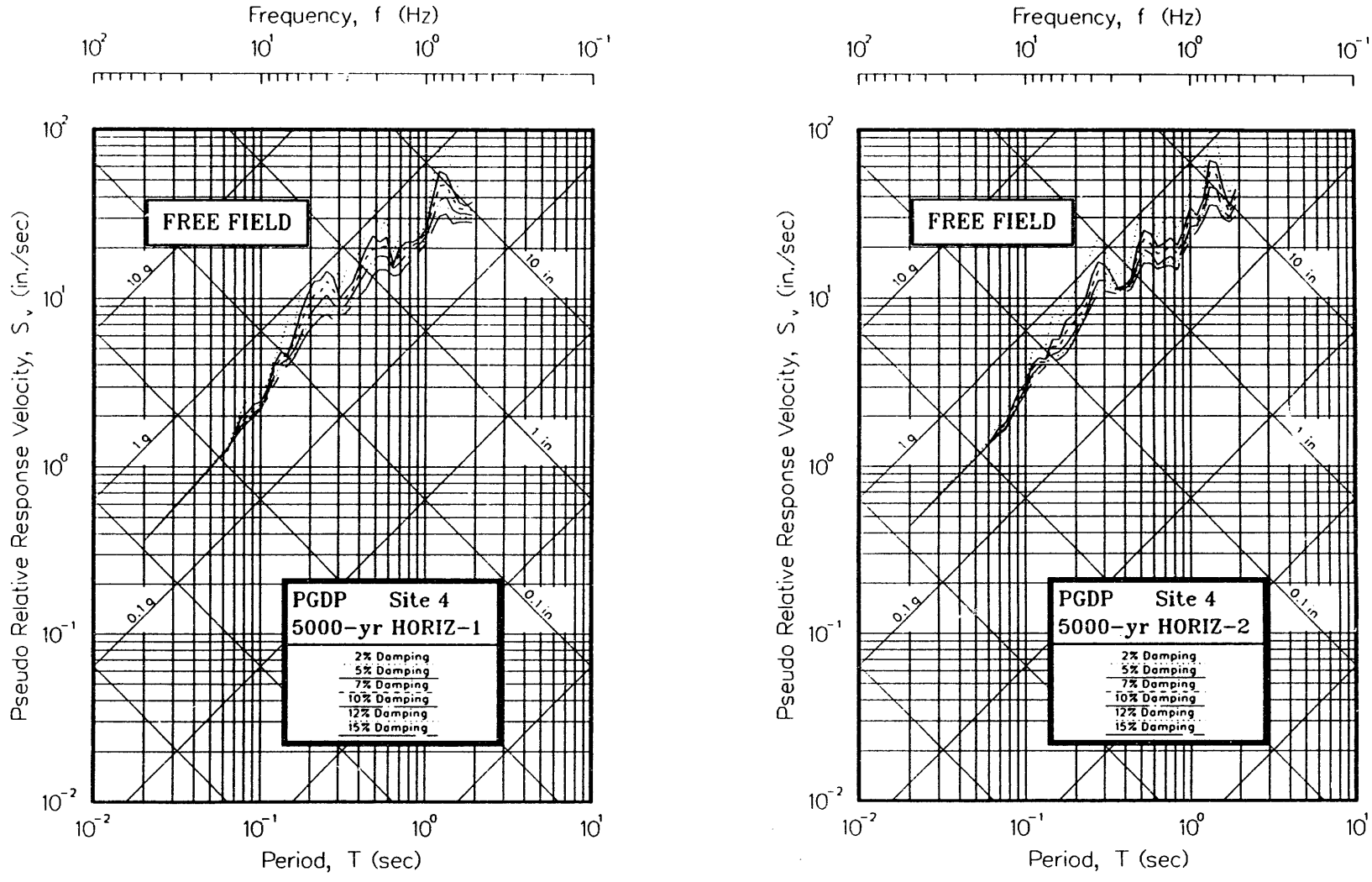

Figure P4. Psuedo-relative velocity spectra in tripartite form at free field for Site 4

APPENDIX Q: ACCELERATION SPECTRA FOR 5000-YEAR EVENT

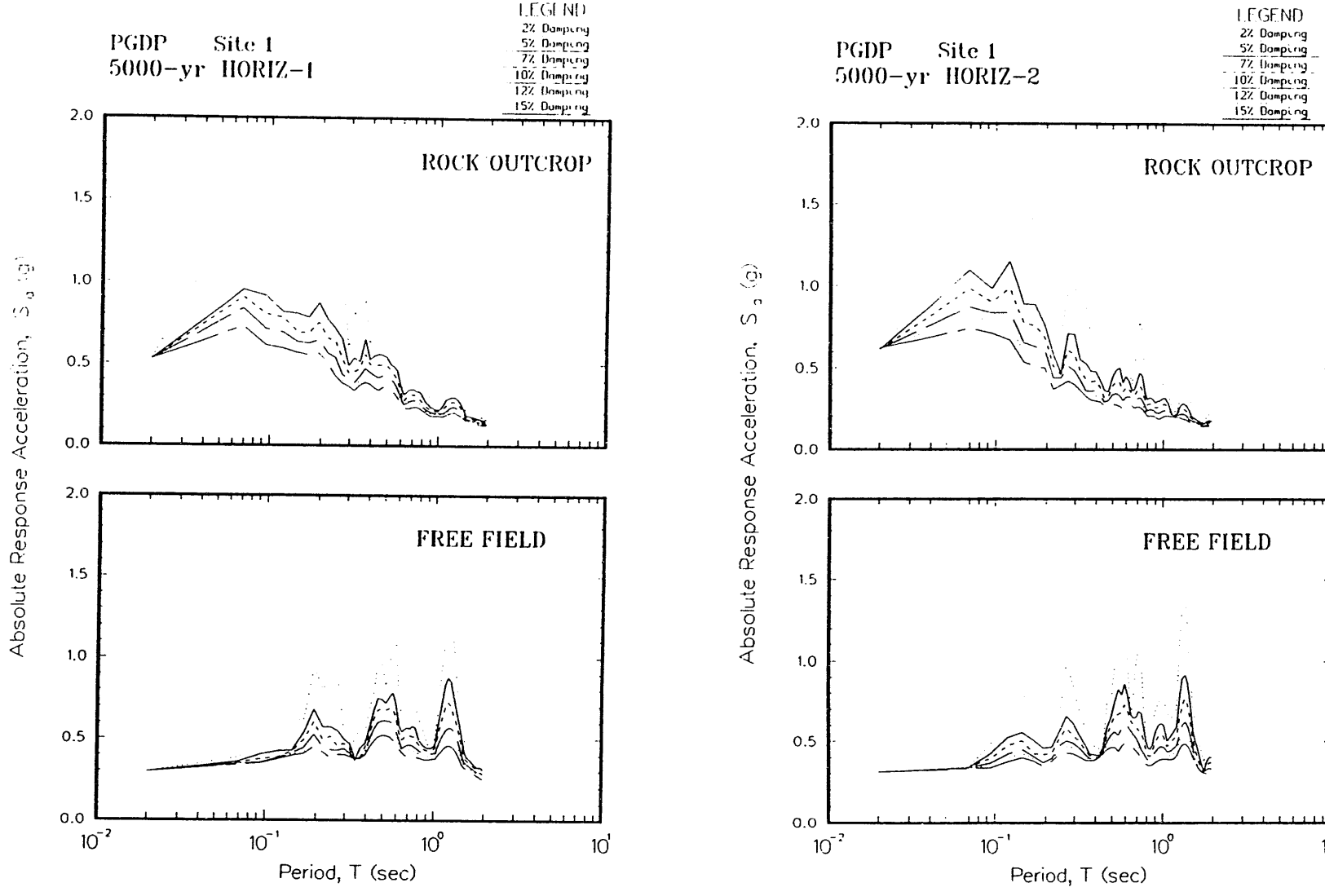

Q2

Figure Q1. Absolute acceleration response spectra at free field for Site 1

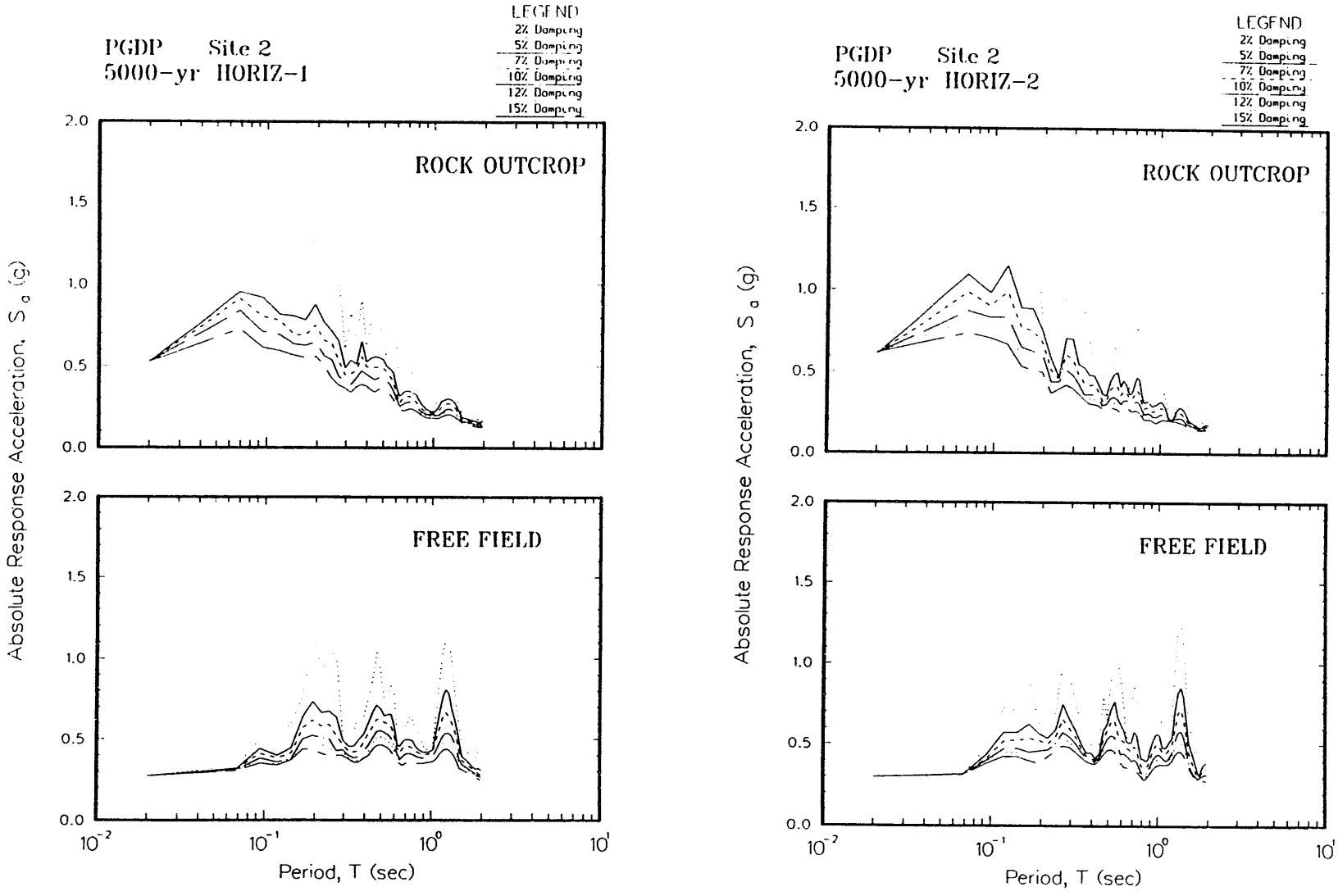

Figure Q2. Absolute acceleration response spectra at free field for Site 2

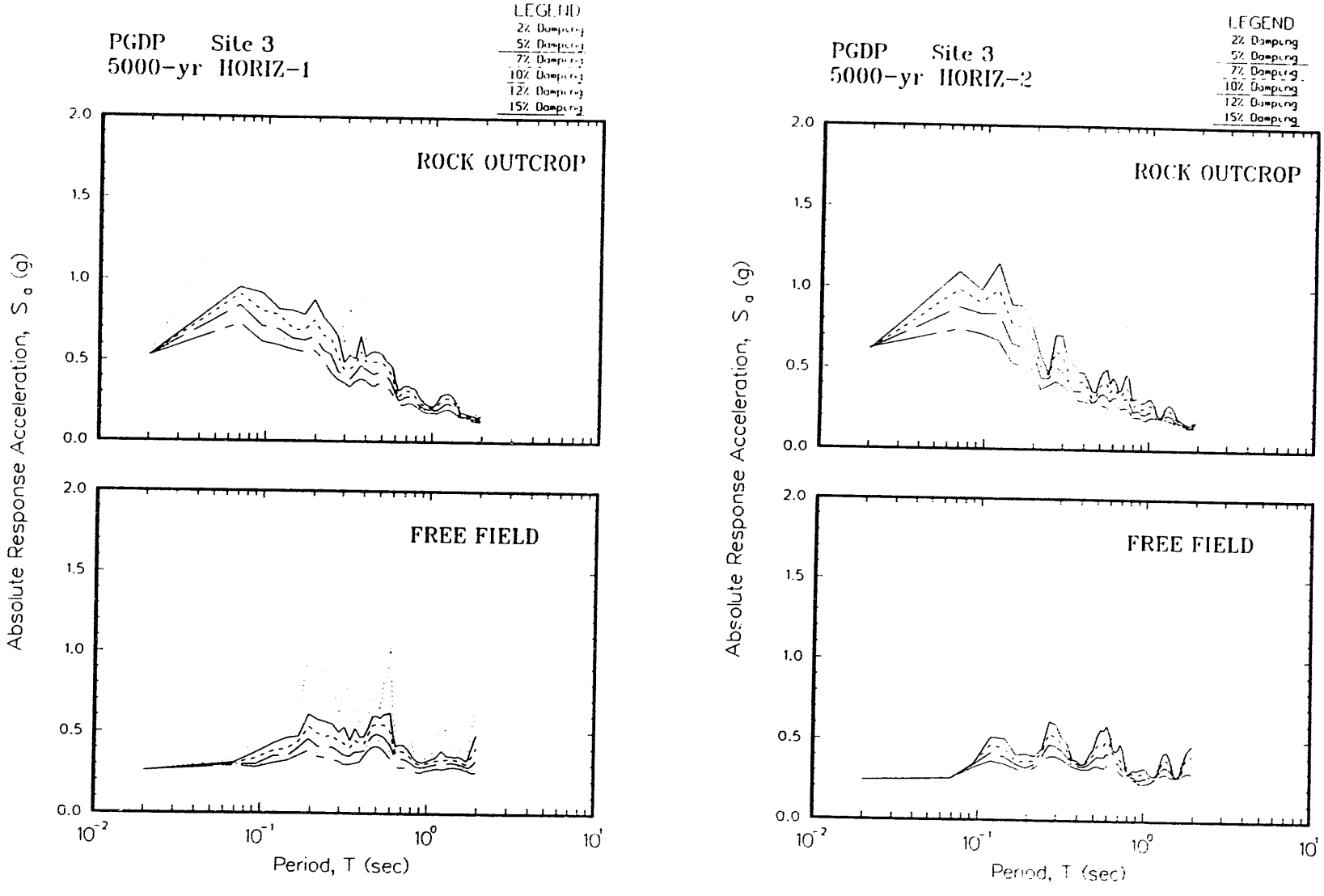

Figure Q3. Absolute acceleration response spectra at free field for Site 3

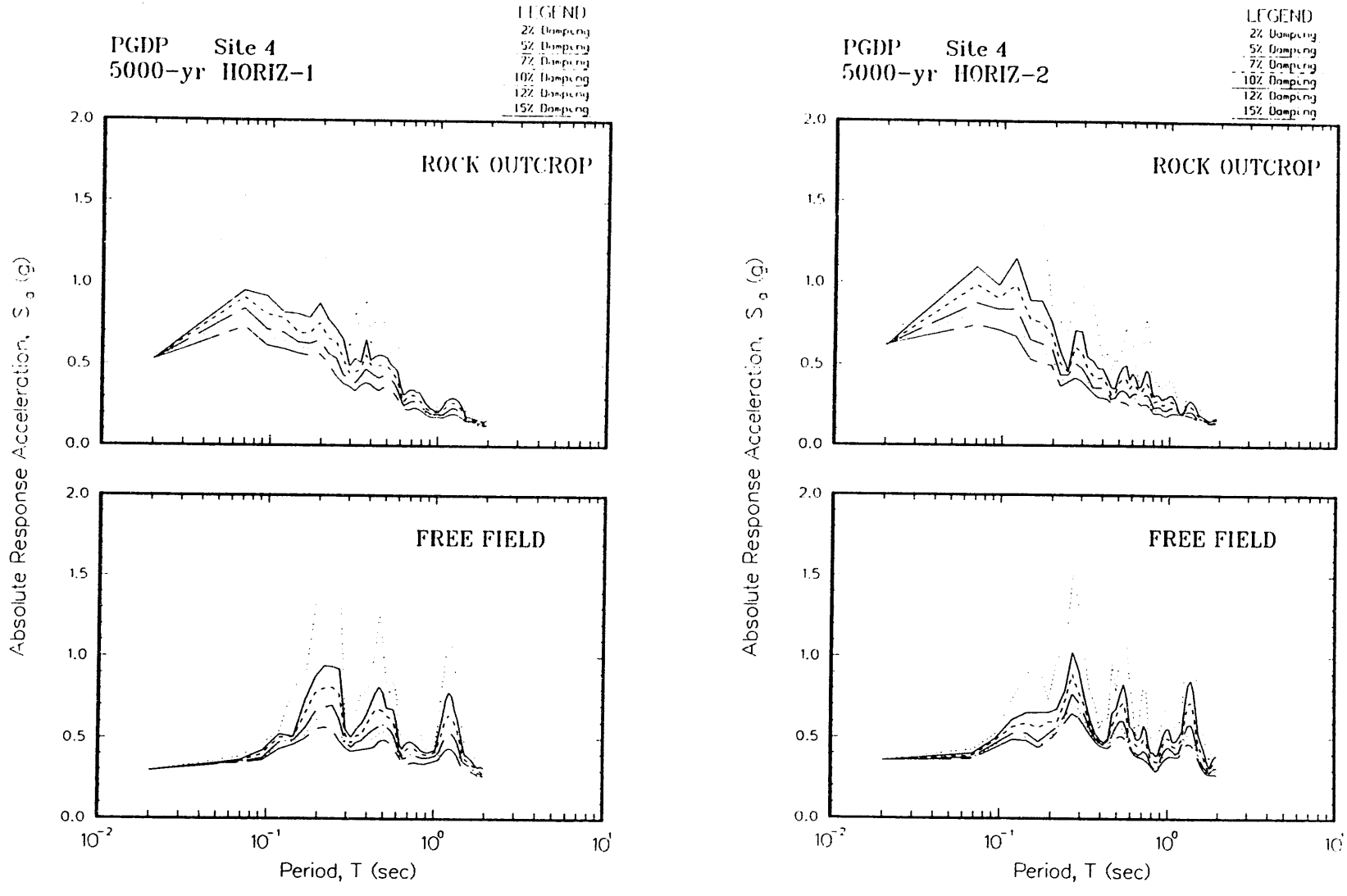

Figure Q4. Absolute acceleration response spectra at free field for Site 4

APPENDIX R: RATIO OF ACCELERATION SPECTRA FOR 5000-YEAR EVENT

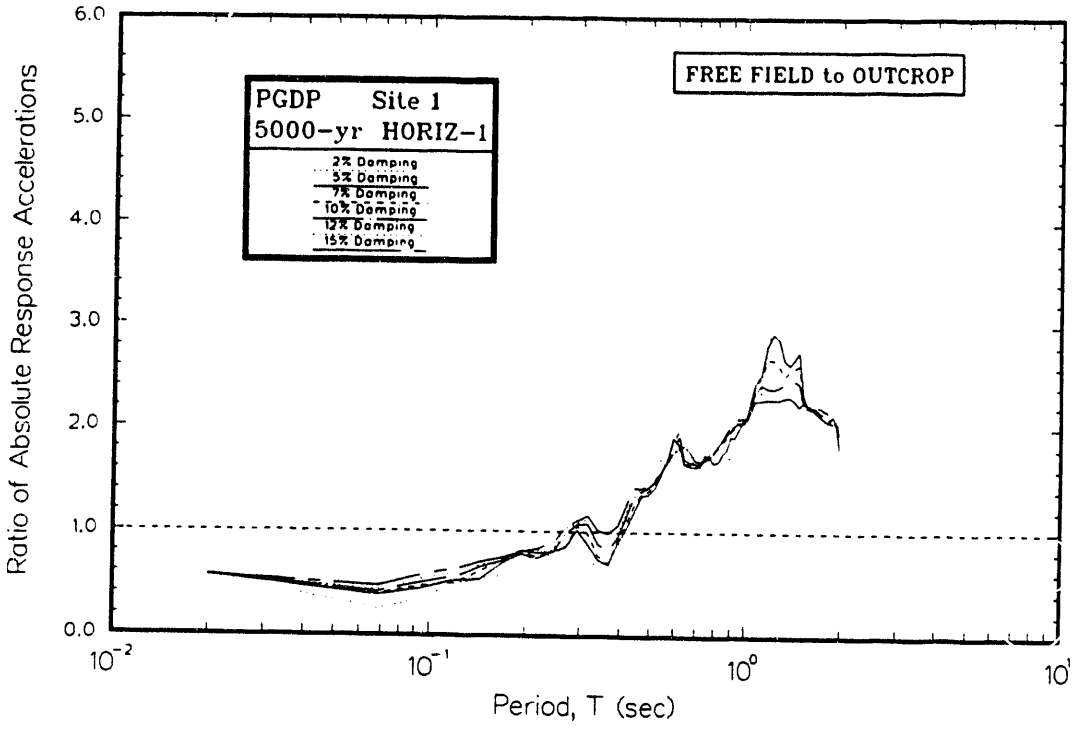

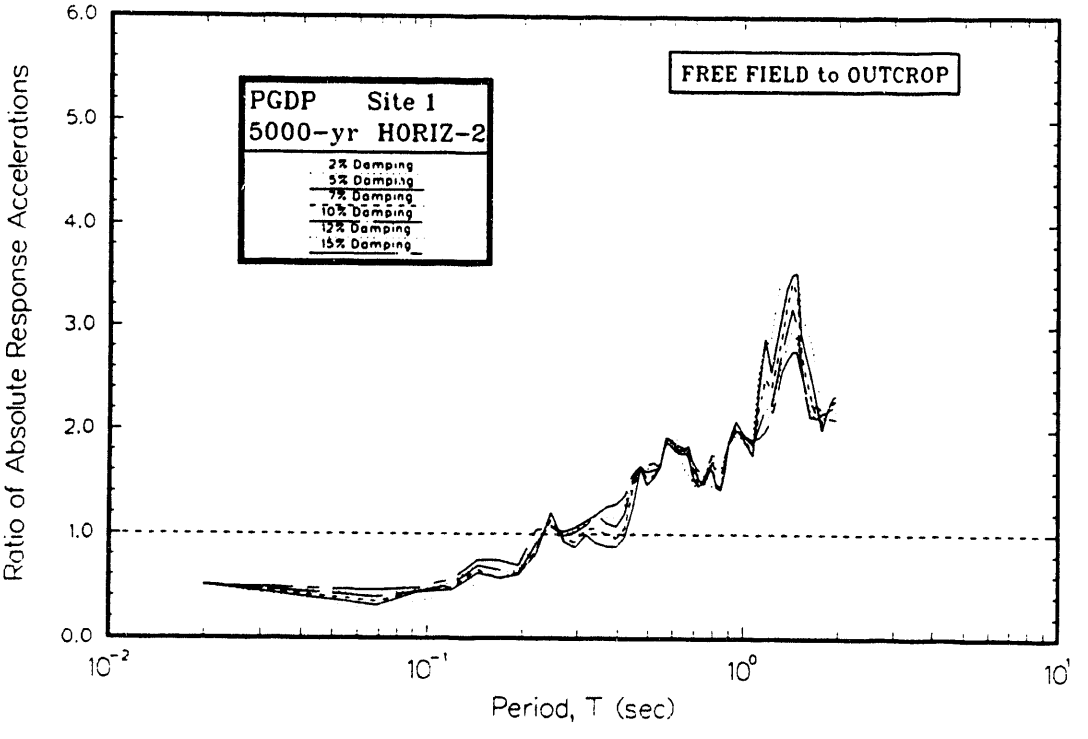

Figure R1. Ratio of absolute acceleration response spectra at free field to rock for Site 1

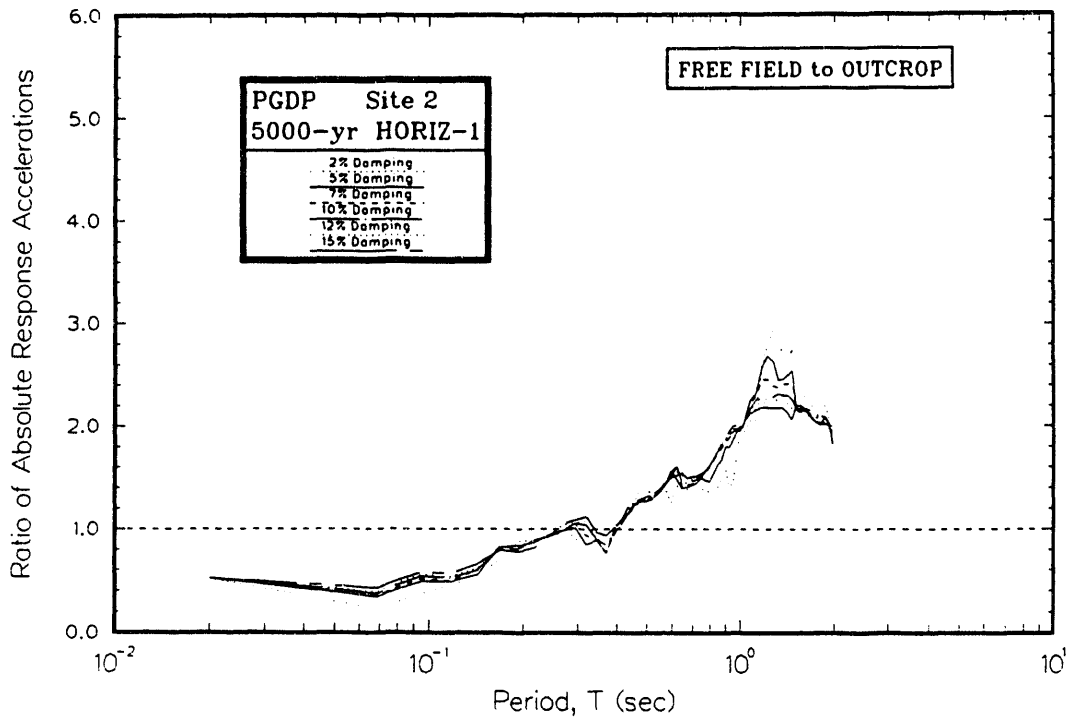

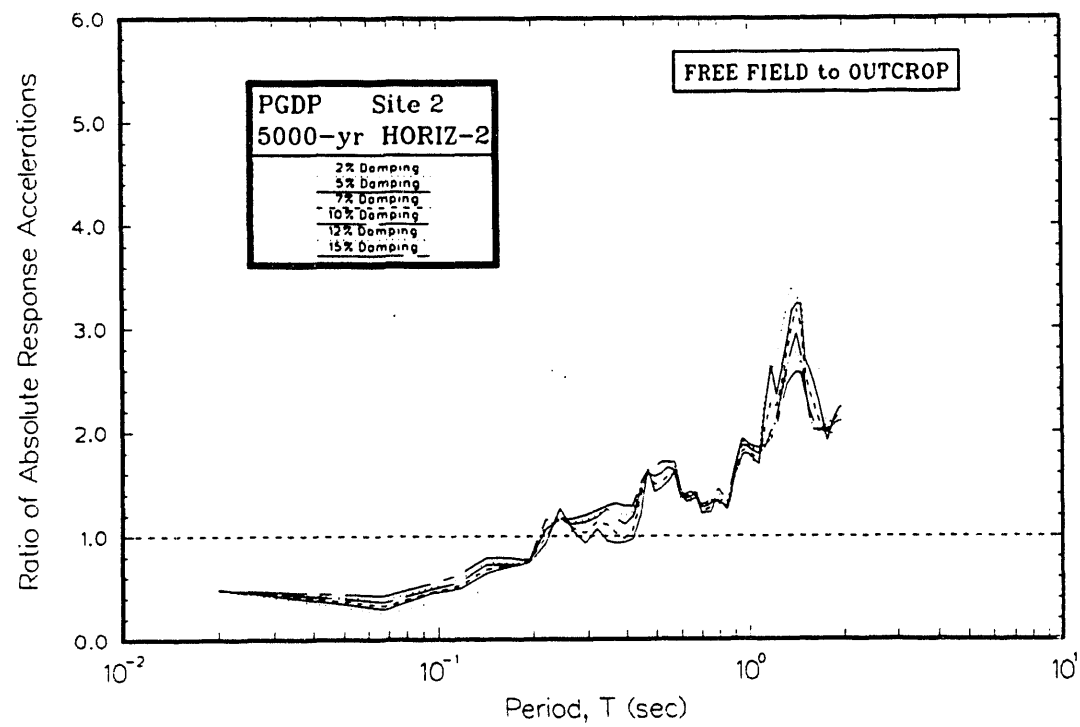

Figure R2. Ratio of absolute acceleration response spectra at free field to rock for Site 2

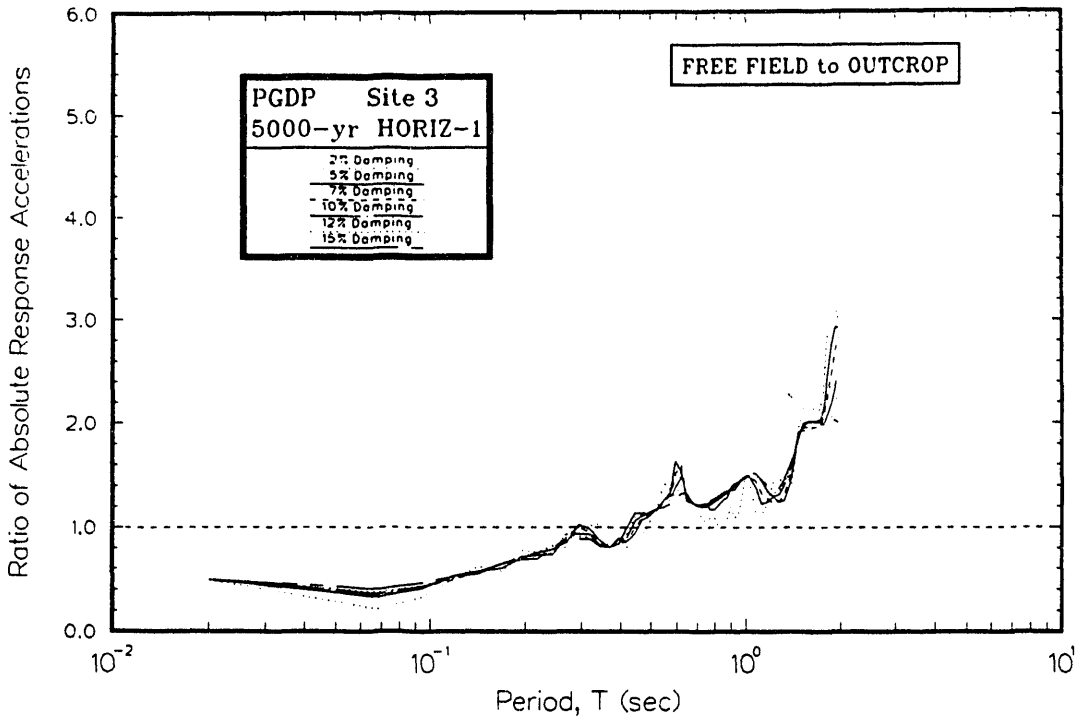

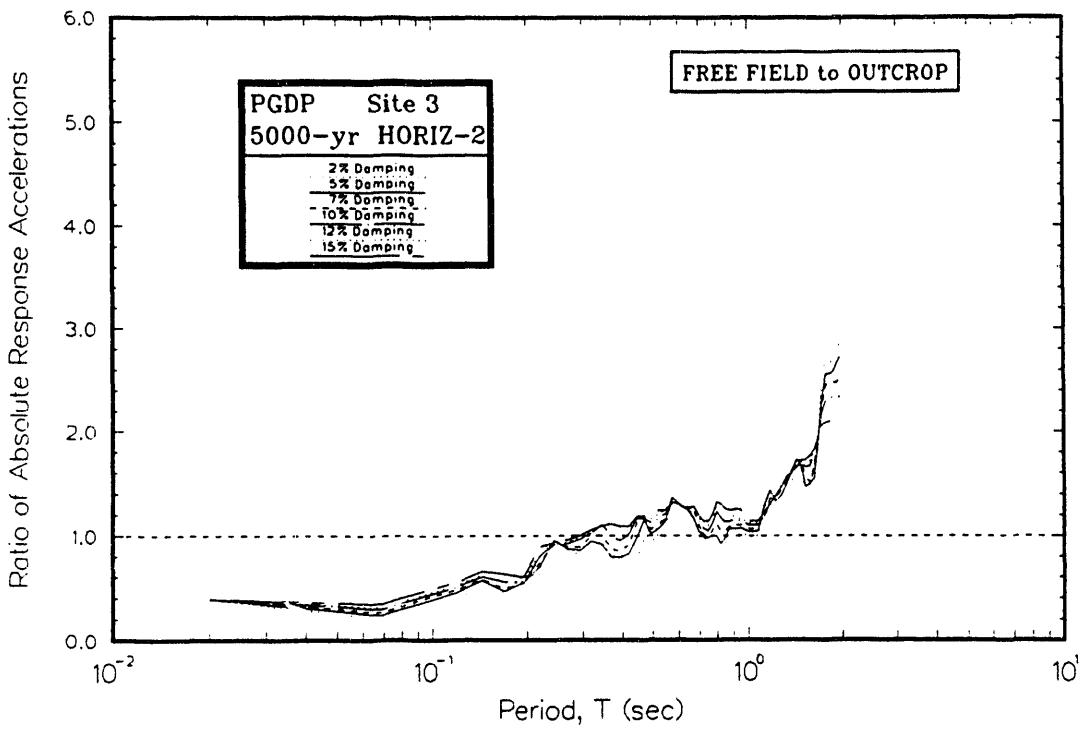

Figure R3. Ratio of absolute acceleration response spectra at free field to rock for Site 3

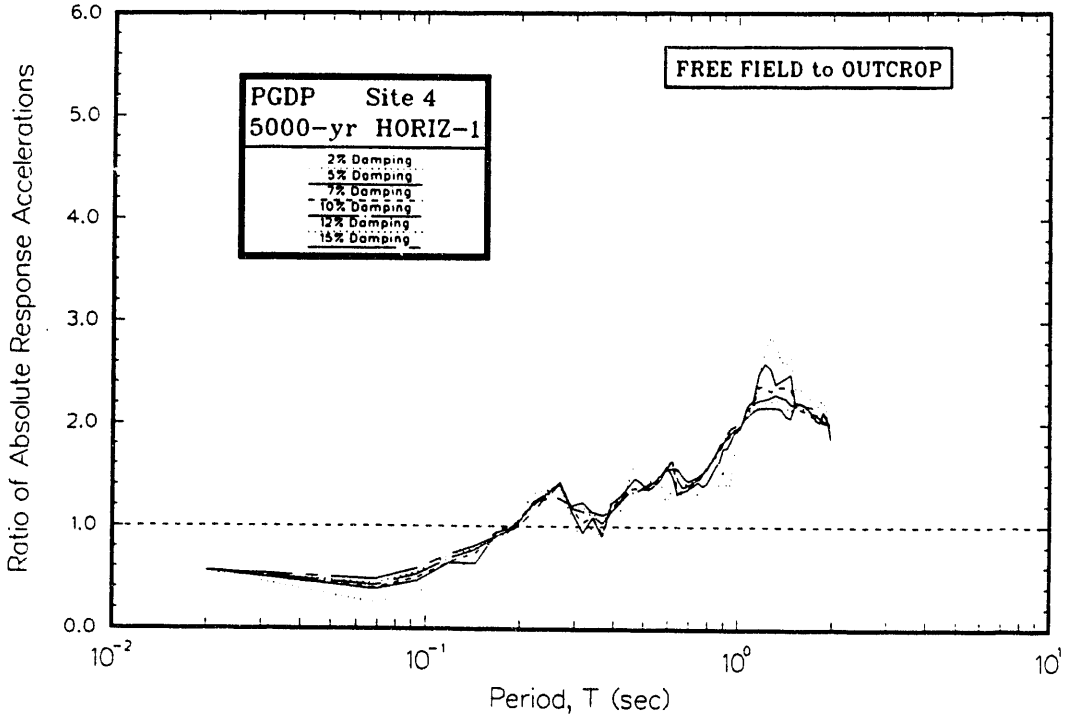

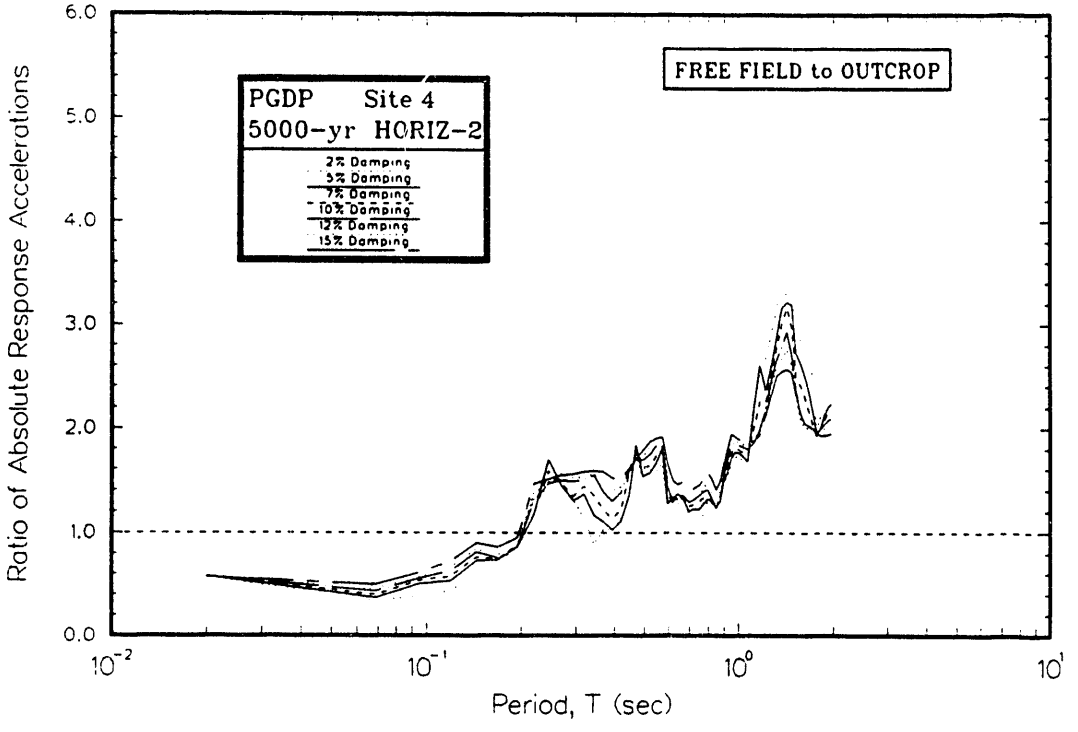

Figure R4. Ratio of absolute acceleration response spectra at free field to rock for Site 4

APPENDIX S: AMPLIFICATION RATIOS FOR 5000-YEAR EVENT

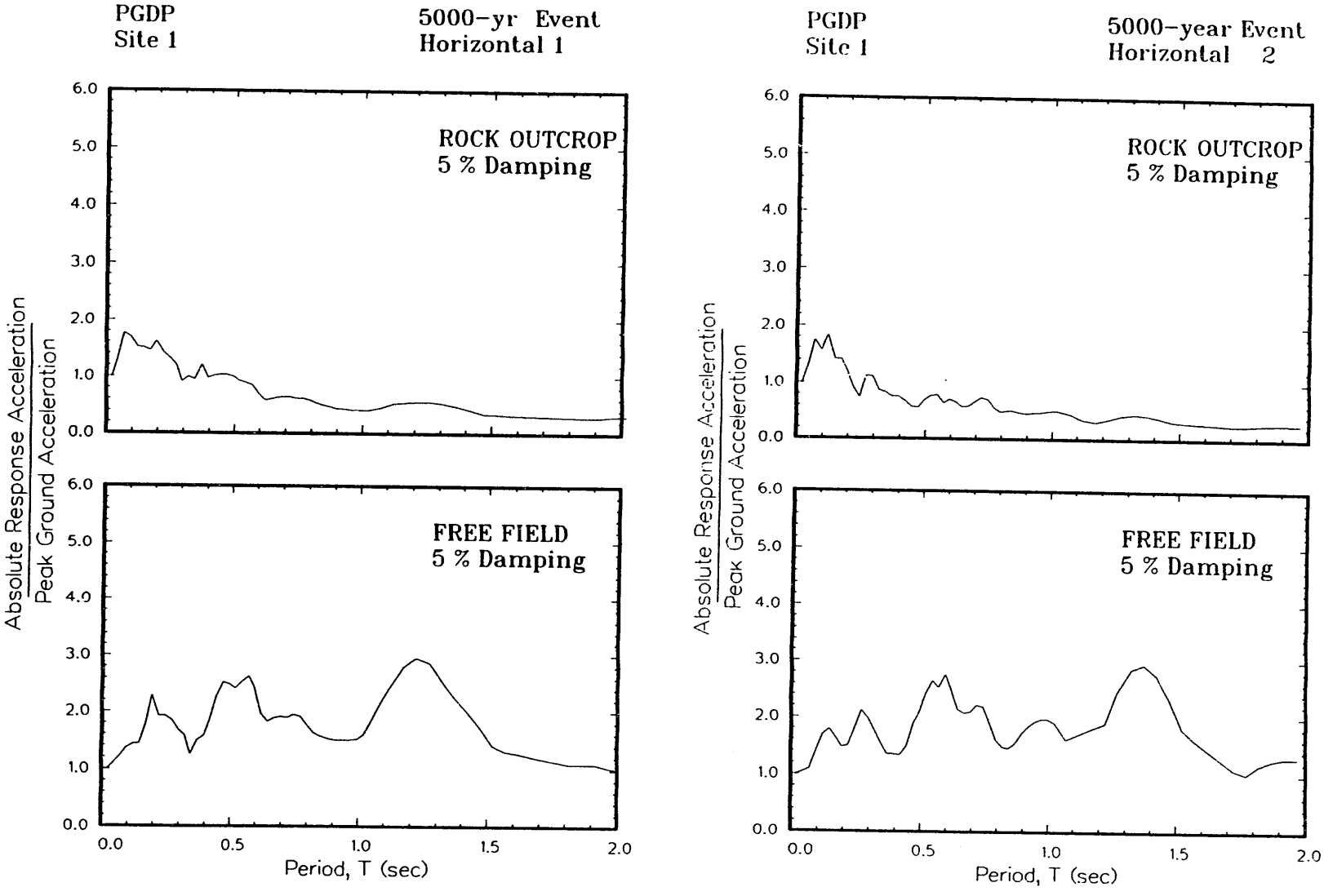

Figure S1. Ratio of amplification of absolute acceleration response spectra to peak acceleration at free field for Site 1

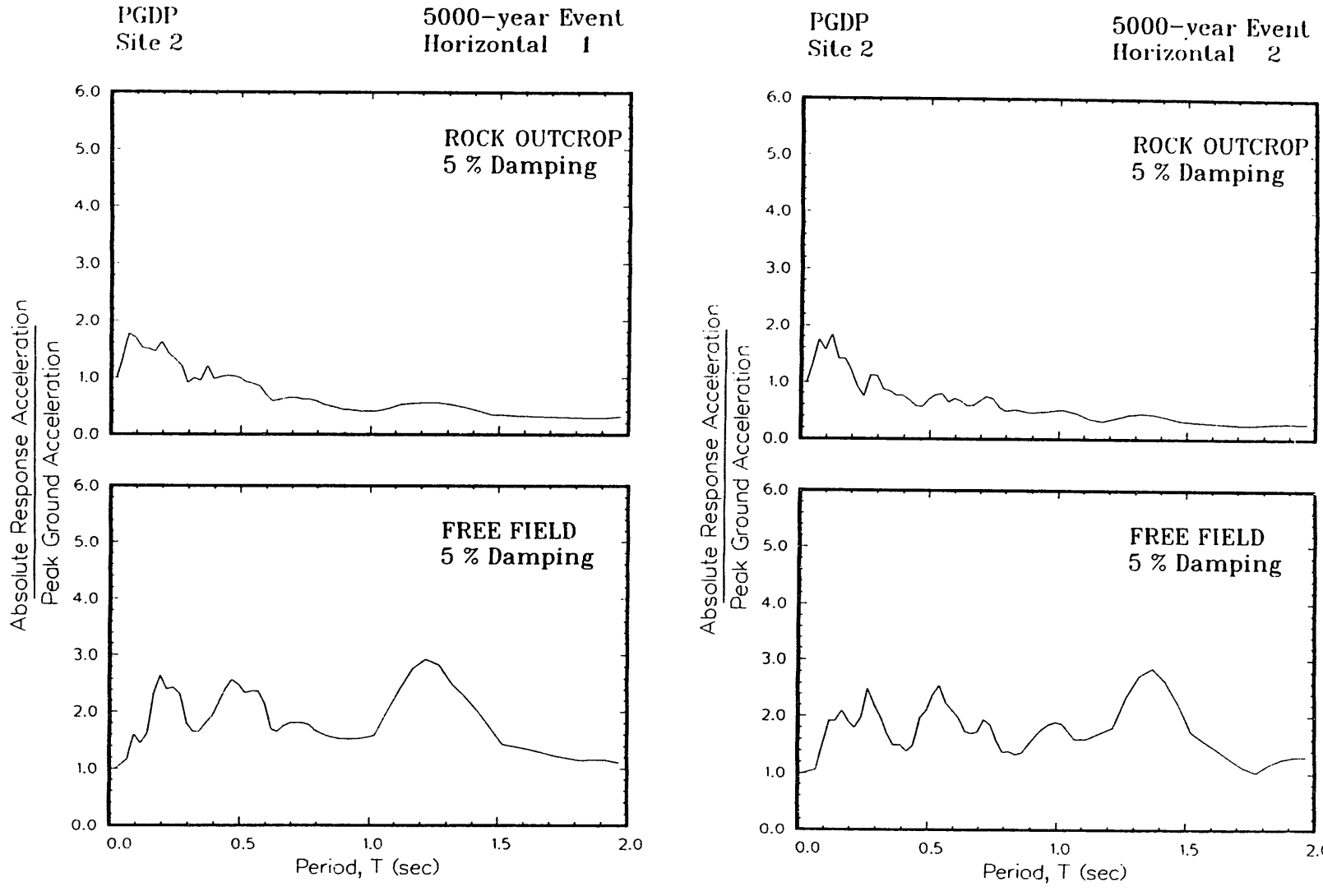

Figure S2. Ratio of amplification of absolute acceleration response spectra to peak acceleration at free field for Site 2

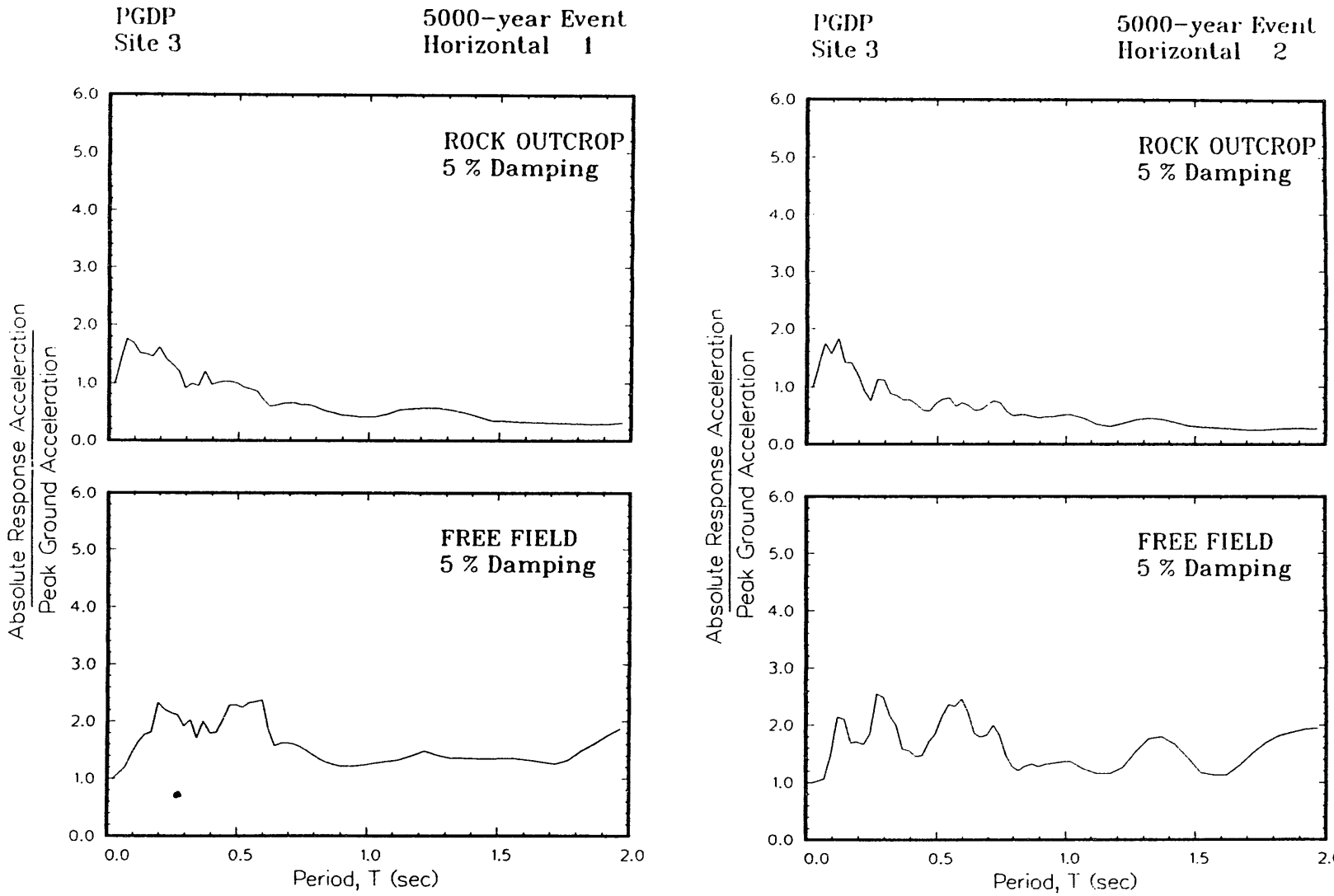

Figure S3. Ratio of amplification of absolute acceleration response spectra to peak acceleration at free field for Site 3

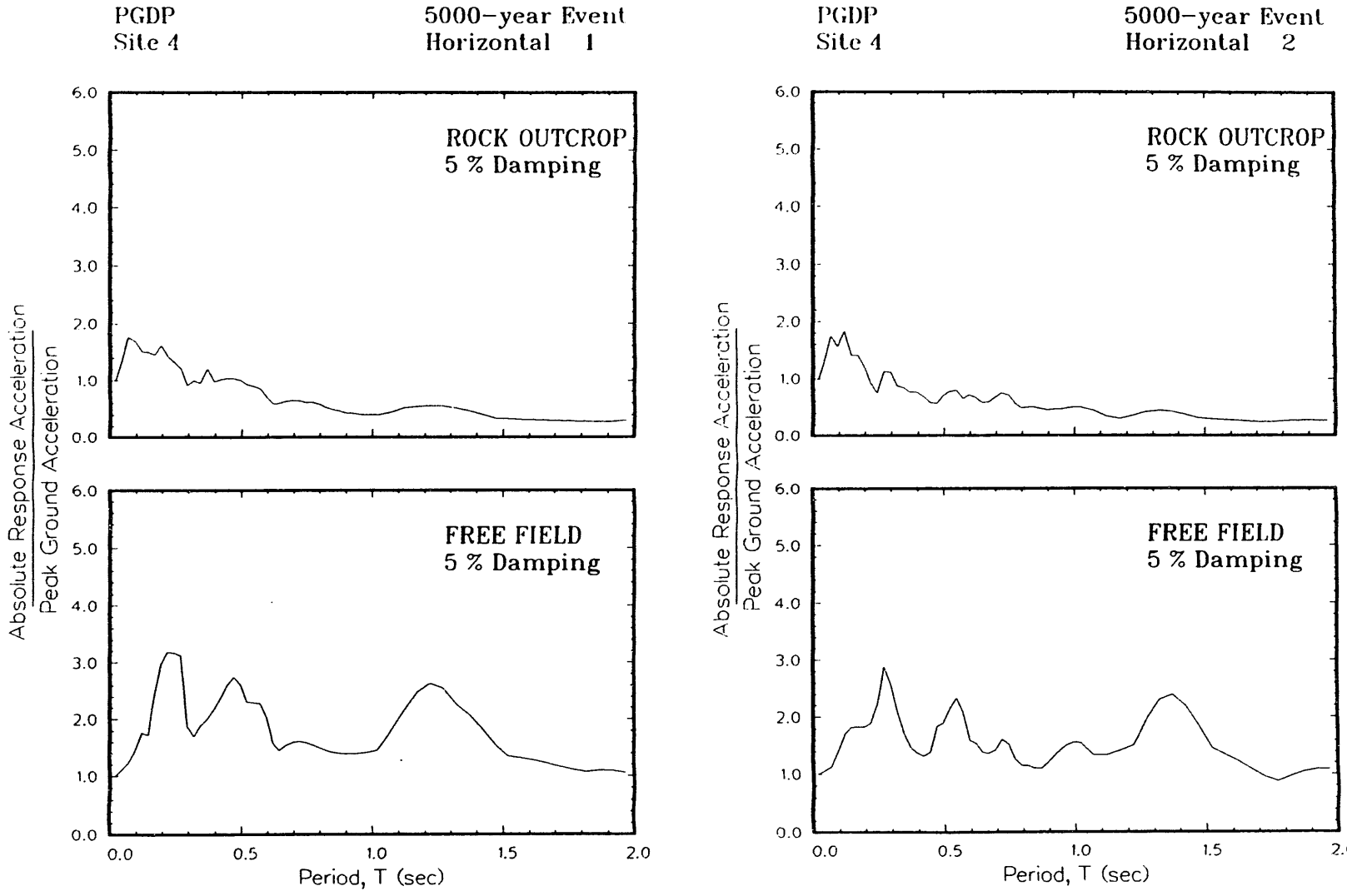

Figure S4. Ratio of amplification of absolute acceleration response spectra to peak acceleration at free field for Site 4

APPENDIX T: SENSITIVITY OF RESULTS TO MAXIMUM SHEAR MODULUS FOR 500-YEAR EVENT

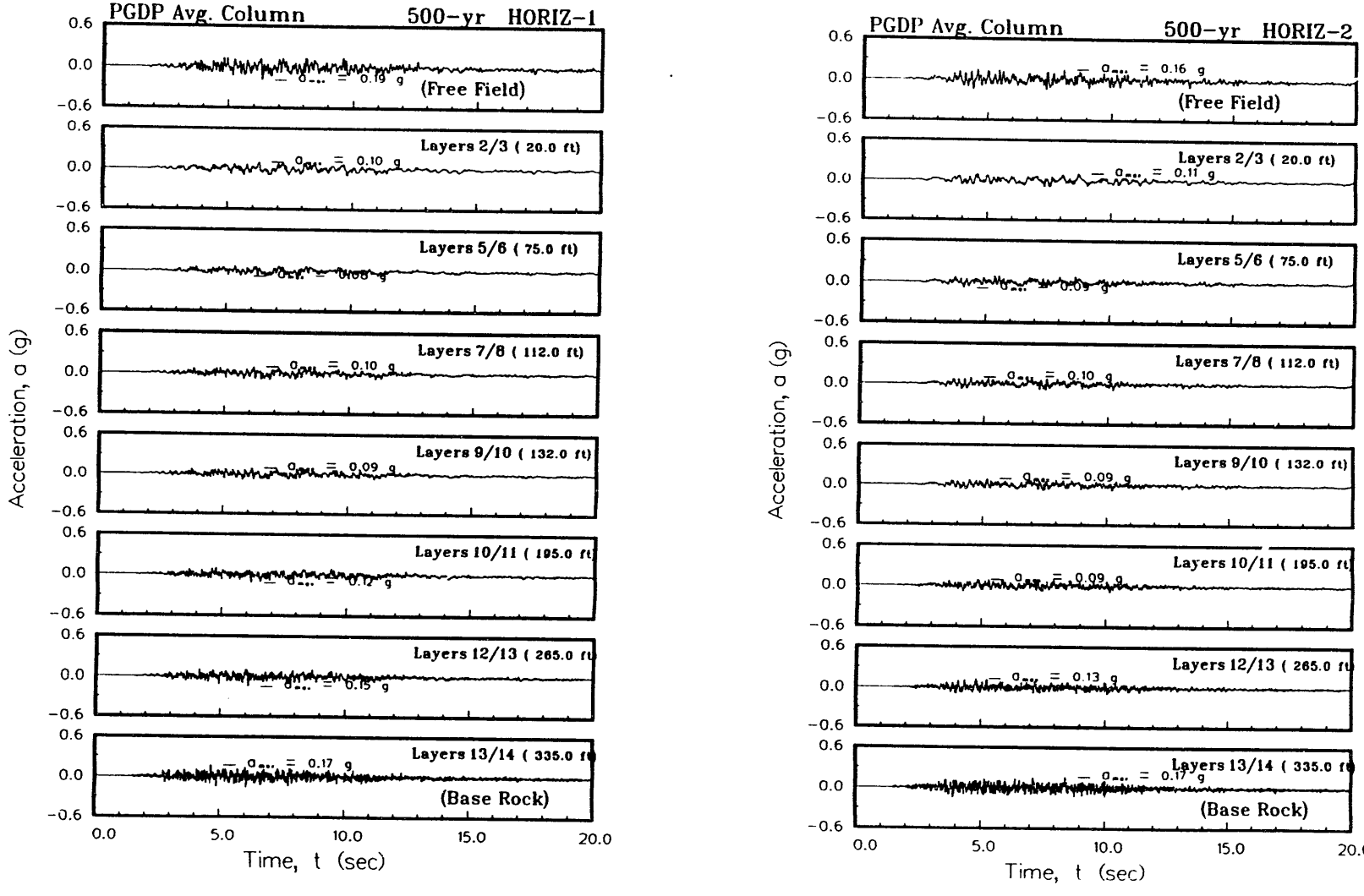

Figure T1. Variation of acceleration with time using best estimate of shear modulus for ave[illegible] column

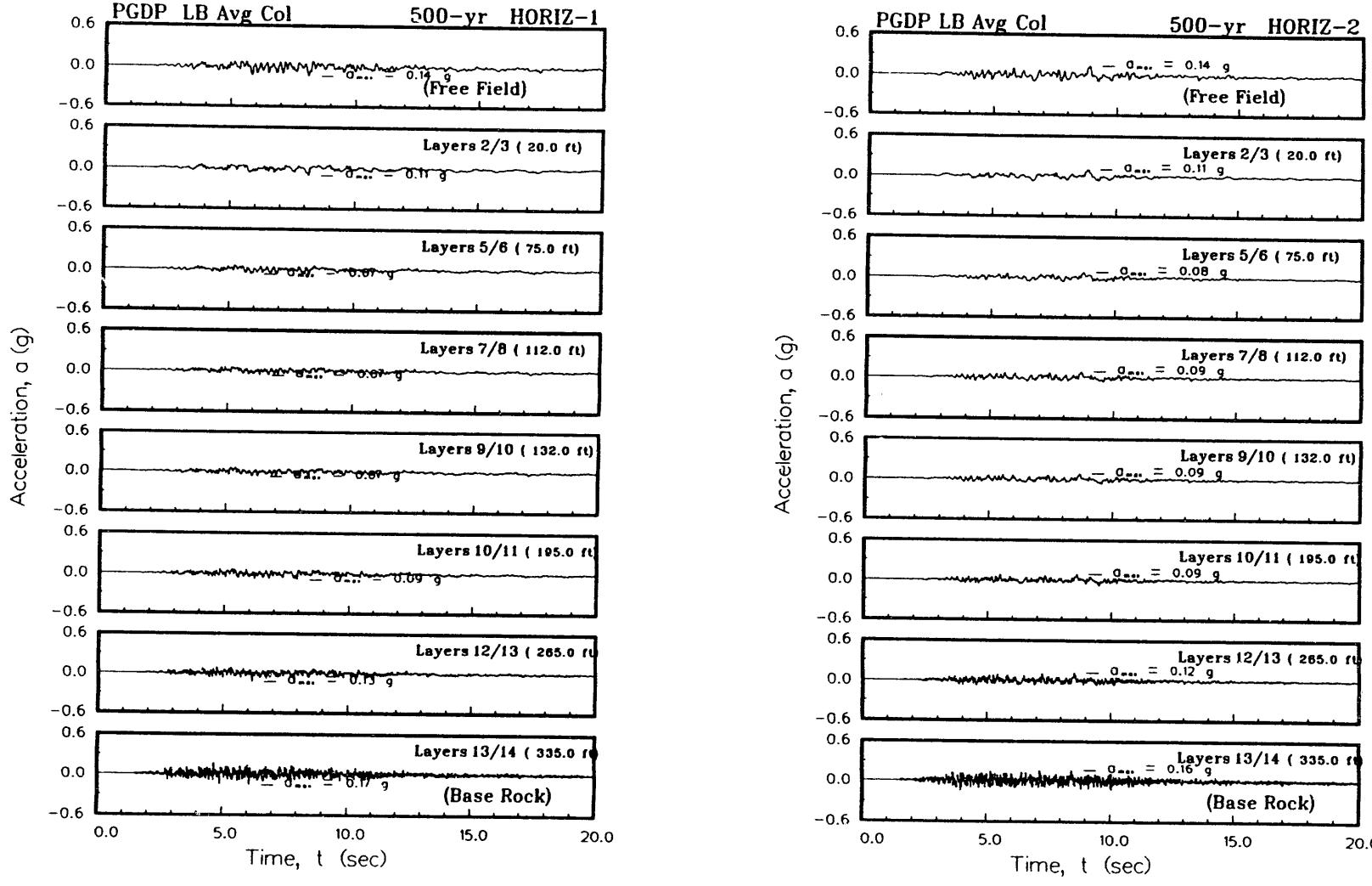

Figure T2. Variation of acceleration with time using lower bound of shear modulus for average column

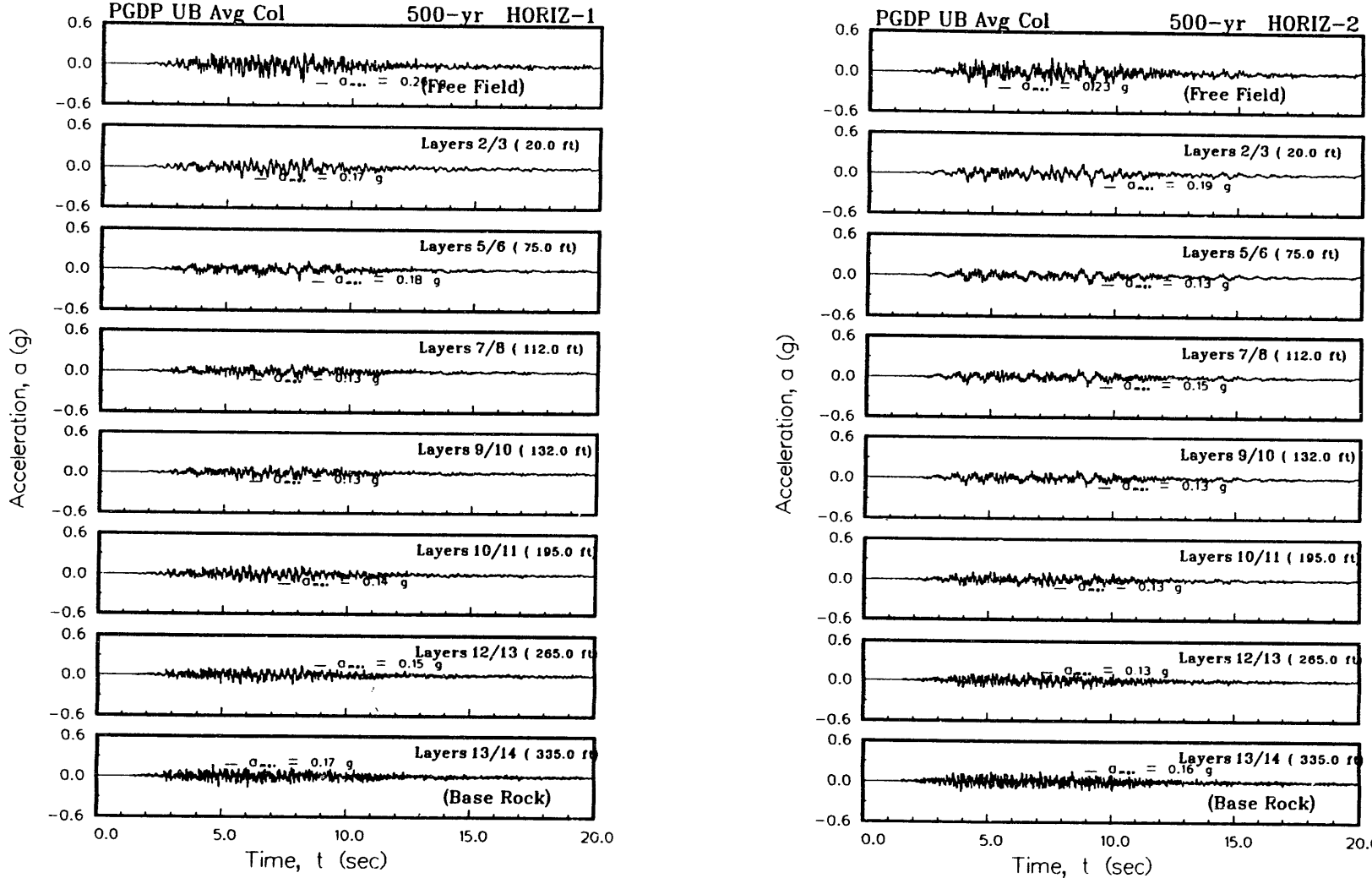

Figure T3. Variation of acceleration with time using upper bound of shear modulus for average column

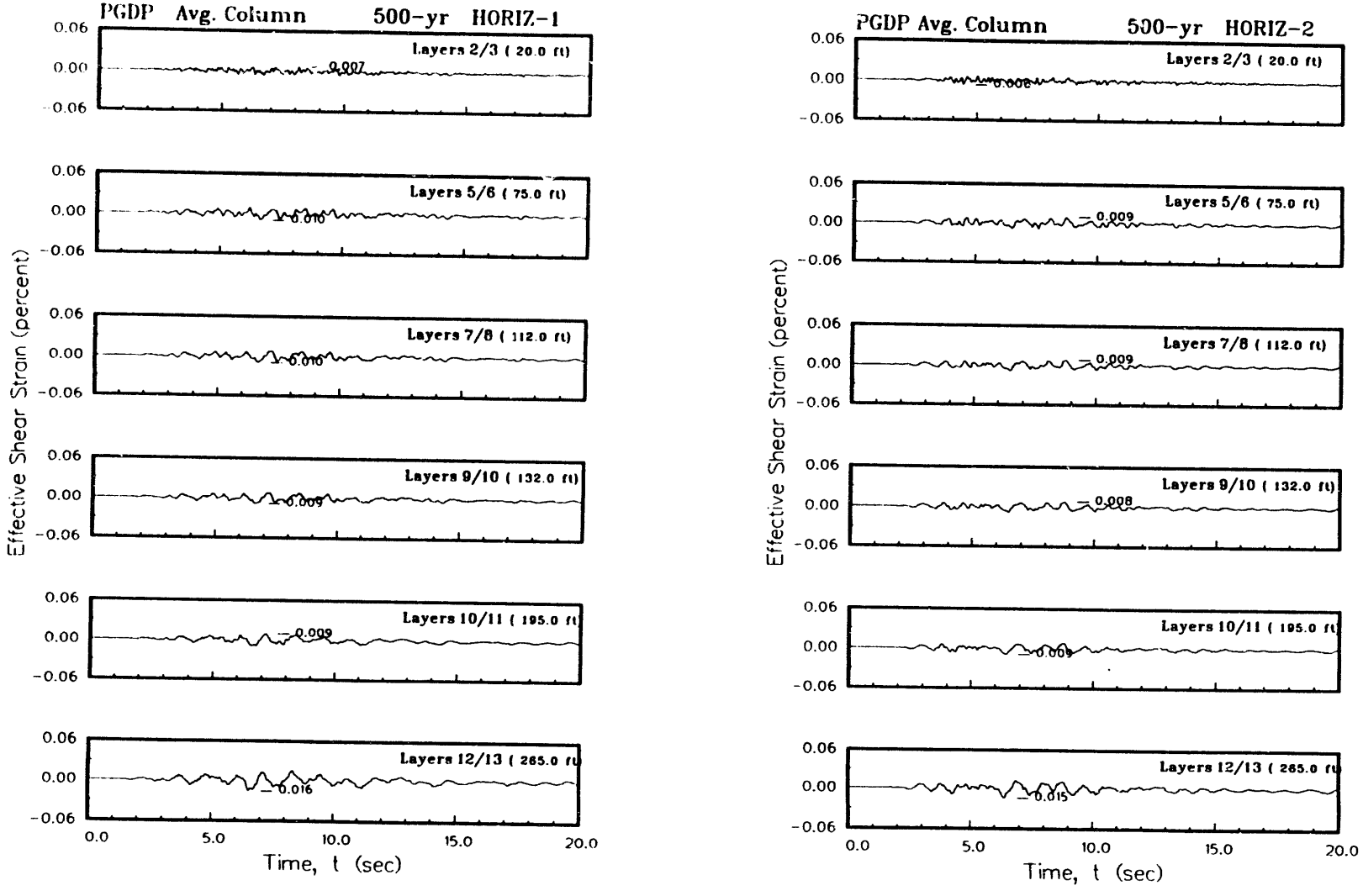

Figure T4. Variation of shear strain with time using best estimate of shear modulus for average column

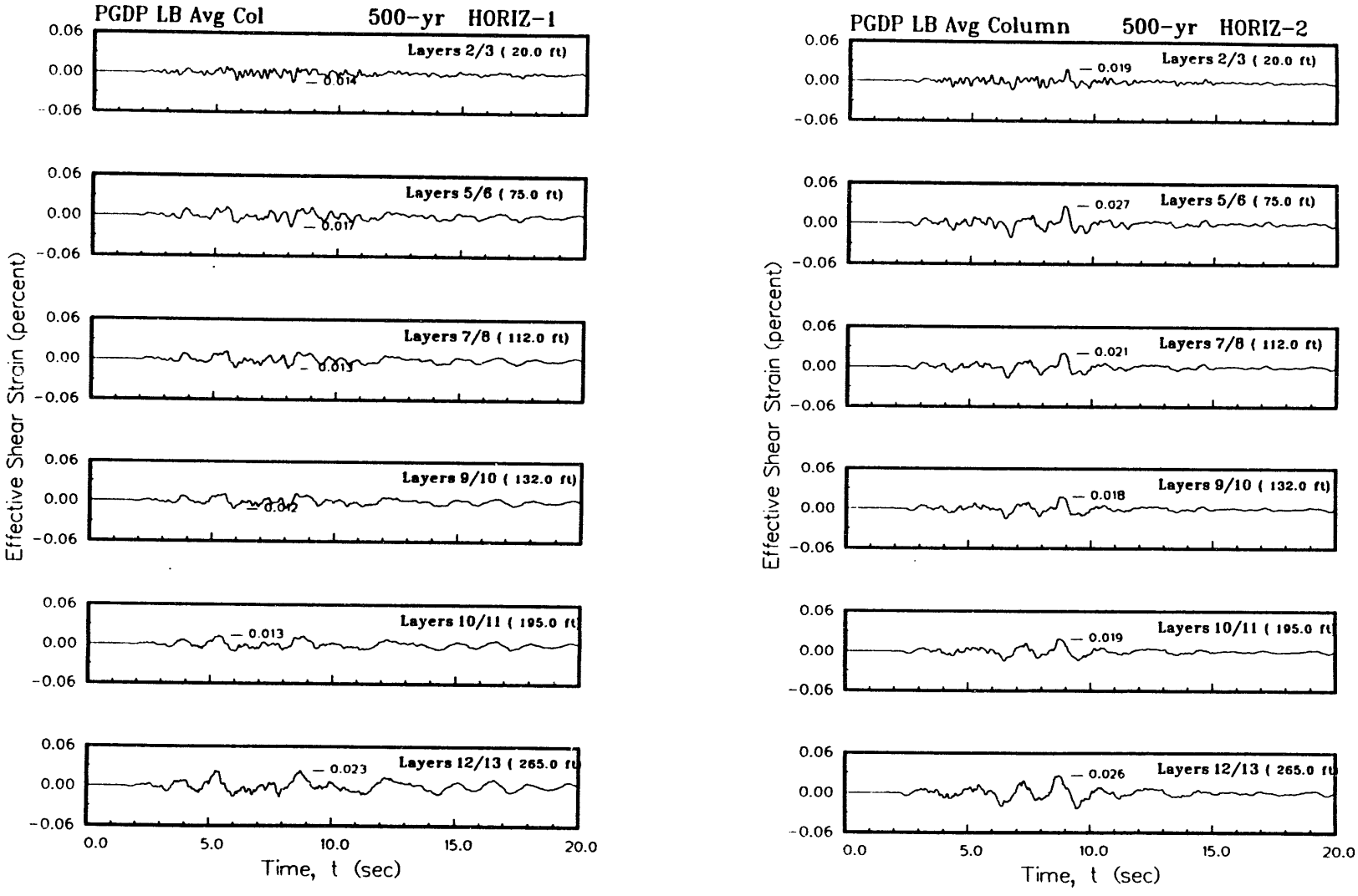

Figure T5. Variation of shear strain with time using lower bound of shear modulus for average column

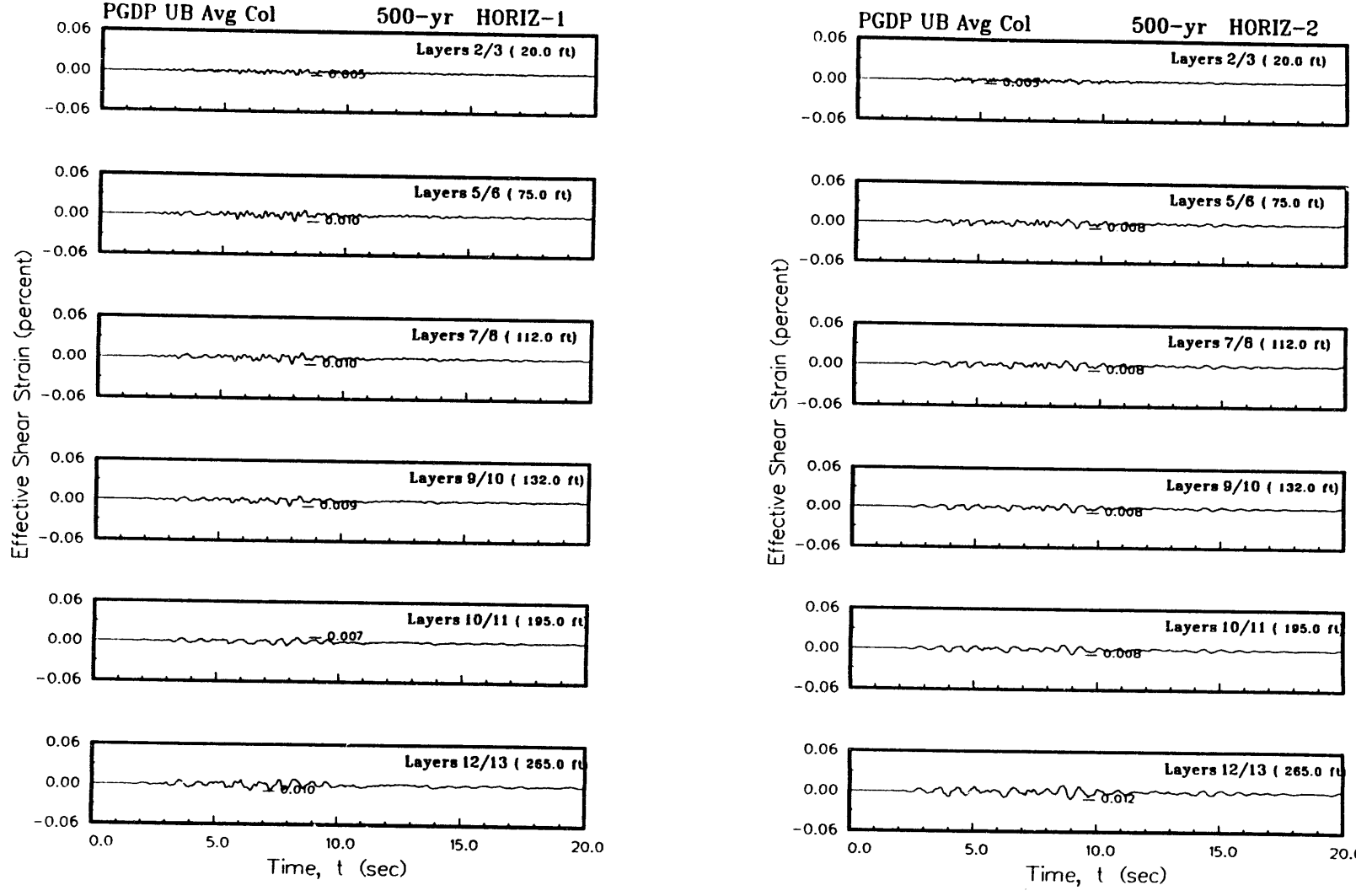

Figure T6. Variation of shear strain with time using upper bound of shear modulus for average column

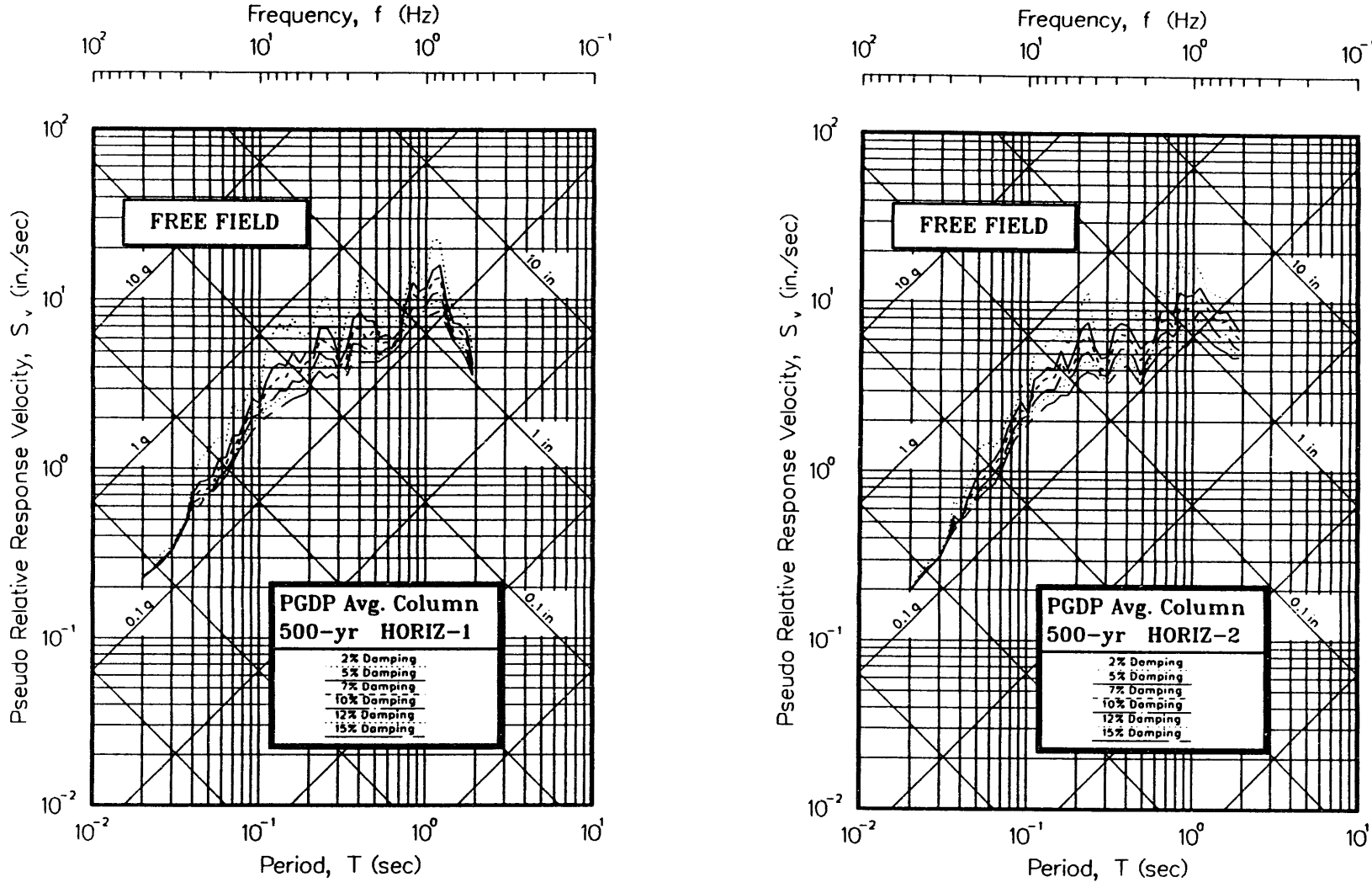

Figure T7. Psuedo-relative velocity spectra in tripartite form at free field using best estimate of modulus for average column

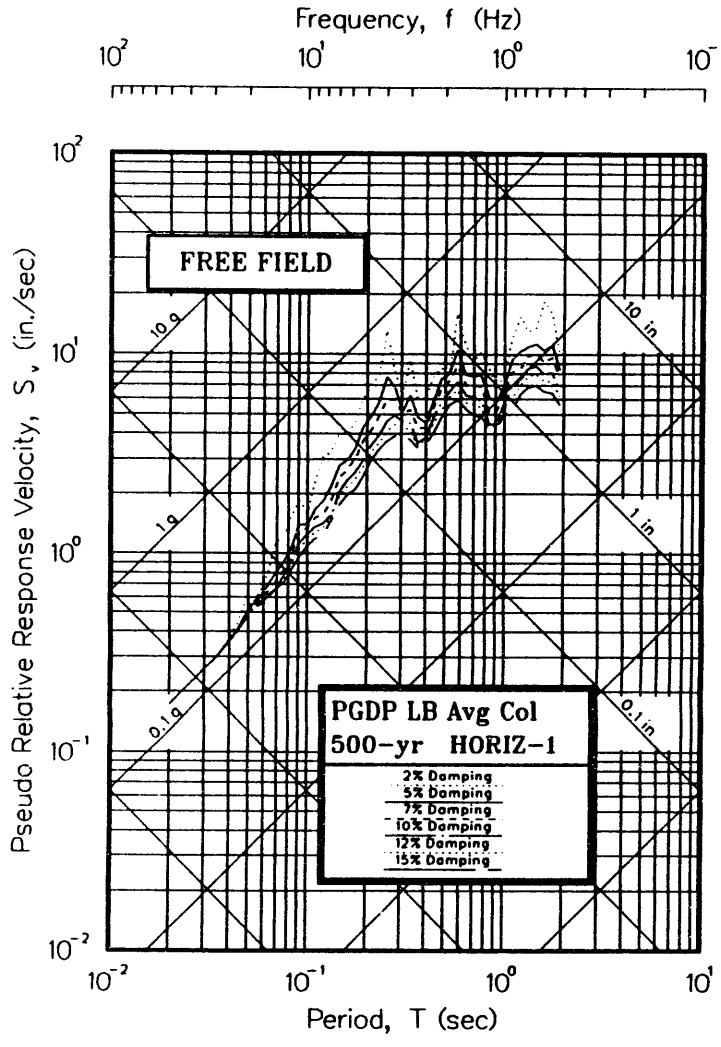

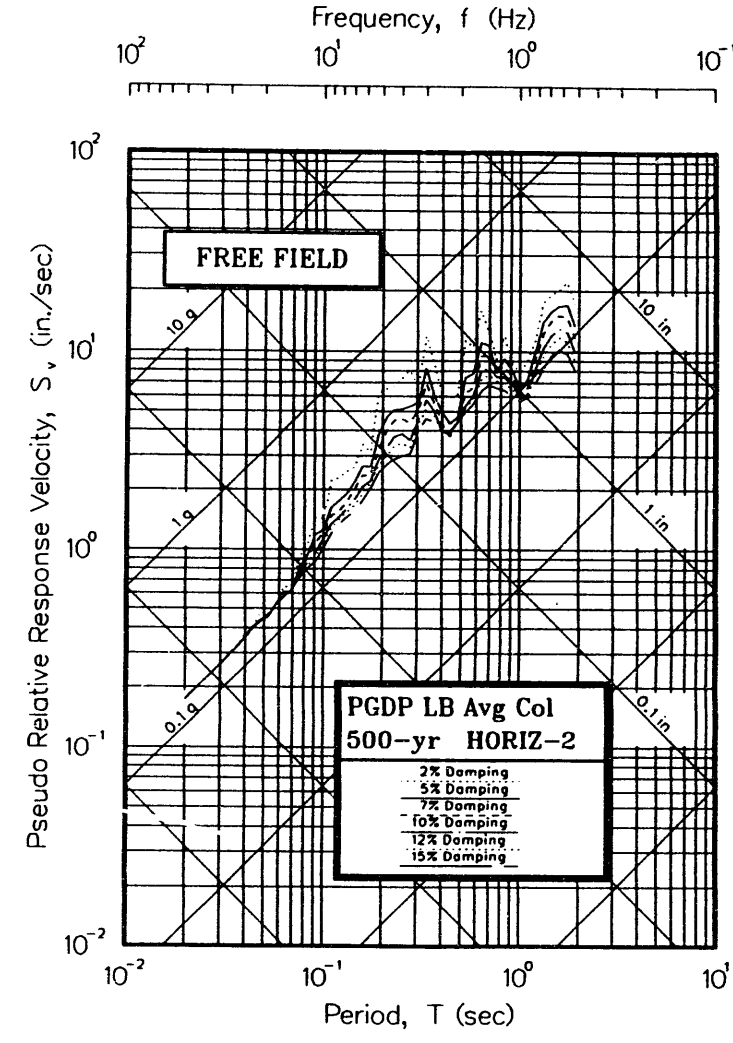

Figure T8. Psuedo-relative velocity spectra in tripartite form at free field using lower bound of modulus for average column

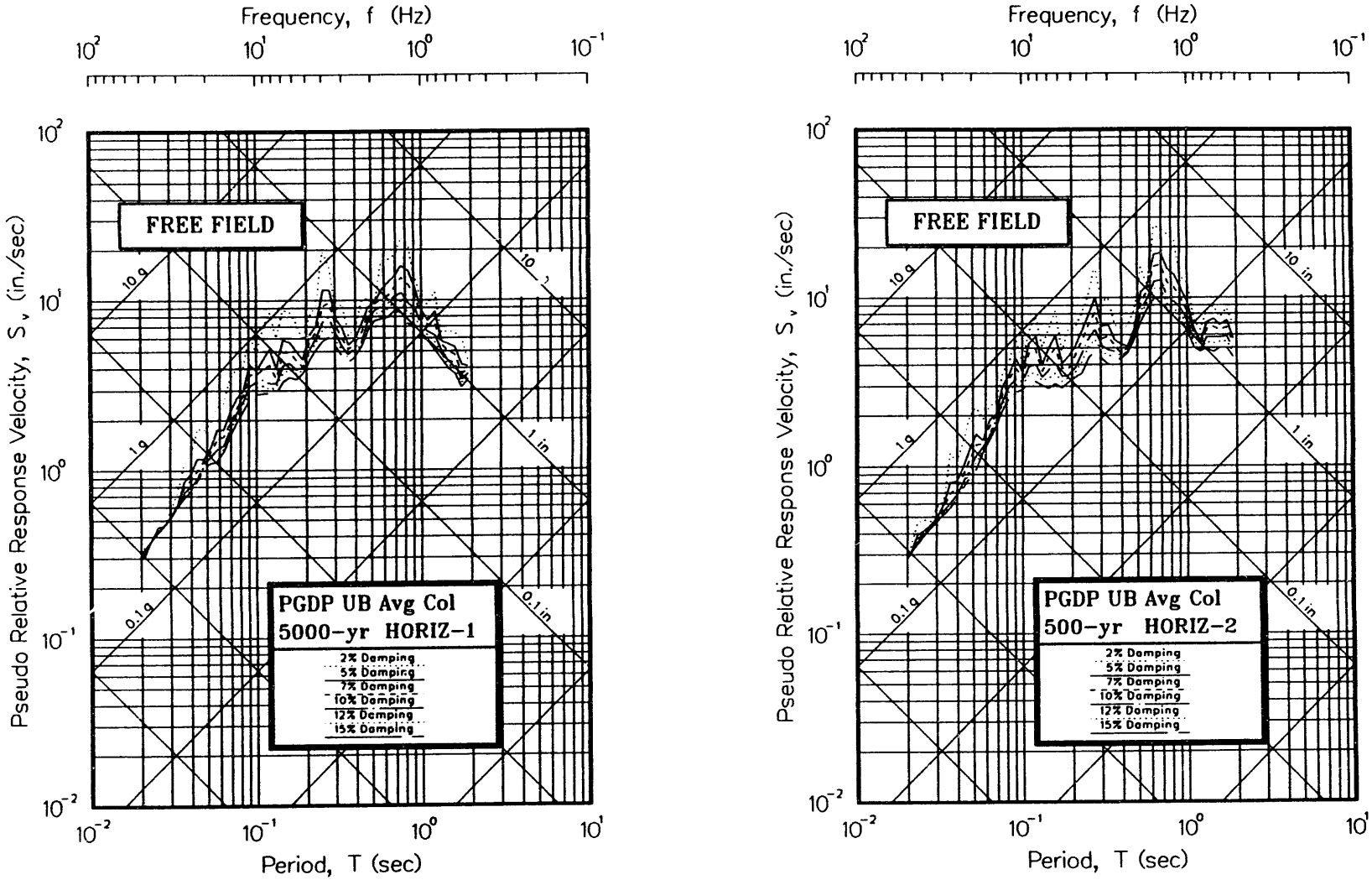

Figure T9. Psuedo-relative velocity spectra in tripartite form at free field using upper bound of modulus for average column

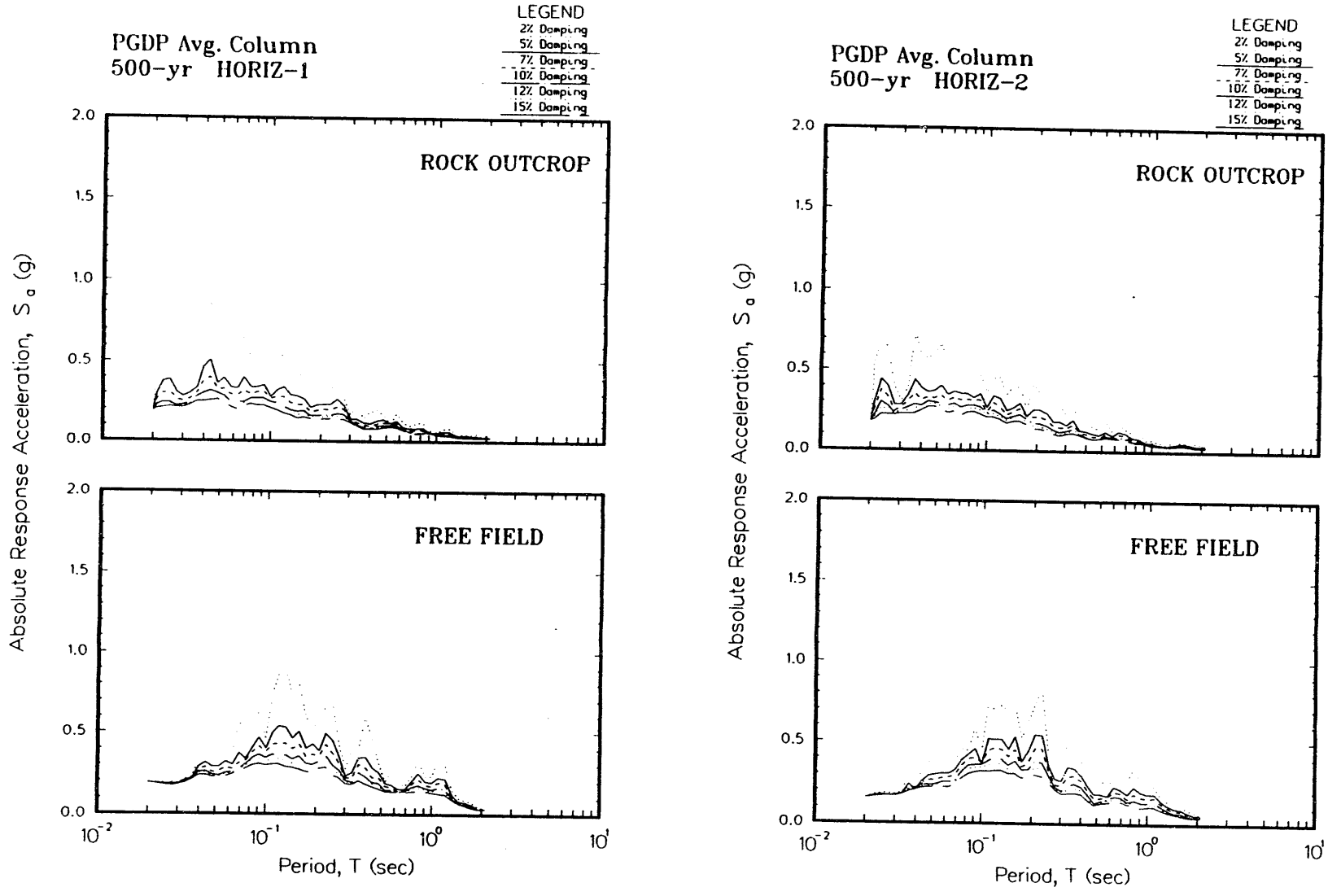

Figure T10. Absolute acceleration response spectra at free field using best estimate of modulus for average column

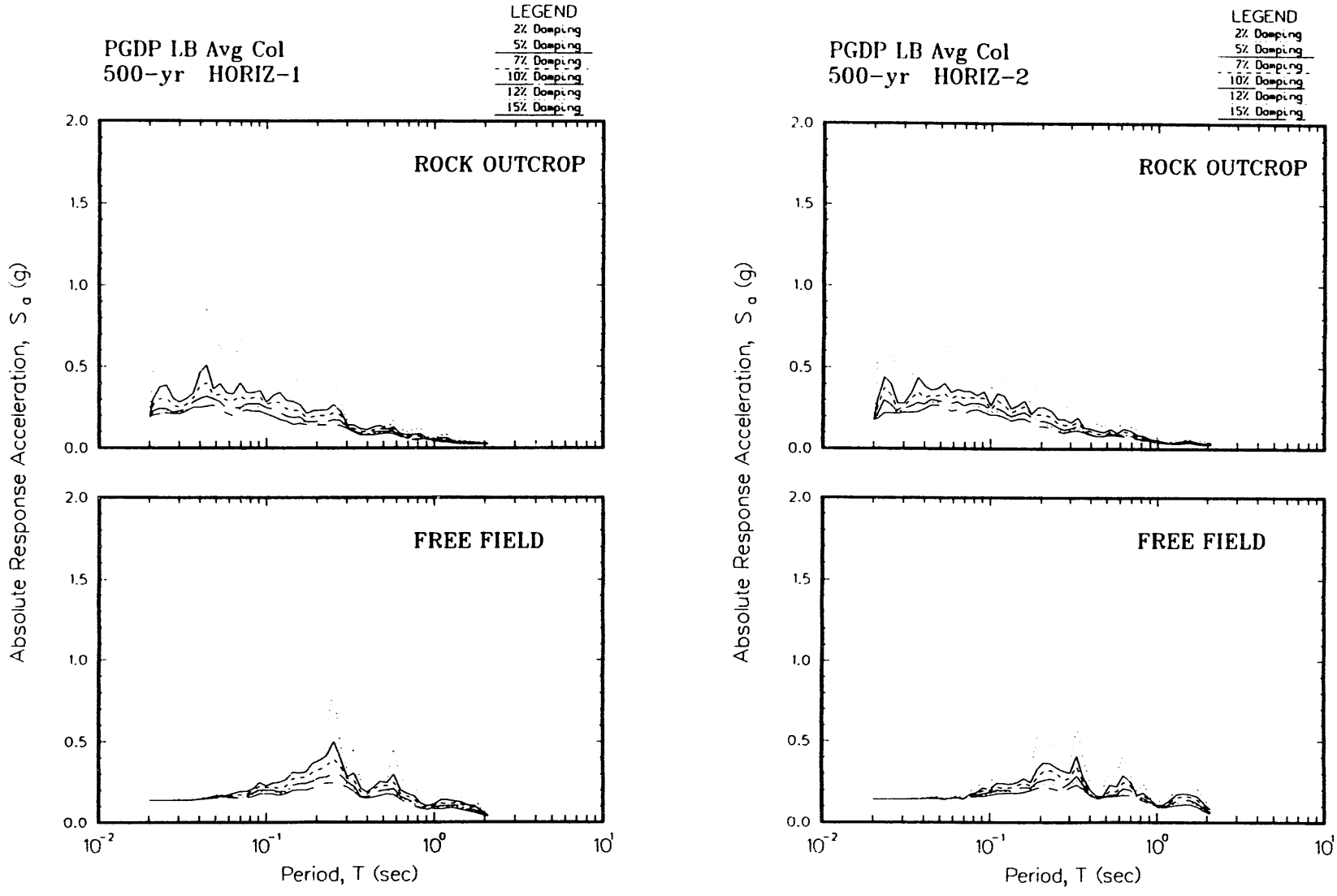

Figure T11. Absolute acceleration response spectra at free field using lower bound of modulus for average column

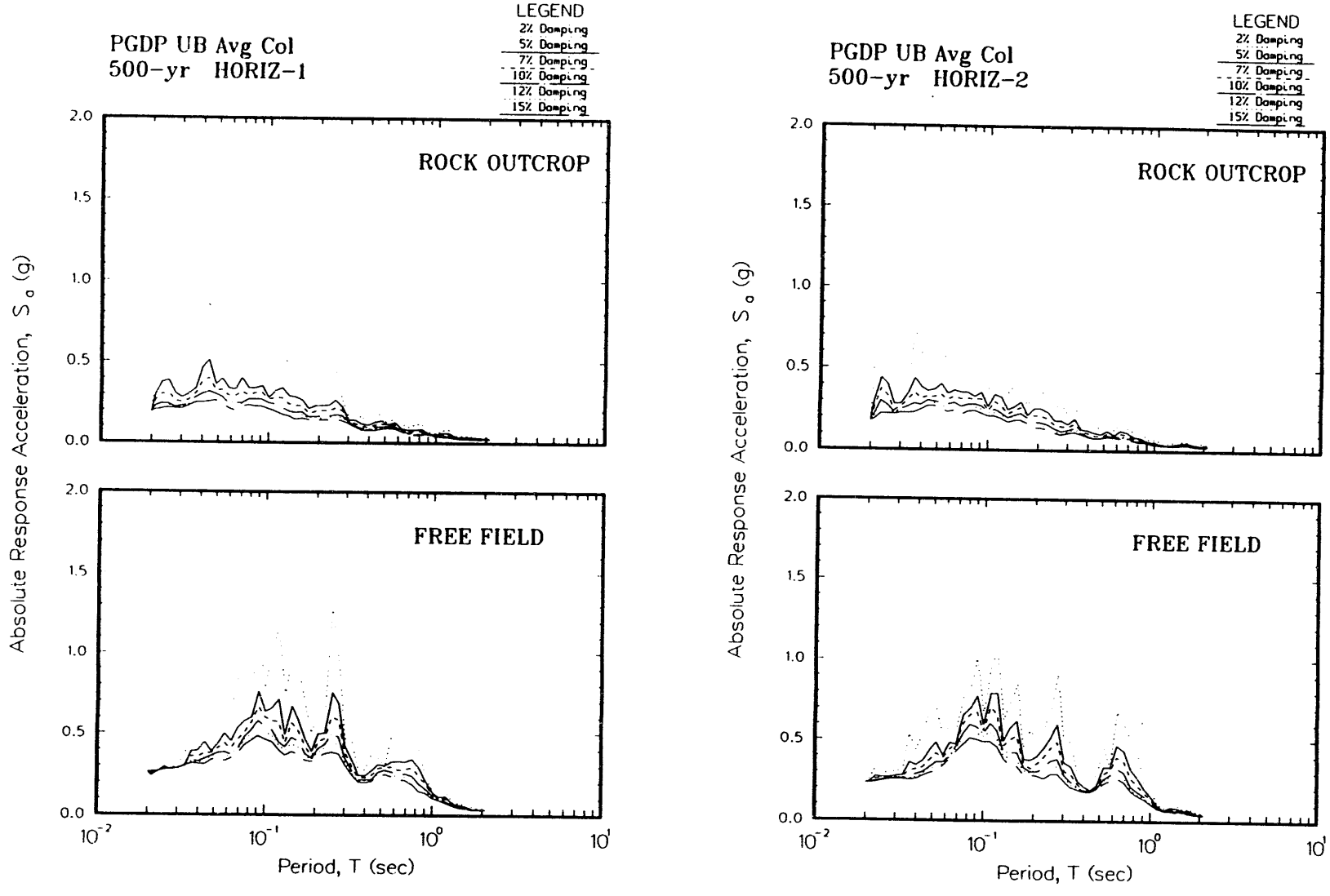

Figure T12. Absolute acceleration response spectra at free field using upper bound of modulus for average column

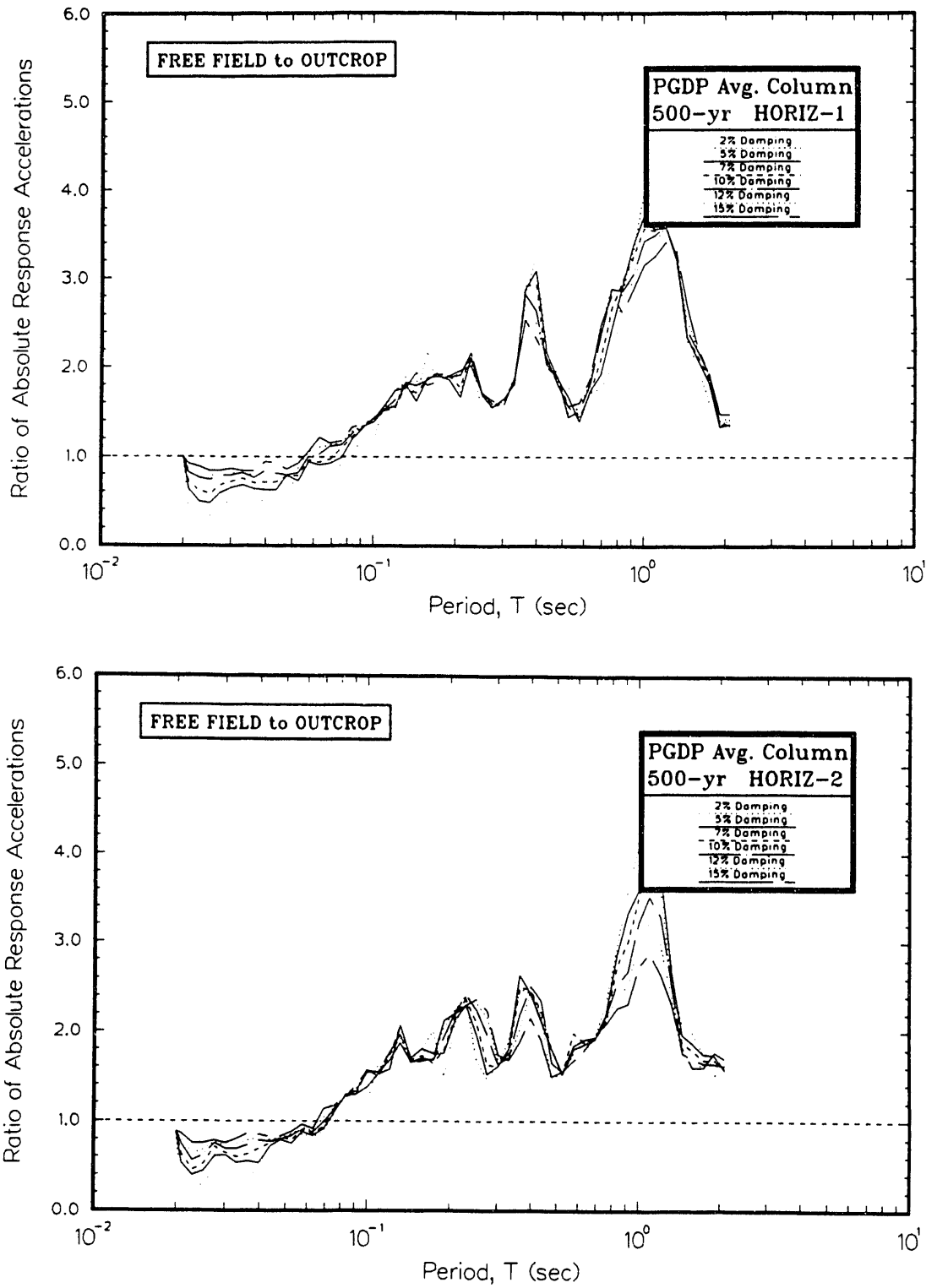

Figure T13. Ratio of absolute acceleration response spectra at free field to rock using best estimate of modulus for average column

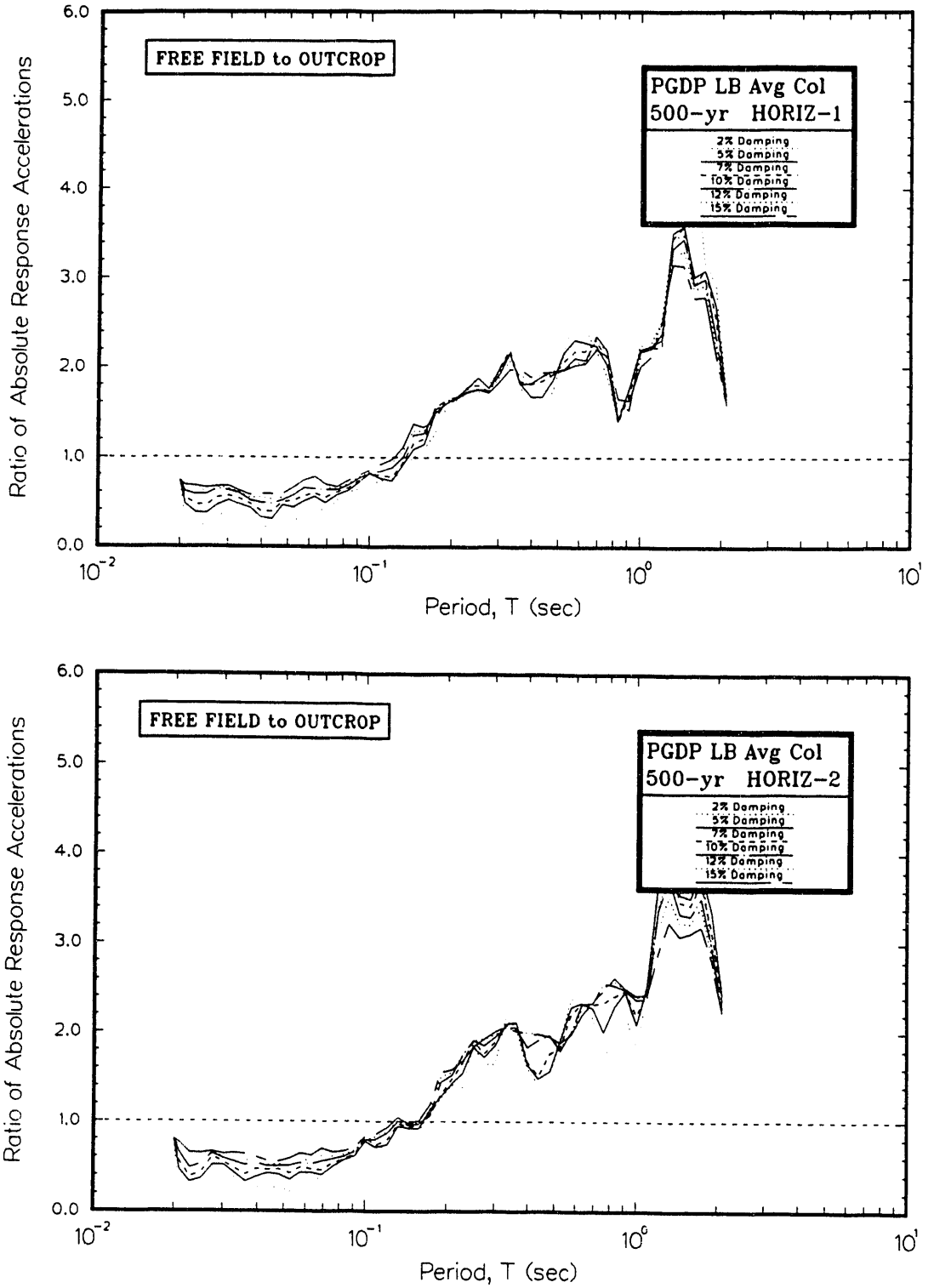

Figure T14. Ratio of absolute acceleration response spectra at free field to rock using lower bound of modulus for average column

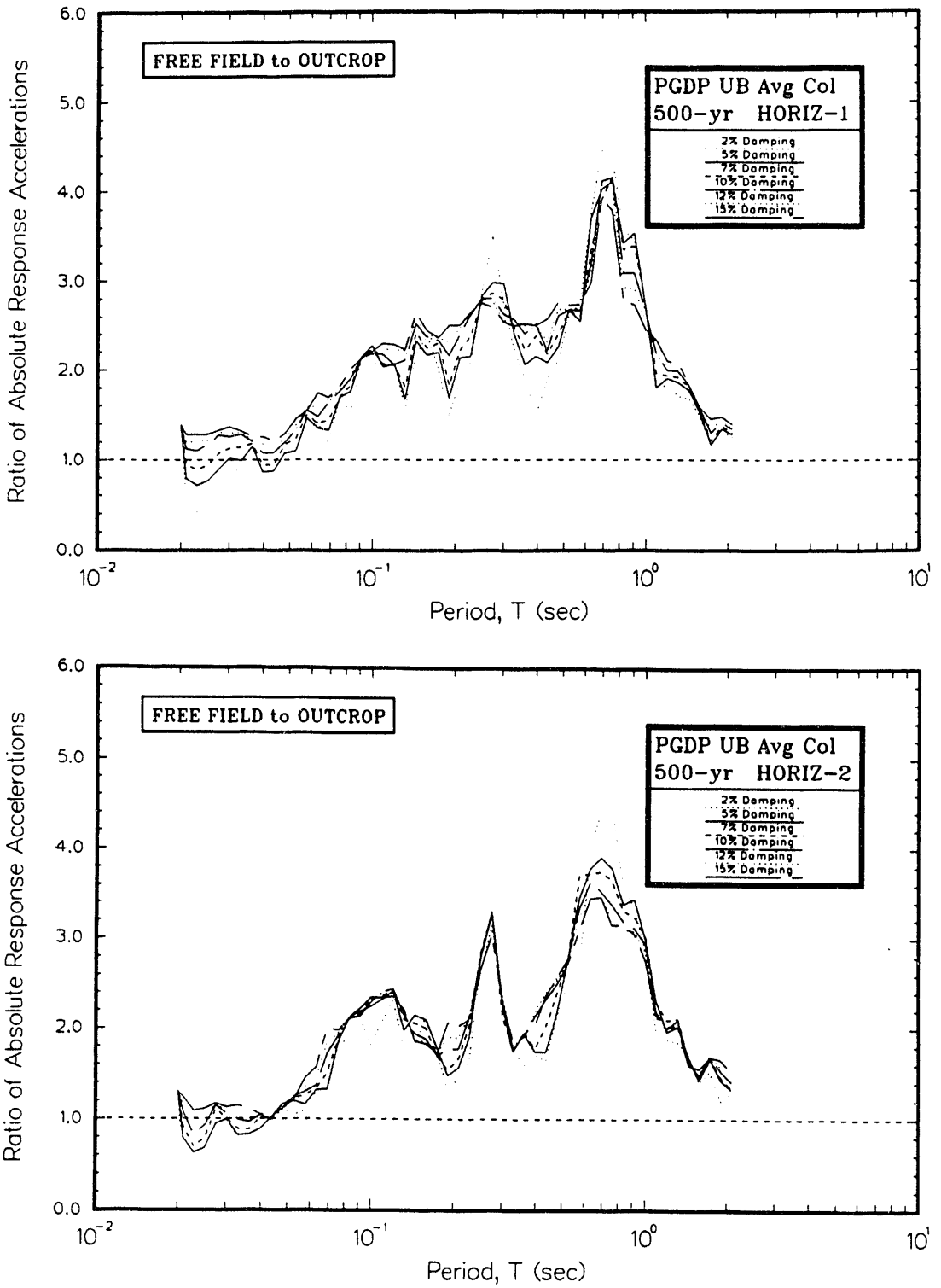

Figure T15. Ratio of absolute acceleration response spectra at free field to rock using upper bound of modulus for average column

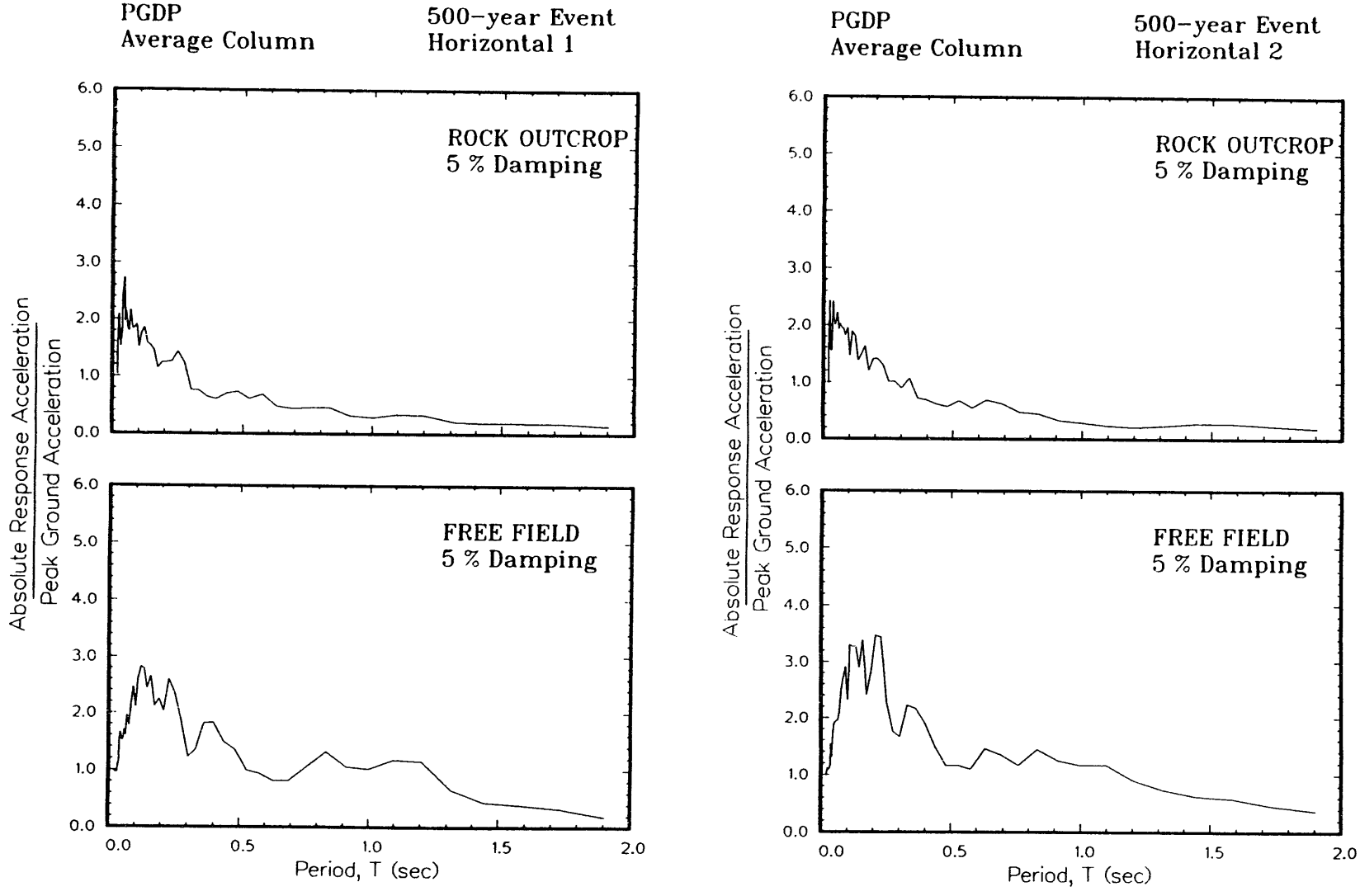

Figure T16. Ratio of amplification of absolute acceleration response spectra to peak acceleration at free field using best estimate of modulus for average column

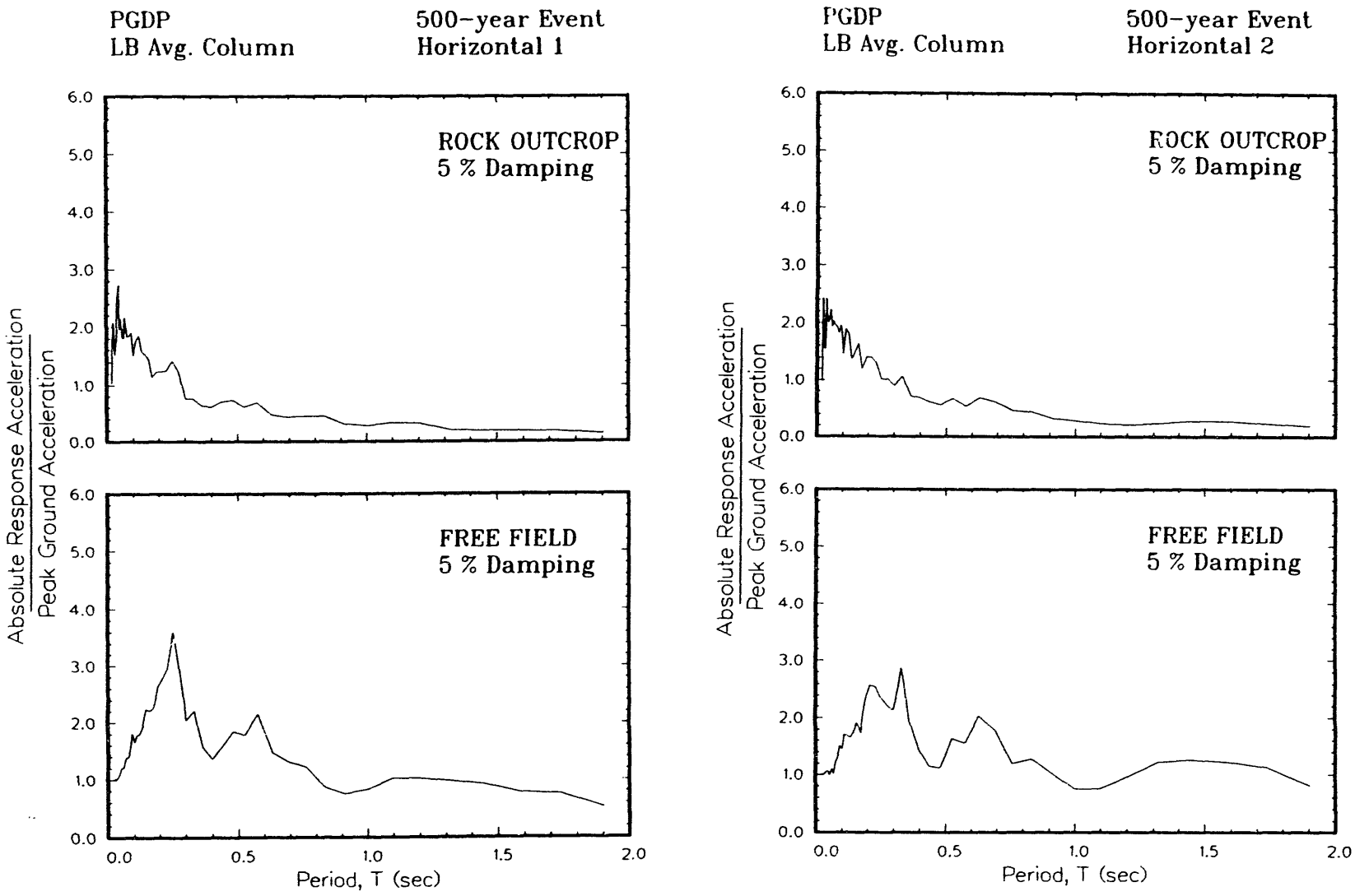

Figure T17. Ratio of amplification of absolute acceleration response spectra to peak acceleration at free field using lower bound of modulus for average column

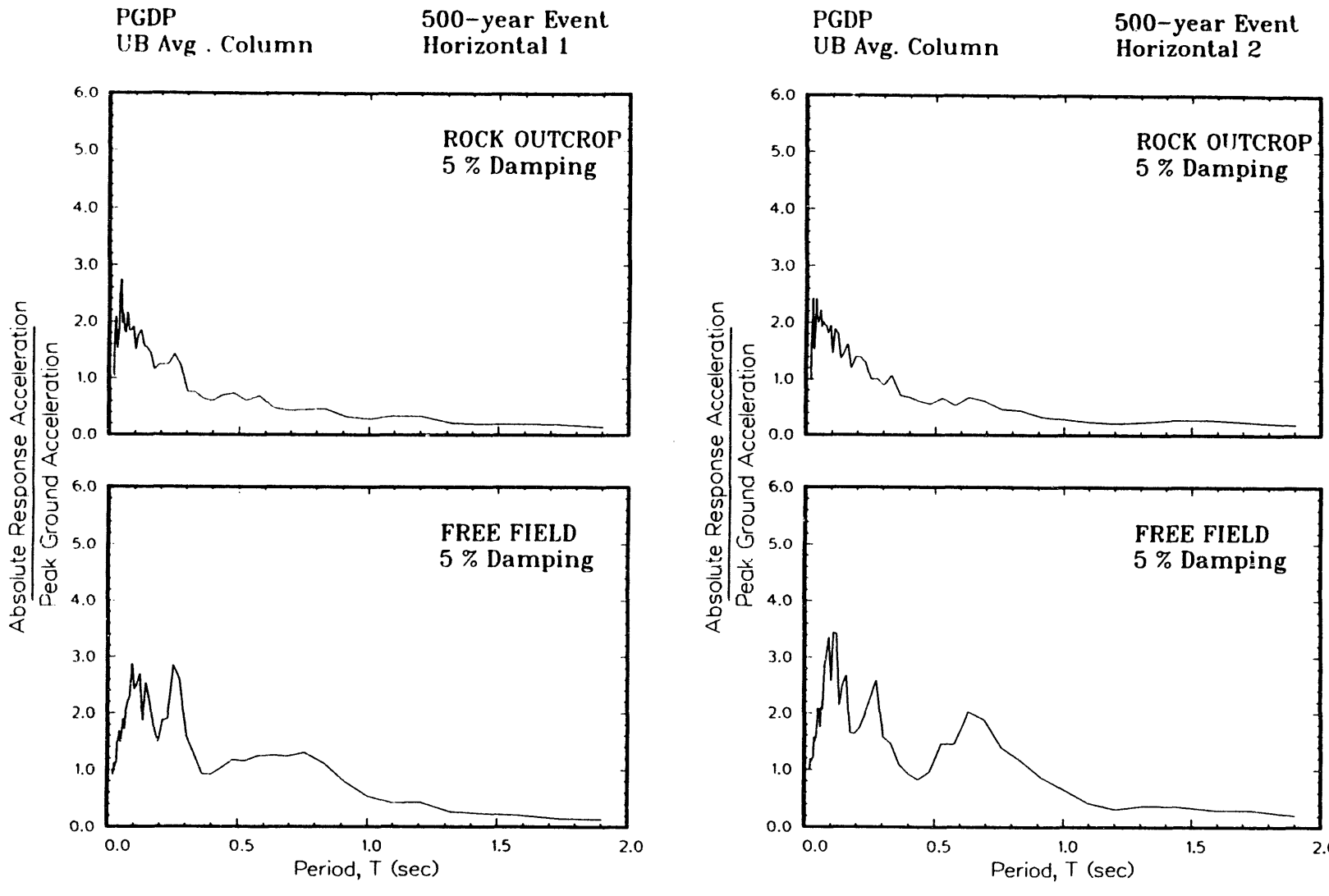

Figure T18. Ratio of amplification of absolute acceleration response spectra to peak acceleration at free field using upper bound of modulus for average column

APPENDIX U: SENSITIVITY OF RESULTS TO MAXIMUM SHEAR MODULUS FOR 1000-YEAR EVENT

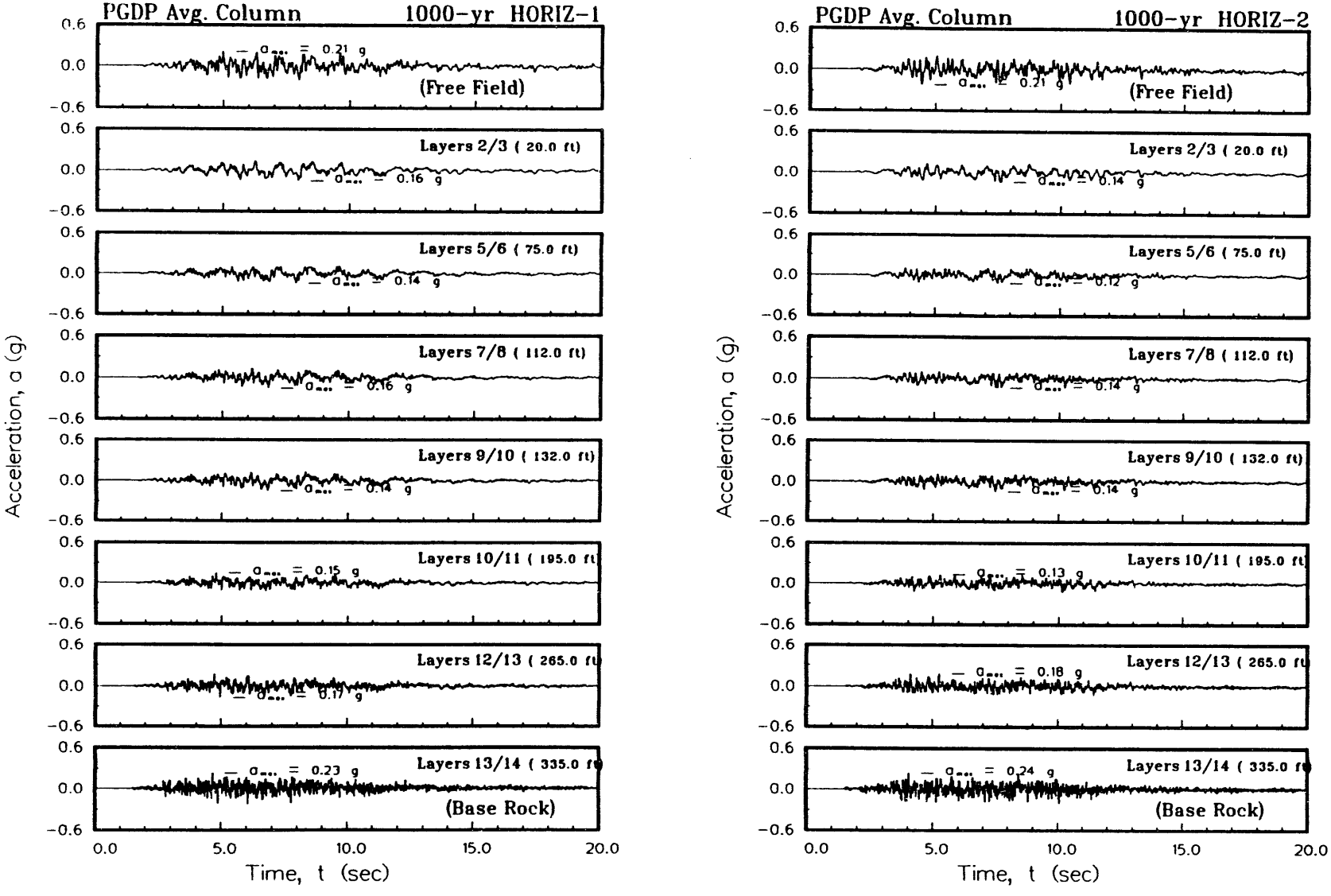

Figure U1. Variation of acceleration with time using best estimate of shear modulus for average column

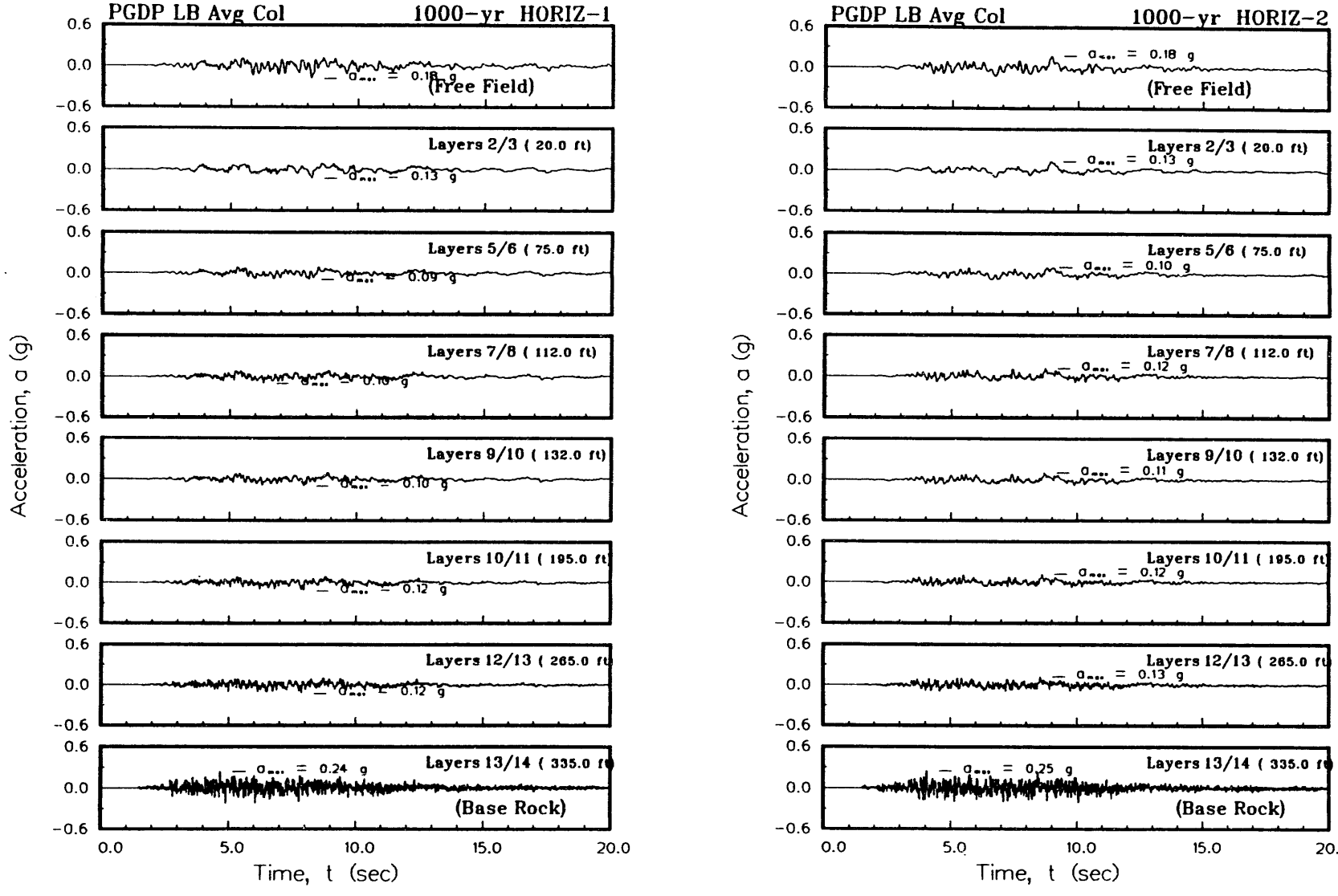

Figure U2. Variation of acceleration with time using lower bound of shear modulus for average column

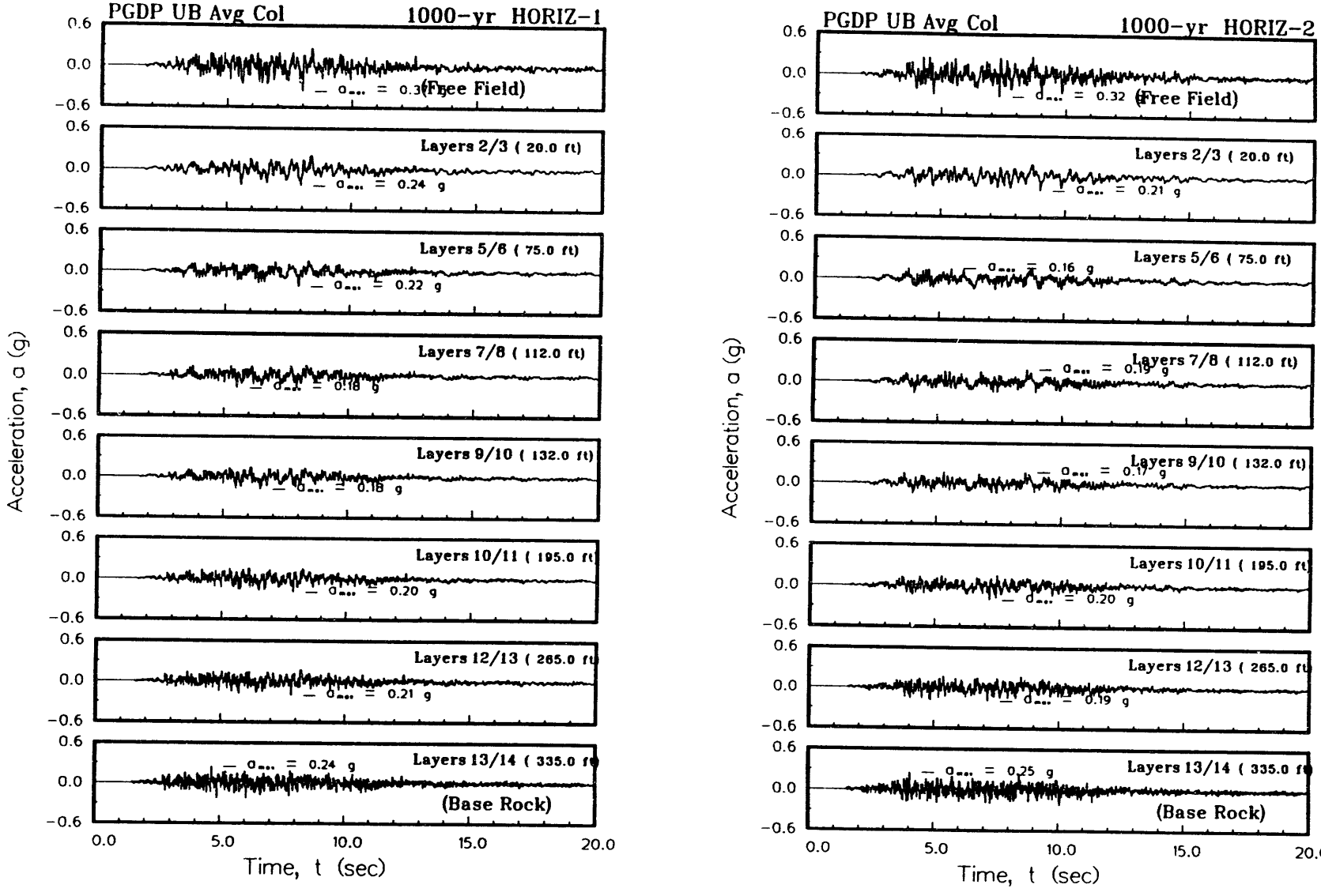

Figure U3. Variation of acceleration with time using upper bound of shear modulus for average column

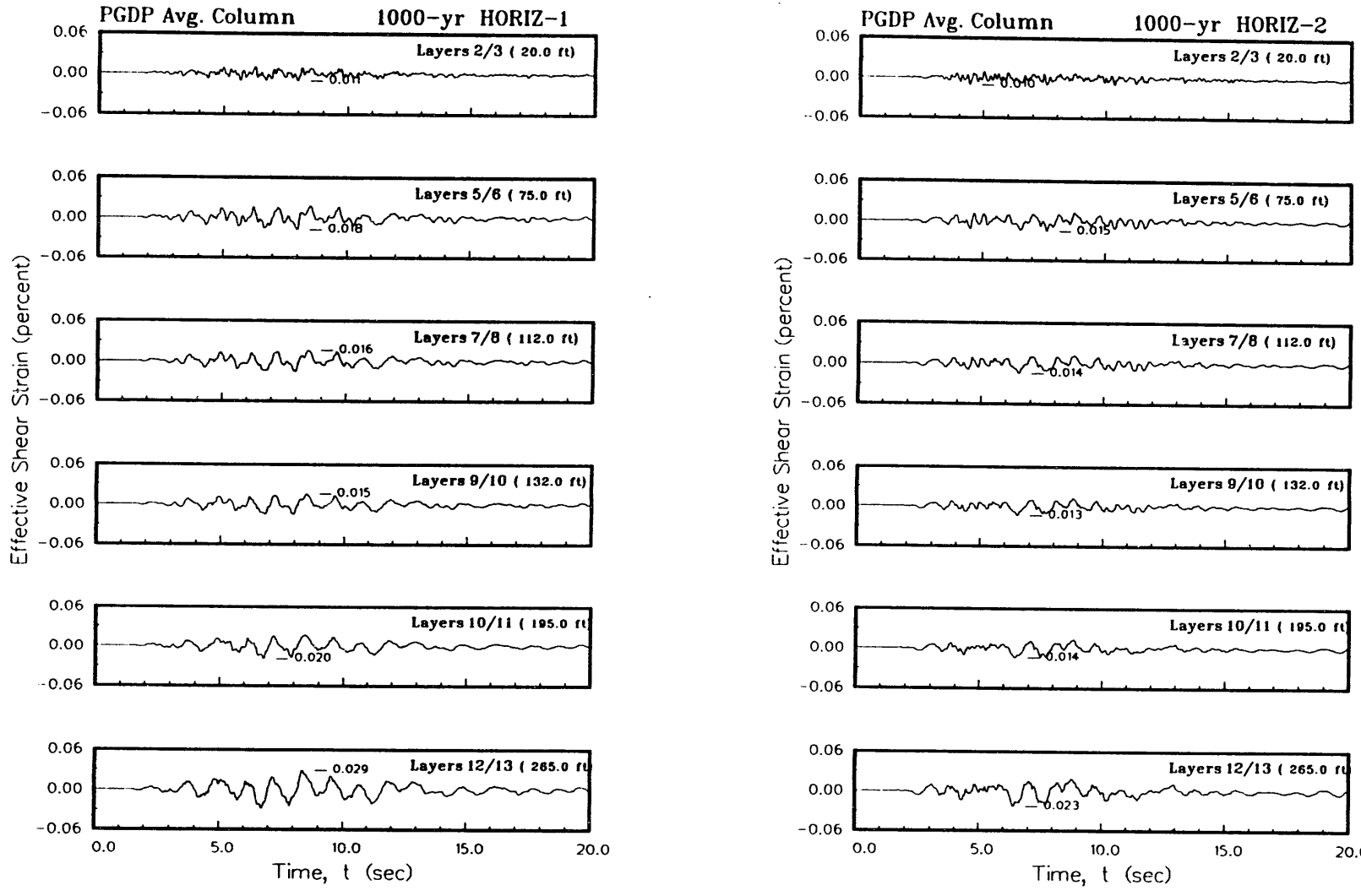

Figure U4. Variation of shear strain with time using best estimate of shear modulus for average column

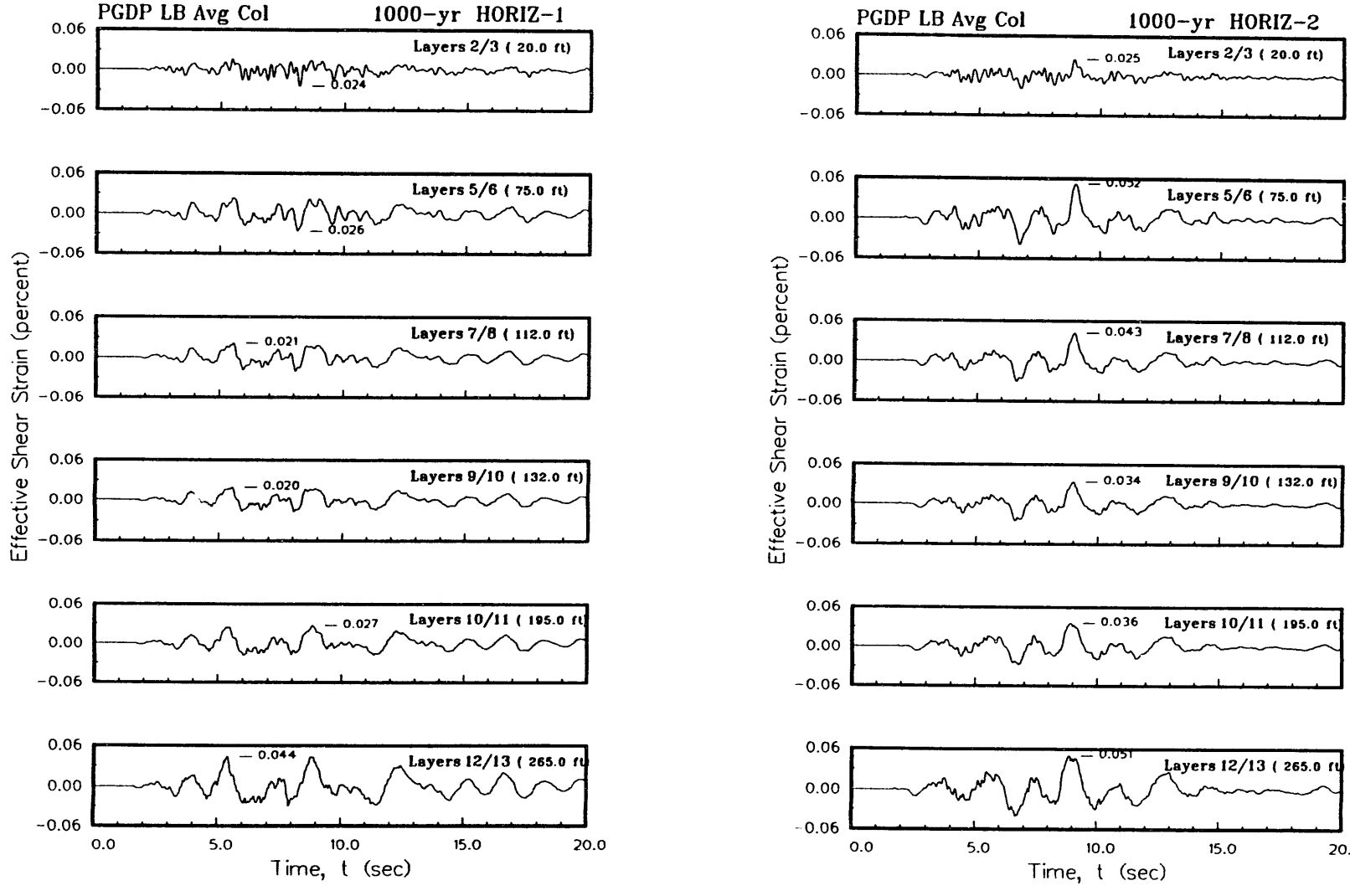

Figure U5. Variation of shear strain with time using lower bound of shear modulus for average column

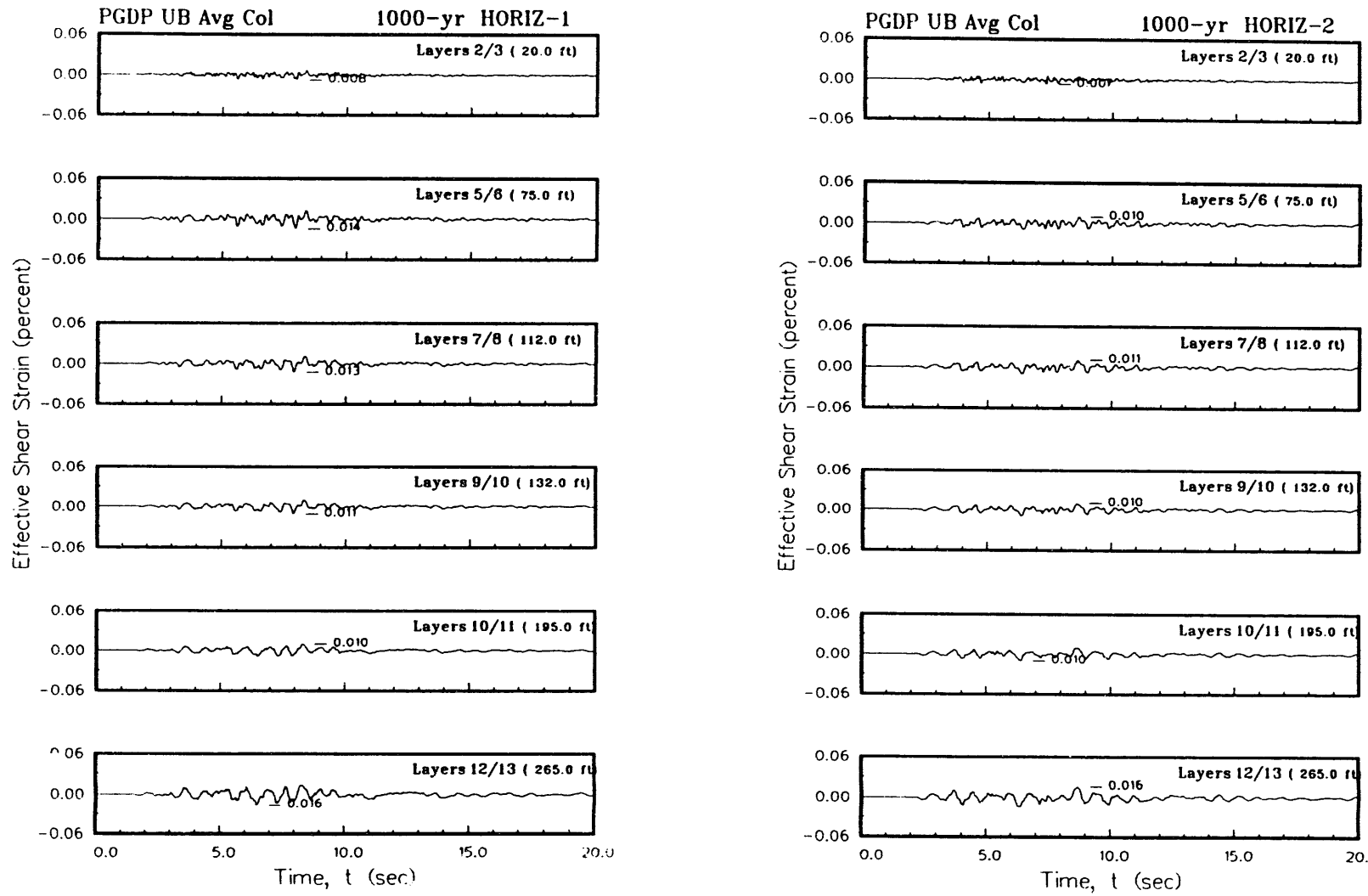

Figure U6. Variation of shear strain with time using upper bound of shear modulus for average column

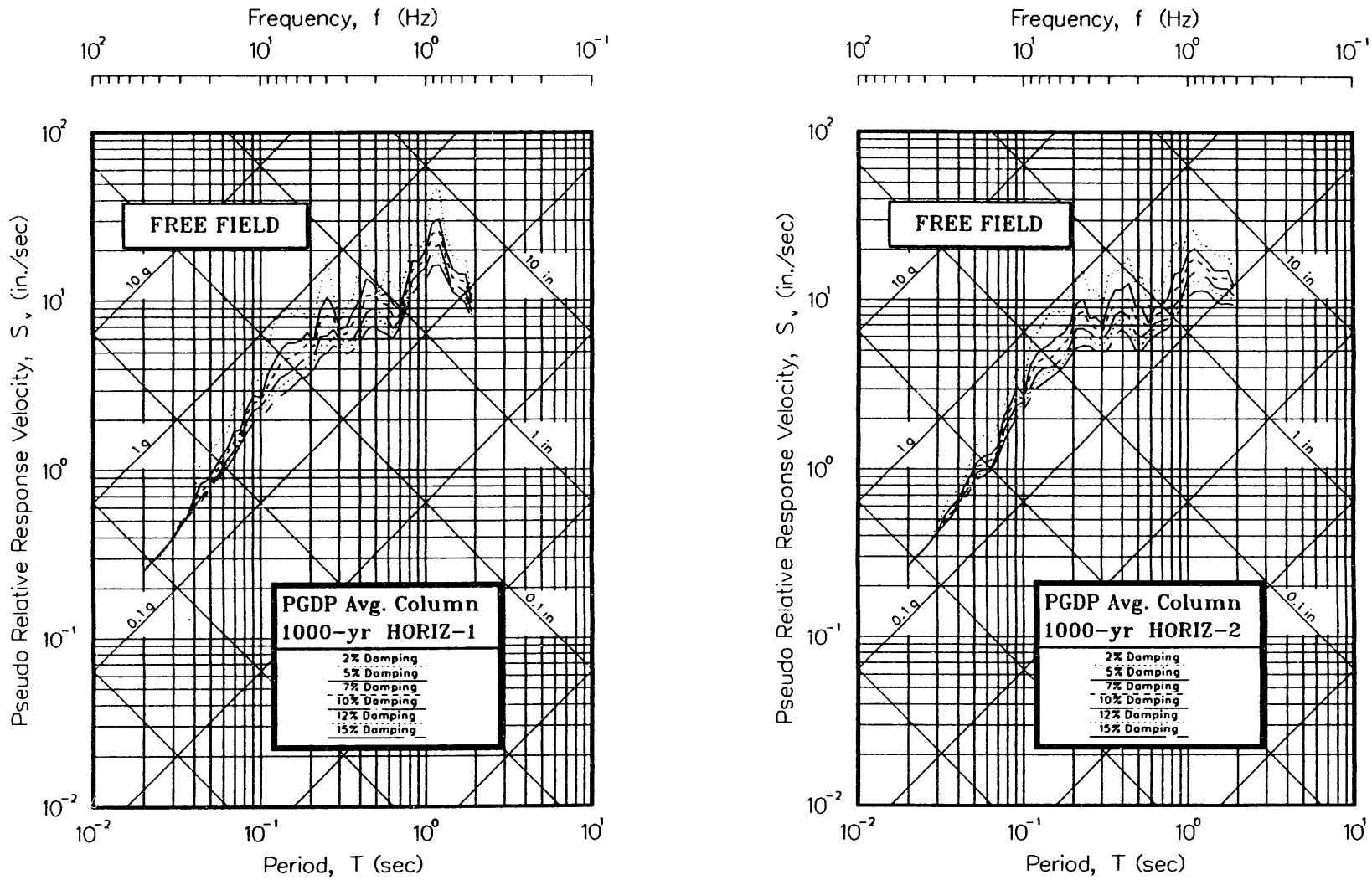

Figure U7. Psuedo-relative velocity spectra in tripartite form at free field using best estimate of modulus for average column

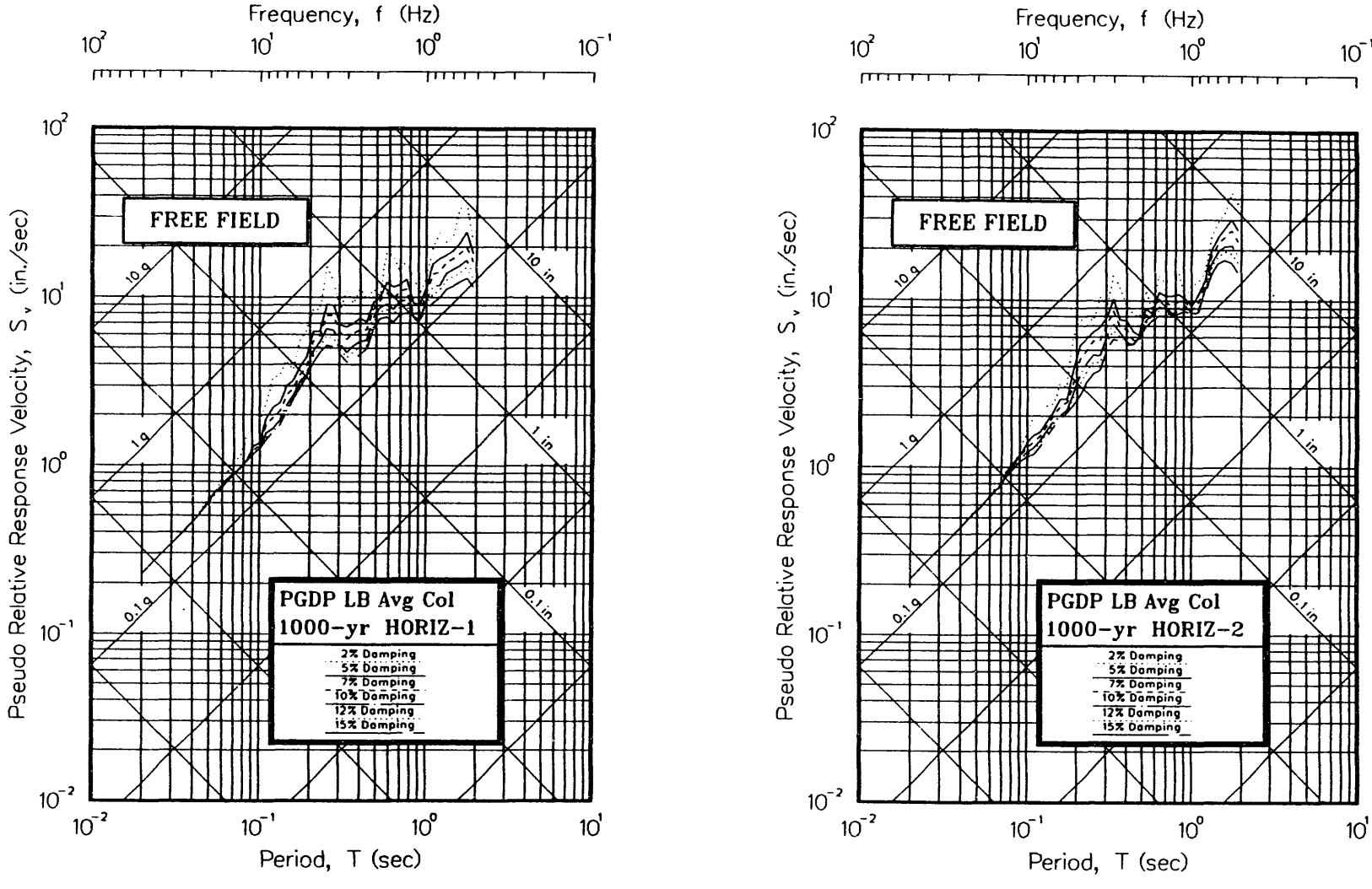

Figure U8. Psuedo-relative velocity spectra in tripartite form at free field using lower bound of modulus for average column

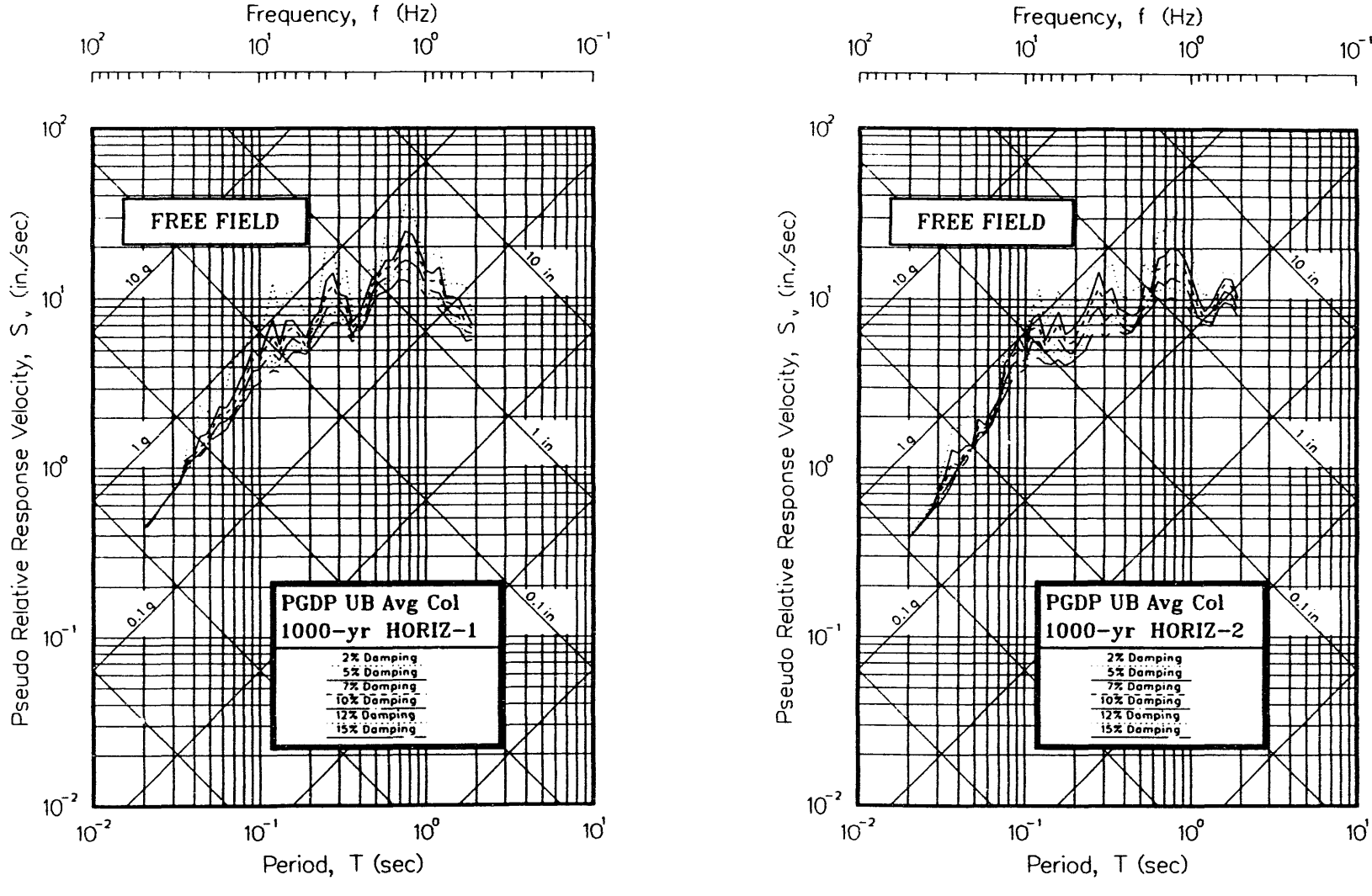

Figure U9. Psuedo-relative velocity spectra in tripartite form at free field using upper bound of modulus for average column

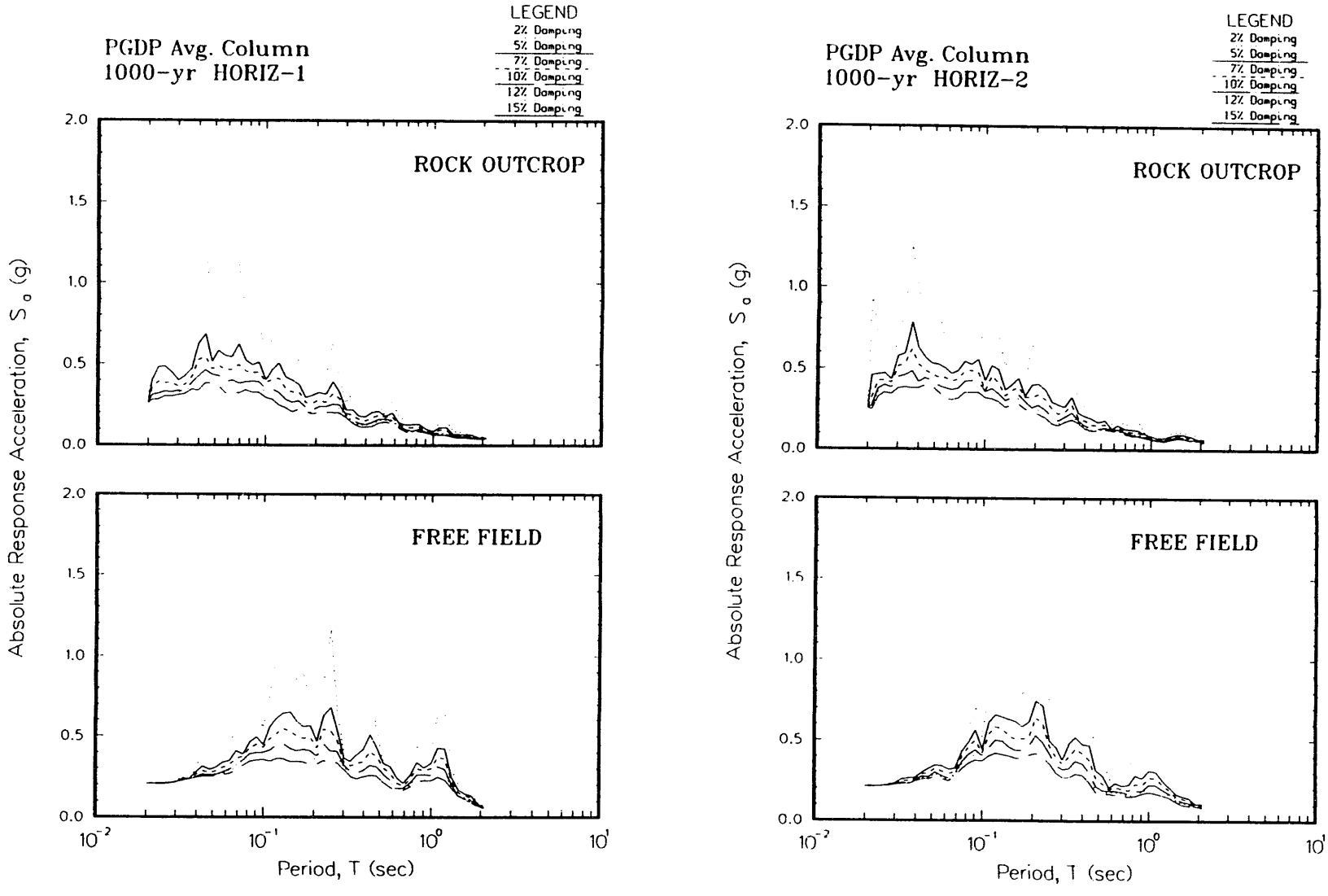

Figure U10. Absolute acceleration response spectra at free field using best estimate of modulus for average column

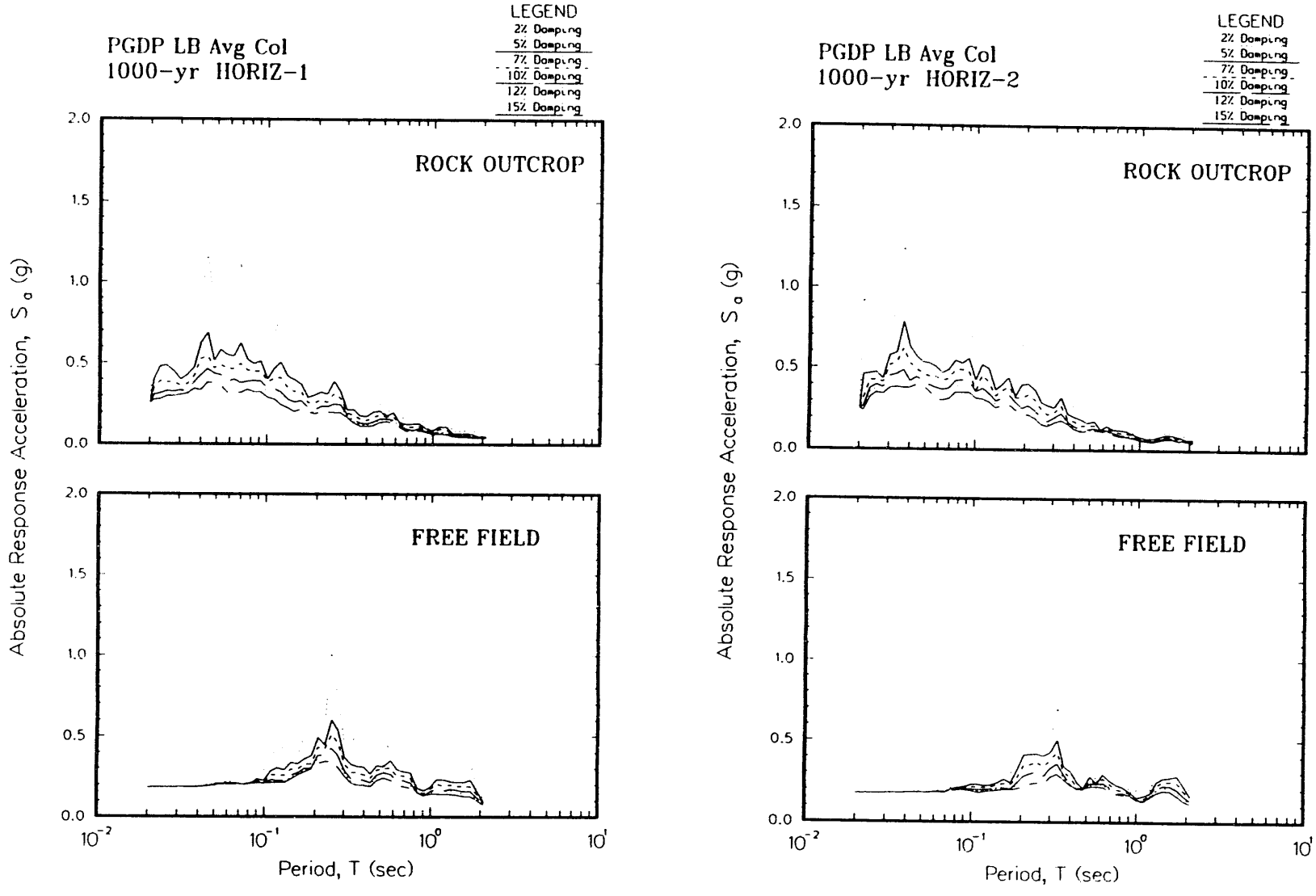

Figure U11. Absolute acceleration response spectra at free field using lower bound of modulus for average column

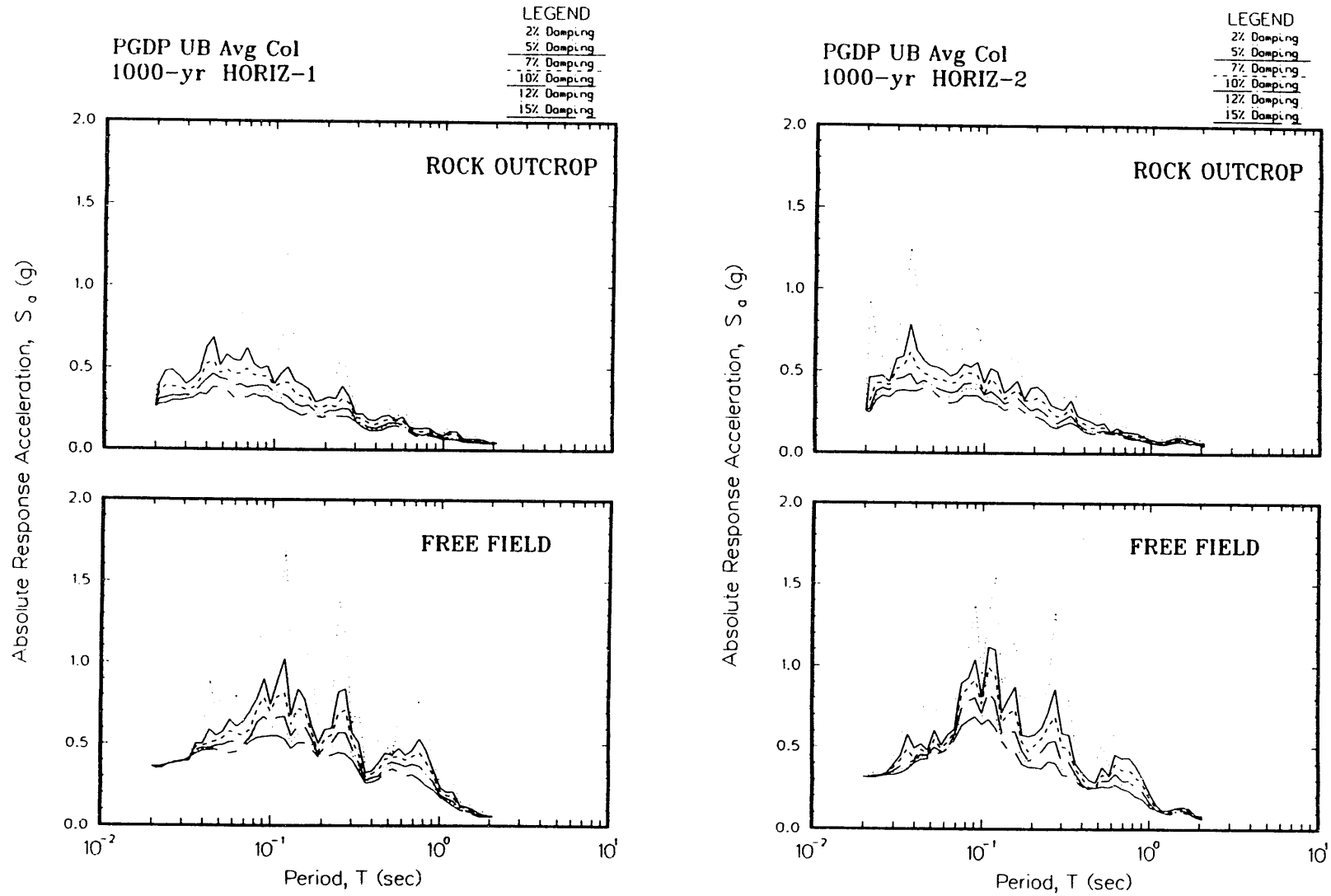

Figure U12. Absolute acceleration response spectra at free field using upper bound of modulus for average column

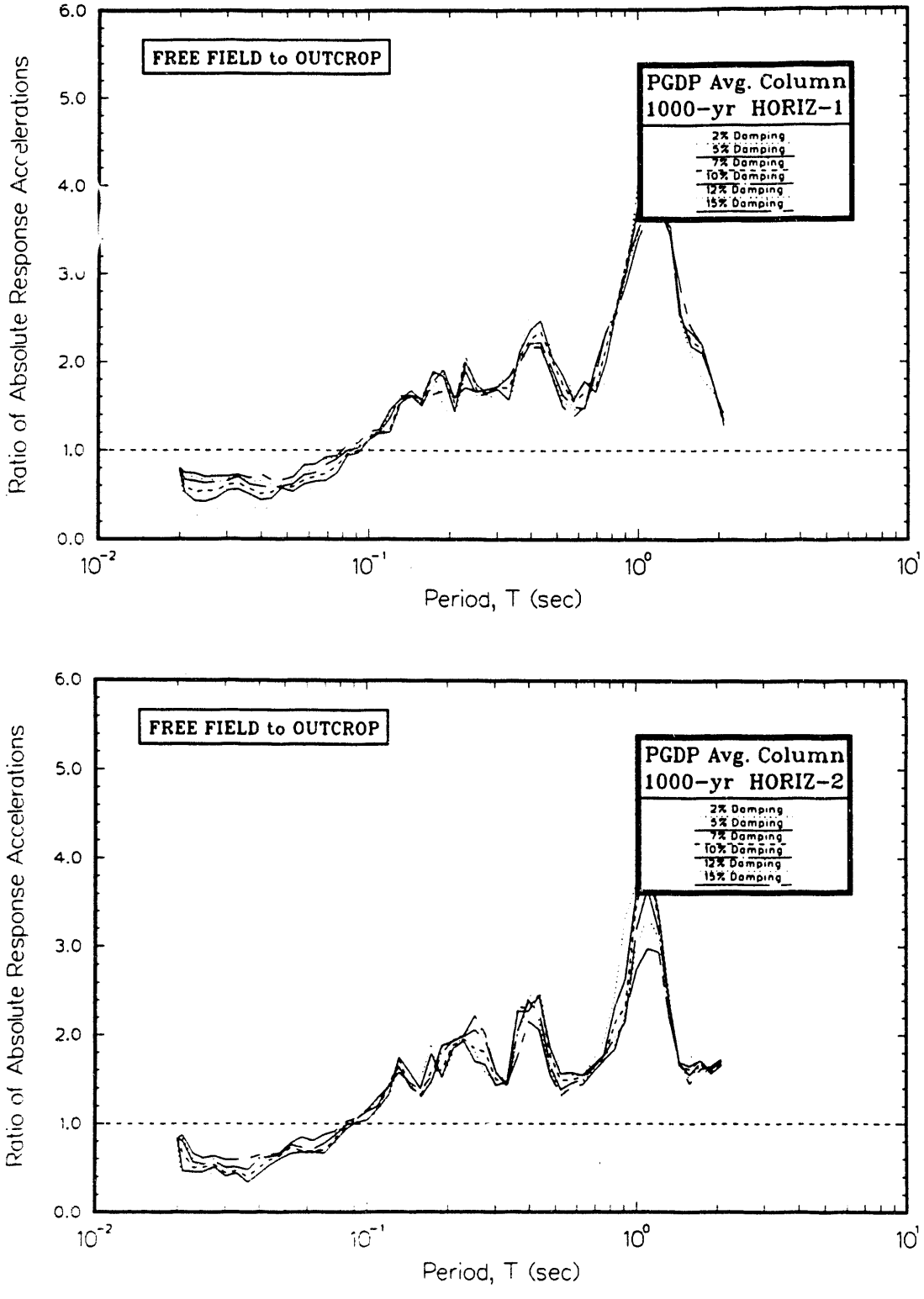

Figure U13. Ratio of absolute acceleration response spectra at free field to rock using best estimate of modulus for average column

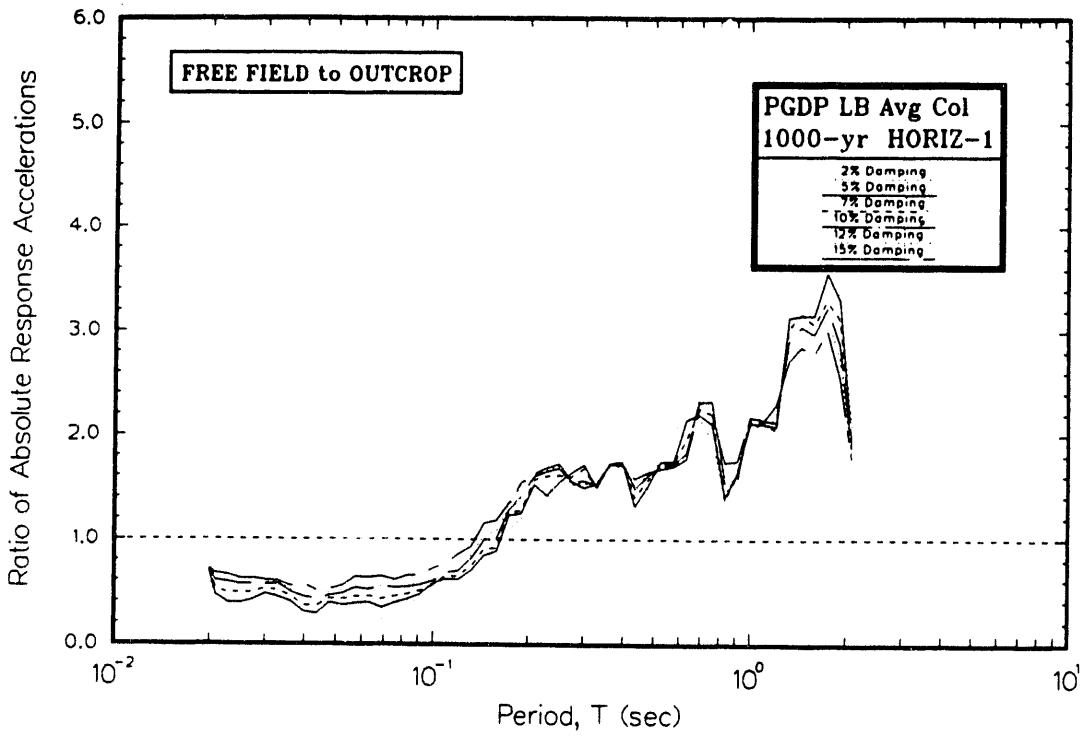

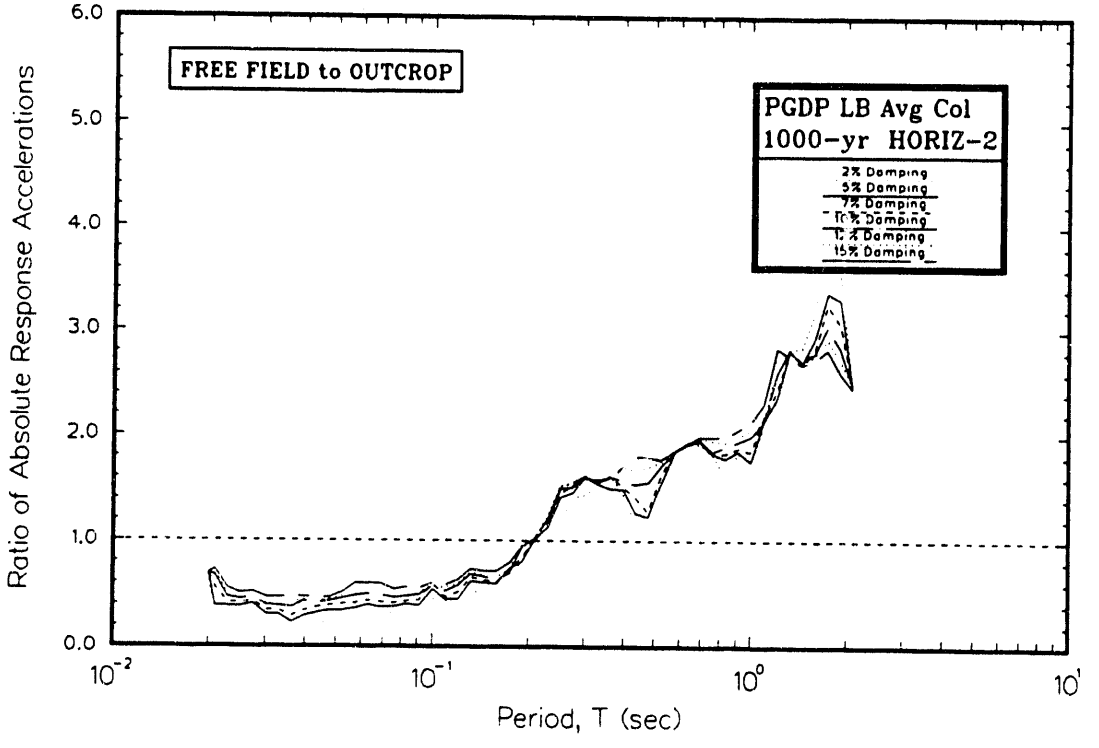

Figure U14. Ratio of absolute acceleration response spectra at free field to rock using lower bound of modulus for average column

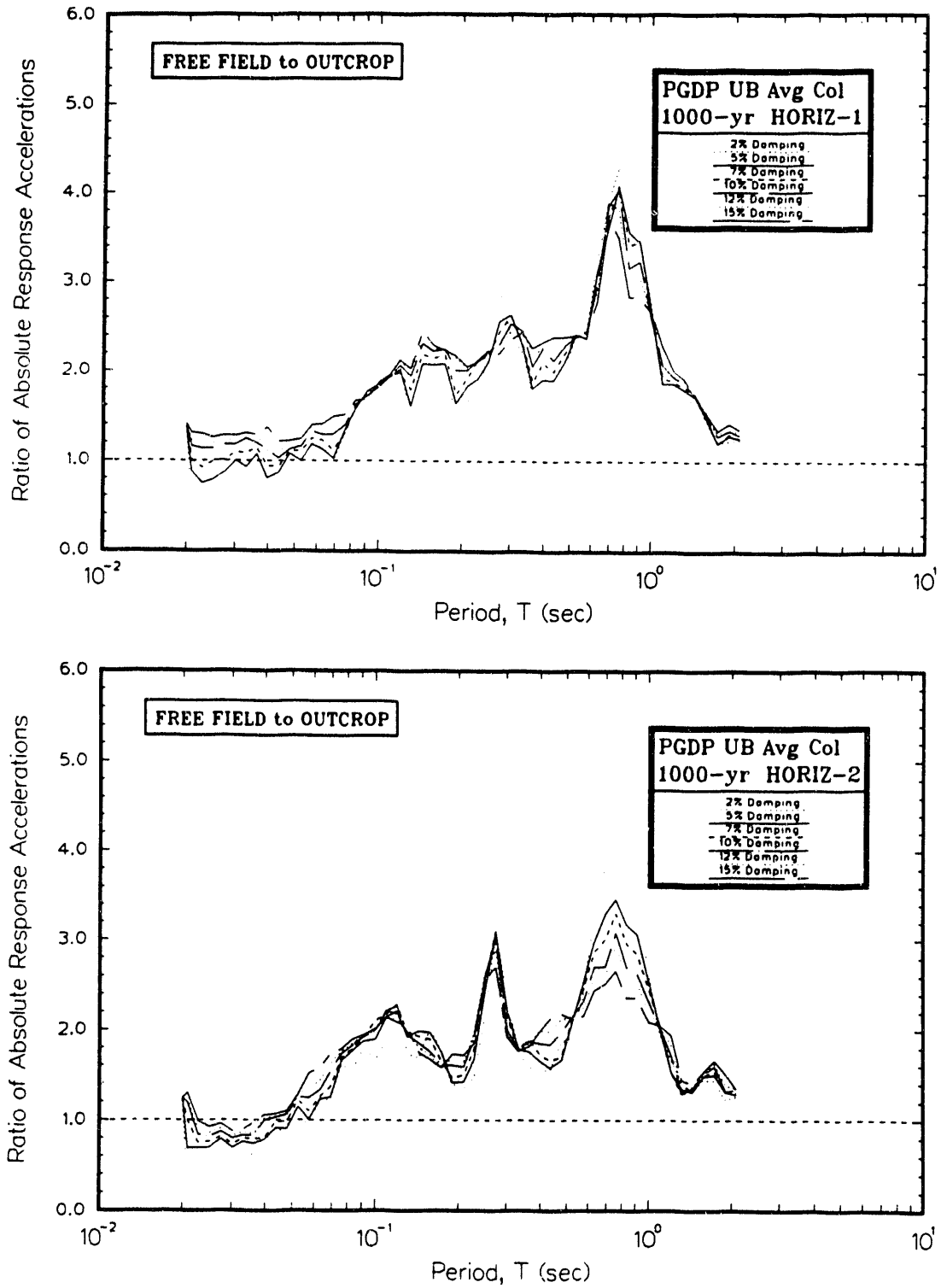

Figure U15. Ratio of absolute acceleration response spectra at free field to rock using upper bound of modulus for average column

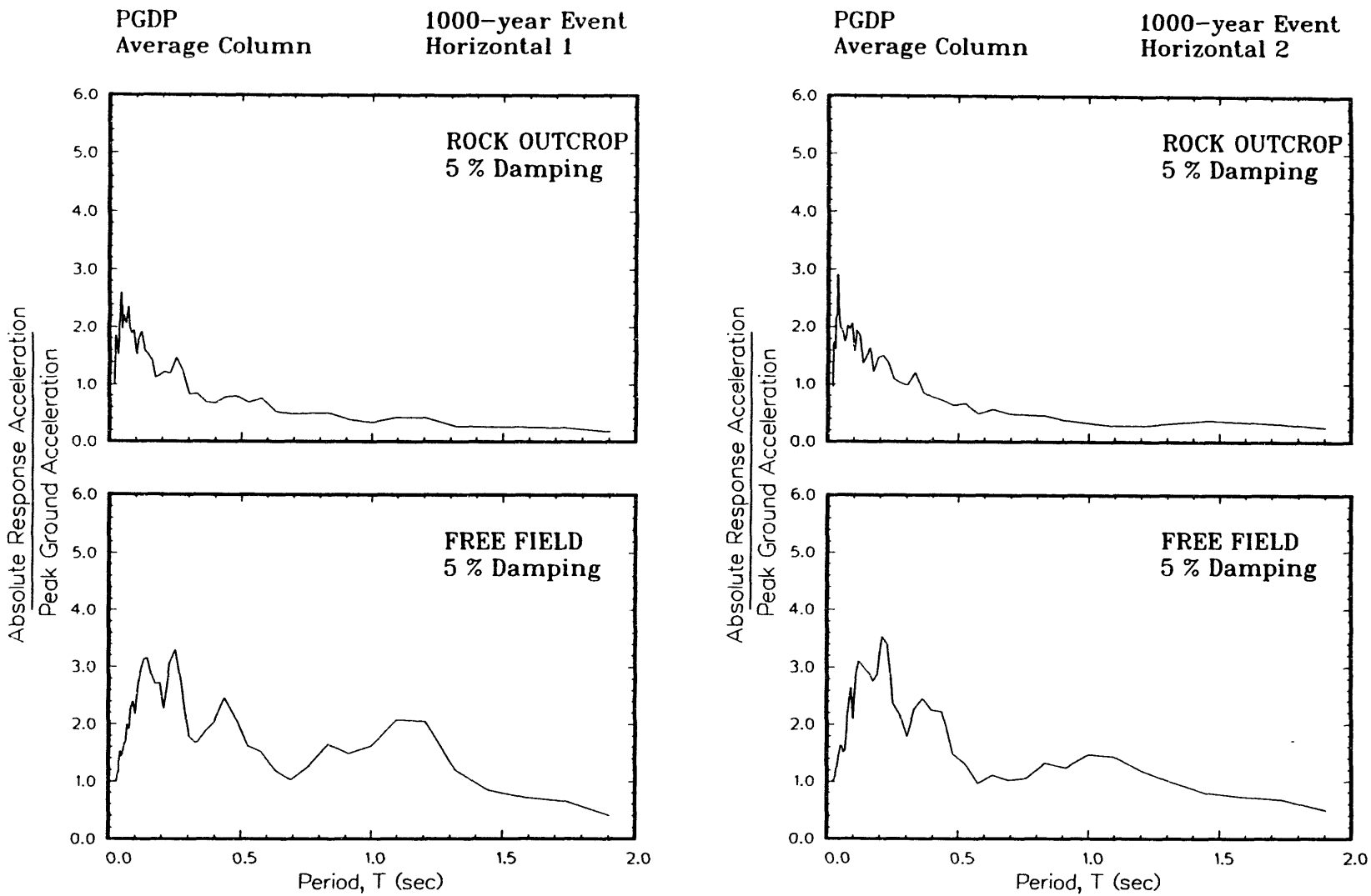

Figure U16. Ratio of amplification of absolute acceleration response spectra to peak acceleration at free field using best estimate of modulus for average column

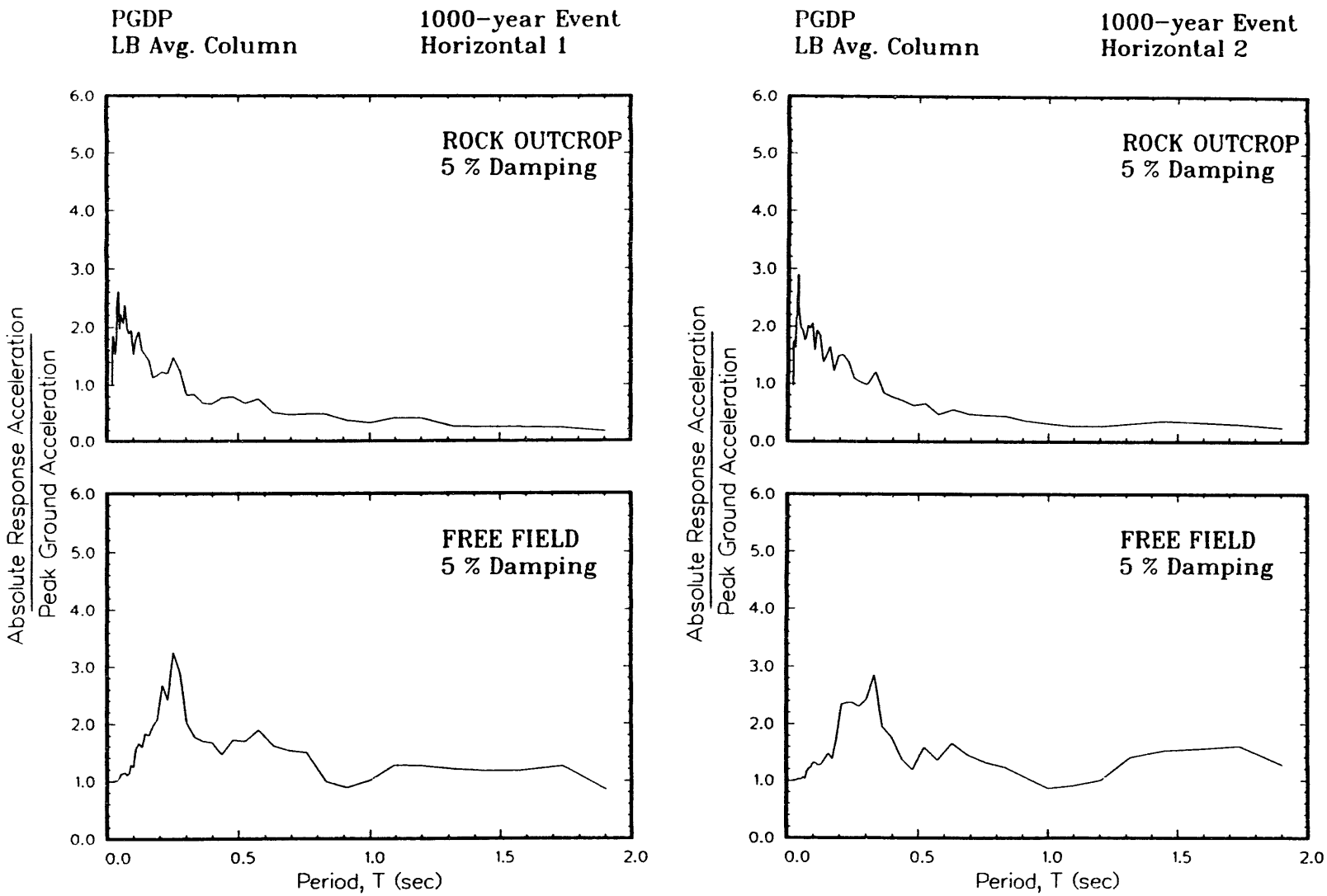

Figure U17. Ratio of amplification of absolute acceleration response spectra to peak acceleration at free field using lower bound of modulus for average column

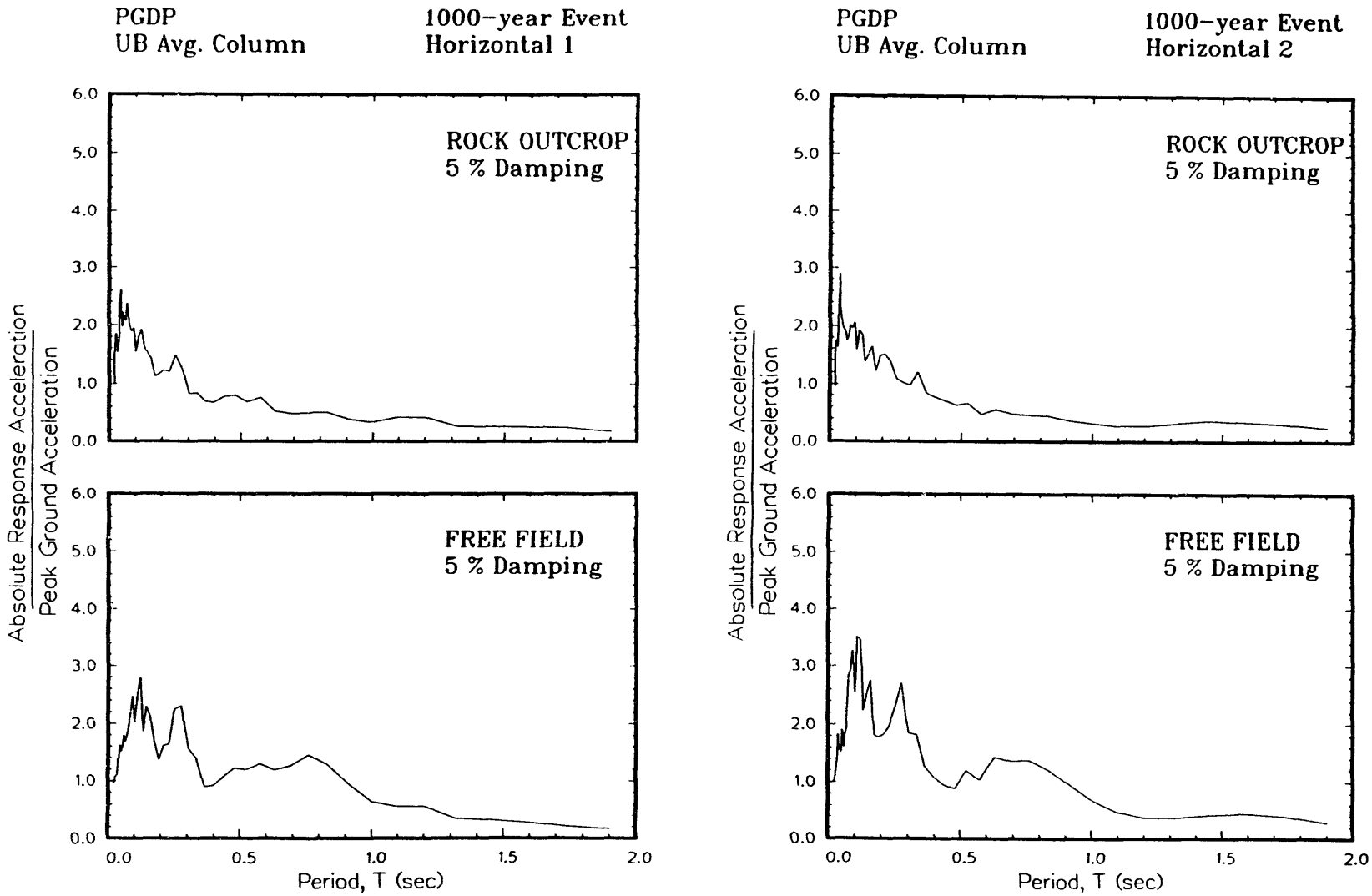

Figure U18. Ratio of amplification of absolute acceleration response spectra to peak acceleration at free field using upper bound of modulus for average column

APPENDIX V: SENSITIVITY OF RESULTS TO MAXIMUM SHEAR MODULUS FOR 5000-YEAR EVENT

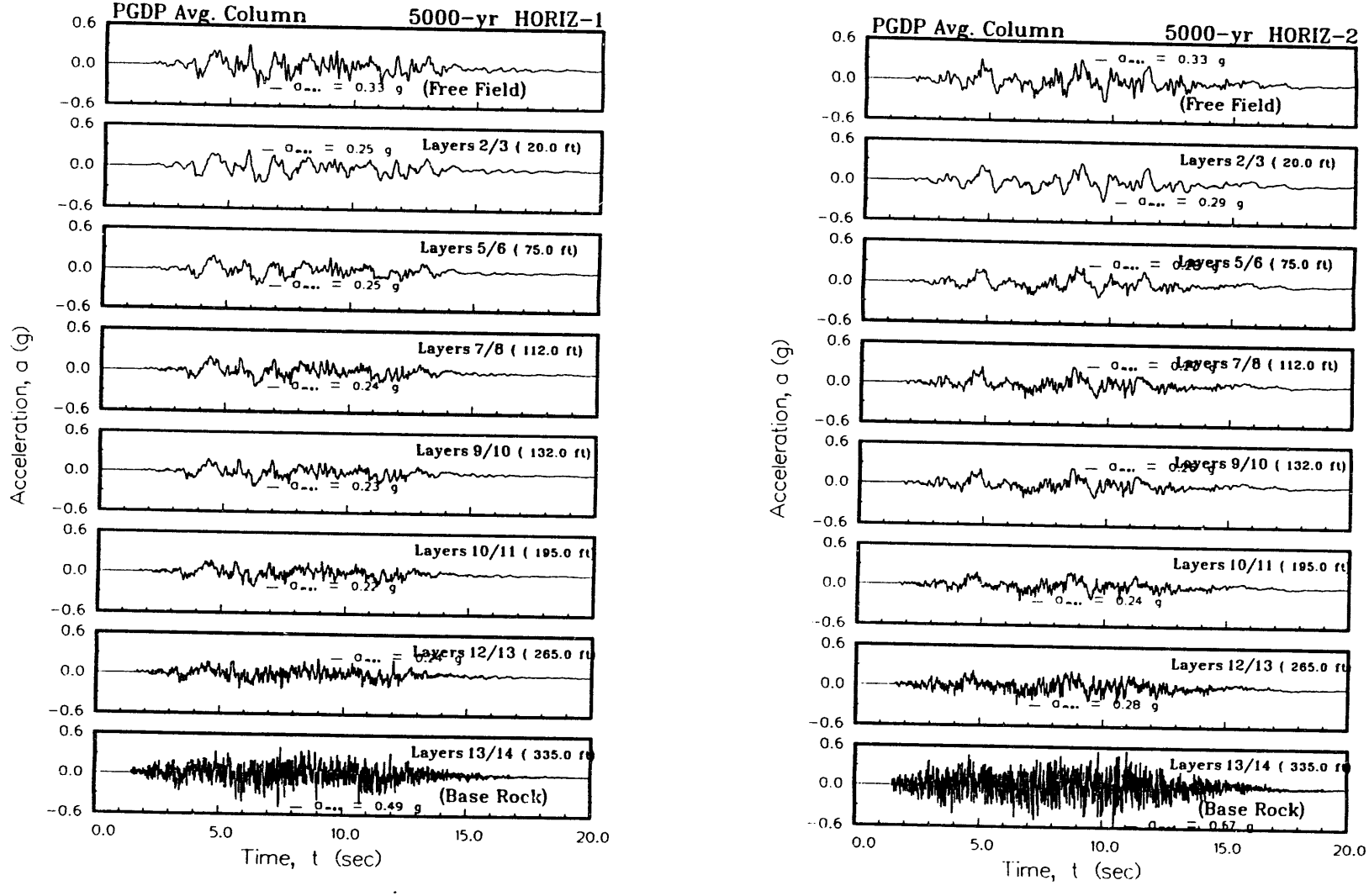

Figure V1. Variation of acceleration with time using best estimate of shear modulus for average column

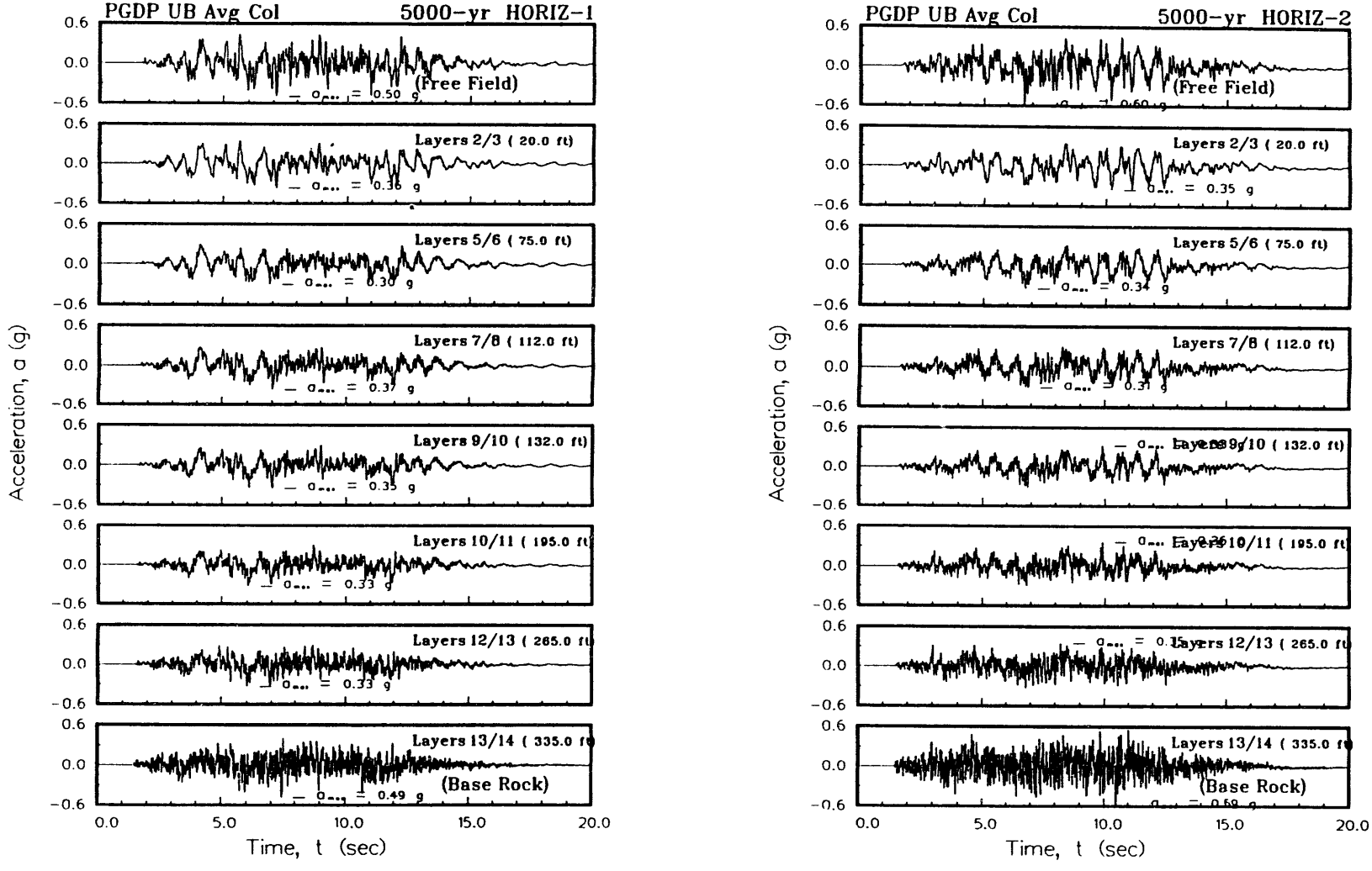

Figure V2. Variation of acceleration with time using upper bound of shear modulus for average column

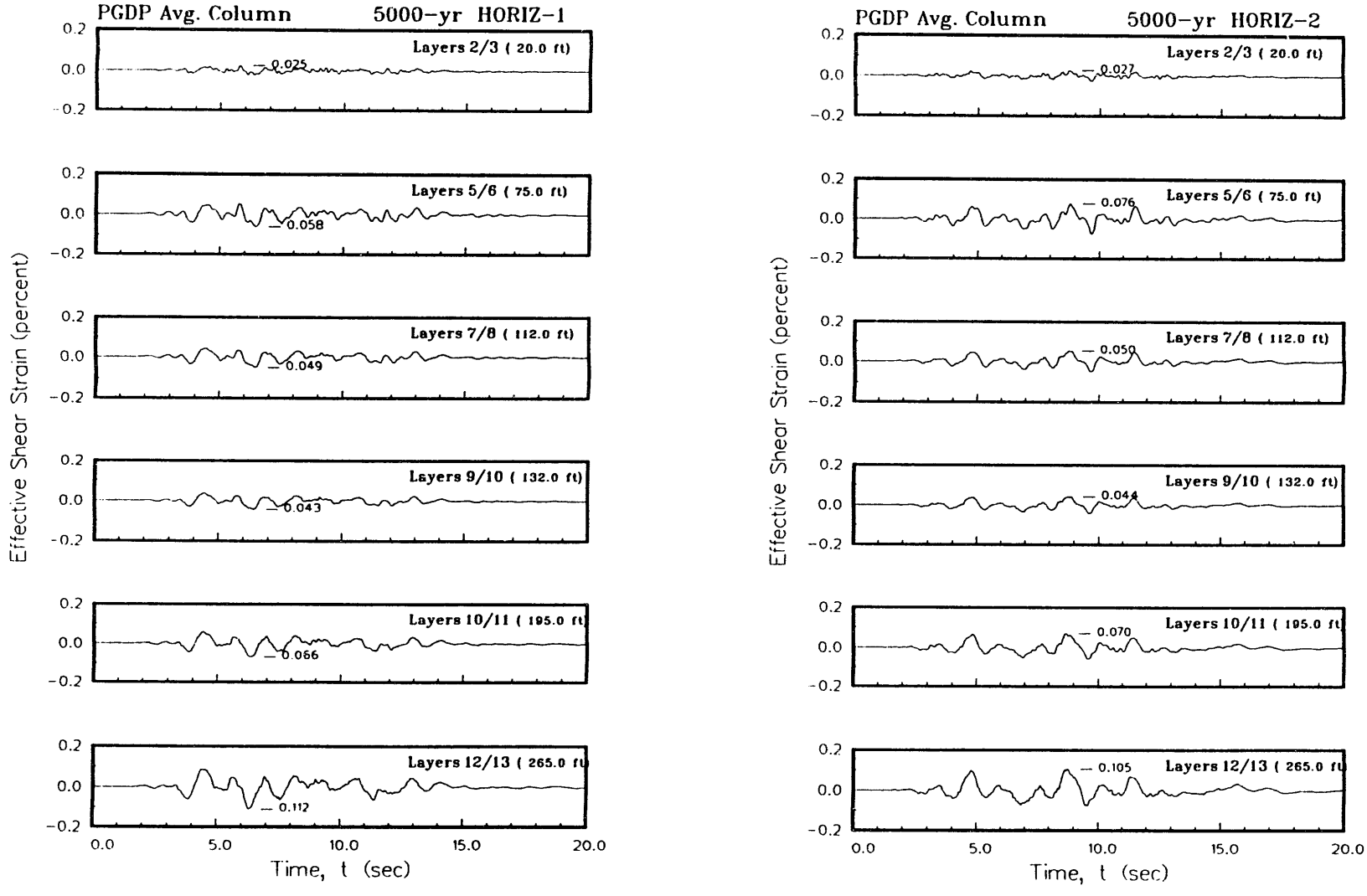

Figure V3. Variation of shear strain with time using best estimate of shear modulus for average column

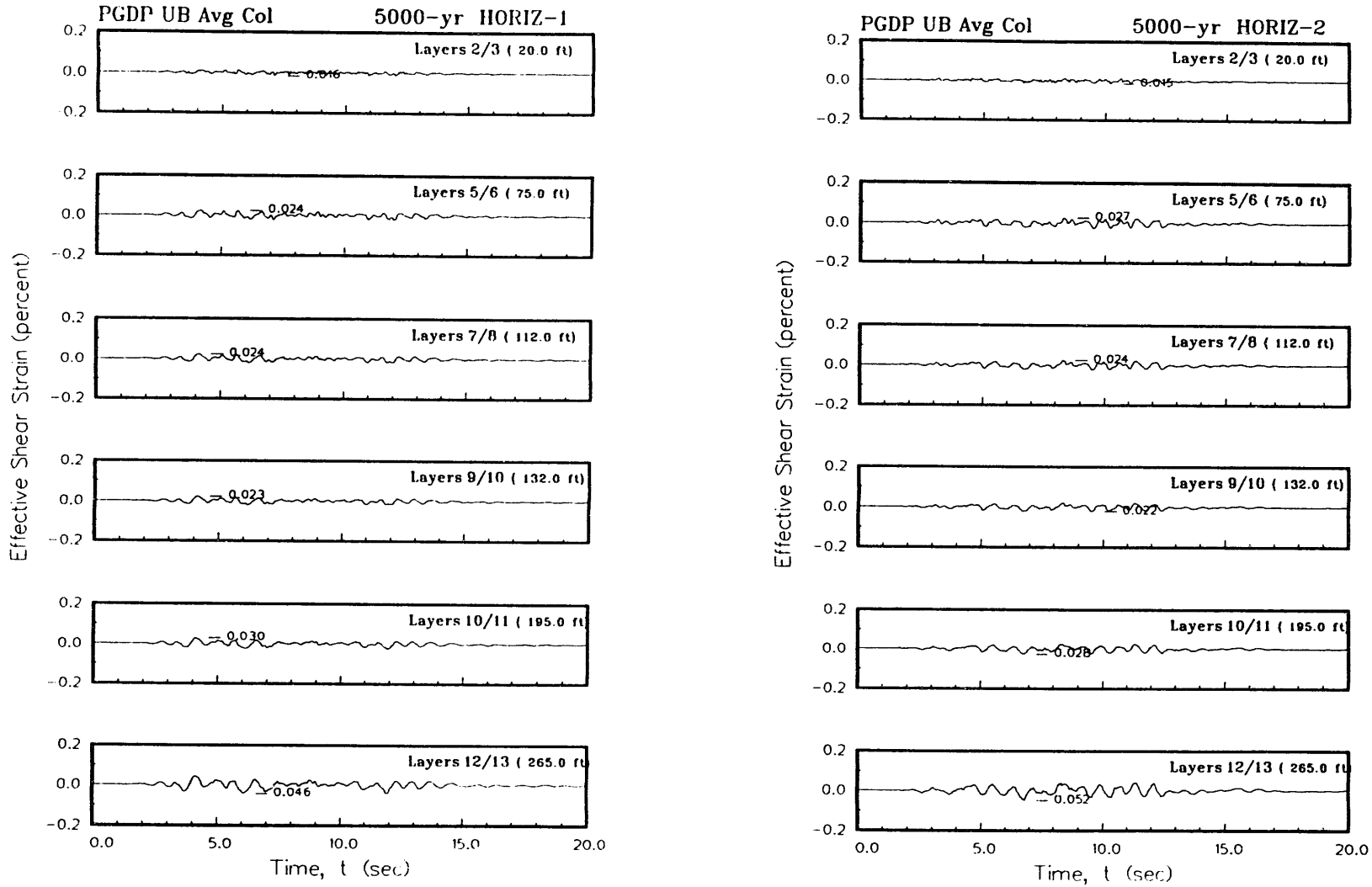

Figure V4. Variation of shear strain with time using upper bound of shear modulus for average column

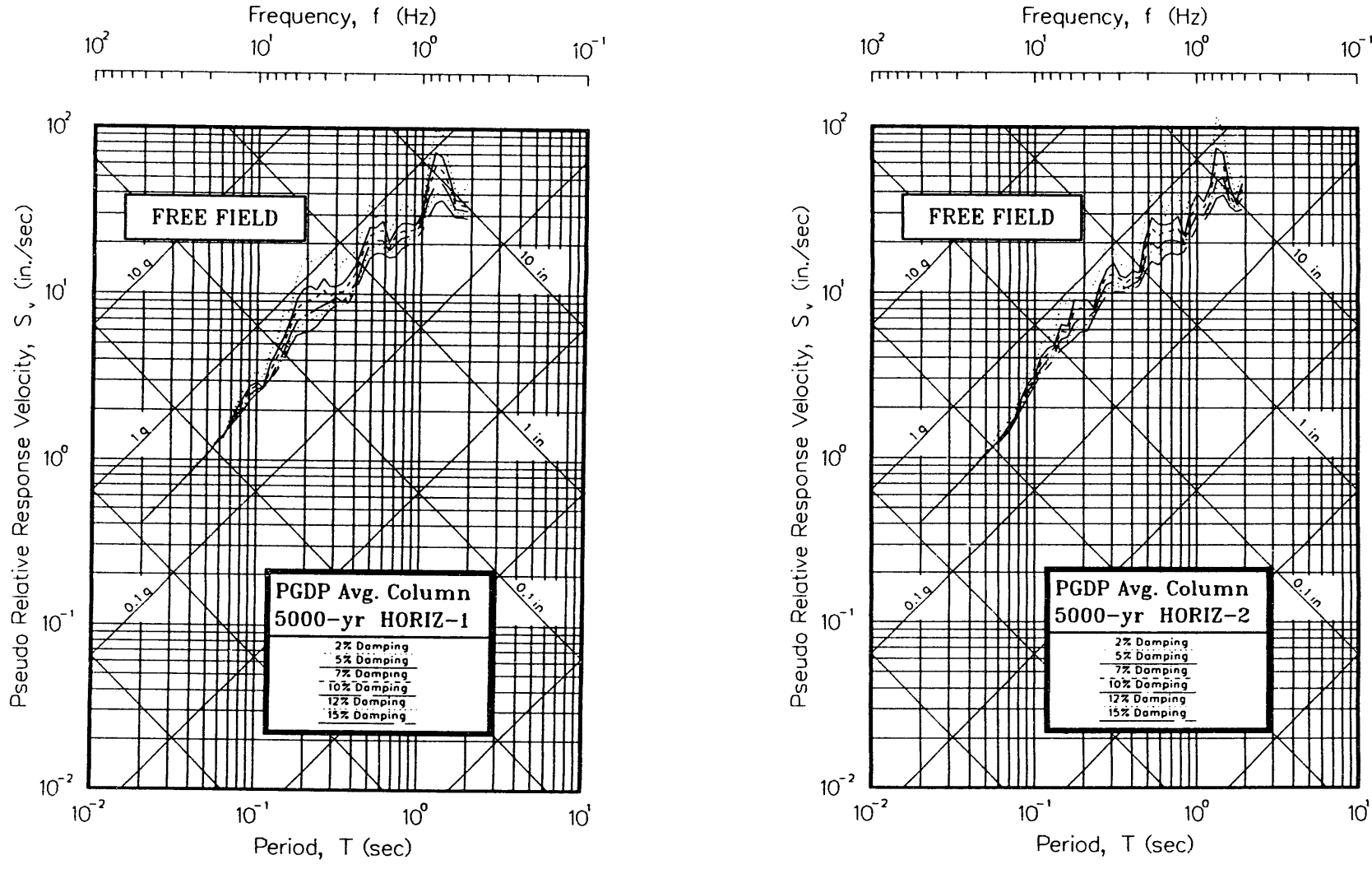

Figure V5. Psuedo-relative velocity spectra in tripartite form at free field using best estimate of modulus for average column

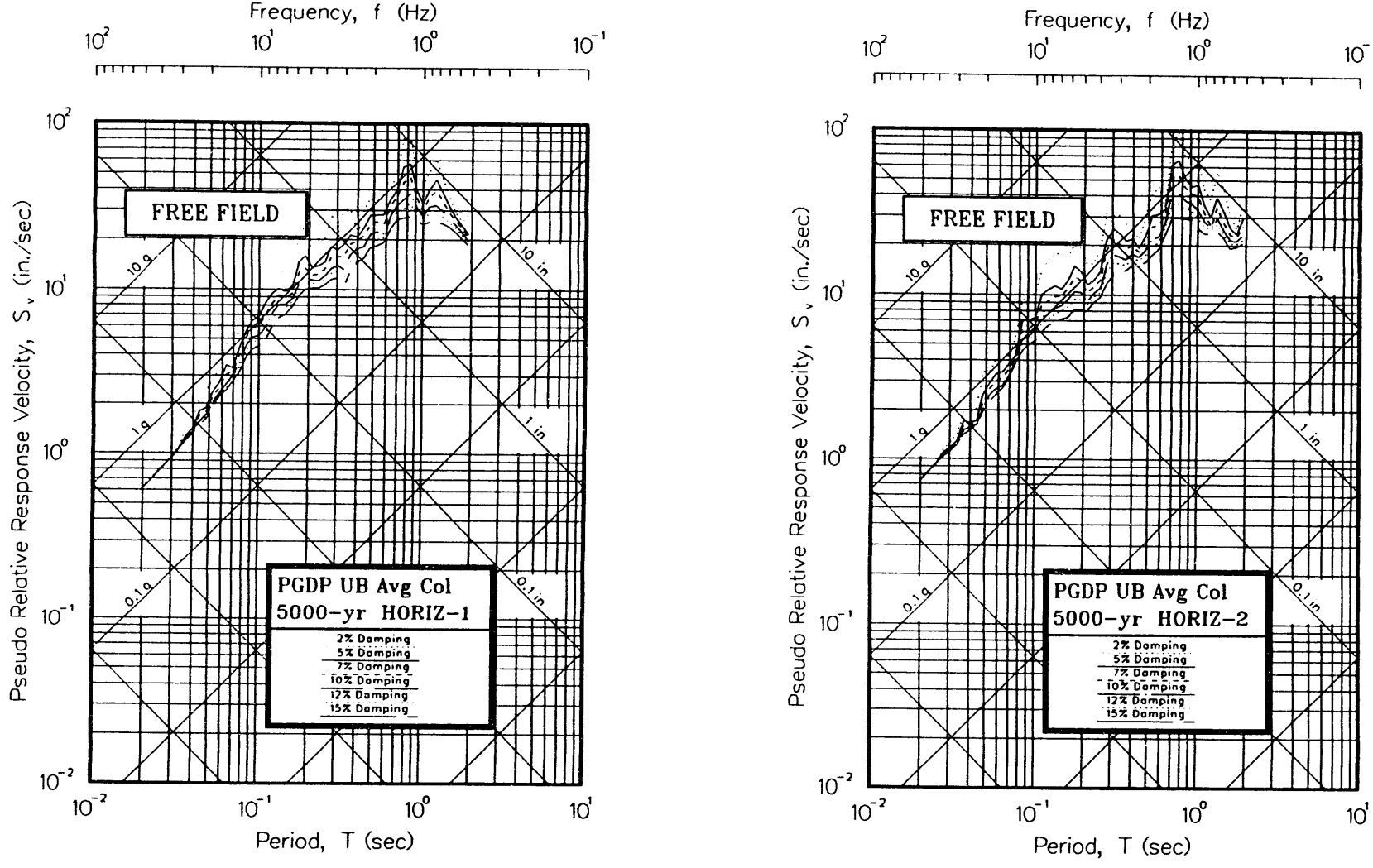

Figure V6. Psuedo-relative velocity spectra in tripartite form at free field using upper bound of modulus for average column

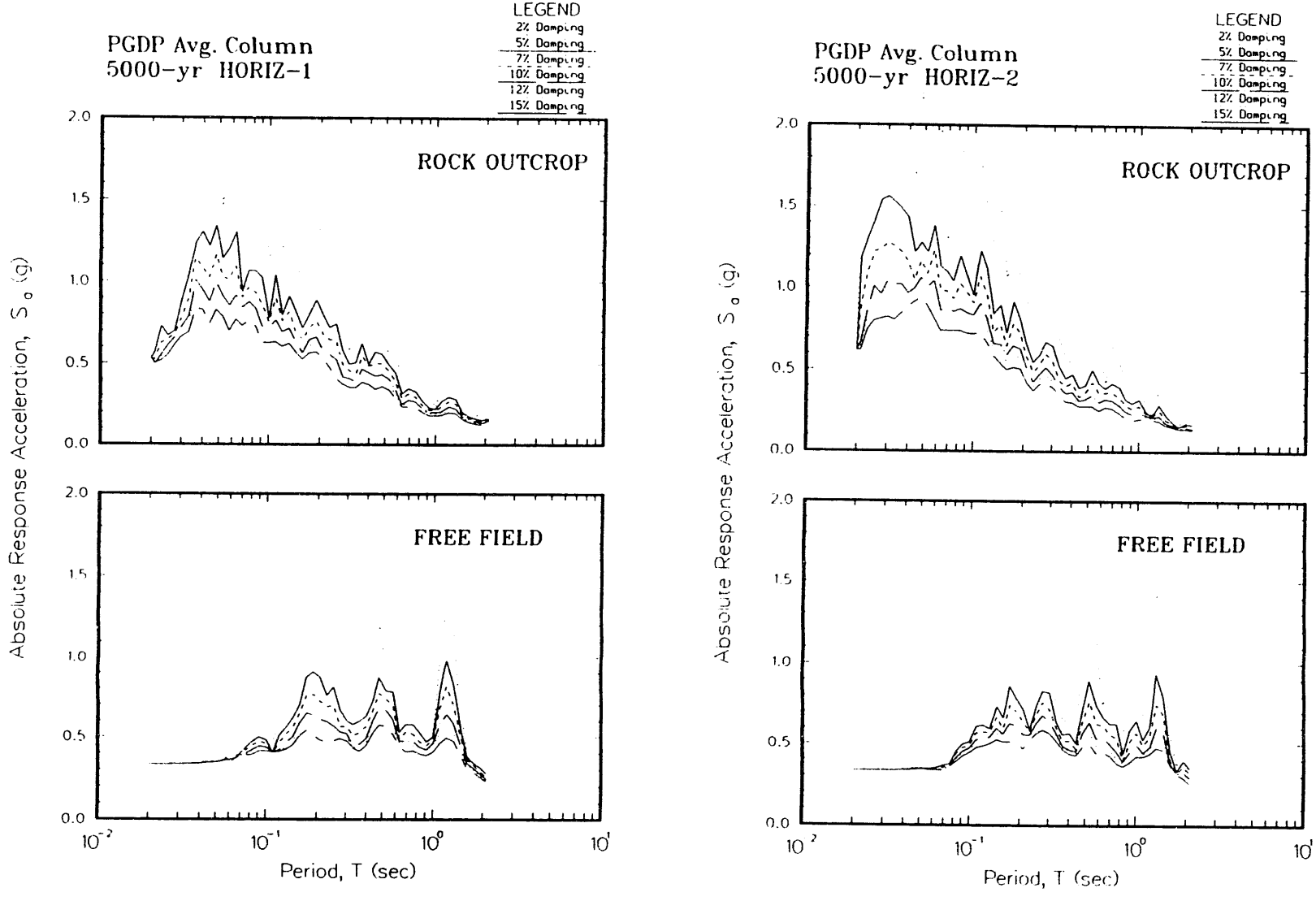

Figure V7. Absolute acceleration response spectra at free field using best estimate of modulus for average column

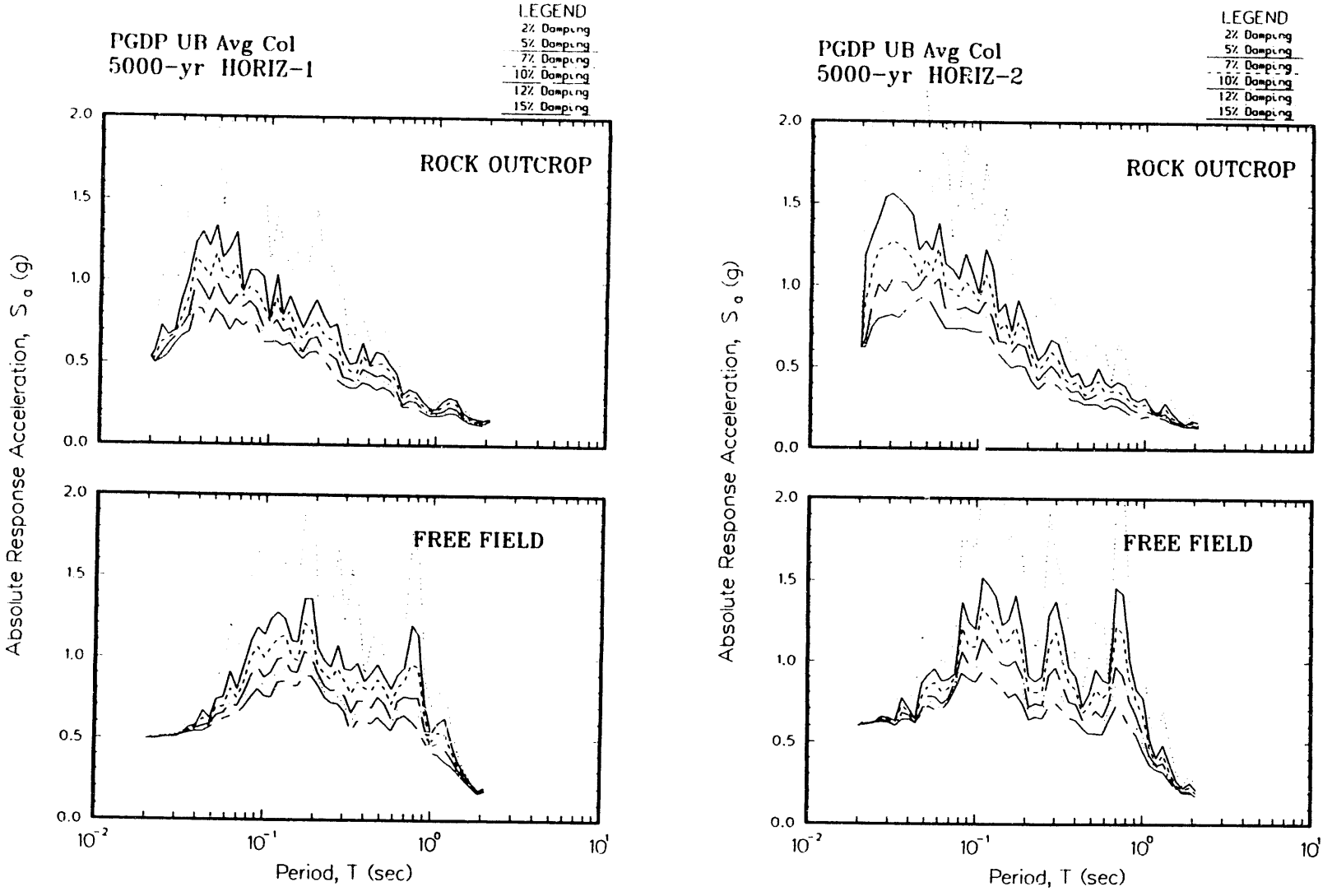

Figure V8. Absolute acceleration response spectra at free field using upper bound of modulus for average column

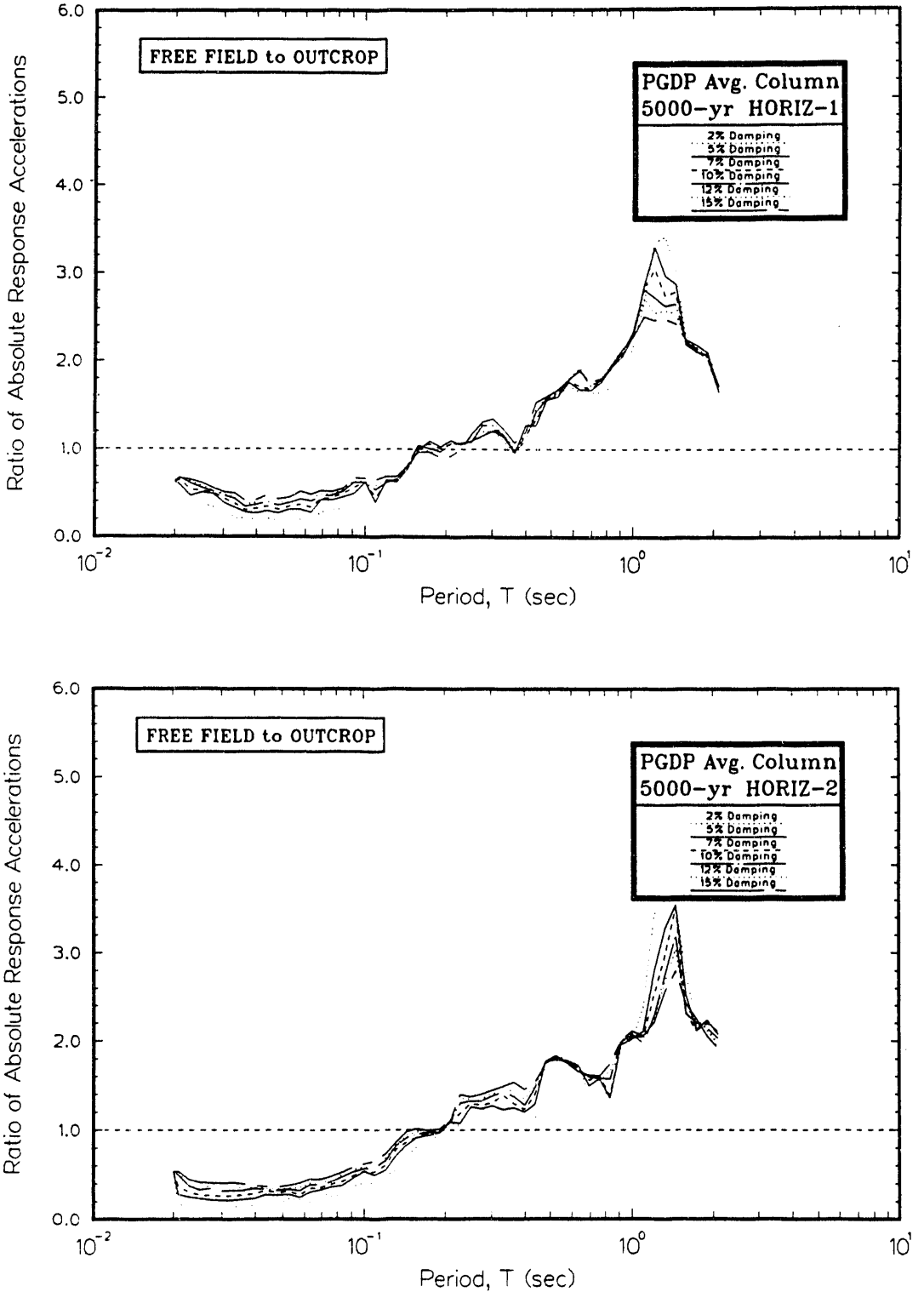

Figure V9. Ratio of absolute acceleration response spectra at free field to rock using best estimate of modulus for average column

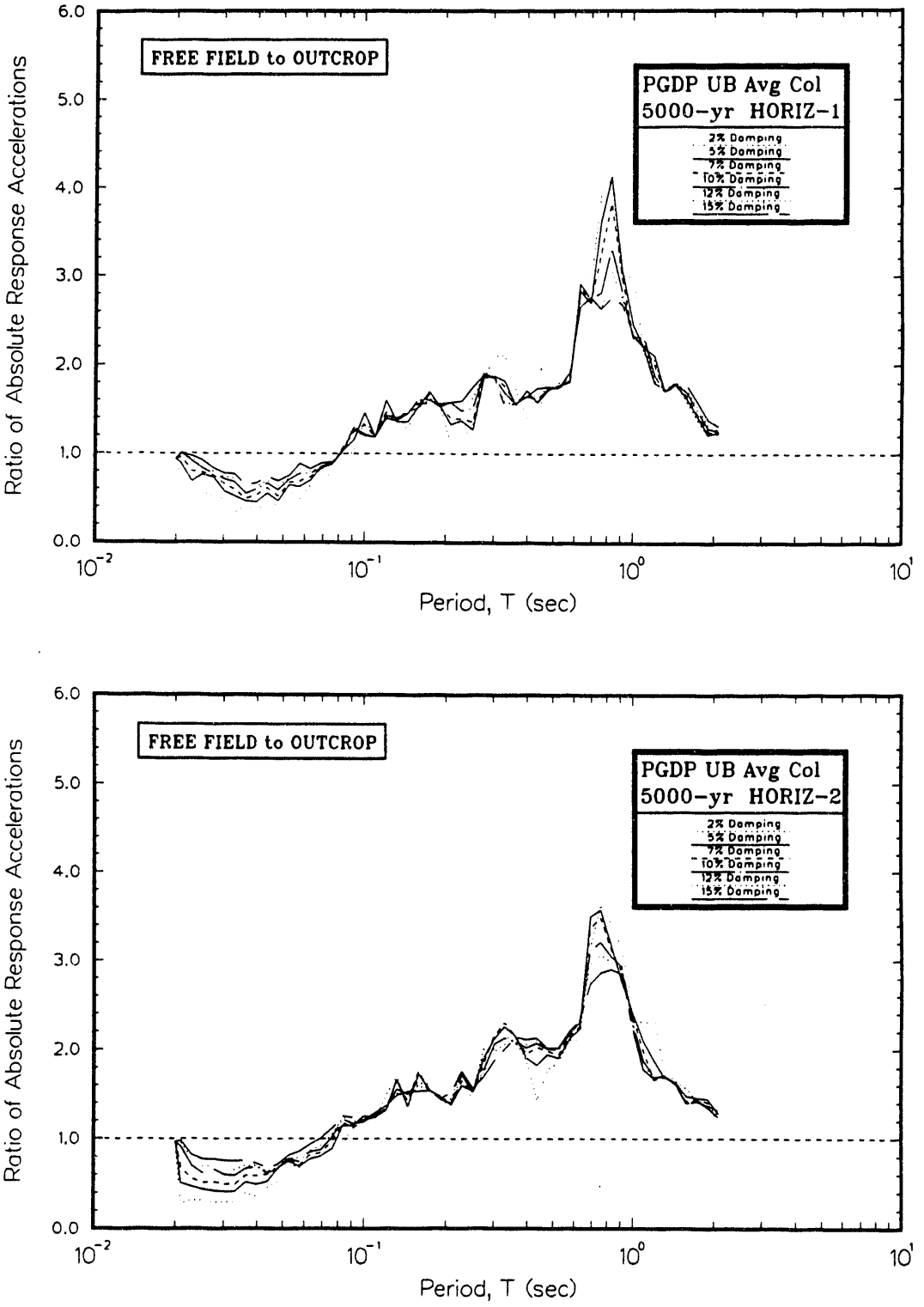

Figure V10. Ratio of absolute acceleration response spectra at free field to rock using upper bound of modulus for average column

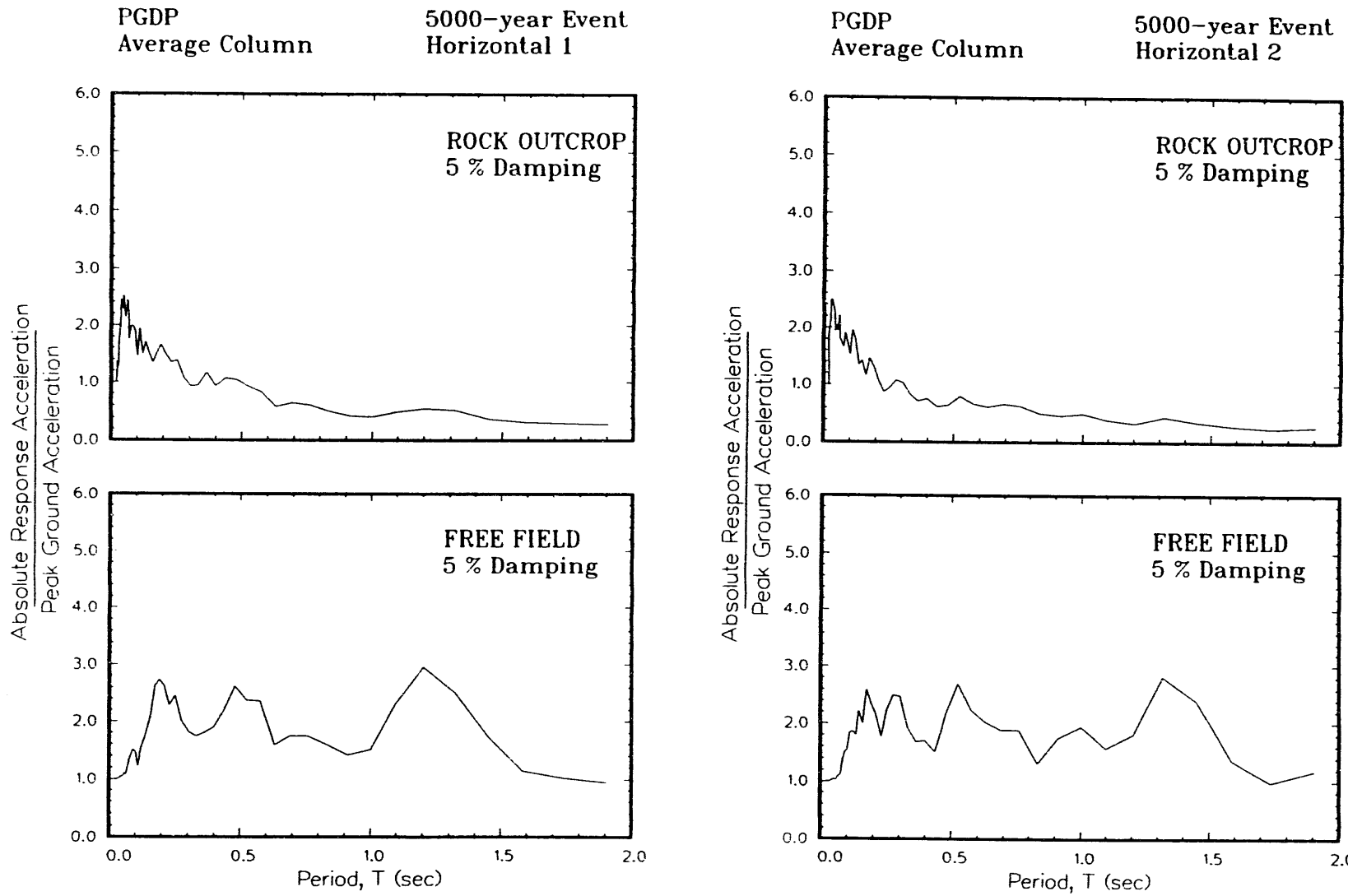

Figure V11. Ratio of amplification of absolute acceleration response spectra to peak acceleration at free field using best estimate of modulus for average column

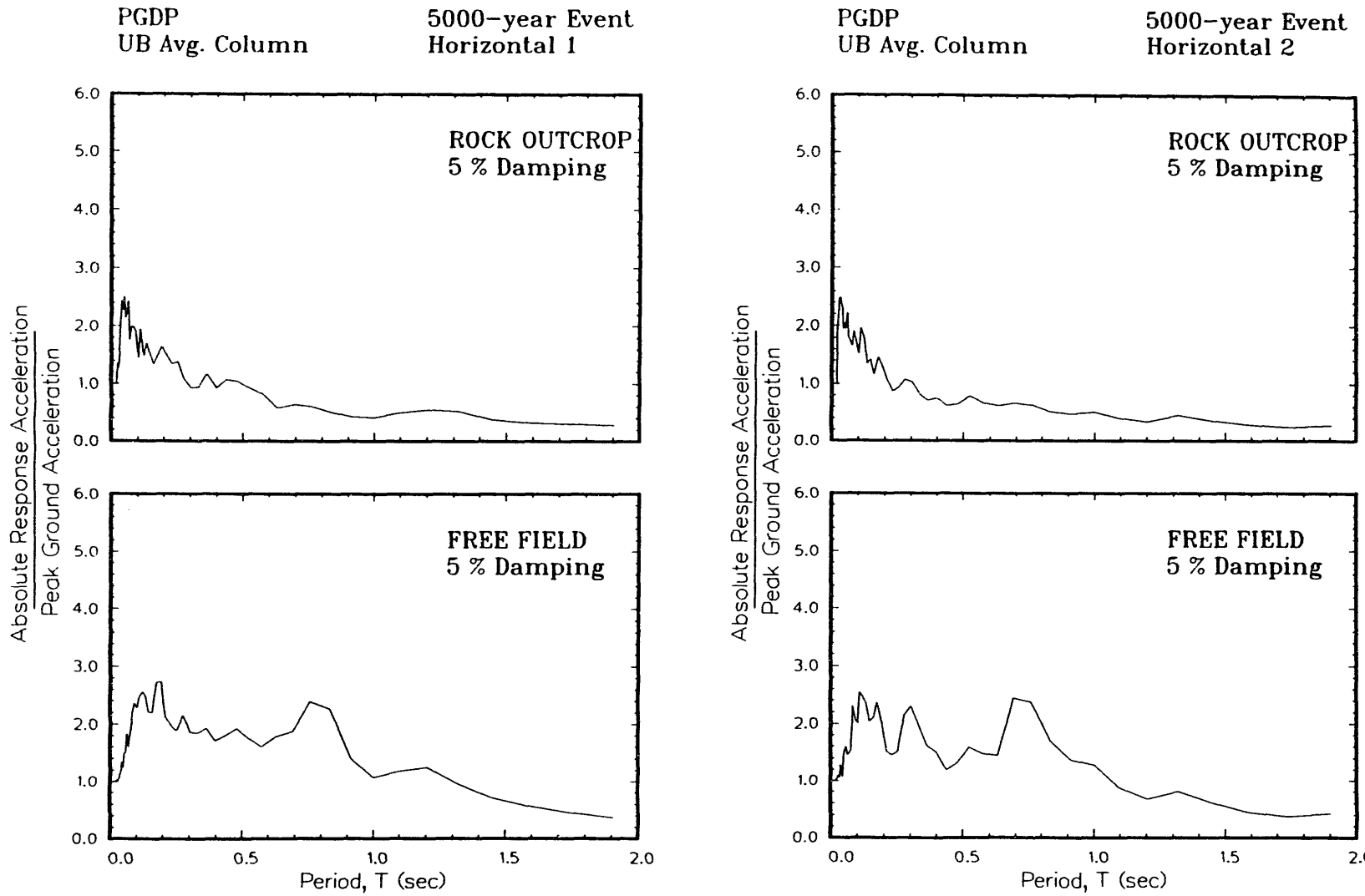

Figure V12. Ratio of amplification of absolute acceleration response spectra to peak acceleration at free field using upper bound of modulus for average column

REPORT DOCUMENTATION PAGE

Form Approved
OMB No. 0704-0188

1. AGENCY USE ONLY (Leave blank)	2. REPORT DATE	3. REPORT TYPE AND DATES COVERED
	August 1993	Final report

4. TITLE AND SUBTITLE
Site-Specific Earthquake Response Analysis for Paducah Gaseous Diffusion Plant, Paducah, Kentucky

5. FUNDING NUMBERS
IAG No.
DE-AI05-910R21971

6. AUTHOR(S)
David W. Sykora and Jennifer J. Davis

7. PERFORMING ORGANIZATION NAME(S) AND ADDRESS(ES)
U.S. Army Engineer Waterways Experiment Station, Geotechnical Laboratory, 3909 Halls Ferry Road, Vicksburg, MS 39180-6199

8. PERFORMING ORGANIZATION REPORT NUMBER
Miscellaneous Paper
GL-93-14

9. SPONSORING/MONITORING AGENCY NAME(S) AND ADDRESS(ES)
U.S. Department of Energy, Oak Ridge Operations,
Oak Ridge, TN 37831-8650

10. SPONSORING/MONITORING AGENCY REPORT NUMBER

11. SUPPLEMENTARY NOTES
This report is available from the National Technical Information Service, 5285 Port Royal Road, Springfield, VA 22161.

12a. DISTRIBUTION/AVAILABILITY STATEMENT
Approved for public release; distribution is unlimited

12b. DISTRIBUTION CODE

13. ABSTRACT (Maximum 200 words)

A site response analysis has been conducted for the DOE Paducah Gaseous Diffusion Plant (PGDP) located southwest of Paducah, Kentucky. Synthetic earthquake records corresponding to three return periods were provided. Geotechnical and seismic geophysical data were collected by others and used to create four individual soil columns for the response calculations and one average column used for the sensitivity analysis. The soils primarily consist of continental deposits of sand, silt, and clay overlying alluvial deposits. Four soil columns were created with a range of total soil thickness from 322 to 364 ft and all material types represented. The shear wave velocities for soil range from 500 fps near the ground surface to 1,600 fps but generally are between 950 and 1,600 fps. The results of calculations using the one-dimensional wave propagation code *SHAKE* indicate that ground motions will be amplified at site periods between 0.1 and 2 sec. Natural site periods range from 0.9 to 1.2 sec. The peak free field accelerations are 0.20, 0.27, and 0.36 g for the 500-, 1000-, and 5000-year events, respectively. A sensitivity analysis of various inputs was conducted.

14. SUBJECT TERMS
Earthquake engineering; Soil amplification; Wave propagation; Site response; Vibration

15. NUMBER OF PAGES
266

16. PRICE CODE

17. SECURITY CLASSIFICATION OF REPORT	18. SECURITY CLASSIFICATION OF THIS PAGE	19. SECURITY CLASSIFICATION OF ABSTRACT	20. LIMITATION OF ABSTRACT
Unclassified	Unclassified		

END

DATE FILMED

10/12/93